# Università degli Studi di Ferrara

DOTTORATO DI RICERCA IN

FISICA

CICLO XXXIV

COORDINATRICE  Prof. Eleonora Luppi

# Nb/Cu QWR superconductive cavities production for the ALPI upgrade in the framework of the SPES facility

Settore Scientifico Disciplinare FIS/01

**Dottorando**

Dott. Andrii Tsymbaliuk

_____
*(firma)*

**Co-Tutore**

Prof. Giorgio Keppel

_____
*(firma)*

**Tutore**

Prof. Diego Bettoni

_____
*(firma)*

Anni 2018/2021

# Acknowledgements

# SCIENTIFIC CONTEXT

# Abstract

The research activity described in this paper is based on the Nb/Cu QWR cavities production technology for the ALPI LINAC upgrade in the framework of the SPES facility.

The ALPI ("Acceleratore Lineare Per Ioni" in Italian) linear accelerator for ions, based in Legnaro National Laboratories, is used for the acceleration of the heavy ions. The ALPI accelerator is composed by quarter wave resonators (QWR), divided onto three brunches: low-β, medium-β and high-β in function on particle velocity.

The SPES ("Selective Production of Exotic Species") project is based in Legnaro National Laboratories and related to basic research in different fields of science. The SPES project is now in the construction stage and ALPI LINAC will be used for acceleration and reacceleration of the radioactive beams of interest for the SPES project. Current acceleration energy of the LINAC is insufficient for the SPES facility, and the upgrade of the accelerator is required.

The increase of the ALPI LINAC total energy and reliability can be done by the addition of two cryostats in the high-β section of ALPI. For this upgrade the production of 8 new Nb/Cu high-β superconductive QWRs and plates, by sputtering technology is fundamental.

The R&D activity in the framework of the Nb/Cu high-β QWR production can be divided in three parts.

The first part was based on the upgrade and modification of the vacuum systems, used for sputtering of the medium-β QWR cavities, plates, and cryostat measurements of the superconductive structures. Due to different substrate geometries of medium and high-β cavities, the sputtering vacuum systems and measurement cryostat were refurbished and modified.

The second part was focused on the definition of the sputtering parameters for the high-β QWR cavities and plates production. The Niobium deposition was made onto quartz samples, placed within the surface of the stainless-steel moke-up QWR cavity. A variation of the sputtering parameters was proceeded for achieving the highest superconductive properties and the equal thickness of the niobium coating within all the quarter wave resonator surface.

After the definition of the sputtering parameters, Nb/Cu high-β QWR cavities and plates were produced. The superconductive performance of the high-β cavities were evaluated at 4,2 K in the refurbished vacuum cryostat.

In the framework of the Nb/Cu high-β QWR production for the ALPI upgrade 10 cavities were produced. Several cavities reached the superconductive target performance and will be assembled in the ALPI accelerator.

The proposed technology is sufficient for further production of the Nb/Cu high-β cavities for the ALPI accelerator.

# Estratto

L'attività di ricerca descritta in questo elaborato è basata sulla tecnologia di produzione di cavità Nb/Cu QWR per l'upgrade del LINAC ALPI nel quadro della struttura SPES.

L'acceleratore lineare per ioni ALPI, basato nei Laboratori Nazionali di Legnaro, è utilizzato per l'accelerazione degli ioni pesanti. L'acceleratore ALPI è composto da risonatori a quarto d'onda (QWR), divisi in tre gruppi: basso-$\beta$, medio-$\beta$ e alto-$\beta$ in funzione della velocità delle particelle.

Il progetto SPES ("Selective Production of Exotic Species") ha sede nei Laboratori Nazionali di Legnaro ed è legato alla ricerca di base in diversi campi della scienza. Esso è ora in fase di costruzione e il LINAC ALPI sarà utilizzato per l'accelerazione e la riaccelerazione dei fasci radioattivi. L'attuale energia di accelerazione del LINAC è insufficiente per la facility SPES e l'upgrade dell'acceleratore è fondamentale.

L'aumento dell'energia totale e dell'affidabilità del LINAC ALPI può essere eseguito con l'aggiunta di due criostati nella sezione high-$\beta$. Per questo aggiornamento è fondamentale la produzione di 8 nuovi risuonatori superconduttivi ad alto-$\beta$ e piatti, prodotti mediante il processo di sputtering.

L'attività di R&D nel quadro della produzione di Nb/Cu high-$\beta$ QWR può essere divisa in tre parti.

La prima parte si è basata sull'aggiornamento e la modifica dei sistemi di vuoto, utilizzati per lo sputtering delle cavità QWR a medio-$\beta$, dei piatti e delle misure tramite un criostato delle strutture superconduttive. A causa delle diverse geometrie del substrato delle cavità a medio ed alto beta, i sistemi da sputtering e il criostato di misura sono stati rinnovati e modificati.

La seconda parte si è concentrata sulla definizione dei parametri di sputtering per le cavità QWR ad alto-$\beta$ e la produzione dei piatti. La deposizione di niobio è stata eseguita su campioni di quarzo, collocati all'interno della superficie della cavità di test in acciaio inossidabile. Si è proceduto ad una variazione dei parametri di sputtering per ottenere le più alte proprietà superconduttive e uguale spessore del rivestimento di niobio all'interno di tutta la superficie del risonatore a quarto d'onda.

Dopo la definizione dei parametri di sputtering, sono state prodotte le cavità QWR e i piatti Nb/Cu high-$\beta$. Le prestazioni superconduttive delle cavità high-$\beta$ sono state valutate a 4,2 K nel criostato rinnovato.

Nel quadro della produzione di Nb/Cu high-$\beta$ QWR per l'aggiornamento LINAC ALPI sono state prodotte 10 cavità, utilizzando la tecnologia di produzione definita nella prima fase dell'attività di ricerca. Diverse cavità hanno raggiunto le prestazioni definite come target per l'instalazione in acceleratore (min 4.5 MV/m @7W) e saranno assemblate nell'acceleratore.

La tecnologia proposta è sufficiente per proseguire nella produzione delle cavità Nb/Cu high-β per ALPI.

# List of Tables

# List of Figures

# List of Acronyms

- AC – Alternating Current;
- ADS – Accelerator Driven System;
- ALPI – in italian "Acceleratore Lineare Per Ioni";
- ANL – Argonne National Laboratory (USA);
- ATLAS – Argonne Tandem LINAC Accelerating System;
- BCP – Buffered Chemical Polishing;
- CB – Charge Breeder;
- CERN – The European Organisation for Nuclear Research (Geneva, Switzerland);
- DC – Direct Current;
- DQWR – Double Quarter Wave Resonator;
- ESS – European Spallation Source (Lund, Sweden);
- FEM – Finite Element Method;
- FNAL – Fermi National Accelerator Laboratory (Fermilab, Chicago, USA);
- FRIB – Facility for Rare Isotope Beams;
- GANIL – in french "Grand Accelerateur National D`Ions Lourds" (Caen, France);
- GPS – General Purpose Separator;
- HF – High Field;
- HIE-ISOLDE – High Intensity and Energy upgrade of ISOLDE;
- HMRS – High-Resolution Mass Separator;
- HPR – High Pressure Rinsing;
- HRS – High Resolution Separator;
- HWR – Half Wave Resonator;
- IFMIF – International Fusion Materials Irradiation Facility (CERN);
- IHEP – Institute of High Energy Physics (Beijing, China);
- IMP – Institute of Modern Physics (China);
- INFN – National Institute of the Nuclear Physics (Italy)
- ISAC – Isotope Separator and Accelerator;
- ISOLDE - Isotope mass Separator On-Line facility;
- IUAC – Inter University Accelerator Centre (New Dehli, India);
- LF – Low Field;
- LIS – Laser Ionization Source;

- LNL – Legnaro National Laboratories (Legnaro, Italy);
- LINAC – Linear Accelerator;
- MF – Medium Field;
- NSCL – National Superconducting Cyclotron Laboratory (Michigan, USA);
- PC – Personal Computer;
- PIAVE – Positive Ion Accelerator for VEry low velocity ions;
- PIP – Proton Improvement Plan;
- PIS – Plasma Ionization Source;
- PVD – Physical Vapour Deposition;
- REX-ISOLDE – Radioactive Beam Experiment of ISOLDE;
- QWR  –  Quarter Wave Resonator;
- RAON – Rare isotope Accelerator complex for ON-line experiments;
- RF – Radio Frequency;
- RFD – Radio Frequency Dipole;
- RFQ – Radio Frequency Quadrupole;
- RIB – Radioactive Ion Beam;
- RISP – Rare Isotope Science Project (South Korea);
- RRR – Residual Resistivity Ratio;
- SARAF – Soreq Applied Research Accelerator Facility (Soreq. Israel);
- SEM – Scanning Electron Microscope;
- SIS – Surface Ionization source;
- SPES – Selective Production of Exotic Species;
- SPIRAL – Production System of Radioactive Ion and Acceleration On-Line;
- SRF – Superconducting Radio Frequency;
- SSR – Single Spoke Resonator;
- TIS – Target Ionisation Source;
- TMP – Turbo Molecular Pump;
- TRIUMF – Tri-University Meson Facility (Canada);

# Chapter 1

# INTRODUCTION

Quarter Wave Resonators (QWRs) are a type of superconductive cavities used for the acceleration of heavy ions. This type of superconductive cavities is now in usage in different accelerators around the world. This is why the development of the most economically efficient production technology of superconductive QWRs is one of the main topics of acceleration physics within last several decades.

From the end of 20th century, the production of QWR cavities by physical vapour deposition (PVD) technology has been studied [1] to replace bulk niobium cavities onto cheaper and easier in machining niobium sputtered copper cavities. Different PVD techniques for production of Nb/Cu sputtered QWR cavities for different accelerators, such as HIE-ISOLDE [2] and ALPI [3], were studied before. For increasing the performance of the sputtered Nb/Cu QWR cavities, further developments and upgrades of production technology are required.

The ALPI ("Acceleratore Lineare Per Ioni" in Italian) is a linear accelerator, placed in Legnaro National Laboratories. The ALPI accelerating cavities are of the QWR type, made from bulk niobium or sputtered niobium onto copper surface [4]. The ALPI accelerator is divided onto three sections, depended on the $\beta$-factor of the QWRs.

The SPES ("Selective Production of Exotic Species") project is based in Legnaro National Laboratories and related to basic research in nuclear physics and astrophysics, production of radionuclides for medical attitudes, generation neutrons for material studies, nuclear technology and medicine [5]. The SPES project is in the stage of construction in Legnaro and it was decided to use ALPI LINAC for acceleration and reacceleration of the Radioactive Ion Beam (RIB) species of interest for the SPES facility. The upgrade of the LINAC for this purpose for a final energy $E_f \sim 10$ MeV/A is required [6].

One of the main scenarios for the ALPI upgrade is assembling two cryostats (4 cavities each) in high-$\beta$ section. In this way the number of the cavities will be more efficiently divided into three different beta branches of the LINAC. This will lead to an improvement of the bean transition and final energy of the accelerator and transmission will be increased. 8 high-$\beta$ Nb/Cu QWR cavities should be produced for arranging the ALPI upgrade [7]. The ALPI LINAC works at the power of 7W and the main performance goals for the cavities, implemented in the high-$\beta$ section are energy of the

acceleration field at working power, that should be higher than 4,5 MV/m; quality factor of the cavity at working power, that should be higher than $1 \cdot 10^8$.

The main aim of this research is to develop technology for the production of sputtered high-β Nb/Cu QWR cavities. Produced QWRs should achieve performance goals, required for implementation in the ALPI LINAC.

Following activities were made for achieving the main goals of the research:

- QWR cavity sputtering vacuum system was refurbished and upgraded;
- Niobium targets were cleaned by the plasma cleaning process;
- Testing of the sputtering systems with niobium deposition onto quartz samples was made;
- Optimal sputtering parameters were defined;
- QWR measurement cryostat was refurbished and upgraded;
- QWR plate sputtering system was upgraded;
- Sputtering of the niobium coating onto copper substrate of the high-β QWR cavities and plates was made;
- Superconductive performance of the produced high-β QWR cavities was defined.

Main part of the research was focused on the production of the Nb/Cu high-β QWR cavities after maintenance of the sputtering systems and test cryostat was finished. A bias sputtering system was used for the production of the QWRs. RF measurements at 4,2 K with refurbished cryostat was made to define superconductive performances of the produced QWRs.

# BACKGROUND AND LITERATURE REVIEW

## Chapter 2

## PARTICLE ACCELERATORS FACILITY

### 2.1. Introduction

The particle accelerator is a machine that uses electromagnetic fields to accelerate the charged particles to the high speeds and energies and to contain them in well-defined beams. Main purpose of the particle acceleration facility development was investigation of the atomic nucleus.

First experimental research of the atomic core was performed with α-particles, obtained from the unstable isotopes decay (Radium), which were accelerated by themselves in the field of the nucleus to the energies of several MeV.

The particle accelerators era starts at early 1930-s, when two acceleration schemes were simultaneously developed with acceleration to 1 MeV. In 1932 Lohn Cockcroft and Ernest Walton built 800 kV constant voltage generator, which started the new research field in the experimental particle physics.

The next great step of the acceleration field development was done in 1944 – 1945. Scientists Veksler in U.S.S.R. and McMillan in U.S. independently conceived the principle of phase stability, which permitted frequency modulation of the acceleration voltage. This principle made possible development of the synchrotrons with acceleration energy 300 MeV. After that work onto acceleration energy increasing was performed.

In the last 1960s, the first major proton storage ring, the ISR, was built in CERN. It stored and collided two proton beams of 28 GeV each, which corresponds to the fixed-target acceleration of 1500 GeV.

The development of each new type of accelerator gave an energy increase. Each accelerator type is eventually replaced by another when it reaches its limit for the higher energy beams producing. The field of the accelerator research has been active and productive over the last several decades [8].

One of the first applications of the particle accelerators was for the proton acceleration and, until the late 1980-s, acceleration facilities were assembled using superconducting cavities of two distinct velocity classes. The high velocity structures were used mostly for the acceleration of the electrons and positrons the $\beta \sim 1$ region (where $\beta$ coefficient is determined by the evaluation of the speed of

accelerated particle to the speed of light). These cavities were made of the series of coupled cells of the specific size.

The low-velocity structures, which were developed for the acceleration of protons and heavy ions, extended to the $\beta \sim 0,2$ region [9]. The variety of low-velocity structures will be described in the next paragraph.

Another separation of the accelerators can be hypothetically done by the type of the used radiofrequency cavities with normal conductivity or superconductivity. Both technologies of the usage normal or superconductive cavities have its advantages and disadvantages, which should be concerned on the stage of projecting the accelerating structure.

Operating with normal conducting cavities do not require cooling down to the superconductive state. The technology of production and operating is simpler, and it is possible to reduce the accelerators production costs, since no constant cooling down and tuning of the structure during operation is needed.

From the other side, superconductive RF structures are more favorable at high energies operating regimes with lower applied beam and RF power. Operating with the SRF accelerating structures requires smaller amplifiers and number of the units in respect to normal conducting cavities at the same working power [10].

## 2.2. Heavy ions particle accelerators.

The ALPI LINAC was constructed for acceleration of the heavy particles, using superconducting RF cavities. Currently active projects, which use similar low velocity structures, obtain high interest for this research.

Among this class of structures are quarter wave resonators (QWR), coaxial half-wave resonators (HWR) and spoke resonators. Since the late 1980-s there has been a growing interest in higher velocity of the heavy particles, which opened the field of usage and development of the low-$\beta$ accelerating structures [9]. This caused increase of the application amount for the non-elliptical cavities (Table 2.1).

Table 2.1. Applications of non-elliptical cavities.

| Application | Maximum β | Accelerated beam | Maximum current |
|---|---|---|---|
| LINACs for nuclear physics research | ~ 0,2 (0,5) | Light & Heavy ions | ~ 1 µA |
| Drivers for radioactive ion beam (RIB) facilities and accelerator driven system | ~ 0,3 – 0,9 | Light & Heavy ions | ~ 0,1 – 30 mA |
| LINACs for radioisotopes production | ~ 0,3 | Protons & Deutrons | ~ 1 – 10 mA |
| Neutron spallation sources | ~ 1 | Protons | ~ 10 – 100 mA |
| Accelerators for material irradiation | ~ 0,3 | Deutrons | ~ 100 mA |
| Compact high-β LINACs | 1 | Electrons | ~ 1 mA |
| Deflecting and crabbing applications | 1 | Electrons & Protons | ~ 1 A |

Increasing field of the usage and applications of non-elliptical cavities increased amount of particle accelerators with different type of low-β structures around the world (Table 2.2.).

Table 2.2. Non-elliptical facilities and projects [11].

| Project | Laboratory | Accelerated beam | Structure |
|---|---|---|---|
| ATLAS | ANL | Heavy ions | Split-ring, QWR (bulk) |
| ALPI | LNL | Protons, deutrons, heavy ions | QWR (bulk and sputtered) |
| ISAC-II | TRIUMF | Heavy ions | QWR (bulk) |
| IUAC | IUAC | Heavy ions | QWR (bulk) |
| ReA3/6 | NSCL | Heavy ions | QWR (bulk) |
| HIE-ISOLDE | CERN | Heavy ions | QWR (sputtered) |
| SARAF | SOREQ | Protons, deutrons | HWR (bulk) |
| SPIRAL-II | GANIL | Protons, deutrons, heavy ions | QWR (bulk) |
| IFMIF | Sacley | Protons, deutrons | HWR (bulk) |
| FRIB | NSCL | Heavy ions | QWR, HWR (bulk) |
| ESS | ESS | Protons | Double Spoke Resonators (bulk) |

| RAON | RISP | Heavy ions | QWR, HWR, Single Spoke Resonators SSR (bulk) |
|---|---|---|---|
| ADS | IMP. IHEP | Protons | HWR, SSR (bulk) |
| PIP-2 | FNAL | Protons | HWR, SSR (bulk) |
| Hi-Lumi | CERN | Protons | Double Quarter Wave Resonators DQWR, Radio Frequency Dipole RFD (bulk) |

One of the major fields of interests in production of the particle acceleration facilities in the last decades is the possibility of substitution bulk niobium accelerating structures onto sputtered cavities. Instant growth of the particle acceleration facilities amount requires development of the cheaper, more reliable and simpler technology of acceleration structures production. From the middle of 1980-s constant development of the QWR cavities production within the sputtering technique is performed.

Currently, there are several acceleration facilities (HIE-ISODE, ALPI), which are built using the sputtered low – velocity structures. History of these facilities development will be described in the next paragraph.

## 2.3. The ISOLDE facility at CERN

## 2.3.1. THE ISOLDE facility

The Isotope mass Separator On-Line facility (ISOLDE) is an on-line isotope separator based in CERN. It was created in 1964 and in 1967 it started delivering radioactive ion beams to the users.

Radioactive nuclei are produced at ISOLDE by impinging the high intensity bunches of the protons (1 – 1.4 GeV) onto thick, heated ISOL targets located at one of two target stations: the General Purpose Separator (GPS) or the High Resolution Separator (HRS) targets. After production, isotopes are filtered by the two magnetic dipole mass separators for the further delivery of the radioactive beam of interest. After separation, the beams are directed to one of several low-energy nuclear physics experiments or an isotope-harvesting area.

The facility was developed for the research activity in the fields of nuclear structure, astrophysics, atomic physics, solid-state physics and fundamental physics.

The last two upgrades of the ISOLDE facility (Figure 2.1) were the upgrade of REX post-accelerator and assembling of the HIE-ISOLDE superconducting LINAC for the re-acceleration of the isotopes to the higher energy.
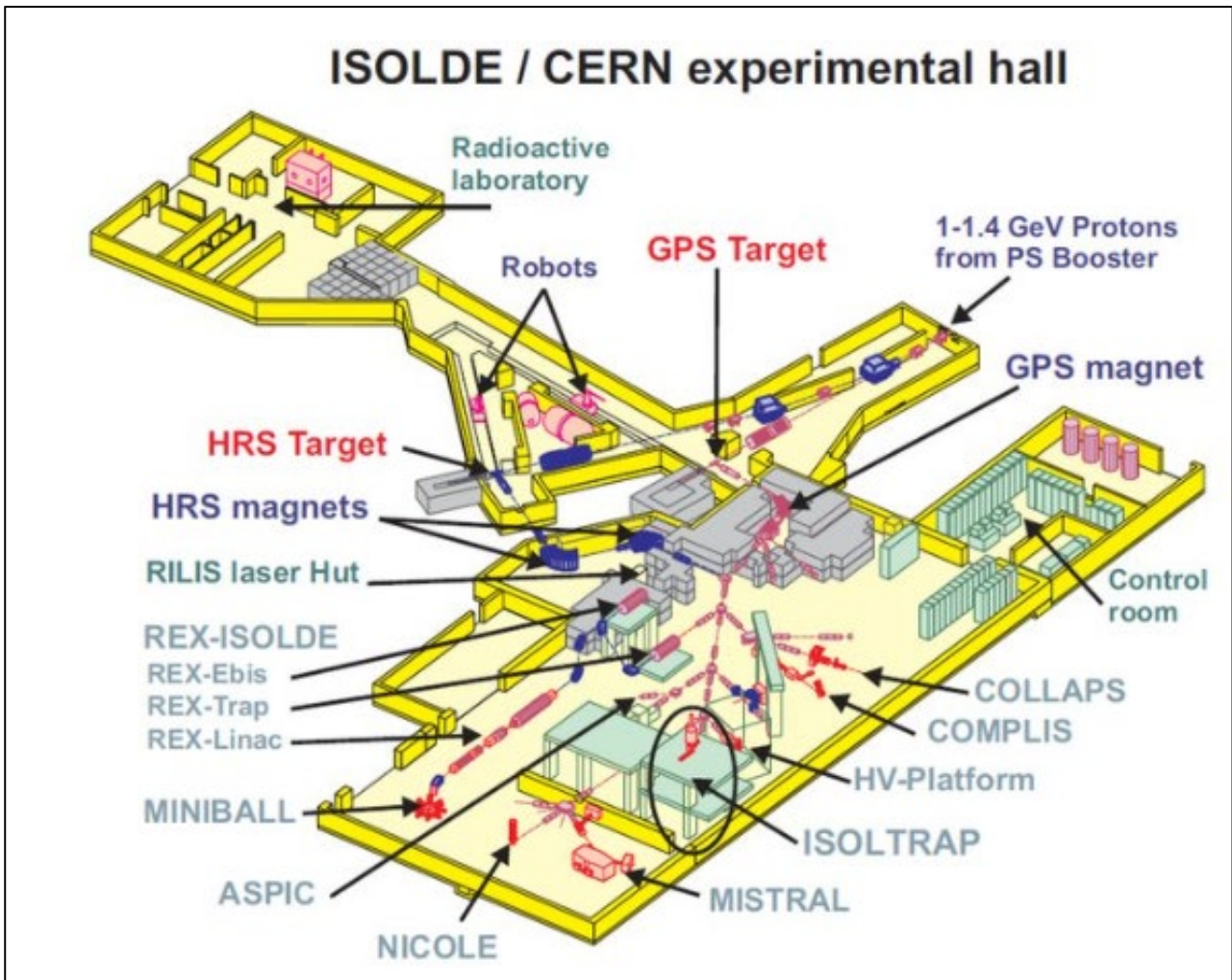
Figure 2.1 – Layout of the ISOLDE facility, including the extension to the experimental hall for the HIE-ISOLDE project.

## 2.3.2. The REX-ISOLDE

The REX LINAC was originally built to accelerate beams with the energy up to 2,2 MeV/u allowing the Coulomb barrier to be reached for isotopes with A < 50. After the upgrade in 2004 the acceleration energy range was increased to 3 MeV/u and extended to reach of the Coulomb barrier to A < 85.

Today REX LINAC (Figure 2.2) consists of the following normal conducting RF structures, operating at the working frequencies 101,28 or 202,56 MHz. Radiofrequency Quadrupole (RFQ) is built to bunch and accelerate beams from the ion source energy from 5 keV/u to 300 keV/u. After RFQ rebuncher is assembled. This is a three-gap slip-ring cavity, which is used to longitudinally match the beam from RFQ into the succeeding IH-structure. 20-gap IS structure is a compact $TE_{11(0)}$-structure, which boosts the beam up to 1,2 MeV/u. 7-gap split-ring resonators provides further acceleration of

the beam up to 2,2 MeV/u. REX LINAC is finished by the 9-gap IH structure with modified drift tube for the acceleration of the beam to the final energy.
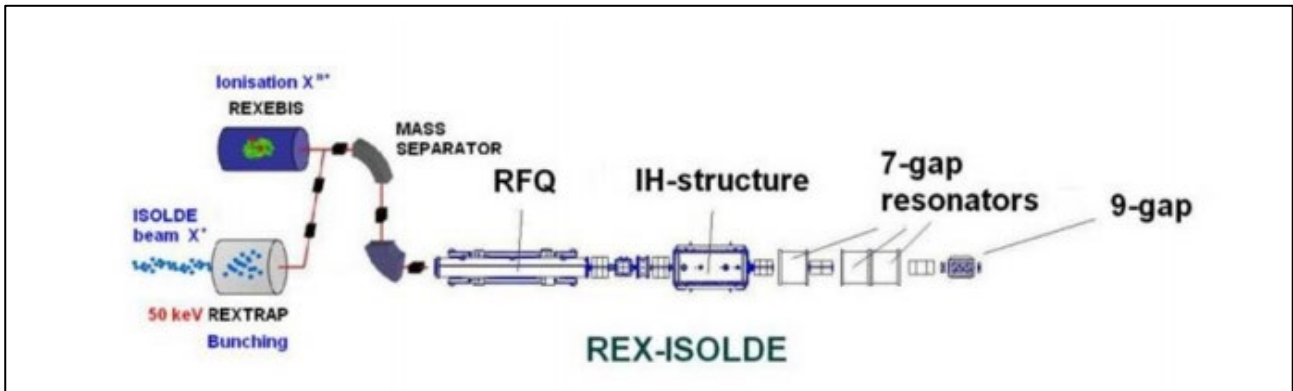


Figure 2.2 – REX LINAC scheme.

## 2.3.3. The HIE-ISOLDE

The HIE-ISOLDE project is based on the major upgrade of the ISOLDE facility for the improvement of the quality and the increase of the intensity and energy of radioactive nuclear beams. The upgrade will replace most of the REX post-accelerator and is based on a compact superconductive LINAC made of the quarter wave resonators and solenoids, housed in six cryomodules.

The energy upgrade comes in the form of a new superconducting linear post-accelerator with 40 MV of the accelerating potential and is divided into the three phases.

The first step is placement of two cryomodules to the REX machine to increase the energy up to 5.5 MeV/u. The second phase is constant adding of the cryomodules up to four items in high-β section to provide the energy of acceleration up to 10 MeV/u. In the end phase all the existing REX accelerator will be replaced with two low-β cryomodules for the improvement of the beam quality and to ensure that the energy is continuous variable between 0,45 – 10 MeV/u.

The design energy of 10 MeV/u was achieved by the implementation of 32 QWR cavities (12 low-β and 20 high-β QWRs). Two different technologies were considered for the production of HIE-ISOLDE QWRs: bulk niobium and niobium coatings sputtered onto the copper substrate. The superconductive LINAC has been designed to achieve the accelerating voltage of 39.6 MV to gain the final energy of 10 MeV/u and a relation A/q to 4.5. The target acceleration field of the HIE-ISOLDE QWRs was chosen 6 MV/m with the working power 7 W for low-β cavities and 10 W for the high-β cavities [12].

## 2.4. The ALPI project at LNL INFN

### 2.4.1. The ALPI project history

The conceptual design of the ALPI project like a superconductive (LINAC) booster for the XTU Tandem in the Legnaro National Laboratories was accepted in 1987. The main aim of the project was to be capable of acceleration all the stable isotopes up to Uranium at energy above the Coulumb barrier. Straight line QWRs were chosen as an accelerating structure for the ALPI project. Their intrinsic mechanical stability and broad velocity acceptance let the ALPI LINAC to operate with different types of the beams. Lead was chosen as superconductor for the first QWRs of the ALPI accelerator due to the relatively easy machining in respect to niobium and positive experience in working with lead (it was used before in SUNYLAC) [13].

The ALPI project was initiated in 1989 after several years of the preliminary research and development activity. The machine was able to host 93 QWRs, but previous research activity onto bulk niobium and niobium sputtered cavities reduced the number of the cavities, needed to reached goal performance of the LINAC, to 74. The shape of the cavities was changed with the target material. Internal cell of the cavity was ending with hemisphere instead of the straight angles. This geometry upgrade reduced peak surface electrical field and simplified the construction of the bulk niobium cavities.

In March 1994 forty-four Pb on Cu accelerating cavities were installed to the ALPI cryostats. Performance of these resonators was limited at 3 MV/m and big part of them were installed in the beam directly, without testing in laboratory. In June 1995, the first cryostat with four sputtered niobium cavities was installed in the machine. They showed good performance (energy of acceleration field was until 7MV/m at 7W) and for the future was decided to replace lead superconductive QWRs onto the niobium sputtered cavities. In the same period new injector PIAVE was installed. This modification made acceleration of the heavy nuclei feasible, increased the beam intensity onto the target on the factor of 10 and extended the use of the ALPI for rare and costly isotopes [14].

In 1998 the first cryostat with 4 low-β resonators was installed after maintenance in the beam line. They showed good performance in superconductive state and were first cryostats with the bulk niobium cavities in the ALPI accelerator. In 1998 also first cryostat with four niobium sputtered cavities was installed in the high-β branch. After success with niobium sputtered high-β cavities was decided to develop technology of the medium-β QWRs Nb sputtering for further exchanging lead cavities onto the niobium sputtered ones [15].

In the period 1999 – 2003 all the Pb on Cu resonators from the medium-β section were replaced onto niobium sputtered cavities. Also, the second cryostat with 4 niobium sputtered cavities was installed in the high-β section. This update increased the ALPI performance from the average acceleration field value of 2,4 MV/m until 4,5 MV/m for the medium-β branch [16].

Dynamical change of the number and type of cavities in the period from start of operation in ALPI in 1995 until final start of the PIAVE working in 2005 is shown on figure 2.3.
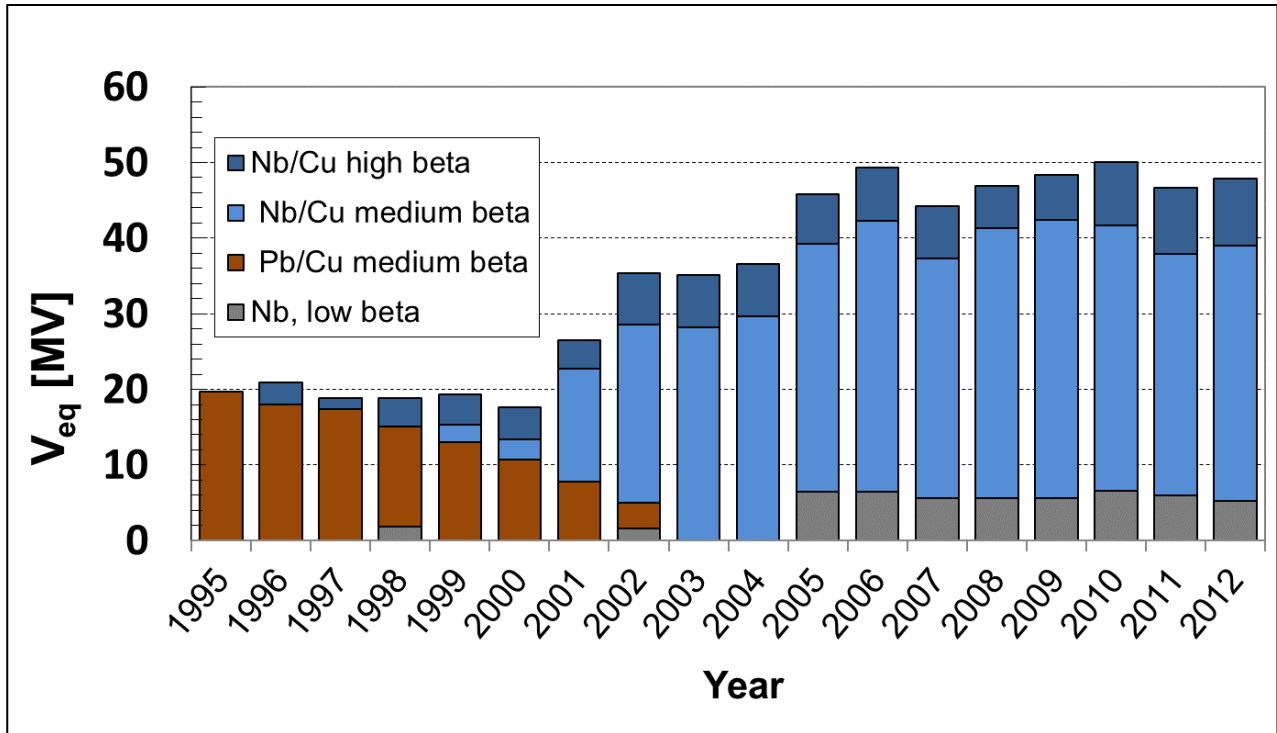


Figure 2.3 – Number and type of the cavities operating in the ALPI between 1995 and 2012 [17].

After 2006 no modification was implemented. In the framework of R&D analysis several medium-β and QWR Cu substrates were machined and sputtered. Produced cavities showed high performance with the average energy of acceleration field 5.5 MV/m [18].

## 2.4.2. The ALPI upgrade for the SPES Facility

"SPES" is an acronym for "Selective Production of Exotic Species". Main goal of the SPES project is providing high-intensity and high-quality beams of the neutron rich nuclei for the further research in nuclear structure, reacting dynamics and interdisciplinary fields (medical, biological and material sciences) [19]. SPES facility is shown on figure 2.4.
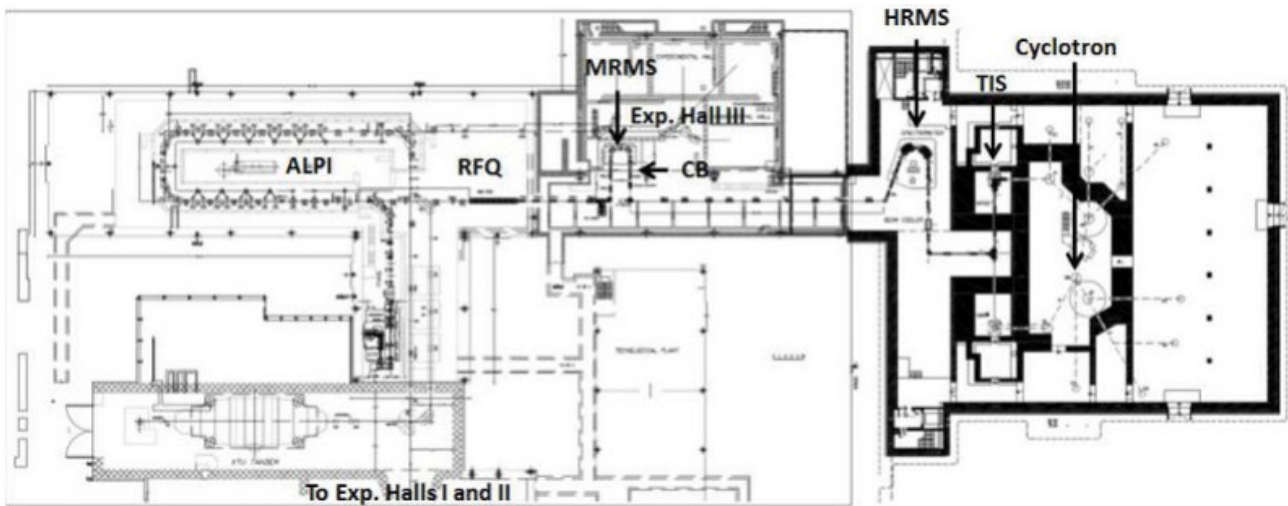
Figure 2.4 – Layout of the SPES facility.

The SPES accelerator starts with the proton cyclotron, producing exotic species via nuclear fission. Target is connected to the ion source system (TIS) (surface (SIS), plasma (PIS) or laser (LIS) ionisation source), from which the desired beam is extracted, containing target particle and contaminations. The beam is transported through Wien filter and the high-resolution mass separator (HMRS) for the contaminations removing. The purified beam is transported through an electrostatic focusing line and delivered an ECR type charge breeder (CB). A CB is the last preparation step of the target beam before the ALPI accelerator. In superconductive ALPI LINAC radioactive ion beam (RIB) is accelerated to the final energy of 10 MeV/A. The next step is transporting of the RIB species of interest into three branches of the experimental hole for further R&D activity [6].

The present configuration of the Legnaro super-conducting acceleration complex (PIAVE Injector and ALPI accelerator) feats the requirements for the SPES facility. Nevertheless, an upgrade of its performances in the overall transmission and the final energy is needed for the proper maintenance of the SPES project.

There are several possible scenarios for increasing of the final energy and transmittance of the ALPI accelerator. For the low-β section upgrade it is possible to assemble 2 cryostats, recovered from the PIAVE, in the start of low-β branch. In this case accelerating efficiency would be favourable for the heaviest ions. From the other side, lightest ones would suffer from the excess of the low-β cavities. However, this upgrade let transporting the beam efficiently, even if some of the low-β cavities were out of order.

For the high-β section upgrade it is possible to place two cryostats in the end of high-β section. In this case, the number of QWRs would be more effectively divided among three different β brunches and the final energy for the lightest ions will increase [7]. On figure 2.5. is shown the proposal of the ALPI LINAC upgrade.
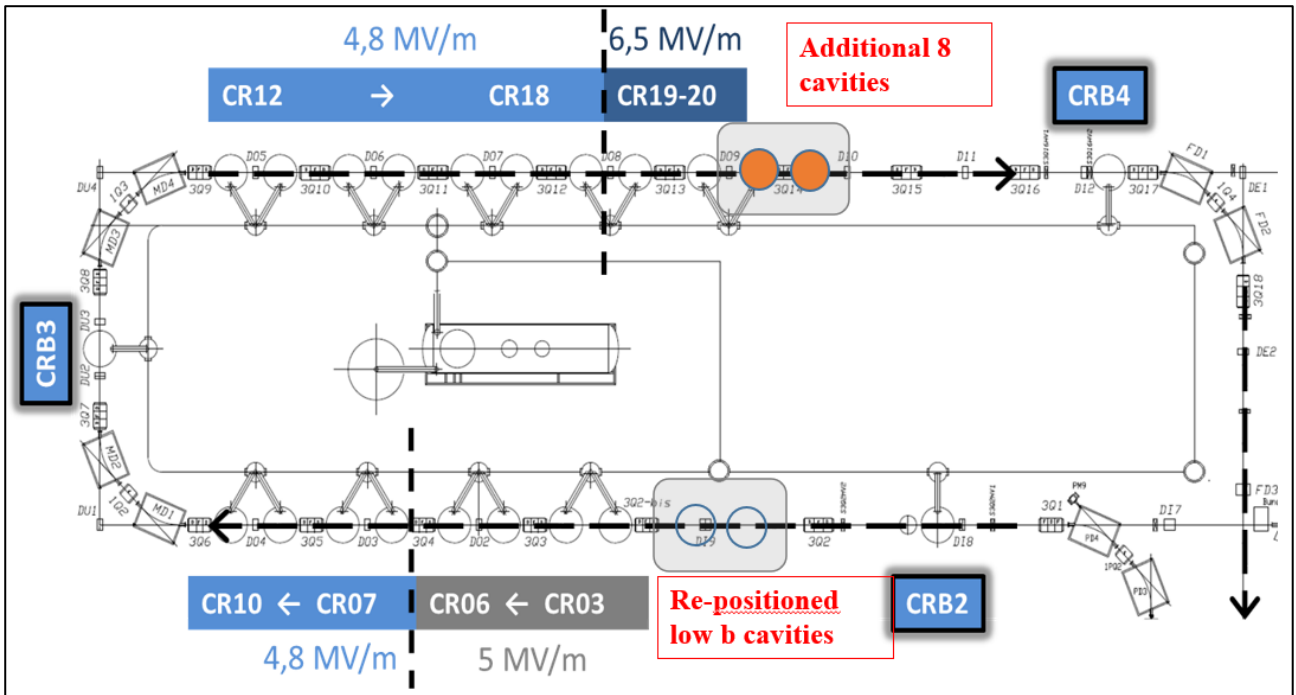


Figure 2.5 – Layout of the ALPI upgrade for the SPES facility.

Research activity of this work is based on the proposed high-β section upgrade of the ALPI LINAC for the SPES facility. The development of the high-β ALPI QWR production technology is the main goal of this work for further production and assembling of the 8 Nb/Cu QWR cavities and plates in the high-β branch of the ALPI LINAC.

# Chapter 3

# FUNDUMENTALS OF SUPERCONDUCTIVITY

## 3.1. Theory of superconductivity

Superconductivity phenomena was discovered in 1911 in the Leiden University in Netherlands. The scientist Kamerling Onnes, with defining the dependence of electrical resistance of Hg from the temperature, discovered, that at 4,2 K resistance of the sampled dropped to zero and did not rise in all the range of the temperatures below 4,2 K. It is important to mention, that decreasing of the resistance was not slightly constant, as in the case of normal conductivity, but it was sudden jump at the specific temperature. This phenomenon was called "superconductivity" (Figure 3.1).
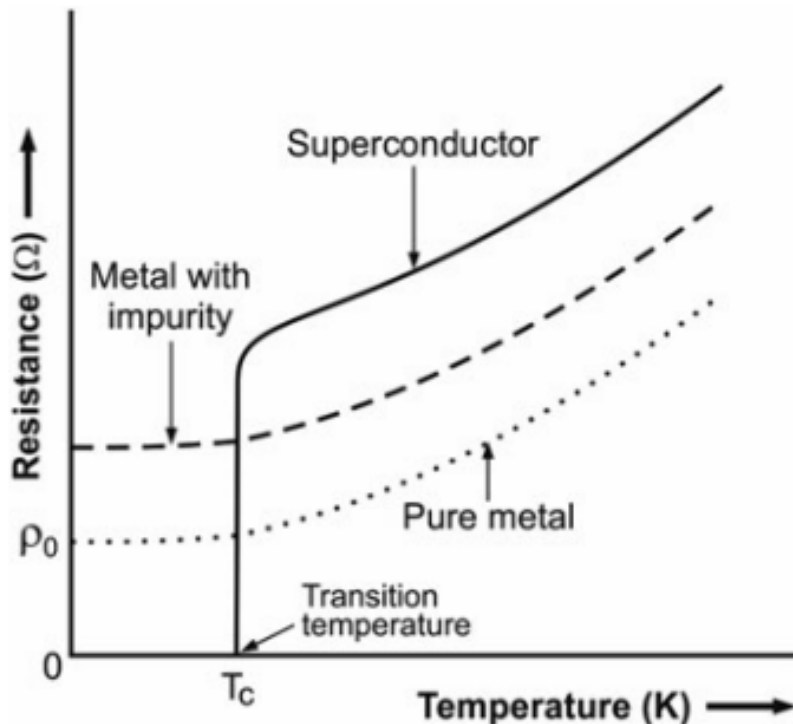


Figure 3.1 – Resistance as function of the temperature in case of normal conductors and superconductors [20].

After discovering of the superconducting properties of mercury, it was found out, that other pure materials (such as indium, lead, aluminium, niobium etc.) and alloys ($Nb_3Sn$, $YBa_2Cu_3O_7$) etc. have superconductive properties. The temperature, at which occurs transition from normal to superconductive state is called *critical* and signed like $T_c$. The highest critical temperature between

pure elements was defined for niobium (9,25±0.02 K) and the lowest temperature of the transition –
for tungsten (0.0154±0.0005 K).

Few years later after the superconductivity discovery, in 1914 was find out, that superconductive state
can be destroyed not only by increasing the temperature of the sample, but also by placing the sample
in certain magnetic field. This magnetic field was called *critical* and signed as $H_c$. Dependence of
critical magnetic field from the temperature is good characterised by the empirical formula (3.1.)
[21]:

$$H_C(T) = H_C(0)\left[1 - \left(T/T_C\right)^2\right]$$
(3.1)

## 3.2. Meissner effect

For 22 years from discovery the superconductivity phenomenon superconductor was considered as
ideal conductor, metal with zero resistivity. At the material temperature, lower than critical (T<$T_c$),
implemented magnetic field do not penetrate in the ideal conductor. By the influence of the magnetic
field, on the surface of the ideal conductor by the Lenz law occurs current, which produces its own
magnetic field and total field in the ideal conductor will be equal to zero. So, ideal conductor in the
external magnetic field has B = 0 in any point of its surface. If the ideal conductor is firstly placed in
the magnetic field at the temperature T>$T_c$ and after cooling down under the critical temperature,
magnetic field penetrates inside at ideal conductive state. The sample has resistance at the high
temperature and magnetic field penetrates inside. During the cooling down of the ideal conductor
under critical temperature, magnetic field remains in the sample.

In 1933, scientists Meissner and Ochsenfeld discovered, that superconductors have different
behaviour. It was observed that metals in the superconductive state have B=0 with external magnetic
field, not depending on the way of transition under the critical temperature. From showing weak
paramagnetic characteristics at the T>$T_c$, superconductor material changes its magnetic behaviour
during transition trough the critical temperature, showing perfect diamagnetism in T<$T_c$. This
discover was shown as one of the main characteristics of the superconductors and was called Meissner
effect. Comparison of the magnetic behaviour in the ideal conductor and superconductor is shown on
figure 3.2.
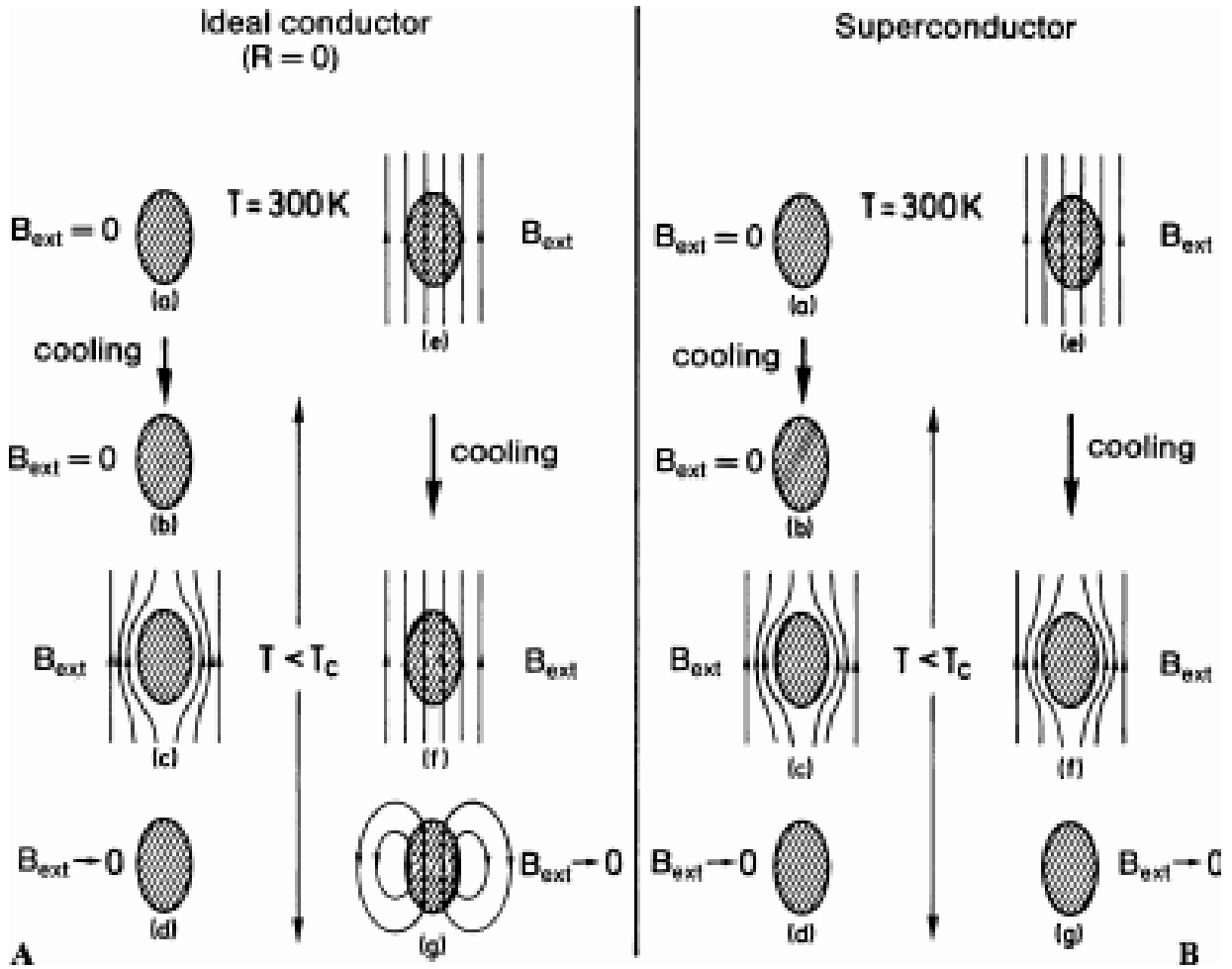
Figure 3.2 – Magnetic behaviour of the ideal conductor – A and superconductor – B [22].

## 3.3. Magnetic properties of superconductors

Superconductors can be divided onto I and II type by the penetration manner of the magnetic flux inside the sample in the superconductive state.

All the elements with superconductive properties, except niobium, refer to the I type of superconductors. The I type superconductors are characterised by the perfect diamagnetism in superconductive state (Meissner effect). There is no magnetic flux penetration in the sample below a critical field $H_0$, that increases, when temperature of the sample falls down below $T_c$. The curve of magnetisation of the I type superconductor $B = B(H_0)$ is shown on figure 3.3a. Superconductivity will be destroyed when the $H_0$ will be equal to the $H_c$, and the field will penetrate in the superconductor, B will be equal to $H_0$.

The magnetic induction and the field $H_0$ are connected with the equation 3.2:

17

$$B = H_0 + 4\pi M \tag{3.2}$$

Where M is magnetization. Dependence of the magnetisation from the magnetic field for the I type superconductors is shown on figure 3.3b.



(a)                                    (b)
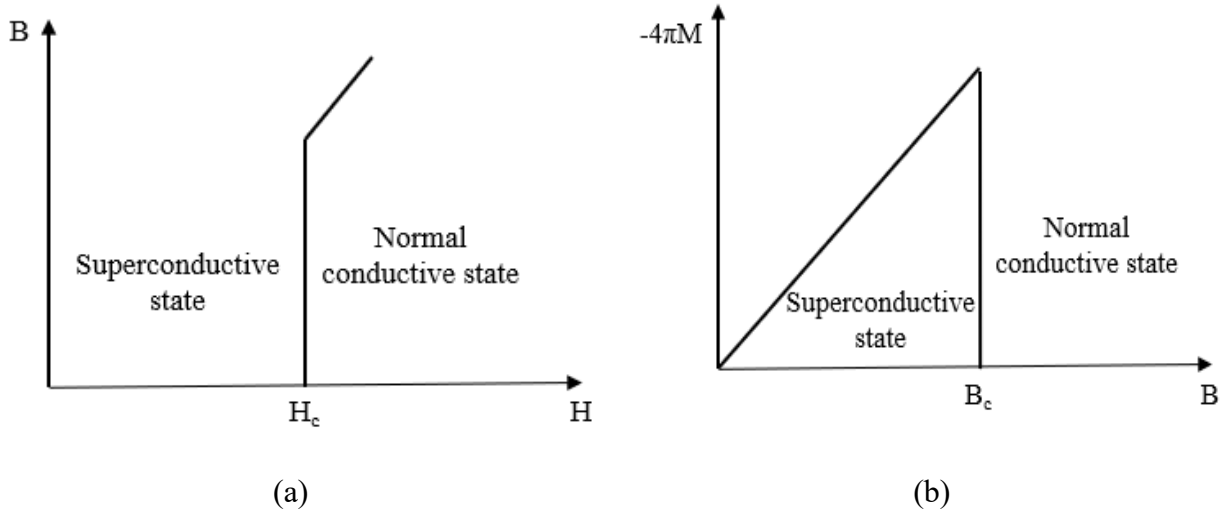
Figure 3.3 – Magnetisation field (a) and magnetisation curve (b) dependences for the I type superconductors.

Niobium, superconductive alloys, and chemical compounds refer to the II type of superconductors. The second type superconductor has two critical magnetic field, which complicates the behaviour of these materials during the magnetic flux penetration. There is no penetration of the flux below a lower critical field $H_{c1}$ *(T)*. Superconductive material transmits into normal state hen the field exceed on upper critical field $H_{c2}$ *(T)*, and the field penetrates perfectly. When the applied magnetic field is between the lower and the upper magnetic field, the flux partially penetrates, and the superconductive material changes its microscopic structure, compiling both normal and superconductive regions, known as mixed state (Figure 3.4).

A.A. Abricosov proposed experimentally confirmed mechanism of the magnetic flux penetration in the superconductors in the mixed state. Magnetic field penetrates partially in the form of thin normal conductive filaments, surrounded by superconductive regions, called vortexes [23].
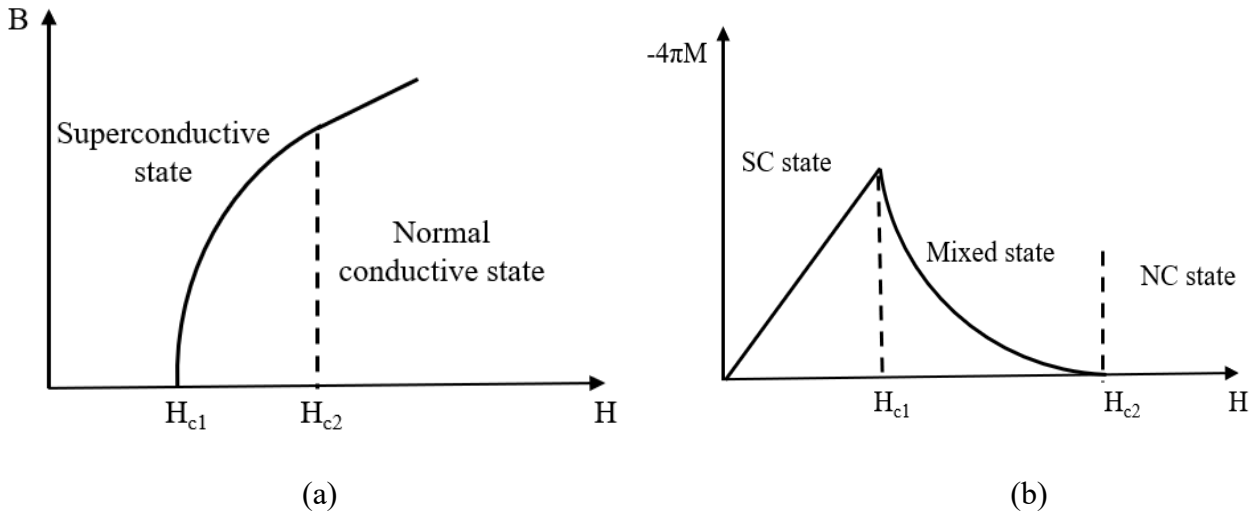
Figure 3.4 – Magnetisation field (a) and magnetisation curve (b) dependence for II type superconductors.

## 3.4. Coherent length

In 1957 scientists Bardeen, Cooper and Schrieffer developed the microscopic theory of superconductivity [24], which is called the BCS theory. It was clear, that superconductivity is new state of electron gas in metals, which displace the unusual property of "infinite high" conductivity. Cooper in 1956 defined, that the ground state of an electron gas (T = 0 K) is unstable if weak attractive interaction between each pair of electrons is added. According to the BCS theory, the electron, which passes through the solid, leaves behind a deformation trail affecting the position of the ions cores. This trail causes an increase of the positive charge density due to the ion cores and has an attractive effect onto the second electron. The lattice deformation causes weak attraction between the pairs of electrons, which called Cooper pairs [22]. The bound state of these two electrons is favourable. The two electrons in the pair have opposite spin and the orbit part of the wave function is symmetric. The coherent length is the length, at which two electrons are correlated and it can be calculated with equation:

$$\xi_0 = \frac{\hbar V_f}{\Delta} \tag{3.3}$$

Where $V_f$ is the Fermi velocity, which characterise the speed of electrons close to the Fermi energy and $2 \cdot \Delta$ is the energy, which is necessary to break the Cooper pair. For the niobium, the coherent length is around 39 nm.

## 3.5. London penetration depth

F. London and H. London made first examination of the magnetic field penetration inside the superconductor interior. Two-fluid model of Gorter and Casimir was settled in the base of their analyses. It was confirmed that magnetic field penetrates in the superconductor on the certain layer by the law:

$$H = H_0 e^{-\frac{x}{\lambda_L}} \tag{3.4}$$

Where $e$ is the charge of the electron and $x$ is the superconductive space. As the result for this equation, characteristic length, at which penetrates magnetic field in the superconductor (London penetration depth) is evaluated by the formula 3.4:

$$\lambda_L = \sqrt{\frac{m}{\mu_0 n_s q^2}} \tag{3.5}$$

Where $m$ is the carriers mass, $q$ is the carriers charge and $n_s$ is density of the superconductive electrons. For the niobium typical value of the London penetration depth is around 32 nm.

In the Gorter and Casimir model all the free electrons of the superconductors are divided onto superconductive with the density $n_s$ and normal conductive with density $n_n$. So, total density of the electrons in the superconductor will define, as:

$$n = n_s + n_n \tag{3.6}$$

Gorter and Casimir suggested that the density of superconductive electrons decrease form $n$ to 0 with increasing of the temperature from 0 to $T_c$ . Dependence of the superconductive electrons number from the temperature of material is described by the formula:

$$n_s(T) = n_s(0) \cdot \left(1 - \left(\frac{T}{T_c}\right)^4\right) \tag{3.7}$$

From the equation (3.4), London penetration depth is dependent from the density of the superconductive electrons, which means, that $\lambda_L$ is dependent from the temperature. After combining equations (3.4) and (3.6), the London penetration depth become:

$$\lambda_L(T) = \lambda_0 \left(1 - \left(\frac{T}{T_c}\right)^4\right)^{-\frac{1}{2}} \tag{3.8}$$

## 3.6. Ginsburg Landau theory

Londons theory did not consider quantum effects of the superconductivity. The Ginsburg Landau theory had become first quantum phenomenological theory of superconductivity. The scientists asserted, that the superconductive state is more ordered, then the normal state, and transition from one to another is phase transition of the second stage (Landau phase transition theory). Ginsburg and Landau characterised superconductive state by a complex "order parameter" $\psi(r)$, which vanishes at the temperature, above $T_c$ and measures the degree of order of superconductivity at position $r$ below $T_c$. From the BCS theory, order function parameter can be described as one-electron function, describing the position of mass centre of the Cooper pair. This function parameter appliable to all the Cooper pairs, since all pairs are in the two-electron state. From the Ginsburg Landau theory, coherent length characterises the distance, at which change of the order of the $\psi$ parameter occurs.

From the Ginsburg Landau theory parameter of characterisation of superconductors by London penetration depth and coherent length is defined:

$$k = \frac{\lambda_L}{\xi_0} \tag{3.9}$$

$k$ is the Ginsburg-Landau parameter, which allows to identify the type of the superconductor:

- $k < \frac{1}{\sqrt{2}}$ means $\lambda_L \ll \xi_0$ , the order function parameter changes slightly in the small part of the coherent length distance, which is typical for the I type of superconductors;
- $k > \frac{1}{\sqrt{2}}$ means $\lambda_L \gg \xi_0$ , which led to the change order function in the distance, smaller than London penetration depth, which is typical for the II type of superconductors.

For niobium $k \approx 1$, and it is a weak II type superconductor.

Pippard in 1950 had published a work [25] about role of the impurities in the superconductor. The study was based on the evidence, that London penetration depth is dependent by the mean free path of the electrons in the superconductive material. This dependence can be described by the equation:

$$\frac{1}{\xi} = \frac{1}{\xi_0} + \frac{1}{\ell} \tag{3.10}$$

Pippard introduced the effective penetration depth:

$$\lambda_{eff} = \lambda_l \cdot \left(\frac{\xi_0}{\xi}\right)^{\frac{1}{2}} \tag{3.11}$$

where $\xi_0$ is the characteristic coherent length of the superconductor. This relation postulate, that the superconducting penetration depth increases with a reduction of a mean free path [26]. For pure superconductor ($\ell \to \infty$) one has $\xi = \xi_0$. In the limit of very impure superconductor, where $\ell \ll \xi_0$, the relation becomes $\xi = \ell$.

The mean free path in the niobium is dependent by interstitial impurities like oxygen, nitrogen, and carbon.

## 3.7 Surface resistance in superconductors at RF current

The remarkable properties of superconductivity are connected with the condensation of charge carriers in Cooper pairs. At *0 K* all charge carriers are condensed and with increasing of the temperature, charge carriers start to be unpaired, which quantity increases exponentially with grows of the temperature until $T_c$. With placing the superconductor in DC field, the Cooper pairs start to carry all the current, shielding the applied field from the normal electrons.

In case of RF fields, superconductors do not have zero resistance at *T* > 0K, although it is very small compared to the normal metals. While the Cooper pairs moves without friction, they do have inertia. The Cooper pairs do not screen electric field perfectly because of inertia. The time-varying electric field couples to the normal electrons to accelerate and decelerate them, which leads to dissipation of the power. With the normal conductive electrons starts creation of the normal conductivity in superconductors with the dissipation of power. The dissipation power can be expressed in terms of a surface resistance:

$$P_{diss} = \frac{1}{2} R_S H^2 \tag{3.12}$$

Since the number of normal electrons decreases exponentially, surface resistance can be defined as:

$$R_S = A\varpi^2 exp\left(-\Delta(0)\big/k_B T\right) \tag{3.13}$$

Where *A* is constant, dependent on the material parameters of superconductor (the penetration depth $\lambda_L(0)$; the coherent length $\xi_0$, the Fermi velocity $V_f$, the mean free path, $l$). $2\Delta$ is the energy gap of the superconductor, energy, that is needed to break the pairing.

At $T_c$ none of the electrons are paired. The quantity of the normal electrons under $T_c$ is proportional to the Bolzman factor ($exp\left(-\frac{\Delta}{k_B T}\right)$). This relation is valid for *T* < $T_c$/2 when $\Delta$(T) reached asymptotic value $\Delta$(0). The equation (3.13) describes two main properties of the superconductive state surface resistance:

22

1. $R_s$ increases with the square of the RF frequency;
2. $R_s$ decreases exponentially with temperature [27].

The detailed expression, based on the BCS theory, of the surface resistance in the limits $T < T_c/2$ and $\varpi < \Delta/\hbar$ is given [26]:

$$R_{BCS} \approx \frac{\mu_0^2 \varpi^2 \lambda^3 \sigma_1 \Delta}{k_B T} \ln \left( \frac{2.246 k_B T}{\hbar \omega} \right) exp \left( -\frac{\Delta}{k_B T} \right) \qquad (3.14)$$

## 3.8. The residual resistance

By the calculations, based on the BCS theory, was predicted existence of the minimum level of $R_{BCS}$. Surface resistance was defined independent from the temperature, saturated at low sample temperature, after experimental evaluation of the surface resistance behaviour with the superconductor temperature change (Figure 3.5).
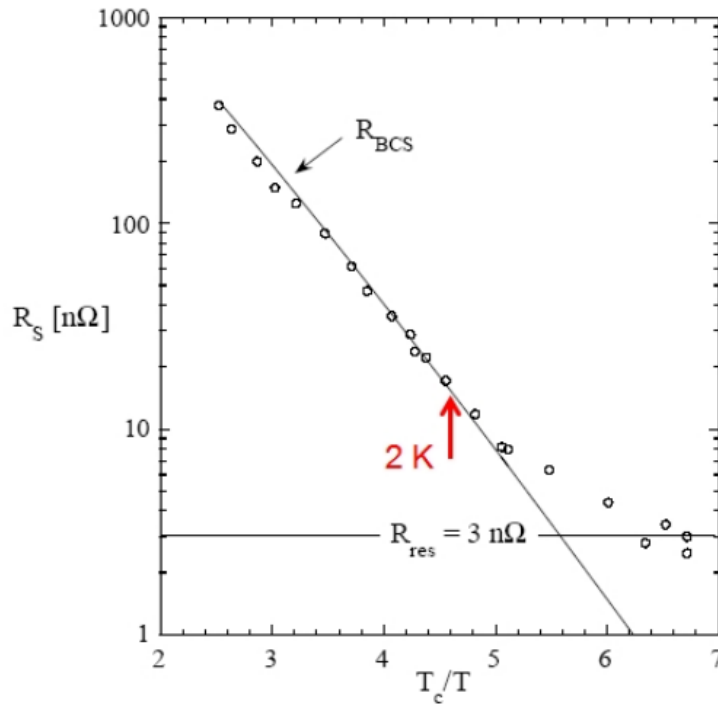


Figure 3.5 – The temperature dependence of the low-field surface resistance of the bulk niobium at 1.3 GHz with saturations to a T-independent value at low temperatures.

The curve of the surface resistance dependence starts to show clear deviation from the predicted exponential dependence with decrease of the temperature towards 0, at the sample temperature, lower

than 2 K, [28]. This T-independent contribution of the surface resistance is called residual resistance [26]:

$$R_s = R_{BCS} + R_{Res} \qquad (3.15)$$

Appearance of the temperature independent part of the surface resistance can be explained by the trapped DC magnetic field due to incomplete Meissner effect in the superconductor sample.

Mainly residual resistance is caused by the imperfections in the superconductive material crystallite structure. There are many cases of the residual losses in the literature, but the mechanism is still not clear. The list of the main reasons of the residual losses is mentioned below:

- Non-ideal surface quality;
- Oxide layer, presented on the superconducting surface;
- Electromagnetic generation of acoustic phonons;
- Trapping of the magnetic flux;
- Superconductor polycrystallinity;
- Hydrogen segregation [29].

It is possible to reach $10 - 20$ n$\Omega$ of residual losses in this material after appropriate preparation of the bulk niobium sample, [27].

From the practical point of view, evaluation of the produced superconducting cavity residual resistance is possible by definition its superconductive performance at the temperature below 2 K.

# Chapter 4

# SUPERCONDUCTIVE RESONANT CAVITIES

## 4.1. Introduction

The main component of the particle accelerators is the detail, which imply the energy to the charged particle for acceleration. This detail is called electromagnetic resonant cavity [27].

A resonant cavity is an energy storage device, which is used for the radiofrequency and microwave range. From electrical point of view, resonant cavities are equivalent for the standard RLC resonant circuit, which operates at frequency $\omega_0 = 1/\sqrt{LC}$. The inductance of the circuit should be done for increasing the resonating frequency of the circuit decreasing. The minimum possible inductance can be achieved in the case of single wire. Next step of increasing the resonant frequency is placing in parallel many single turns inductances until enclosing two capacitor plates by the metallic sheet, that short circuit the capacitor. Resulted structure is so-called "pill-box" resonant cavity [28].

Basically, the resonant cavity is any volume enclosed by metallic walls, that contains oscillating electromagnetic fields. The electromagnetic energy, that is stored in the cavity, is applied to the charged particle beam for the acceleration. The range of the resonant frequencies of the applied accelerating cavities is 3 kHz – 300 GHz.

The electromagnetic field inside the accelerating cavity is the solution for the wave equation:

$$\left(\nabla^2 - \frac{1}{c^2}\frac{\partial^2}{\partial t^2}\right)\begin{Bmatrix} E \\ H \end{Bmatrix} = 0 \tag{4.1}$$

With the boundary conditions $\hat{n} \times E = 0$ and $\hat{n} \times H = 0$, where $\hat{n}$ is the unit vector, normal to the surface. Due to the solution of the equation (4.1), resonator modes with the specified boundary conditions can be divided into three groups, based onto the direction of the electric and magnetic fields:

- TE$_{mnp}$ modes with transverse electric field;
- TM$_{mnp}$ modes with transverse magnetic field (and longitudinal component of the electric field);
- TEM modes is significant for the spoke cavities due to complicate geometry of the acceleration structure.

Where parameters $m$, $n$, $p$ are the directions indices in the cylindrical coordinates.

Schematic model of the electromagnetic fields, stored within the "pilled-box" (TM$_{010}$) accelerating cavity is showed on figure 4.1.
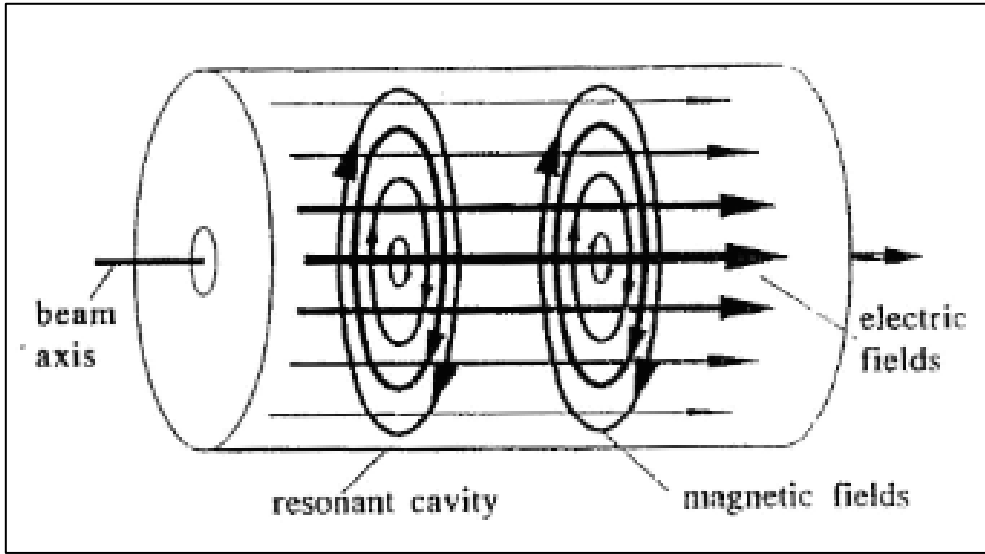


Figure 4.1 – Electric and magnetic fields for a TM$_{010}$ made inside the pilled-box cavity [29].

## 4.2. Cavity fundamentals

The charged particle obtains some acceleration energy during the travel through the RF cavity. Assuming the electron moving with the speed of light, it is possible to postulate, that particle enters on the cavity beam axis in time $t = 0$ and leaves at the time $t = d/c = T_{cav}$, where $d$ – is conducting face of the cavity. Charged particle sees the time-varying electro-magnetic field during the transition. Time of the transit through the cavity and obtaining the acceleration energy is:

$$T_{cav} = \frac{d}{c} = \frac{\pi}{\omega_0} \tag{4.2}$$

Where $\omega_0$ is the angular frequency of the acceleration mode.

The acceleration voltage of the cavity can be defined by the following equation:

$$V_c = \left| \frac{1}{e} \times maximum\ energy\ gain\ possible\ during\ trasit \right| \tag{4.3}$$

The acceleration voltage is given by the line integral of energy, seen by the electron $E_z$:

$$V_c = \left| \int_0^d E_z(p = 0, z) e^{i\omega_0 z/c} dz \right| \tag{4.4}$$

The average energy of the acceleration field, that electron always sees during the transfer, is given by the equation:

26

$$E_{acc} = \frac{V_c}{d} \qquad (4.5)$$

There are main parameters, which characterise the acceleration RF cavities superconductive performance, which are the stored energy ($U$), the surface resistance ($R_s$), the dissipated power ($P_d$), the geometry factor ($G$) and the quality factor ($Q_0$), the peak surface electric field ($E_{pk}$) and the peak surface magnetic field ($H_{pk}$).

Some part of energy is dissipated in the walls of the RF structure due to non-zero resistance of the cavity walls during the storage of the energy inside the cavity. This loses of the energy can be characterised by the surface resistance, which is defined by the power dissipation via the area unit ($dP_d/ds$) due to the Joule heating:

$$\frac{dP_d}{ds} = \frac{1}{2}R_S|H|^2 \qquad (4.6)$$

Where $H$ is the local magnetic field.

The dissipation power can be defined by an integration, taken over interior cavity surface:

$$P_d = \frac{1}{2}R_s \int_S |H|^2 ds \qquad (4.7)$$

An important parameter, which is characterised by the stored energy and the power dissipation of the cavity, is quality factor:

$$Q_0 = \frac{\omega_0 U}{P_d} \qquad (4.8)$$

The time average energy in the electric field is equal to the energy in the magnetic field. The total energy can be defined by an integration over the volume of the cavity:

$$U = \frac{1}{2}\mu_0 \int_V |H|^2 dV \qquad (4.9)$$

Taking in consideration equations (4.7) and (4.9), the quality factor can be defined as:

$$Q_0 = \frac{\omega_0 \mu_0 \int_V |H|^2 dV}{R_s \int_S |H|^2 ds} = \frac{G}{R_s} \qquad (4.10)$$

Where

$$G = \frac{\omega_0 \mu_0 \int_V |H|^2 dV}{\int_S |H|^2 ds} \qquad (4.11)$$

$G$ – is the geometry factor of the cavity. It is defined by the geometry of the cavity.

One of the important criteria of the RF cavity is how big acceleration energy can be applied to the charged particle. The main limitation of this parameter are the peak surface electric field ($E_{pk}$) and the peak surface magnetic field ($H_{pk}$). The peak surface magnetic field cannot exceed critical magnetic field of the superconductor due to the transition of the material into the normal conducting state and the quench of the superconductor. The high peak surface electric field can cause field emission in the high electric field region. It is important to minimise the ratio between the peak fields and the acceleration field for maximization of the acceleration field [26].

## 4.3. Overview of the superconductive structures

There are three main types of the acceleration structures: high – β, medium – β and low – β, where β = v/c (v is speed of acceleration particle and c is speed of light) [30]. Classification of the acceleration structures by the β coefficient is shown on figure 4.2.
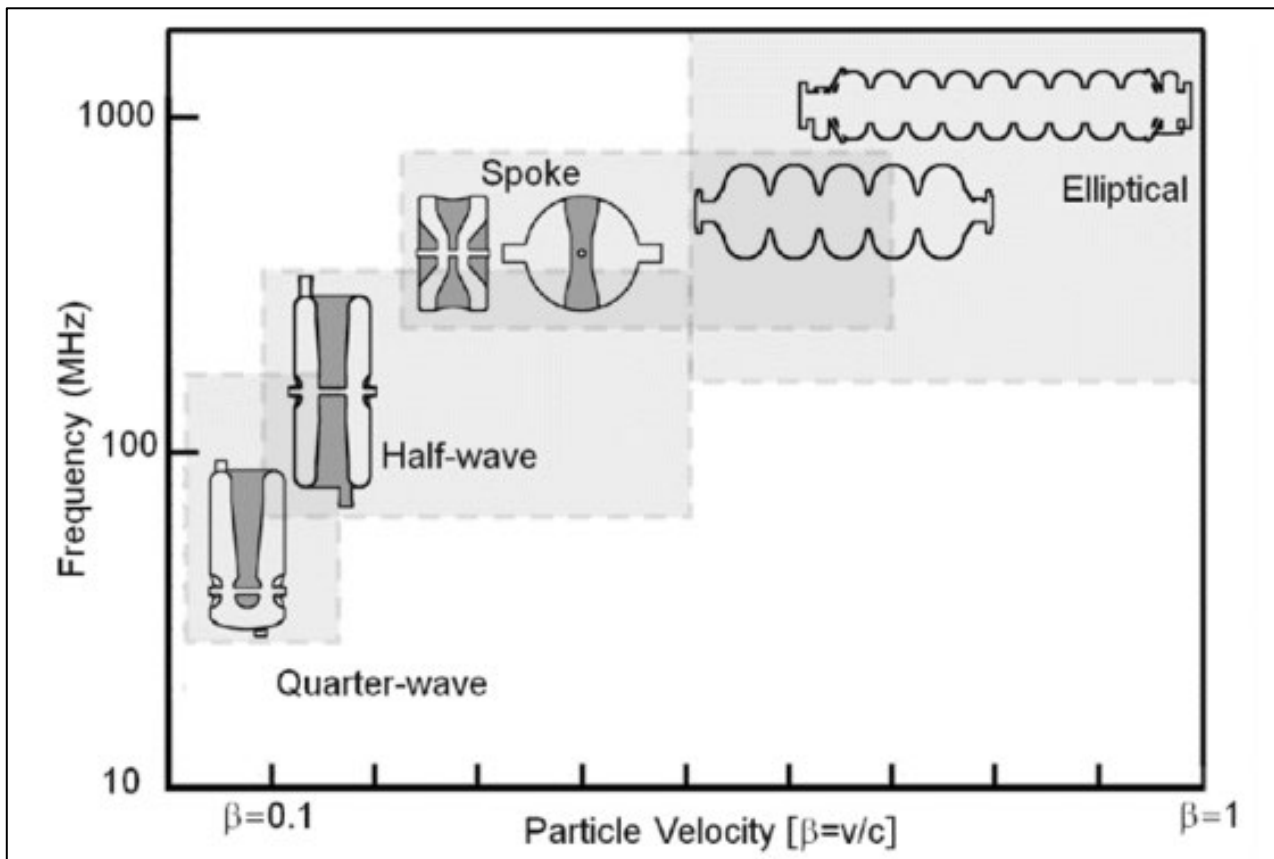


Figure 4.2 – Classification of the acceleration structures.

The high – β structures, based on TM$_{010}$ resonant cavities, are used for the acceleration of electrons, positrons, or high-energy protons with β ~ 1. A typical high – β acceleration cavity consists of a chain

of coupled cells with the cavity gap length $\beta\lambda/2$, where $\lambda$ is the wavelength corresponding to the frequency choice of the accelerating structure.

The medium – β structures are used for acceleration of protons with the energies, less than 1 GeV as well as for ions. At the higher $\beta$ range, there are "foreshortened" speed-of-light structures with the longitudinal dimensions, scaled by the β factor. The spoke resonators with single or multigap are mostly used near region $\beta = 0,5$. Elliptical shaped cells for $\beta < 0,5$ become mechanically unstable as the accelerating gap shortens and cavity walls become nearly vertical. The necessity working in low RD frequency, favoured for ion and proton applications, makes the elliptical cells very large, producing a constructure problems and structural weakness.

The low – β structures are used for acceleration of heavy ions with $\beta = 0,01 – 0,2$. The acceleration gap is proportional to $\beta\lambda/2$, so the low frequency is necessary to provide a significant acceleration length. There is a big amount of low – β structures, which depend onto the resonant transmission line either quarter-wavelength, or half-wavelength. The medium – β spoke resonators and low – β structures operate in TEM-like mode [30].

## 4.4. Quarter wave resonators (QWR)

The low - β resonators have been used for heavy ion acceleration for more than three decades. The short independently phased cavities provide flexibility in operating and beam delivery.

The superconductive quarter wave resonators were firstly developed in 1981 for the heavy ion acceleration. The QWR is a resonant structure, which is composed from the coaxial transmission line, shorted at one end and "open" from another end, a quarter from the fundamental wavelength from the shorted end. The most common use of the QWR is in the acceleration of low velocity ions, where QWRs were made from the variety of different materials: lead-plated copper, niobium explosively bounded to copper, bulk niobium and niobium sputtered onto the copper substrate [31].

Cross section view and mechanical parameters of the ALPI quarter wave resonator are shown on figure 4.3.
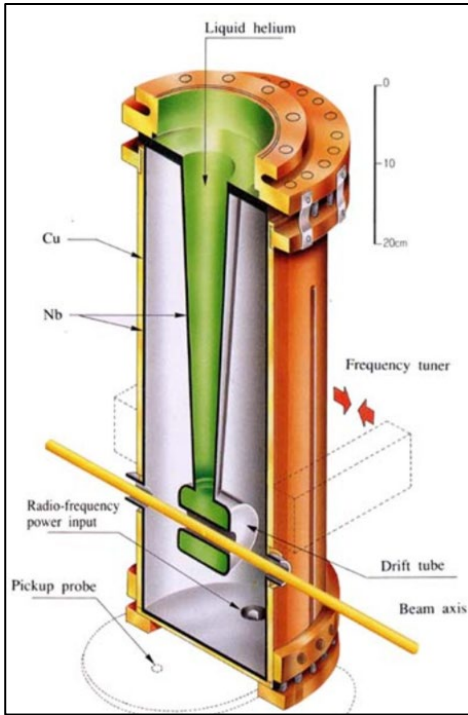
| Cavity | QWR High β |
|---|---|
| No. of Cells | 2 |
| Frequency, [MHz] | 160 |
| $β_0$ , [%] | 13 |
| Design gradient $E_{Acc}$ , [MV/m] | 5.5 |
| Active length, [mm] | 120 |
| Inner conductor diameter, [mm] | 60 |
| Mechanical length, [mm] | 566.5 |
| Gap length, [mm] | 197 |
| Beam aperture diameter, [mm] | 20 |
| U/ $E_{Acc}^2$ , [mJ/(MV/m)$^2$] | 65 |
| $E_{pk}$/ $E_{Acc}$ | 4.5 |
| $H_{pk}$/ $E_{Acc}$ , [Oe/MV/m] | 110 |
| RSh/Q , [Ω] | 140 |
| Γ = RS · $Q_0$ , [Ω] | 29 |

|(a)|(b)|

Figure 4.3 – The ALPI superconductive QWR cavity cross section view (a) and mechanical parameters (b) [32].

ALPI QWRs can be divided into three groups, according to the β coefficient: low – β (β = 0,056); medium – β (β = 0,11) and high – β (β = 0,13) cavities. Different ALPI QWR types has different structure and technical characteristics, such as mechanical length, geometry factor etc. In figure 4.3. (b) are mentioned main technical characteristics of the high – β ALPI QWR cavities.

## 4.5. Niobium properties

Niobium is 41$^{st}$ element of the periodic table. It is a transition metal of the V group and 5$^{th}$ period. This element is used in different fields, such as metallurgy, nuclear physic science, space sciences and jewellery. In the last century it was discovered that niobium has the highest critical temperature for the superconductive state transition within all the pure elements.

The niobium is a lustrous, grey, ductile, paramagnetic metal. Its crystal system is based on the body centric cubic, and it's considered a refractory metal due to its very high melting point. Physical properties of niobium are shown in table 4.1.

Table 4.1. Niobium properties [33].

| Characteristic | Value |
|---|---|
| Atomic number | 41 |
| Atomic mass, [g/mol] | 92,91 |
| Melting point, [°C] | 2468 |
| Boiling point, [°C] | 4927 |
| Atomic volume, [$m^3$] | $1,8E^{-29}$ |
| Vapor pressure at 1800 °C, [Pa] | $7E^{-6}$ |
| Density at 20 °C, [$g/cm^3$] | 8,56 |
| Lattice structure | body-centred-cubic |
| Lattice constant, [Å] | 3,030 |
| Hardness at 20 °C cold-worked, [HV 10] | 110 – 180 |
| Hardness at 20 °C recrystallized, [HV 10] | 60 – 110 |
| Young`s modulus at 20 °C, [GPa] | 104 |
| Poisson`s ratio | 0,35 |
| Linear coefficient at thermal expansion at 20 °C, [m/(m·K)] | 52 |
| Electrical conductivity at 20 °C, [1/(Ω·m)] | $7E^{-6}$ |
| Specific electrical resistance at 20 °C, [(Ω·$mm^2$)/m] | 0,14 |
| Superconductive transition temperature, [K] | 9,26 |
| Specific heat at 20 °C, [kJ/(kg·K)] | 0,27 |

## 4.6. Motivations of the niobium thin film onto copper QWR cavities

It is well-know, that among all the pure metals, niobium with its high critical temperature and critical magnetic field is the most useful material for the fabrication of the superconductive SRF cavities. It is inert, can be machined, deep drawn, welded and it is available in the bulk and sheet form [34]. However, bulk Nb QWR cavities remain very expensive and difficult in the machining due to the complicate shape of the cavity. The usage of the substrates with higher thermal conductivity and lower cost can simplify the fabrication process and decrease the cost of the cryomodules.

One of the strongest motivations of using copper as a substrate and producing of Nb/Cu thin film QWR cavities is to provide increased thermal stability to prevent the breakdown of superconductivity. The thermal conductivity of copper at 4,2 K is between 300 and 2000 W/(m·K), depending on the material cleanliness. The thermal conductivity of 300 RRR niobium is 75 W/(m·K) at 4,2 K [35].

Higher thermal stability of Nb/Cu thin film QWRs compared to the bulk niobium cavities simplify the conductance of the heat, generated by the defects inside the superconductive material.

The cost of the copper material is ten times lower, then the cost of niobium. The cost for fabrication and operation Nb/Cu SRF structures is sufficiently lower in comparison to the bulk niobium cavities regarding big dimensions and weight of the QWRs.

The mechanical stability of the QWRs with the copper substrate made the cavity more resistant to mechanical resonance and insensitive to deformations, caused by the drift of the He bath pressure. The usage of the Nb/Cu instead of bulk niobium QWRs simplify resonator control system, decrease possibility of the leak occurring in the vacuum joints and allows operation of the cavity up to the maximum reachable cryogenic power.

The Nb/Cu thin film cavities are not affected by the Q-disease (chapter 4.8), so processing of the fast cooling through the critical temperature range and continuous maintaining of the cavity at 4,2 K is not necessary.

Thin film fabricated QWRs are not sensitive to the small magnetic fields, so they do not need magnetic shields for attenuation the earth magnetic field [16].

Within the advantages, Nb/Cu thin film cavities have several disadvantages, which cause for limited usage of these cavities in particle accelerators. One of the main disadvantages of these cavities is strong decrease of the quality factor with increasing of the energy of acceleration field. This limitation will be discussed in the next paragraph.

Nevertheless, R&D activity in the field of the high-quality thin film QWRs fabrication is very perspective due to the benefits, which can be gained with substitution of the bulk niobium QWRs onto thin film cavities.

## 4.7. Basics of the Q-slopes

The Q-slopes in the thin film cavities is a complex problem, which can be caused by different physical processes. Since, Q-drops in thin film cavities can have the same reasons, as in case of bulk niobium cavities, it is sufficient to overview the behaviour of the Q-slopes appearance in the bulk and thin film cavities separately.

## 4.7.1. Q-slopes in the bulk niobium cavities

The "Q-drop" or "Q-slope" denominates the strong degradation of the bulk niobium superconducting cavities quality factor at the acceleration gradients ~ 20 MV/m. An absence of the electron emission or X-rays confirms that field emission is not the major reason of these losses. It is noticed global heating and local heating spikes within the equator region (region with the highest magnetic field) in the Q-drop regime due to temperature arrays maps.

At first it was considered as a typical feature of the BCP cavities since the KEK group could show that electro-polishing process did not give significant Q-drop [36]. Later the CEA/Saclay group discovered that an in-situ bake at the temperature range between 90 – 120 °C for 48 hours partially remove the Q-drop problem [37]. The same was shown later in the electropolished cavities at DESY. It was noticed that the baking effect is generally more pronounced in the electro-polished cavities. A small residual Q-drop remained after the baking process in case of chemically polished (BCP) cavities.

The Q-drop problem can be caused by several reasons. Low RRR material, for example, shows higher resistance at low fields, stronger Q-slope and earlier Q-drop of the cavity.

B. Visentin proposed modification of the baking process for elimination of the Q-drops. It is possible to decrease the processing time to 3 hours with increasing of the baking temperature to 145 °C. This modification allows to significantly shorten the cavity preparation process [38]. Since both baking conditions effect on the same oxygen profile of the niobium surface, it can be noticed possible role of the oxygen in the Q-drops phenomenon.

It is possible to divide the Q-slope of the bulk niobium cavity into three distinct zones for better understanding the Q-drops problem: low field (LF), medium field (MF) and high field (HF) regions (Figure 4.4). Each region has different mechanisms and the quality factor behaviour with increasing of the $E_{acc}$, which will be described below.
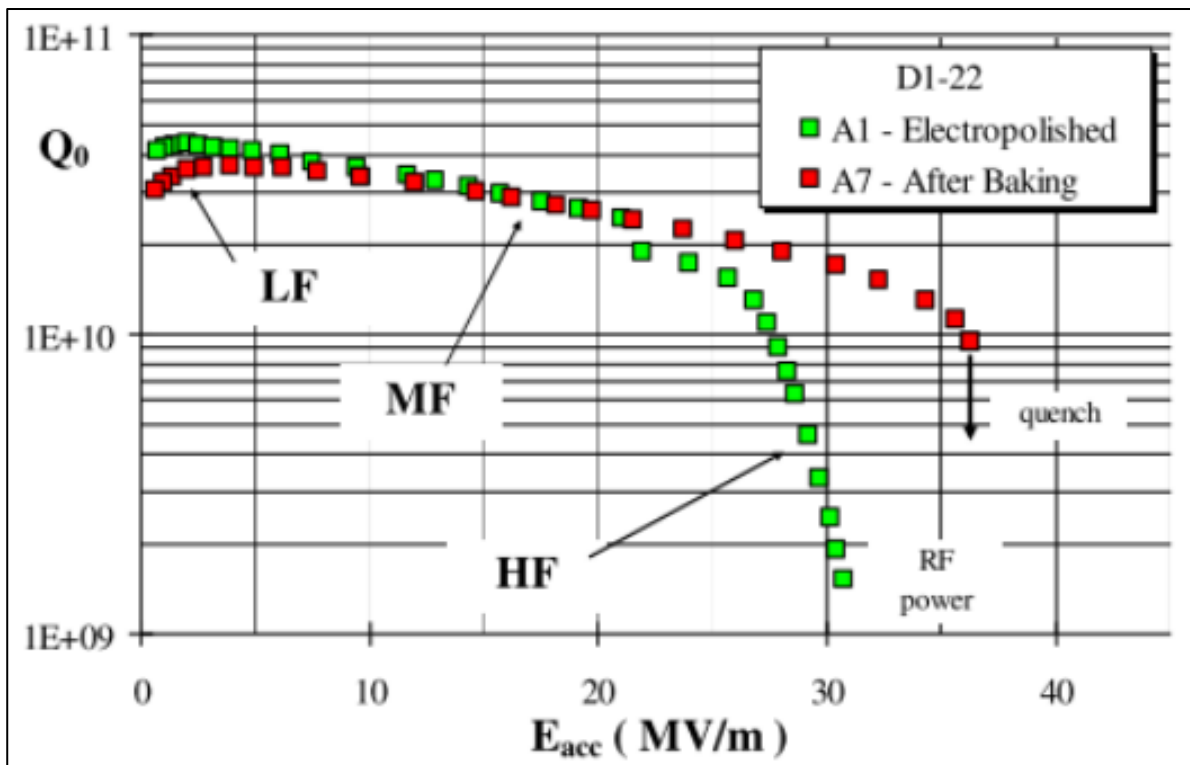
Figure 4.4 – Low field, medium field and high field Q-slopes of the bulk niobium cavities [30].

## 4.7.2. Low field Q-slope

The quality factor rises and reaches the maximum value (near 15 – 20 mT) with increasing of the RF magnetic field from zero. The Q rises by about 40 % and in the maximum, it reaches the traditional BCS value.

The reason of the Q-drop in the low fields, according to Halbrittel [39], is presence of $NbO_x$ clusters located at the oxide-metal interface. Surface analysis shows that the niobium surface is covered by a few monolayers of hydrocarbon and water followed by about 5 nm of $Nb_2O_5$, under which are clusters of $NbO_x$ formations. Presence of localised subclusters in the gap region increase surface resistance and case Q-drop.

This theory could explain some experimental observation. First of all, the LF Q-drop could be caused by additional clusters due to interstitial oxygen diffusion after cavity baking. Indeed, the LF Q-slope is restored as before baking after hydrofluoric rinse of the baked cavity (Figure 4.5). Considering, that hydrofluoric acid removes the niobium oxide and new oxide layer rebuilds after some period of time, the LF Q-drop origin in located in the oxide layer or in the oxide-metal interface such as $NbO_x$ cluster.
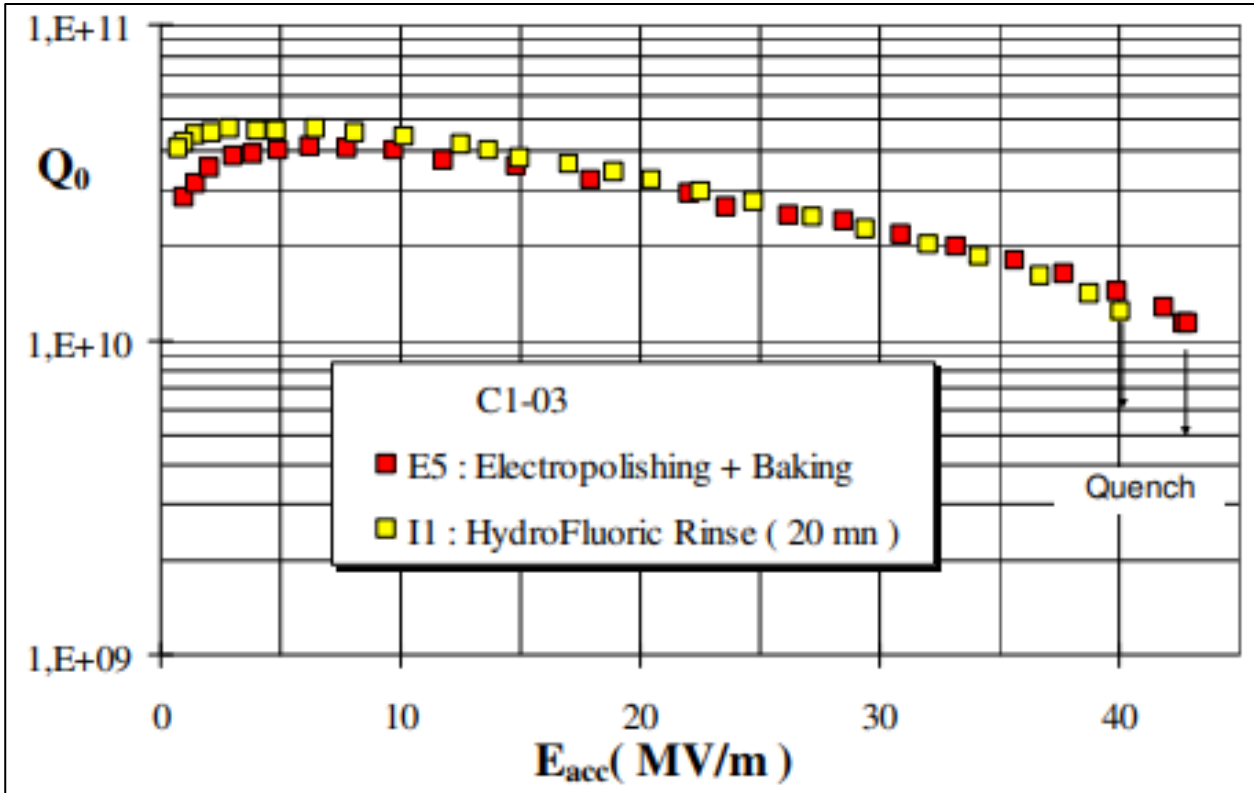
Figure 4.5 – Low field Q-slope modification after hydrofluoric acid rinse [38].

### 4.7.3. Medium field Q-slope

The medium field Q-slope can be quite strong dropping the Q by a factor of $2 - 3$ from 2 to 25 MV/m, and another factor of 2 out of 40 MV/m.

The linear and quadratic increase of the surface resistance in this region on the peak surface magnetic field $B_p$ have theoretical been established. The linear dependence (equation 4.12) is linked to a hysteresis loss due to Josephsons fluxions in weak links (oxidation of grain boundaries). Quadratic dependence (equation 4.13) is caused by the surface heating due to the thermal impedances of Nb and Nb-He interface.

$$R_s = a + bB_p \qquad (4.12)$$

$$R_s = R_0 \left( 1 + \gamma \frac{B_p^2}{B_c^2} \right) \qquad (4.13)$$

Where $B_c$ is the thermodynamic critical field of niobium and $R_0$ is the surface resistance at small magnetic fields [38].

## 4.7.4. High field Q-slope

At the highest fields, the quality factor starts to decrease rapidly. The onset peak surface magnetic field for the Q-drop falls starts at $80 - 100$ mT ($E_{acc} = 20 - 25$ MV/m). Experimental results show that the RF magnetic field is mainly responsible for the Q-drop in the HF region, rather than electric field. Temperature maps of the cavities at high field regime show strong heating of the surface in the high magnetic fields region as well as spatial nonuniformity of the heating.

Another convincing results for the magnetic field dominance in the reasons of the HF Q-drops comes from the measurement of both TE and TM modes cavities in the high field region. In case of dominance of electric field, as the main factor for the HF Q-drop, a cavity, which operates in TE mode, should not show Q-drop, since there is no surface electric field in the TE mode. After measurement, both cavities, operating in TE and TM modes, showed significant Q-drops.

The mechanism of the sudden increase of the surface resistance in the HF region is yet not clear. Several alternative theories were proposed, but none of them can explain some experimental data of the measurements in this area [30].

## 4.7.5. Q-slopes in thin film cavities

Superconducting cavities produced by the thin film coating of Nb or Nb compounds ($Nb_3Sn$, NbN, NbTiN etc.) is attractive alternative to the bulk niobium cavities, as was described in the paragraph 4.6. The main disadvantage of thin film cavities is the continuous decrease of the quality factor versus $E_{acc}$. (Figure 4.6).
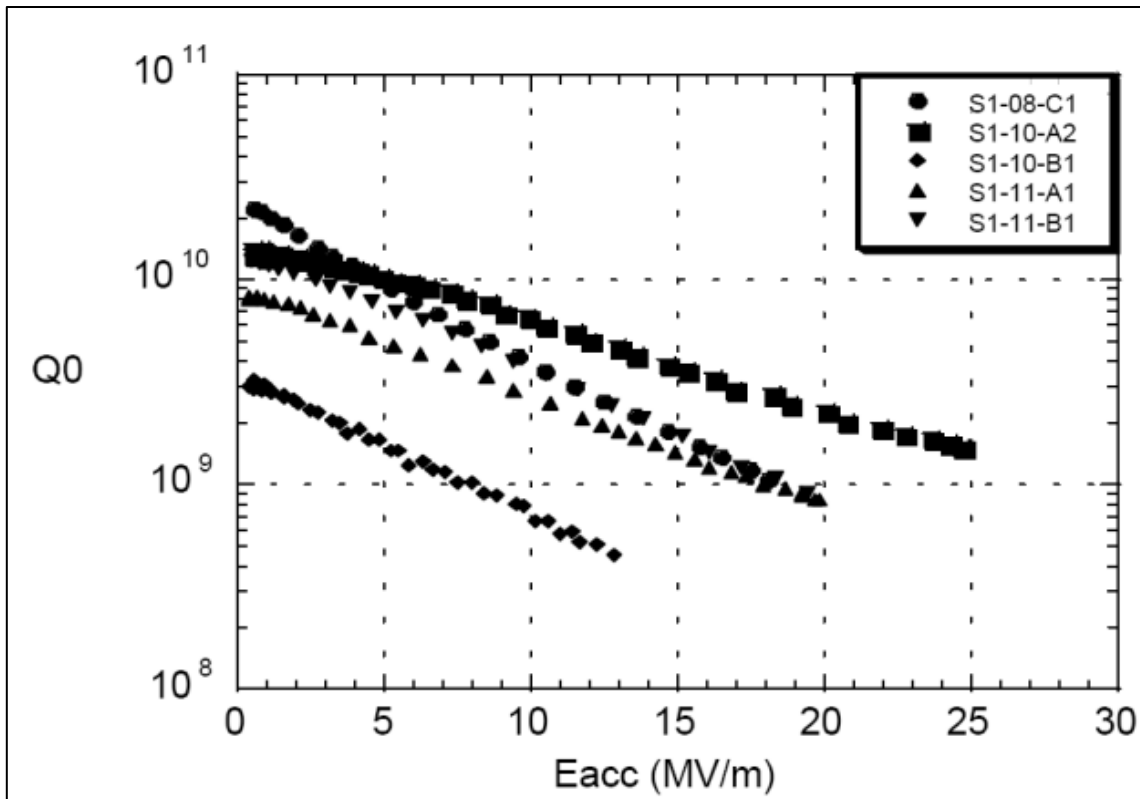
Figure 4.6 – Example of the typical Q-slope at 1.8 K for Nb coatings on copper cavities (1.5 GHz) [39].

Superconductive energy gap dependence with the magnetic field could explain thin film Q-drop with low value of the $\ell/\xi_0$ key parameter (ratio between the electron mean free path and the coherent length of the Cooper pair). The losses can be explained by the nature of the niobium coating itself, due to the penetration of the Josephson fluxons in the weak links (oxidised sputtered boundaries) [40].

If to compare dependence of the quality factor of the cavity to $E_{acc}$ of thin film cavities, it can be noticed significant difference (Figure 4.7). For bulk niobium cavities quality factor is relatively constant in all range of the field. Indeed, for thin film sputtered cavities the Q-slope starts from higher values in the LF region, but with increasing of the field quality factor rapidly drops.
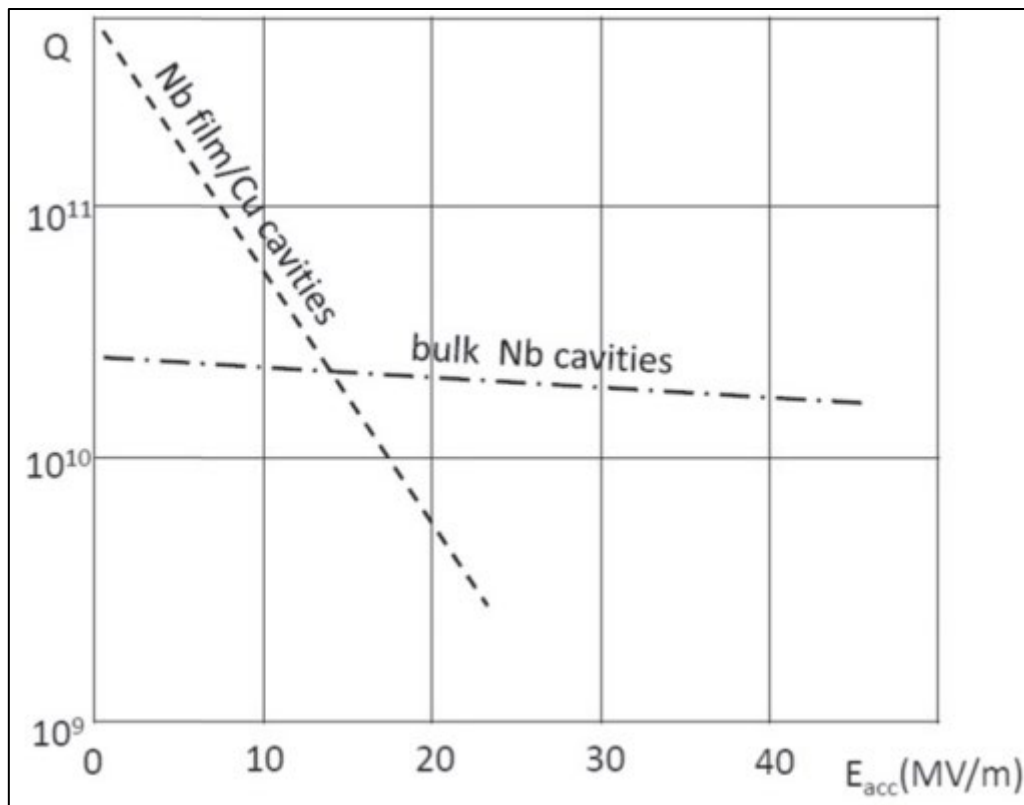
Figure 4.7 – Q factor versus accelerating field for bulk niobium cavities compared to thin film cavities [41].

## 4.7.6. Reasons and experimental solutions of the thin film cavities Q-slopes

The reason underlying the strong Q-drop for the thin film cavities is still unknown. There are several theories, which underline specific reasons as major for the Q-drop of thin films cavities. These reasons will be discussed in this chapter.

*Quality of the sputtered film.*

C. Benvenuti in his research [42] connect rapid drop of the quality factor in thin film cavities with the residual resistance of the produced films. The RRR of the bulk niobium cavities reaches 300, while the RRR of the sputtered niobium thin films is around 30. The quality of the deposited thin film is strongly dependant on the impurities contamination, the macroscopic film defects, the deposition parameters, the base system pressure etc. It is possible to decrease surface resistance of the Nb coating and move the quality factor drop further in the HF region of the Q-slope with increasing of the deposited film quality.

*Hydrogen and Oxygen migration.*

Hydrogen is well known source of the niobium coatings contamination. Hydrogen permeates across the copper substrate and diffuses inside niobium lattice during the film growth. Hydrogen migration process causes increase of impurities and forming of the hydrogen pollution of the deposited coating, which effect onto the Q-slope of the produced cavities. Oxygen can also migrate through the copper surface and include into the niobium coating during formation. One of the possible solutions of this problem is deposition of the metallic interlayer between the substrate and the thin film. There were several attempts in CERN with deposition of the titanium layer onto the copper before niobium, but Q-slopes of the cavities with interlayer showed the same behaviour as directly Nb/Cu sputtered cavities [43].

*Thermal feedback.*

The power dissipated by the RF field produces a temperature difference between the inner superconducting cavity surface and the helium bath, proportional to dissipated power and thermal boundary resistance. This difference induces the thermal feedback, since, adjusting the surface magnetic field, the power leads to the temperature increase, which causes surface resistance increase. The magnitude of the Q-slope in this model depends on the thermal boundary resistance between the inner cavity surface and the bath. So, the higher copper thermal conductivity plays in favour of thin film Nb/Cu QWRs, where thermal feedback is less relevant in respect to bulk niobium cavities.

*Nb/Cu interface and adhesion problems.*

Due to the thermal feedback model, the high thermal boundary resistivity increases the Q-slope of the Nb/Cu cavity. Thermal boundary resistivity ($R_b$) consists of thermal niobium film resistivity ($R_{Nb}$), grain boundary resistivity ($R_{Nb/Cu}$) and copper substrate thermal resistivity ($R_{Cu}$). Thermal resistivities of niobium film and copper substrate can be negligible due to the high copper thermal conductivity and low thickness of the niobium film. So, thermal resistivity of the Nb/Cu interface takes major part of the thermal boundary resistivity. Good adhesive contact in the Nb/Cu interface plays a critical role in the thermal boundary resistivity value and the Q-slope behaviour of the Nb/Cu cavities.

There is no miscibility range between copper and niobium at the usual film deposition temperature (150 °C) due to the phase diagram (Figure 4.8). The Nb/Cu is considered as a classical example for the non-miscible systems.
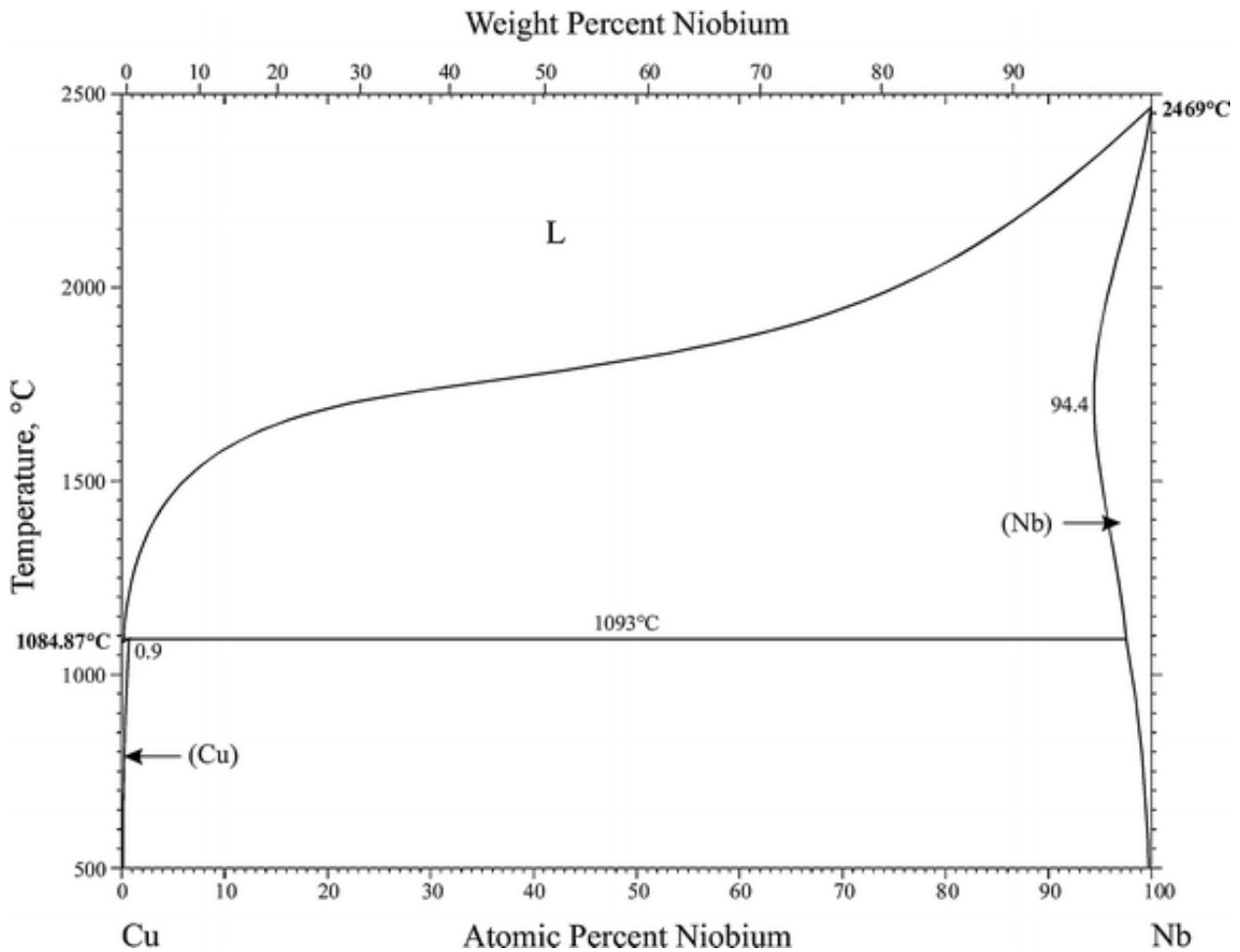
Figure 4.8 – The Cu/Nb phase diagram.

The problem of the niobium film adhesion on the copper system is not well understood. There are several reasons, that causes poor thermal contact between niobium and copper, such as bad adhesion of the thin film; stress inside the niobium film, which causes further relaxation, cracking and desorption of the film; copper oxides, powder, or other contaminations; micro-voids at the interface due to the self-shadowing of the film growth.

*Experimental solution for the thin film cavities improvement.*

There are several experimental strategies, that should be taken in consideration during the development of the Nb/Cu cavity deposition processes.

Proper technology of the substrate surface preparation can decrease amount of the impurities, copper surface roughness and this will case better adhesion and quality of the deposited niobium thin film on the copper substrate. Increasing of the substrate temperature will both decrease the void volume and the mean surface roughness of the nucleation film.

40

Rising of the kinetic deposition energy, released from the bombarding particles to the growing film, will increase the film adhesion. This effect can be achieved by using of the bias sputtering with action of the plasma bombardment of the growing film.

Buffer layer of a metal, miscible on both material can increase adhesion and prevent migration of hydrogen and oxygen in the niobium coating.

Finding appropriate parameters of the sputtering regime, where the film internal stresses are released, will prevent cracking and desorption of the coating from the substrate [41].

## 4.8. Limitations on SRF cavities

There are several most important limitations of the Q-slopes of SRF cavities. Main mechanisms of the SRF limitations are shown on figure 4.9.
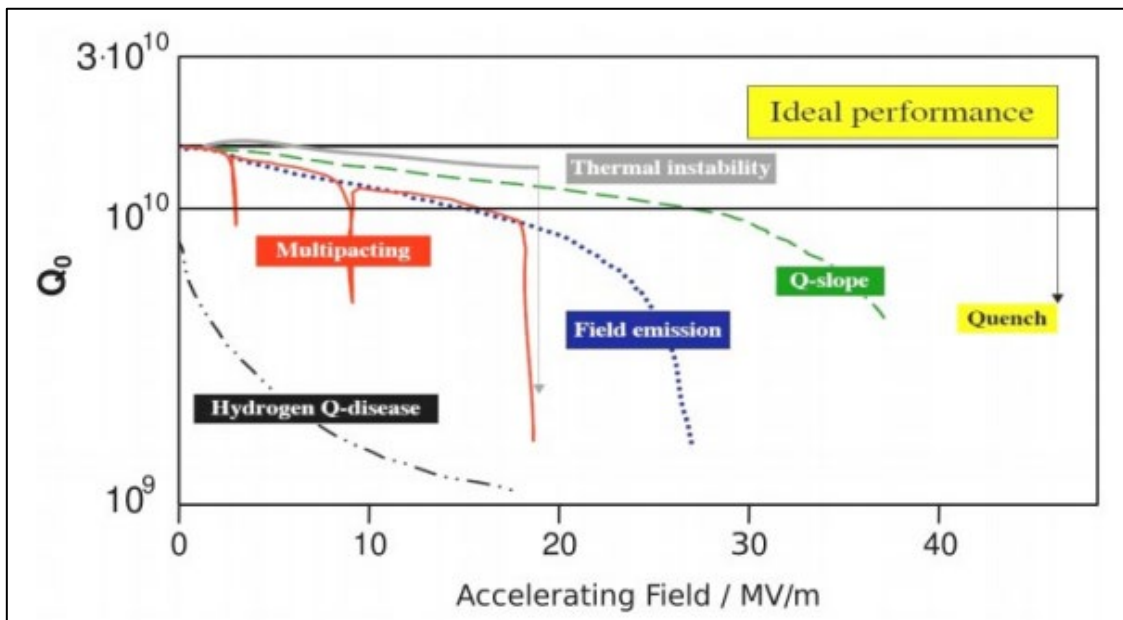
Figure 4.9 – Performance limitations of the quality factor or energy of the acceleration field in the Q vs E curve [44].

## 4.8.1. Hydrogen Q-disease

An important residual loss mechanism effects on the quality factor of the SRF cavities at $E_{acc} \approx 0$ MV/m when hydrogen dissolves in the bulk niobium RF surface. This residual loss (commonly referred as "Q-disease") depends on the quantity of the dissolved H, the rate of cool down to the liquid helium temperature and amount of other impurities or atomic-sized defects in the niobium surface. Nb-H phases harmful to the superconductivity can form at the temperature range 100 – 150

K, when the hydrogen concentration is higher than 100 – 200 at. ppm. With increasing of the time, spent in the dangerous zone, hydrogen regions grow in the nucleation centres due to the mobility of H at these temperatures. Below 77 K, H mobility is small enough to arrest the growth of the hydride centres [30].

The hydrogen contamination of the niobium lattice can be caused by the mechanical treatment (forming, electron beam welding etc.) and preparation (chemical treatment, BCP, water chemical preparation, electrochemical treatment etc.) processes of the SRF cavities [45].

One of the main methods of elimination of the hydrogen contamination during the chemical preparation is the control of the temperature of the etching solution below 15 °C. Reducing of the amount of hydrogen in already polluted SRF cavity is possible by additional baking of the cavity at the pressure, lower than $10^{-6}$ mbar at a temperature 600 °C for 10 – 12 hours (or 700 – 900 °C for 1 – 2 hours) [29].

## 4.8.2. Multipacting

Multipacting (multiple impact electron amplification – MP) is a resonant process in which large amount of electrons absorbs RF power, decreasing the cavity field. An electron is emitted from one of the structure`s surfaces. The emitted electron is accelerated by the RF fields and eventually impacts the wall again, thereby producing the secondary electrons. The number of secondary electrons depends on the surface characteristics and on the impact energy of the primary electron. After that, secondary electrons are accelerated and produce another generation of emitted electrons. This form of multipacting is called "one-point" or "one-surface" MP. Scheme of the typical trajectories of the order one, two and three is shown on figure 4.10 in the cylindrical cavity.
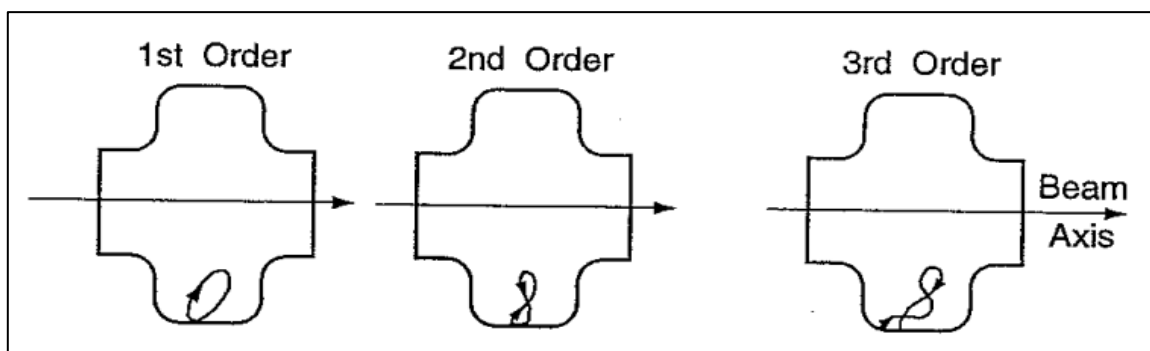


Figure 4.10 – Typical one-point multipacting trajectories for the order one, two and three [27].

 Free electrons, created by the multipacting process, absorb RF power, reduce quality factor and the field cannot be increased until the multipacting barrier is "processed".

Mechanism of the multipacting effect is similar for elliptical and spoke cavities. The multipacting effect can be avoided by the modification of the shape of the SRF cavity and building "multipacting free" structure. In case, when modification of the shape is impossible, removing of the MP barrier can be done by the slight increasing of the RF power in the multipacting region. After short period of time multipacting vanishes and the quality factor value returns to the previous quantity.

## 4.8.3. Field emission

In the high surface electric field region, the main limitation mechanism is field emission. Electrons are confined inside the metal and under normal circumstances the energy of electron is insufficient to enable it to escape from the surface. The electron must be given extra energy in the form of the thermal energy (thermionic emission) or the radiation energy (photoemission) to escape from the metal. The wave function of the electron is attenuated rapidly outside the surface potential barrier. Instead, if the barrier is thin enough, attenuation is not complete and there is a finite probability that some electrons will tunnel through the barrier and escape into vacuum. The escaped electrons can hit the walls of the cavity or flanges, causing radiation [27].

Due to the field emission, the quality factor of the SRF cavity starts to decrease steeply because of the exponentially increasing electron currents emerging from the particular emitting spots on the surface. Field emission can be detected by the increase of the current in the cavity beam pipe and increase of the x-ray intensity by the radiation detectors outside the cryostat. A detailed temperature map (Figure 4.11) shows line heating along the longitude at the location of the emitter.



(a)                                                                                              (b)
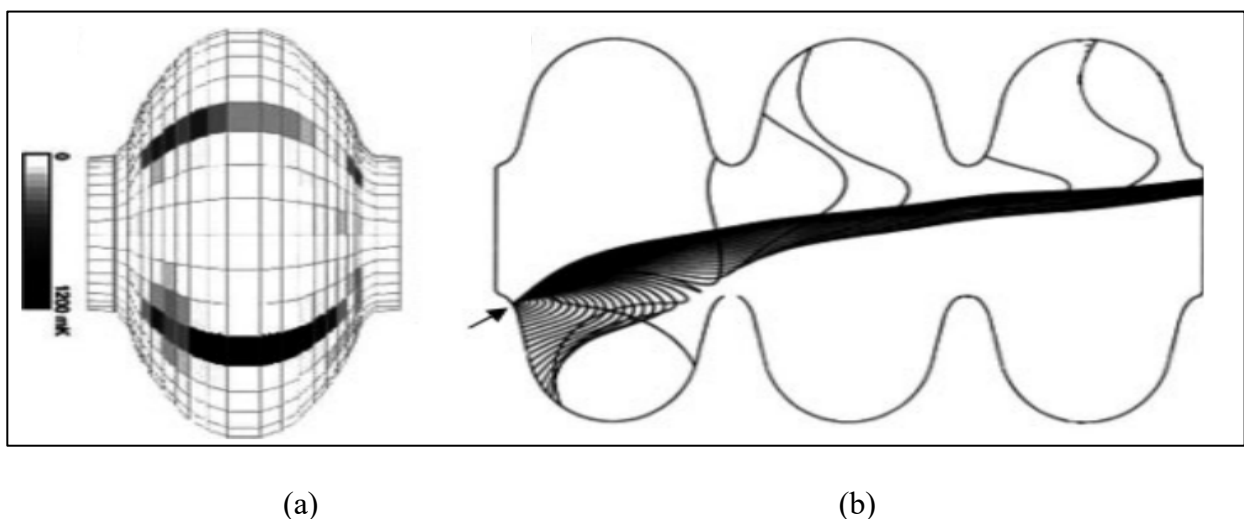
Figure 4.11 – (a) Temperature map from the heating of impacting field emitted electrons; (b) Calculated field emitted electron trajectory in a three-cell 1,5 GHz cavity at Epk = 50 MV/m [4].

Field emission mechanism is similar for cylindrical and spoke cavities. It can be avoided by the better treatment and water high pressure rinsing of the cavity surface for the fields up to 25 MV/m [46].

## 4.8.4. Thermal breakdown

One of the phenomenon, that limits the achievable fields, is thermal breakdown, also known as a "quench". Thermal breakdown is concentrated in the sub-millimetre-size regions ("defects") that have higher RF loses, than the surface resistance of an ideal superconductor.

In case of DC, supercurrents flow around defects. At the RF frequencies, the reactive part of the impedances causes the RF current to flow through the defects, producing Joule heating and increasing the temperature of the defect. When the temperature of the defects overcome the critical temperature of the material, the superconducting regions surrounding the defects become normal conducting, increasing power dissipation. Further increasing of the normal conducting islands results increase of the dissipated power and thermal instability (Figure 4.12).



(a)            (b)
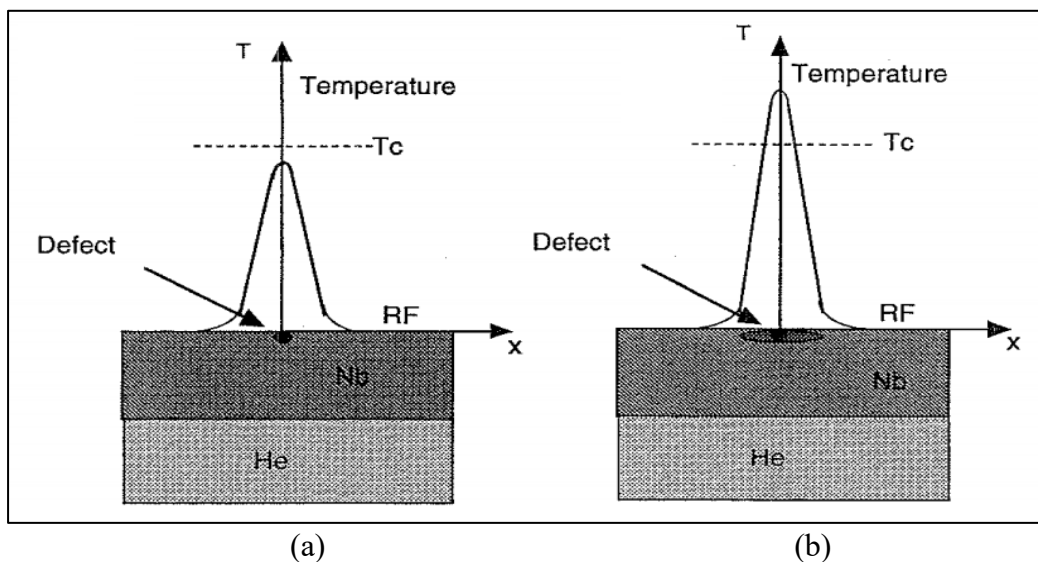
Figure 4.12 – Thermal breakdown of the niobium cavity: (a) – at the low field temperature of the defect is lover then the critical temperature of the niobium; (b) – with increase of the field, temperature of the defect surrounding area starts to be higher, than critical, creating normal conductive islands and causing power dissipation increase.

The field, at which occurred thermal breakdown, is dependent on the different factors, such as quantity and size of the defects in the superconductive film, thermal conductivity of the bulk niobium and heat transfer process from the niobium surface to the helium bath. The "big" sized defects (diameter ≈ 1 mm.) of the surface are caused by manufacturing errors and can be eliminated by the

mechanical grinding. In case of smaller defects, the useful solution can be increasing thermal conductivity of the bulk niobium [27].

## 4.9. Theory of the QWR RF measurement

The basic RF parameters, that characterize QWR superconductive performance (quality factor ($Q_0$), maximum energy of acceleration field ($E_{acc}$), field emission and quality factor as a function of gradient) can be defined during the RF test at the cavity temperature of 4,2 K. System, used for the RF measurement is described in the paragraph 6.4.

For the ALPI QWR cavities these cold tests are done with the cavity vertical holding. Normally, these tests are done at or near critical coupling when the transferred RF signal frequency is similar to the QWR resonant frequency. In this case the required RF source should have few hundreds of watts, which is enough to overcome the walls and field emission power losses.

The following equations are generally used for the low temperature measurements of the SRF cavities.

Stored energy is defined by the equation:

$$U = \frac{E^2}{\omega_0} \frac{L}{\left(r/Q\right)} \tag{4.14}$$

Where $E$ – electrical field, [V/m]; $\omega_0$ – cavity frequency; $L$ – electrical length, [m]; $r/Q$ – geometric shunt impedance, [$\Omega$/m].

$$P = \frac{U\omega_0}{Q} = \frac{E^2}{Q} \frac{L}{\left(r/Q\right)} \tag{4.15}$$

Where $P$ is the total power, [W].

Intrinsic quality factor can be calculated by the equation [47]:

$$Q_0 = G/r_s \tag{4.16}$$

Where $G$ is geometry factor, [$\Omega$]; $r_s$ – surface resistance, [$\Omega$].

The RF signal is transferred to the QWR through the forward line to the Coupler antenna. From the QWR signal is received by the measurement system from pick-up antenna through the reflected line. The system, used for RF measurements, is described in the chapter 9.

The total power loss $P_{tot}$ can be defined as the sum of the power, dissipated in the cavity walls $P_d$ and the power leaks in the coupler $P_{cpl}$ and pick-up $P_{pk}$ antennas:

$$P_{tot} = P_d + P_{cpl} + P_{pk} \qquad (4.17)$$

For characterization of the cavity with couplers, "loaded" quality factor $Q_L$ can be defined as:

$$Q_L = \frac{\omega U}{P_{tot}} \qquad (4.18)$$

The energy in the cavity decays exponentially with a time constant, $\tau_L$

$$\tau_L = \frac{Q_L}{\omega} \qquad (4.19)$$

Decay time is measured experimentally and by evaluation of the $\tau_L$ it is possible to determine $Q_L$. Equation (4.19) is useful for determining of the Q of the cavity, connected to input and output RF lines. Due to this, loaded Q also considers leakage of the power from the pick-up and coupler antennas. Substitution of the (4.17) into (4.18) shows connection between loaded Q and quality factor of each measured component:

$$\frac{1}{Q_L} = \frac{1}{Q_0} + \frac{1}{Q_{cpl}} + \frac{1}{Q_{pk}} \qquad (4.20)$$

The quality factor for each dissipated power can be defined as:

$$Q_o = \frac{\omega U}{P_d} \qquad (4.21)$$

$$Q_{cpl} = \frac{\omega U}{P_{cpl}} \qquad (4.22)$$

$$Q_{pk} = \frac{\omega U}{P_{pk}} \qquad (4.23)$$

The (8.8) can be rewritten by definition the "coupling parameters" [27]:

$$\beta_{cpl} = \frac{Q_0}{Q_{cpl}} \qquad (4.24)$$

$$\beta_{pk} = \frac{Q_0}{Q_{pk}} \qquad (4.25)$$

Coupling parameters gives the information about strength of coupling interaction with the cavity. In case when the $\beta$ power leakage from the couplers is higher in respect to power, dissipated in the cavity walls, system set up at "over coupled conditions". The proper measurement conditions are reached,

46

when $\beta_{pk} \ll 1$. In this case power leakage on the pick-up antenna is minimum. For transferring of the all signal to the cavity, system should be measured at "critical coupling" conditions ($\beta_{cpl} = 1$). In this case measurement system is matched to the cavity electrical impedance.

In case of critical coupling the incident power is the sum of dissipated power in the cavity walls and reflected power, that goes out from the pick-up port. At critical coupling, dissipated power can be defined as:

$$P_d = P_i - P_{ref} \tag{4.26}$$

When the cavity is critical coupled, it is possible to calculate quality factor as:

$$Q_0 = \left(1 + \beta_{cpl} + \beta_{pk}\right)Q_L = 2Q_L = 2\omega\tau_L \tag{4.27}$$

$$Q_{pk} = \frac{2\omega\tau_L(P_i - P_{ref})}{P_{pk}} \tag{4.28}$$

Next step is increasing of the input power to rise the stored energy $U$. $Q_{pk}$ is stable in this case because it is dependent onto the geometry of the cavity. In case of power input, $Q_0$ can be defined as:

$$Q_0 = \frac{Q_{pk}P_{pk}}{P_i - P_{ref} - P_{pk}} \tag{4.29}$$

The gradient can be calculated as [48]:

$$E = \sqrt{Q_{pk}P_{pk}\frac{r/Q}{L}} \tag{4.30}$$

# Chapter 5

# THIN FILM DEPOSITION

## 5.1. Introduction

Thin film coatings of certain material are used for the modification of the surface properties of the bulk material. Combining of the properties of two materials can modify physical properties and decrease economical costs of the final product.

Typically, thin films are in the range of thickness from few to thousands of nanometers. One of the main used processes for the thin film deposition is PVD (acronym for Physical Vapor Deposition) techniques. PVD processes are based on atomistic growth of the film, in which material is vaporized in form of atoms or molecules from the solid or liquid state, transported through the vacuum or low pressure gaseous (or plasma) environment, and deposited onto the substrate material.

The main general categories of PVD processes are sputter deposition, vacuum deposition (evaporation), arc vacuum deposition, and ion plating. Each process has advantages and disadvantages and is used for modification of the substrate surface according to the specific tasks of the final product, such as increasing of hardness, thermal or electrical conductance of the bulk material etc. [49].

## 5.2. Sputtering process

## 5.2.1. Bases of the sputtering process

Sputtering process can be described in several steps. First step of the process is bombardment of certain material (target) by the suitable high-energy particles. Bombardment with ions ($Ar^+$ in this research activity) occurs due to application of the negative potential to the target material (creating voltage between target cathode and grounded substrate) and migration of the charged argon ions, extracted from the electropositive plasma, to the negatively charged material. At the low voltage region, applied to the electrodes, the current is created by the small number of carriers, presented in the sputtering gas, when the voltage applied. Negative potential increase leads to the current density growth due to the increase of the charge carriers number, so-called secondary electrons. With further growth of the current density voltage breakdown occurs, which can be noticed by the decrease of the electrode voltage. At this voltage region number of $Ar^+$ ions, produced by the collision with one secondary electrons, is high enough to produce another secondary electrons. This normal discharged region is characterized by self-sustainability of plasma.

The energy transfer between charged particles and atoms in the target crystallite lattice occurs due to the plasma bombardment. Target material obtain enough energy from this collision for breaking the interatomic connection and escaping from the surface.

After breaking the target lattice, ejected atoms migrate through the inter electrode environment and can be used for the forming of thin films on the other bulk material (substrate).

Inert gas plasma is normally used in the sputtering processes for accelerating charged particles electrically towards the target surface. After migration to the bulk material, target atoms start to adsorb onto the substrate surface and form thin film coating layer by layer.

Generally, sputtering process can be defined as erosion process of the target surface under the influence of the high-energy particles with further thin film growth onto the substrate surface.

Mechanism of the sputtering process is described in figure 5.1.
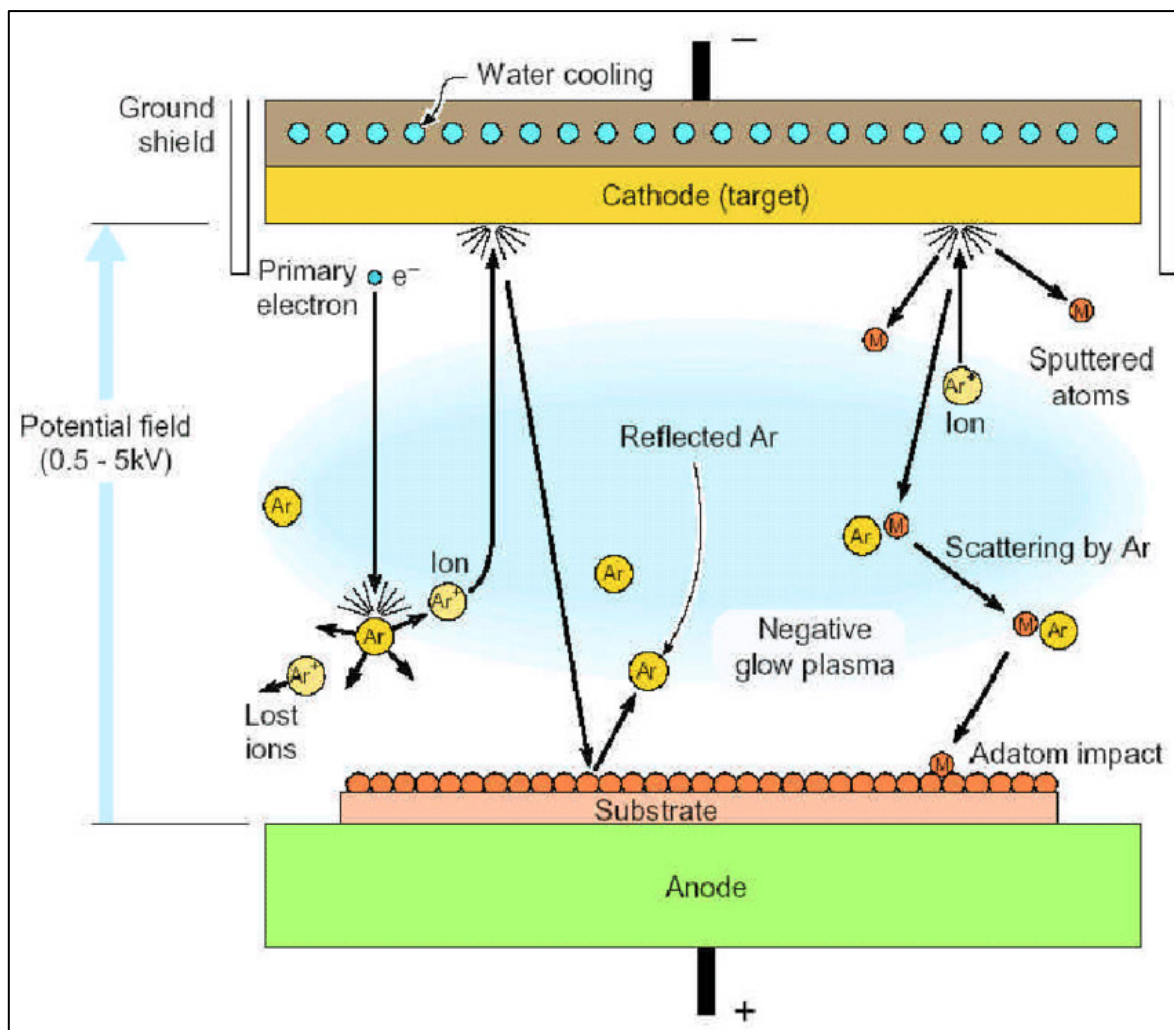


Figure 5.1 – Scheme of the sputtering process in the DC sputtering configuration [50].

## 5.2.2. Mechanism of the sputtering process

Two theoretical models have been proposed for the description of the sputtering process:

1. Thermal vaporization theory
2. Momentum transfer energy

The scientists Hippel (in 1926), Sommermeyer (in 1935) and Townes (in 1944) supported the thermal vaporization theory and for the first half of the 20th century it was considered to be the most suitable sputtering mechanism. According to this theory, the surface of the target is heated enough to be vapourised due to charged ion bombardment.

In 1956 Wehner suggested momentum transfer energy as the most important mechanism of the sputtering process, which is based on the emittance of the target atoms due to momentum transfer from the charged ions due to collision. Sputtering event is initialised by the first collision and target surface atoms, followed by second and third collision between atoms in the target surface cells according to this theory. Figure 5.2. shows initial collisions in the target surface region.
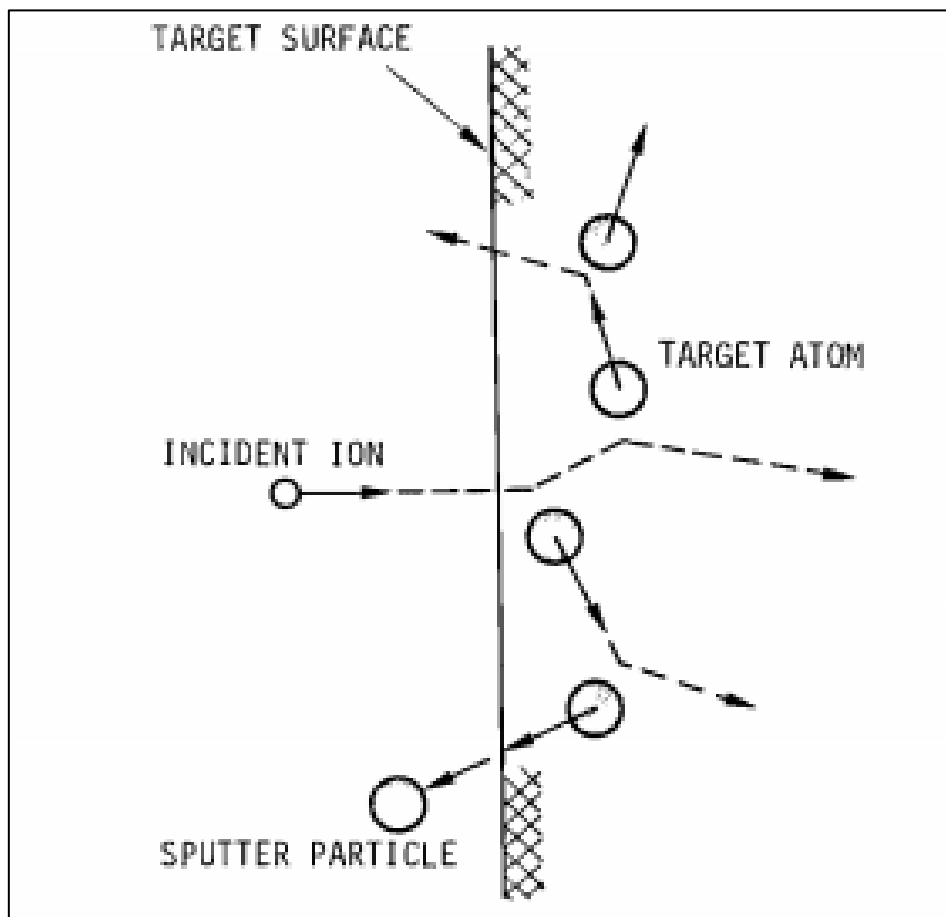


Figure 5.2 – Initial of the sputtering event due to elastic-collision theory [51].

During the sputtering process, number of secondary events can occur: secondary electron emission, secondary positive and/or negative ion emission, emission of radiation (photons, x-ray), reflection of the incident particles, heating, chemical dissociation or reaction, bulk diffusion, crystallographic changing, backscattering.

Secondary effects can affect sputtering process in general and quality of the coating. Several rules should be scheduled in order to perform high-quality coating deposition. Charged ions should be directed to the surface of the target material for the atom erosion "Free" atoms of the target material should be able to travel through the vacuum (plasma) environment with the less amount of collisions with other particles and the less moving impedance as possible.

The concept of mean free path is used for characterisation of the movement of the particles inside the sputtering environment. The mean free path is the distance, on which particle can travel without collision with other particles. The particle can save higher amount of its energy with lower amount of collision during its migration. This will influence onto the amount of sputtered particles, thickness of the film onto the substrate material and deposition rate of the sputtering system. Higher sputtering pressure will decrease deposition rate of the process.

The sputter yield Y determines the erosion rate of the sputtering targets. It is defined as the number of atoms, removed from the surface of the material per incident ions and is given:

$$Y = \frac{atoms\ removed}{incident\ ions} \qquad (5.1)$$

Sputtering yield is dependent on several factors, such as energy of incident particles, mass of incident particles, target material, incident angles of particles and crystal surface of the target material.

Dependence of the sputtering yield onto the ion energy can be described as first constant growth with increasing of the energy. At low energy region the incident ions collide with the surface atoms of the target and the number of dissipated atoms will be proportional to the incident energy. The highest sputtering rate is observed at the energy region of 10 keV. Sputter yield decrease with increasing of the ion energy from 10 keV to 100 keV due to the energy dissipation of the incident ions deep in the target material.

Sputter yield vary with the angle of the incident particles. The yield increase with the incident angle value and reaches maximum at the range of the angle between 60° and 80° (figure 5.3). With further angle increase, the yield decreases rapidly [52].

52
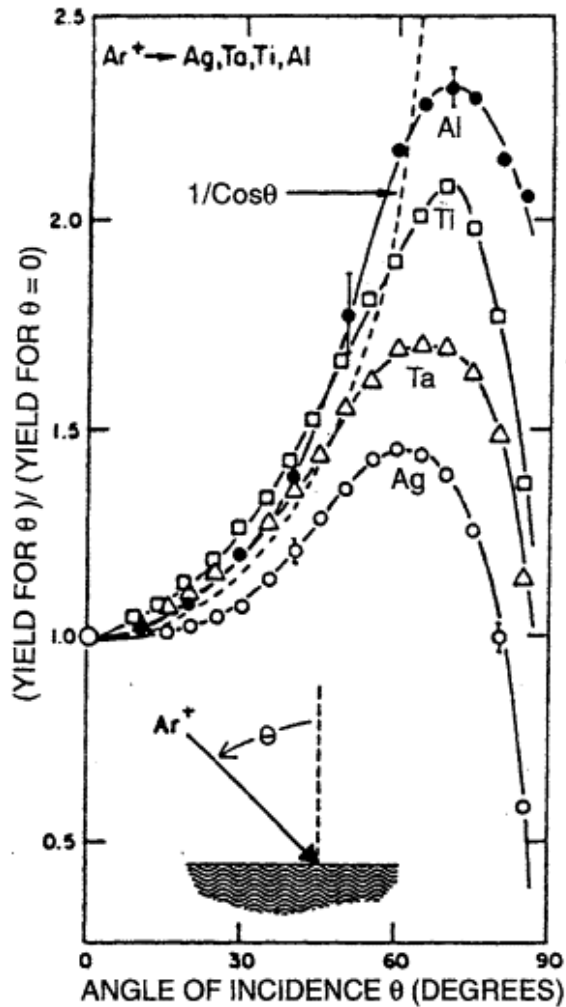
Figure 5.3 – The sputter yield dependence from the angle of incident particles for different materials [53].

## 5.3. Sputter deposition technologies

### 5.3.1. Sputtering configurations

Different sputtering techniques are used for more than 150 years, starting from gas discharges and plasma physics. Currently, sputter deposition is practiced by a variety of different techniques. One of the most commonly used (Figure 5.4) are:

- DC diode sputtering;
- RF diode sputtering
- magnetron sputtering;
- Biased diode/magnetron sputtering;
- ion beam deposition.
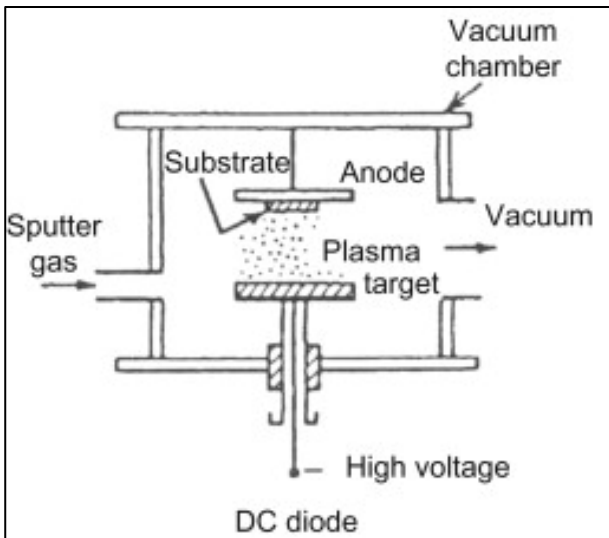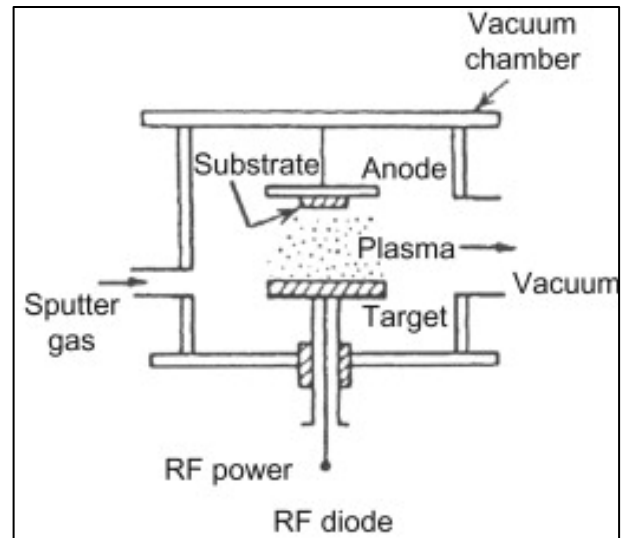
(a)                                                      (b)
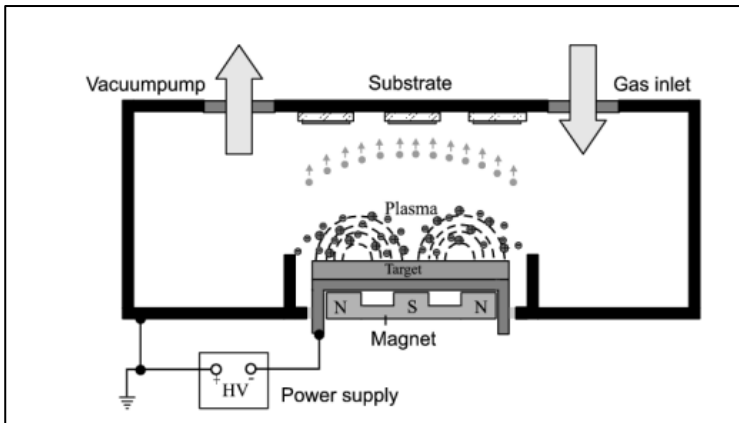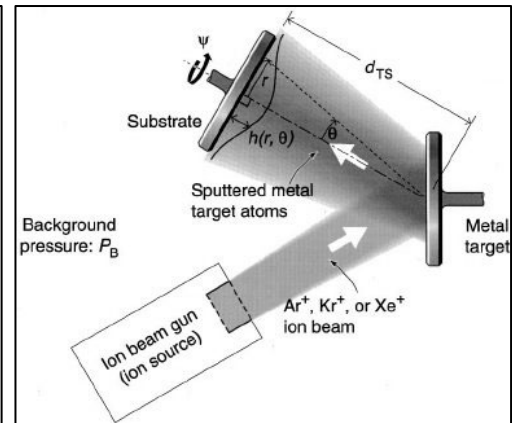


(c)                                                      (d)

Figure 5.4 – Simplified schemes of the most commonly used sputtering techniques: (a) – DC diode sputtering; (b) – RF diode sputtering; (c) – magnetron sputtering; (d) – ion beam deposition.

All of these techniques have its advantages and disadvantages, which makes them suitable for film deposition of the different materials variety for different products [54].

Biased sputtering technique is one of the most suitable for the superconductive thin film deposition for the different type of acceleration cavities due to its advantages, which will be described in the next paragraph.

## 5.3.2. Bias sputtering

Bias sputtering methodology is one of the most useful techniques of the basic ion sputtering thin film deposition techniques. One of the first usage of the bias sputtering technology was in 1962 [55]. The scientist Frerich tried to produce superconductive films of tantalum and niobium. He found out, that with asymmetric AC "protected sputtering" technique he could deposit metallic bright thin films, which reproduced superconductive properties of the bulk material. After his discovery, bias sputtering started to be widely used for the superconductive thin films production.

The main difference from the "classical" DC sputtering is placing substrate under some negative potential (bias) in respect to ion plasma. In parallel of the target material bombardment due to plasma interaction, thin film, that was formed on the substrate surface, is also influenced by the plasma charged particles due to the bias voltage.

The main source of contamination of the thin film during DC sputtering are residual gases inside the vacuum chamber, vacuum pump backstreaming and impure sputtering gasses. These gasses and impurities can be absorbed on the substrate surface before arriving of the additional sputtering material. Also, trapped impurities and gasses are entrapped in the film structure during the coating deposition. These contaminations and its migration inside the thin film is greatly effect on the physical properties of the coating, especially where superconductivity is concerned. Slight ionic bombardment of the created substrate films during the deposition due to the substrate bias voltage causes selective removal of loosely bound or absorbed particles (residual gasses, oxides etc.) while permitting some net deposition of the pure target material [56].

Making the research of the bias sputtering mechanism, Vratny and Harrington [57] suggested two additional mechanisms, which could coexist with the formed theory and explained some of anomalous changes in the film resistivity. Better quality of the sputtered film can be caused by cleaning-up due to an intense ion flux at the substrate surface. Also, on the structure of the film can influence trapping of the bombardment ions into the surface substrate.

Grant and Carter [58] continued research onto the trapping mechanism during the bias sputtering. They studied both trapping and releasing processes of the bombardment ions within the substrate surface. These scientists proved experimentally release mechanism of the bombardment ions and residual gasses from the structure of thin films and substrate surface during the bias sputtering.

Depending on the impurity removal from the films, with bias sputtering it is possible to produce physical changes within the crystal structure of the sputtered deposit (recrystallization, defect removal), which influence on the final quality and electric properties of the final coating.

### 5.3.3. Diode bias sputtering

Regarding advantages of the bias sputtering technique, it was decided to use diode bias sputtering for production of the Nb/Cu high-β ALPI QWR cavities. Usage of the diode sputtering technique instead of magnetron sputtering can be explained by the specific construction of the ALPI QWR cavities. Niobium cathode should be thin enough for preventing short circuits and arcs during the deposition process due to small distance between inner conductor and external walls of the QWR. With the absence of place for the cool down and magnet system inside the niobium cathode it was decided to use bias diode sputtering technique as an appropriate for the high quality ALPI QWR production.

Regarding the advantages of the bias diode sputtering technique, there are some disadvantages, which should be considered during the production of the superconductive thin films with this technology. Within the others sputtering techniques, deposition rate of the diode sputtering is the lowest due to the processing of "classical" DC sputtering (without magnetic field, as in case of magnetron sputtering) with further plasma influence onto the thin film. Another negative side of this technology is more complex sputtering apparatus, needed for the bias diode deposition performance. Usage of the additional bias potential regards additional power supply implementation, which increase the total cost of the sputtering system sufficiently.

Nevertheless, bias sputtering technique is an appropriate solution for high-β Nb/Cu superconductive ALPI QWR cavities production due to cleanliness and physical characteristics of the produced coatings, relatively easy control of the film thickness and uniformity of the deposit within the complicate substrate surface.

### 5.4. Thin film growth

The continuous film growth process can be summarised as controlled growth of the substrate surface absorbed nucleus in three-dimensional scale, formation of a network structure with other nucleuses for growing the continuous film [52].

During the sputtering process, growth of the film occurs atom by atom. With variation of the sputtering parameters, it is possible to achieve high control of the film growth with specific microstructure and physical properties of different materials.

Scientists Movchan and Demchishin in their study [59] onto thick films of nickel, titanium, wolfram and oxides of aluminium and zirconium found out, that due to the temperature of the substrate, coatings can be divided onto three zones by its structure and properties. It was discovered that hardness, strength and plasticity of the same material in different zones is different. Scientists

assumed, that the main reason of different physical properties is difference in microstructural lattice of the formed material at different forming temperature.

Thornton continued the research in this field and updated Movchan and Demchishin model with introduction of additional axis with pressure of the working gas argon and fourth structural zone with 20 – 250 μm. (Figure 5.5)
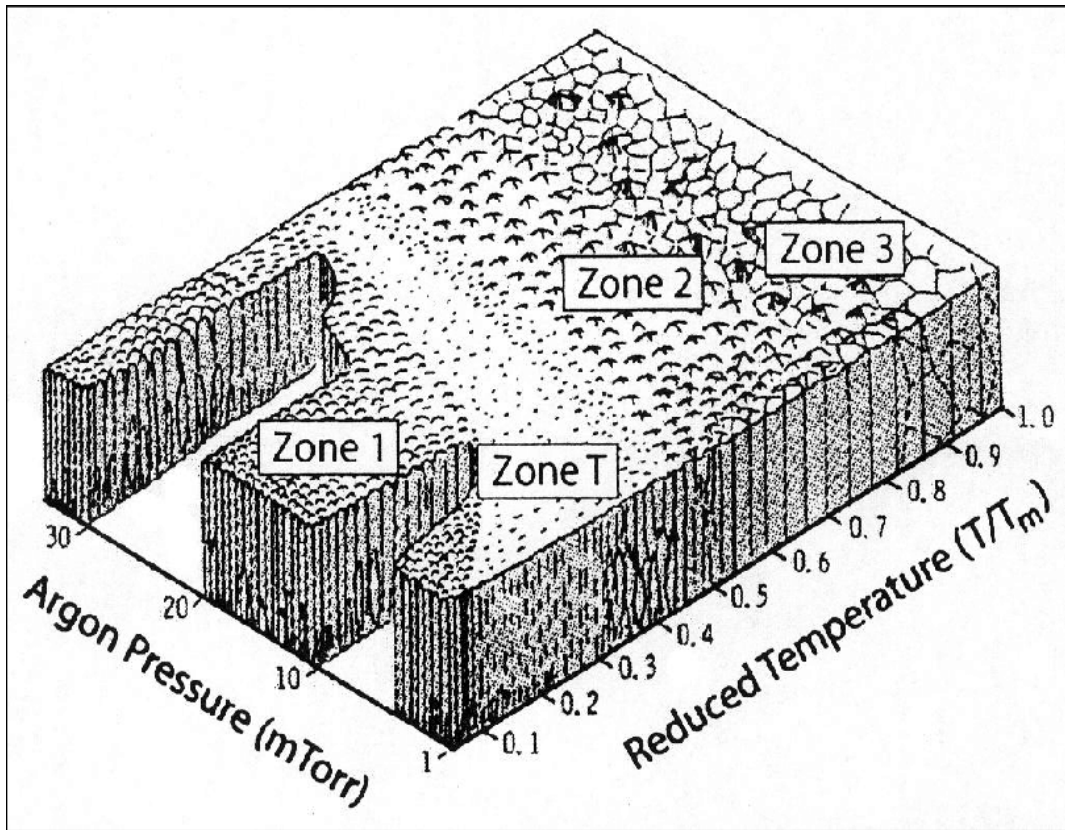


Figure 5.5 – Thornton structural model for films, produced by sputtering [60].

According to the Thornton model, depending on the technical parameters, types of the film growth can be divided onto four zones.

Zone 1. The film structure in the cross-section is cone columnar crystallites with intermediate pores. Specific crystallite structure formation is caused by the low substrate temperature and the low surface diffusion coefficient of absorbed atoms. High roughness of the deposit can be explained by anisotropic conditions of nucleation and formation of the crystallites.

Zone T. Transition zone between zone 1 and zone 2 can be characterised by the crystallite structure, similar to the zone 1, but with less fibrous crystallites and higher density of the film. The films, produced in this zone, are characterised with good mechanical properties, high density in respect to

zone 1, high microhardness, reflectivity, and tensile stress. Dense films with physical properties, which corresponds to the zone T, can be obtained using low sputtering pressure about 0.001 mbar. The low sputtering pressure moves zone T to the lower reduced temperature and allow produce dense films at low $T/T_m$.

Zone 2. Film in this zone is characterised with dense columnar structure and smooth surface. Specific crystallite structure can be explained with growing of the grain size due to the film forming temperature increase.

Zone 3. Structure of the deposits, formed in the zone 3 characterised by equiaxial crystallites, formed at high substrate temperatures and in the dominance of the lattice diffusion. The hardness of the thin films, formed in zones 2 and 3 is higher, then in 1 and T [61].

## 5.5. Internal stress in thin films.

All the metallic and inorganic thin films are in the state of stress. The total stress of a thin film is composed of a thermal stress and an intrinsic stress. The thermal stress occurs due to the difference in the thermal expansion coefficient of the coating and substrate materials. The intrinsic stress is due to the accumulative effect of the crystallographic flaws that are built layer by layer during deposition. The internal stresses in thin film can seriously influence on the deposit properties.

Thermal stress occurs during temperature change of the deposit, that takes place at the final deposition stages or during annealing cycles. Thermal stress can cause material diffusion inside the deposit with further holes or defects production. Intrinsic stresses in the films are similar to the ones, formed in the bulk materials. This total stress compound is associated with various lattice defects, created by deformation.

An idealized representation of the total stress generated in the thin film as function of $T/T_m$ is shown in figure 5.6, where T is deposition temperature and $T_m$ is the coating material melting point.
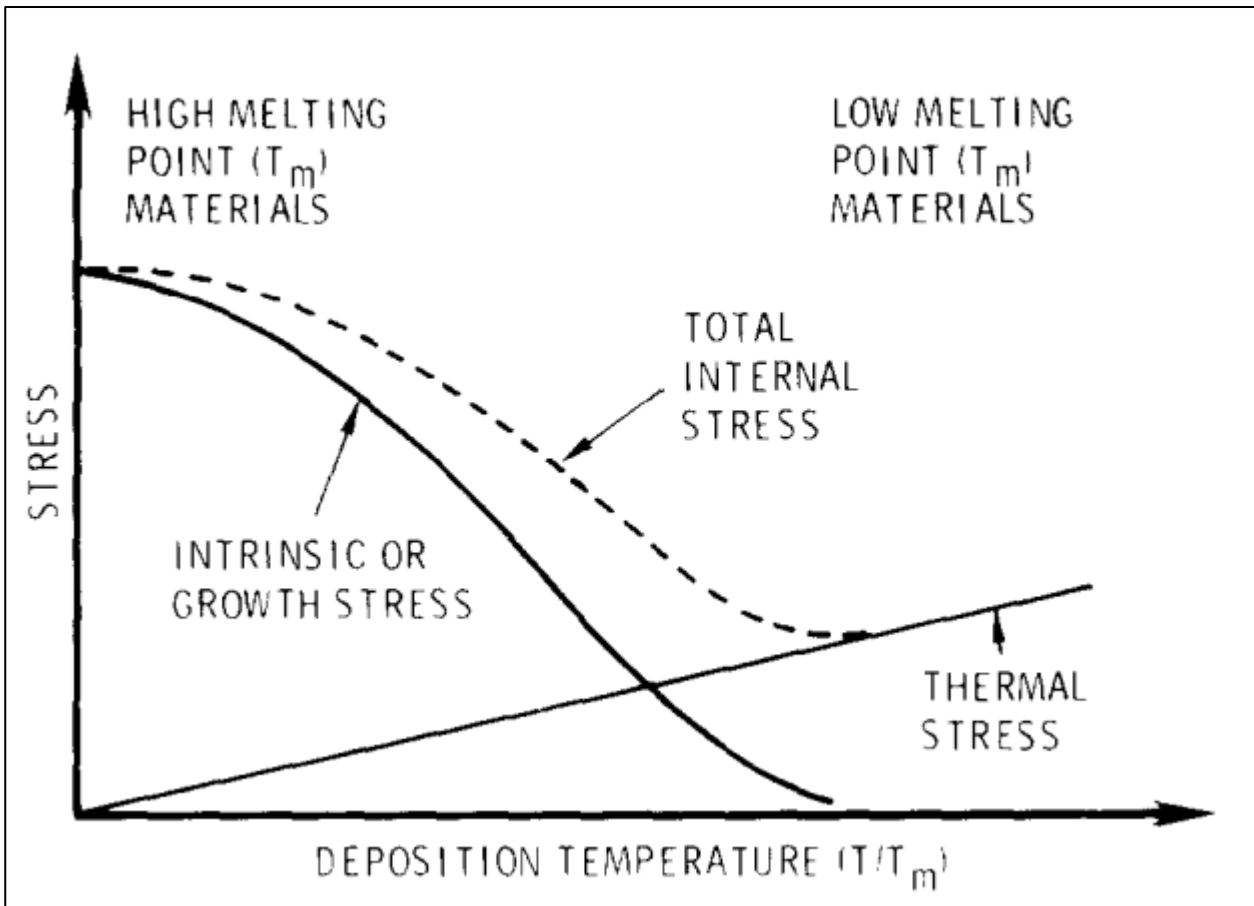
Figure 5.6 – Schematic representation of intrinsic and thermal stress contributions [62].

The sputtering temperature $T$ is assumed to be higher, then the final temperature of dissemblance (room temperature) so the tensile stress is generated during the substrate cooling down. At low $T/T_m$ the intrinsic stress is the dominant part of the total internal stress. The intrinsic component is reduced when $T/T_m$ exceed 0.25 – 0.3 and with further increase of the deposition temperature thermal stress becomes dominant.

High internal stress in the niobium film cause degradation of the superconducting performance of the deposit. Total thin film stress is strongly dependant on the deposition parameters. Decreasing of the film stress is important parameter, that should be considered during the deposition process set-up.

Increasing of the deposition temperature can be good solution also for the niobium thin film internal stress decrease. Several research works showed also promising results in stabilisation of the internal film stress by the sputtering temperature growth. Deposition of the different materials with cylindrical magnetron showed constant decrease of the internal thin film stress with $T$ increasing (figure 5.7).
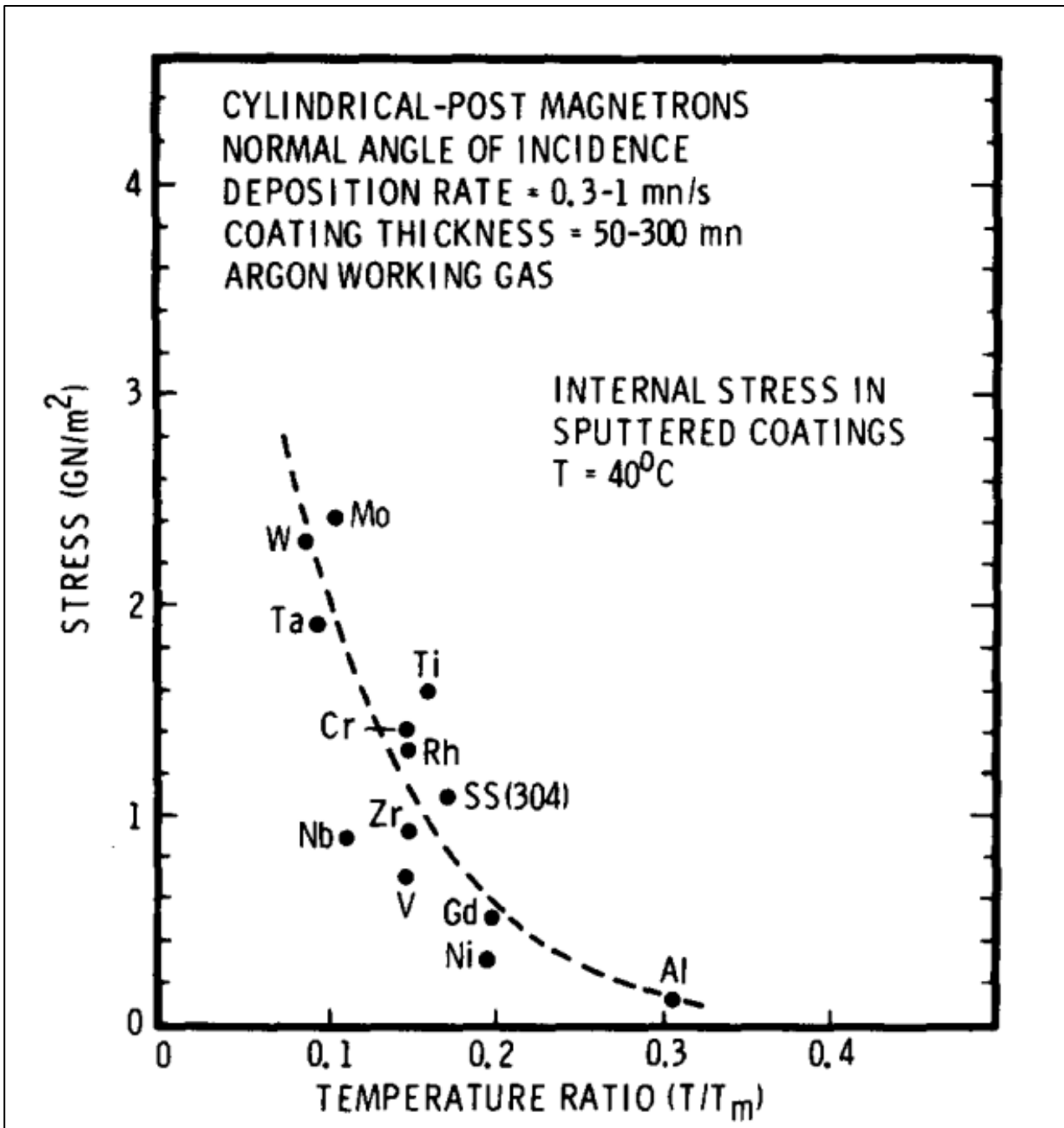
Figure 5.7 – Dependence of the internal stress in the metal coating onto temperature ratio [62].

Another factor, that causes stress in thin films is sputtering parameters. The film`s intrinsic stress is the cumulative result of chemical and microstructural defects produced during coating forming. It can be divided on tensive and compressive stress, which can be generated due to physical vapour deposition process. Excessive stress can produce film cracking and desorption due to tensile stress, while compressive stress can cause film decohesion by buckling. Between the other, intrinsic stress can be caused by incorporation of oxygen, hydrogen, water vapor or inert gas in the crystallite deposit

lattice [63]. For that reason, cleanliness and low base pressure of the sputtering system is fundamental for obtaining low stress thin films.

Thin film stress of the sputtered niobium films can be changed by varying of the argon pressure. Dependence of the intrinsic film stress nature onto argon pressure is showed on figure 5.8.
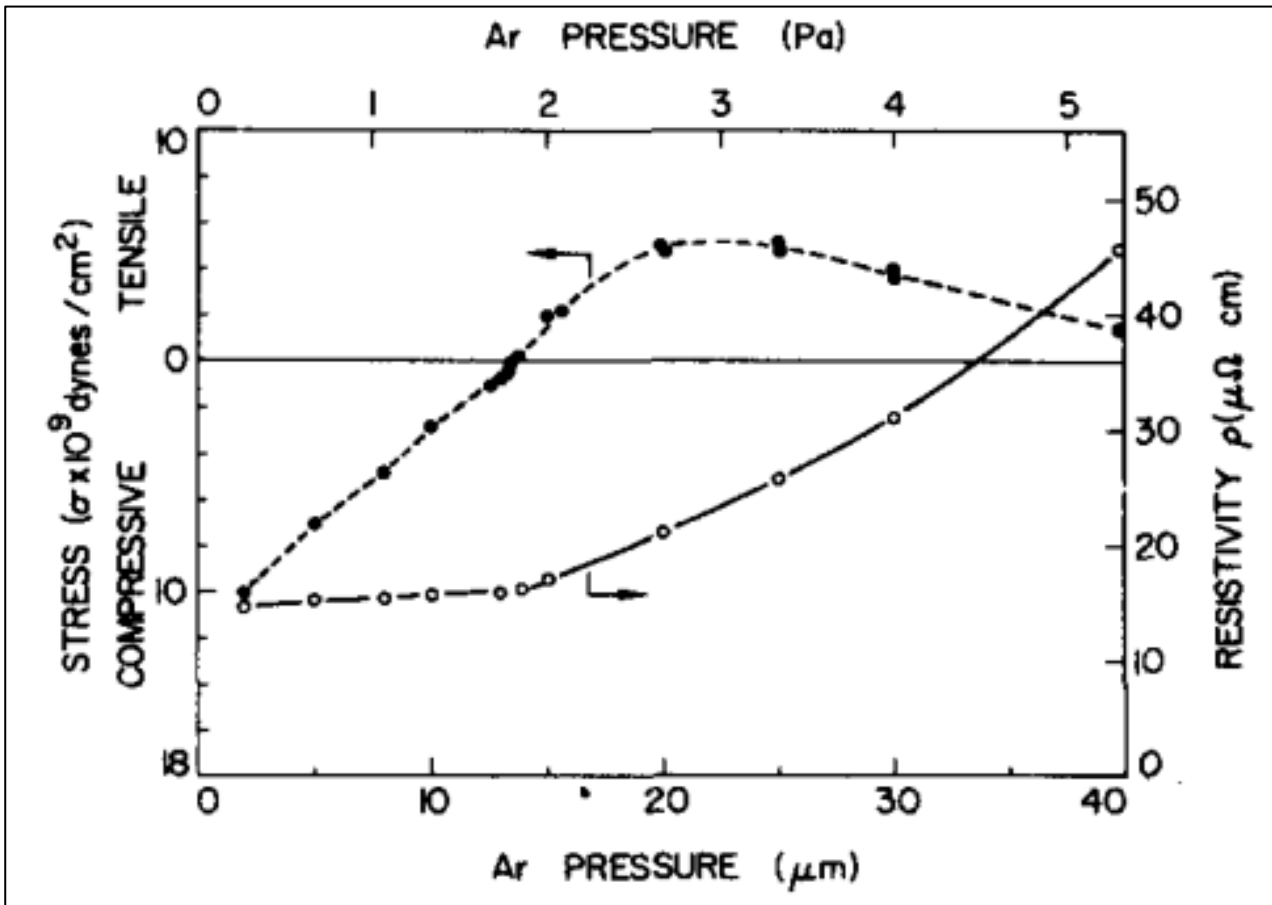


Figure 5.8 – The stress ( ● ) and the room temperature resistivities ( ○ ) of niobium films prepared at various pressure [64].

Internal stress is quite sensitive to the argon pressure. At low deposition pressure, compressive stress is dominant, but with increasing argon pressure to transition value of 1,9 Pa (0,019 mbar) stress starts to be tensile. Further increase to 2.7 (0,027 mbar) Pa causes tensile stress to reach its maximum. After that deposition pressure growth decrease tensile stress of the niobium coating [64].

## 5.6. Characterisation techniques

For characterisation of the structural, physical and superconductive parameters of the deposited niobium thin films before the ALPI QWR production several techniques and apparatus were used. Thickness of the coating was defined for the deposition rate evaluation. Microstructure, $RRR$ and $T_c$

of the niobium deposit were analysed for evaluation of the uniformity and superconductive properties of thin films.

## 5.6.1. Thickness measurement

Thickness measurement of the produced niobium thin films is made for characterisation of the deposition rate of the sputtering system at certain parameters:

$$D.R. = \frac{Coating\ thickness}{Sputtering\ time} \qquad (5.2)$$

Thickness is measured with profilometer DEKTAK 8. Profilometer is an apparatus, that drags a stylus and records the topological profile of the surface. Profilometer is also a device for evaluation of relative surface roughness. DEKTAK 8 can also operate in either contact or non-contact modes and may use optical or stylus techniques to make the measurement [65].

The profilometer DEKTAK 8 has the following features:

1. Combines high repeatability, low-force sensor technology, and advanced 3D data analysis;

2. 7.5 angstrom, 1 sigma step height repeatability and a vertical range of up to 1 mm;

3. Scan lengths range is from 50 μm to 200 mm;

4. Scan speed range is from 3 to 200 seconds;

5. Low force sensor option offers stylus forces down to 0.03 mg;

6. Maximum sample thickness, that can be measured, is 76.2 mm. and weight is 2.5 kg;

7. Profilometer equipped with two cameras: top – down view and 45° view.


Front view of the profilometer, used for the thin films thickness measurements is shown on figure 5.9.
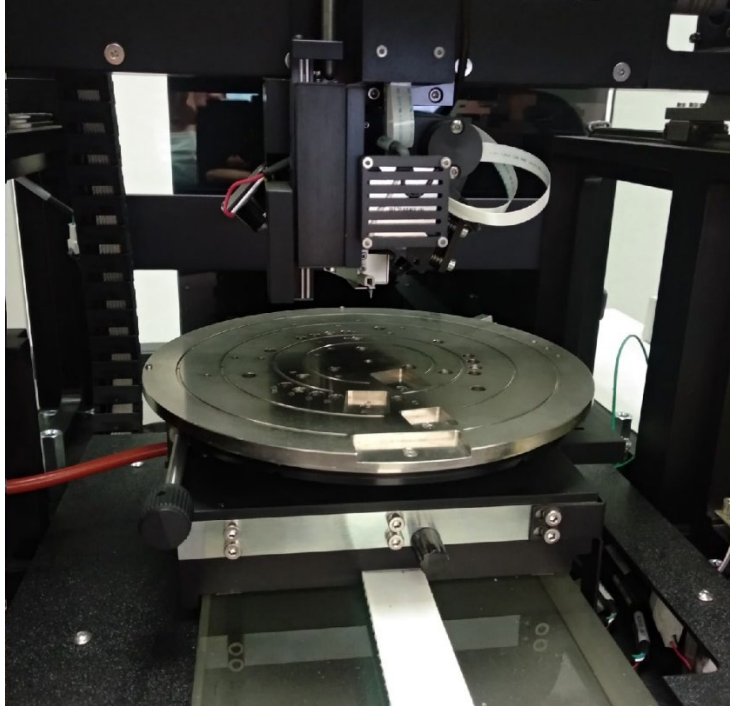
Figure 5.9 – Front view of the DEKTAK 8 profilometer.

## 5.6.2. RRR and $T_c$ measurements

Superconductive properties of the produced niobium thin films are characterised with the measurements of RRR and $T_c$.

The residual resistivity ration (*RRR*) is a common indicator of the level of cleanliness of the superconductive films. The main impurities, residual gasses, hydrogen and oxygen inside of the crystalline structure of the films act as scattering centres for unpaired electrons and reduce the RRR. High RRR values indicate high material cleanliness for recrystallized materials and are defined by the equation:

$$RRR = \frac{R_{300K}}{R_{10K}}$$
(5.3)

In the practical estimation, there are several experimental methods for *RRR* and $T_c$ definition:

1. DC-method for RRR determination at $T_c$ (for niobium $T_c \sim 9.3$ K);
2. DC-method for RRR determination by extrapolation electrical resistivity curve *ρ(T)* to 4.2 K.;
3. DC-method for RRR determination by supressing the niobium superconductive behaviour with a magnetic flux and extrapolation *ρ(B)* curve at 4.2 K to the zero magnetic field *B*;

4. AC-eddy current method as a non-destructive method performed directly on the cavity surface;

5. AC inductive method for *RRR* determination [34].

General DC-method is used for the definition of the *RRR* and $T_c$ of the superconductive niobium thin films.

The temperature was measured by the Cernox temperature sensor. 4-pins system (Figure 5.10a) is put in contact to the surface of the niobium coating, deposited onto the quartz sample. The warm-up and cool-down procedures are performed by inserting the holding system with the sample (Figure 5.10 b) into the liquid helium Dewar. A DC current of 5 mA is applied to the sample and the resulting voltage is measured to define the resistance. A dedicated software acquires the data and builds the plot of the temperature dependence of the measured resistance during cooling down of the sample.
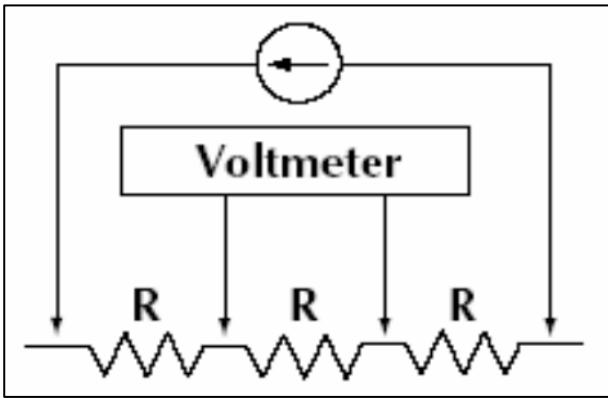


(a)                                                             (b)

Figure 5.10 – Scheme of the 4-point method (a) and top view of the quartz sample holder (b).

$T_c \pm \Delta T_c$ was measured from the electrical resistivity curve $\rho(T)$ by the following equation:

$$T_c = \frac{T(90\%) + T(10\%)}{2}$$

(5.4)

The error $\Delta T_c$ was calculated with the equation:

$$\Delta T_c = \frac{T(90\%) - T(10\%)}{2}$$

(5.5)

Where *T(90%)* and *T(10%)* are the temperatures, which corresponds to the 90% and 10% of the resistance before the transition relatively.

## 5.6.3. Microstructural analysis

Microstructural analysis of the produced niobium thin films is done using scanning electron microscope (SEM) XL-30 TMP.

Scanning electron microscope is an apparatus, which provides information about surface topography, crystalline structure, chemical structure and electrical behaviour of the analysed films (specimen). In the SEM XL-30 TMP the incident electrons from the gun have energies from 2 to 40 keV. Maximum resolution of the tool is from 3.5 nm to 25 nm depending on the incident electron energy.

XL-30 TMP is equipped with the tungsten filament, which produces thermal emission electrons. There are two objective lengths of 45° and 60° for magnification of the image.

There are cathodoluminescence detector, Robinson backscatter electron detector and various EDX detectors, which collect data of the emission of secondary electrons, Auger electrons, X-rays and light and send it to the software.

# EXPERIMENTAL PART

Experimental research activity, carried out in the framework of the ALPI upgrade project, is described in the second part of this thesis.

Three vacuum systems were used during the research activity. Two vacuum systems were used for niobium deposition of the copper QWR cavities and copper plates. A test cryostat was used for the RF measurement of the coated QWR cavities. Layouts, 3D-models, upgrade and assembling activity of the vacuum systems, used for the high-β Nb/Cu QWR cavities and plates deposition and superconductive performance characterisation, are described in chapter 6.

The quality of the deposited niobium thin film is in strict dependence on the sputtering parameters of the deposition process. Niobium deposition tests onto quartz samples were done for the characterisation of the sputtered thin film properties. Thin films parameters were compared for verification of the optimal sputtering parameters. The definition of the sputtering parameters, used for the QWR cavities and plates further production, is described in chapter 7.

The production of the high-quality Nb/Cu QWRs and plates requires appropriate substrate preparation. Machining and preparation of the copper substrate surface before the niobium deposition is a complicate process, which consists of several surface treatment techniques. Niobium deposition is a long-term process, which needs a correct set-up and constant control. The methodology, used for the QWR cavities and plates substrate preparation and niobium coating processing, is described in chapter 8.

Radiofrequency measurements at 4,2 K are made for the definition of the coated high-β QWRs superconducting performance. The results of the RF measurements characterise the quality of the coated QWRs. The methodology of the RF measurements, with the obtained results, are mentioned in chapter 9.

The comparison of the measured results with superconductive performance of the QWRs, used in currently active projects, can characterise the quality of the produced Nb/Cu high-β QWR cavities. The analysis of the niobium deposition process and RF measurements results of the coated Nb/Cu high-β QWR cavities are described in chapter 10.

# Chapter 6

# VACUUM SYSTEMS

## 6.1. Introduction

The cleanliness of the vacuum system is fundamental for the coated quarter wave resonator production with high superconductive performance. High performance of the produced QWRs requires high-quality niobium coating. The ultra-pure niobium deposit is in strong dependence with the ultra-high vacuum of the sputtering system. Higher vacuum and a good preparation of the system causes lower amounts of impurities in the niobium deposit, better adhesion between deposit and the substrate and higher quality of the produced QWR in general.

Vacuum systems for sputtering and cryostat measurements of ALPI Nb/Cu QWR cavities remained in inactivity for more than 15 years. These systems were used for production and evaluation of the medium-β Nb/Cu QWR cavities in the past [16]. For the production of the cavities with different shape, cleaning, upgrade and modification of these systems were necessary. Three main systems were used for the production and characterization of the high-β Nb/Cu QWR cavities: the cavity sputtering system, the plates sputtering system [66] and the test cryostat. Layouts, modifications and activities done for the assembling of these vacuum system will be presented in this chapter.

## 6.2. Cavity sputtering system

## 6.2.1. Layout of the system

Bias diode sputtering is a complicate technique, which requires the usage of an appropriate apparatus for the deposition and control performance. In paragraph 6.2 layouts, 3-D modelling and upgrade activities of this system. will be described

The layout of the cavity sputtering vacuum system is shown in figure 6.1.

| Scroll pump | ⊚ |
|---|---|
| Turbo molecular pump | ◎ |
| Gauge | Ⓐ |
| Gate valve | ⋈ |
| Leak valve | ⋈ |
| Manual valve | ⋈ |
| Manometer | ⊘ |
| Reducer | ⤼ |
| Flow measurement | ⊗ |
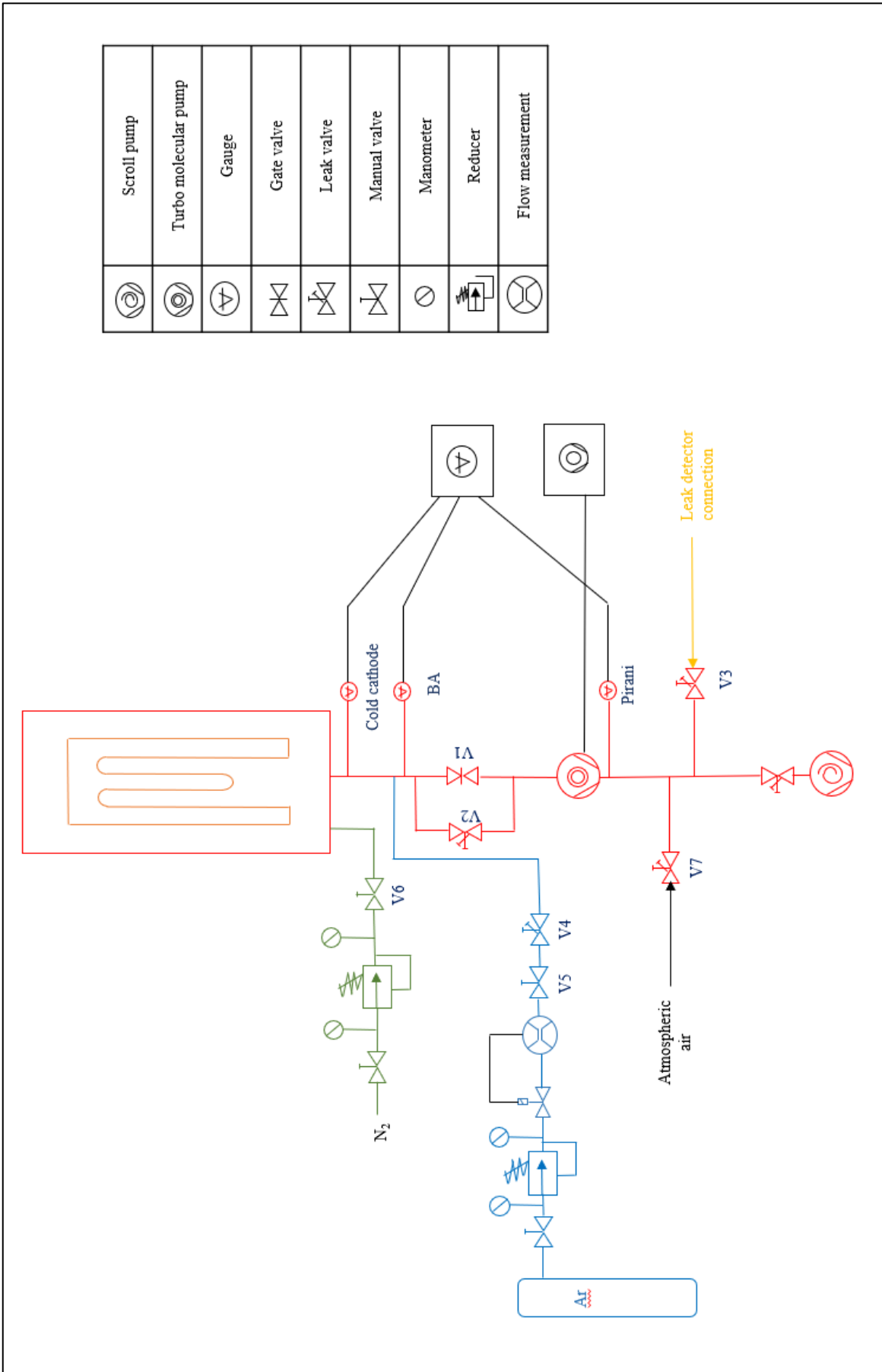
Figure 6.1 – Layout of the cavity sputtering vacuum system.

The vacuum chamber is connected to the pumping line, which starts from the gate valve Varian V1. The by-pass with the leak valve V2 is used to decrease the gas flux during sputtering and protects the turbo molecular pump from damages. On the other side of the gate valve, a pumping module is connected, consisting of a turbomolecular levitation and primary scroll pump. The characteristics of the vacuum pumps used in this system will be described in paragraph 6.2.3.

The leak detector unit is connected to the vacuum line between the turbo molecular and the primary pumps through the leak valve V3.

The deposition process of niobium is made using the extra pure argon gas. The argon inlet gas line is connected to the leak V4 and shut off V5 valves, which are connected to the vacuum system. Inlet pressure of both gas lines, connected to the system, is controlled by the pressure regulators. An additional leak valve V4 in the argon inlet line increases the possibility to precisely control of argon flux in the system.

The venting of the chamber is performed with nitrogen gas through the gas line, that is connected to the shut off valve V6. The area behind the gate valve is vented by the atmospheric air, which is connected to the leak valve V7.

The application of the negative potential to the target material is necessary for the initialisation of the ions bombardment of the niobium cathode and deposition processing. The use of the bias diode sputtering technique complicates the sputtering system. A scheme of the electric connection of the QWR sputtering system is shown in figure 6.2.
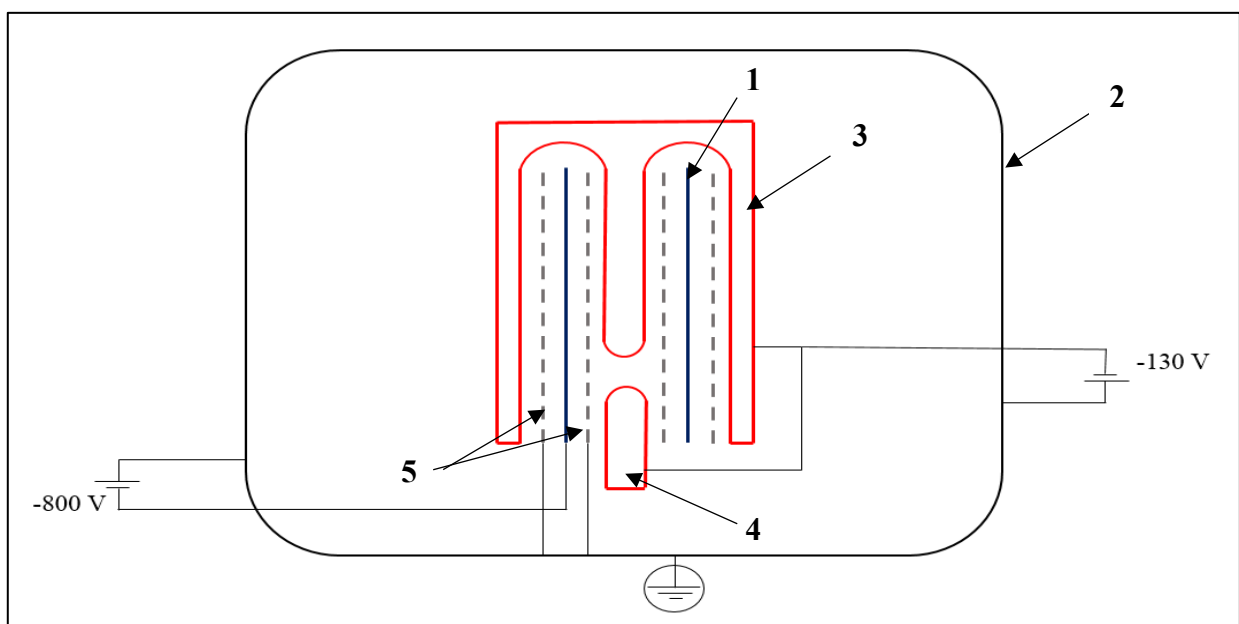


Figure 6.2 – Scheme of the QWR sputtering system electric connection.

As shown in figure 6.2, voltage of -800 V is created between niobium target *(1)* and grounded chamber *(2)* for performing the bombardment of the niobium material by the argon plasma. The application of the negative potential to the QWR cavity *(3)* and counter electrode *(4)* in respect to the grounded chamber with -130 V is performed for processing the bias diode sputtering. Grounded titanium net *(5)* is placed between the niobium and QWR surface for biased deposition performance.

A counter electrode is assembled to the vacuum system in front of the QWR inner conductor for obtaining uniform coating thickness in the bottom part of the copper substrate. The influence of the counter electrode position in respect to the QWR onto the quality of the obtained niobium coating will be described in chapter 10. After schematic projection, 3D model of the QWR sputtering system is made.

## 6.2.2. 3D model of the internal part of the vacuum chamber

The 3D layout of the cavity sputtering system is designed using Solidworks® software. Cross section of the side (a) and bottom (b) view of the cavity sputtering system are shown in figure 6.3.



(a)                                                                                          (b)
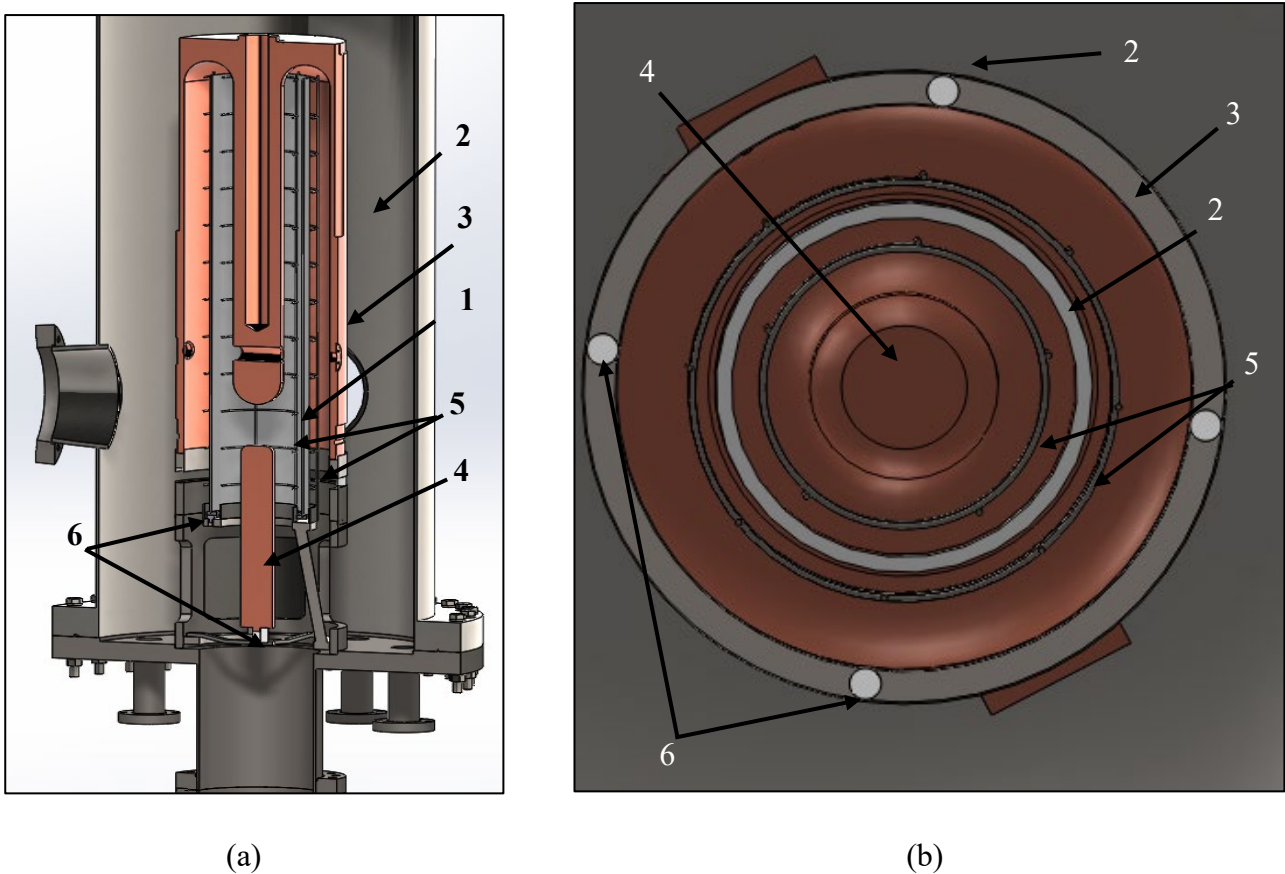
Figure 6.3 –Section view of the side (a) and bottom (b) of the cavity sputtering system.

Niobium cylinder (1), QWR cavity (3) and counter electrode (4) are assembled on the ceramic parts (6) to avoid the electric contact between the parts of the system with negative potential and grounded chamber (2). Titanium nets (5) between niobium target and QWR cavity are in direct contact with the grounded vacuum chamber.

The next stage of the QWR sputtering system construction after designing is refurbishing and upgrade, described in the next paragraph.

## 6.2.3. Refurbishing and upgrade of the system

Total refurbish and upgrade of the cavity sputtering system is needed before processing of the QWR sputtering.

All the vacuum system was disassembled, vacuum chamber and main flange were cleaned in ultrasound bath with the soap Rodasteel® and cleaned vacuum chamber was assembled [67]. Upgraded vacuum system for high-β QWR sputtering is shown on figure 6.4.
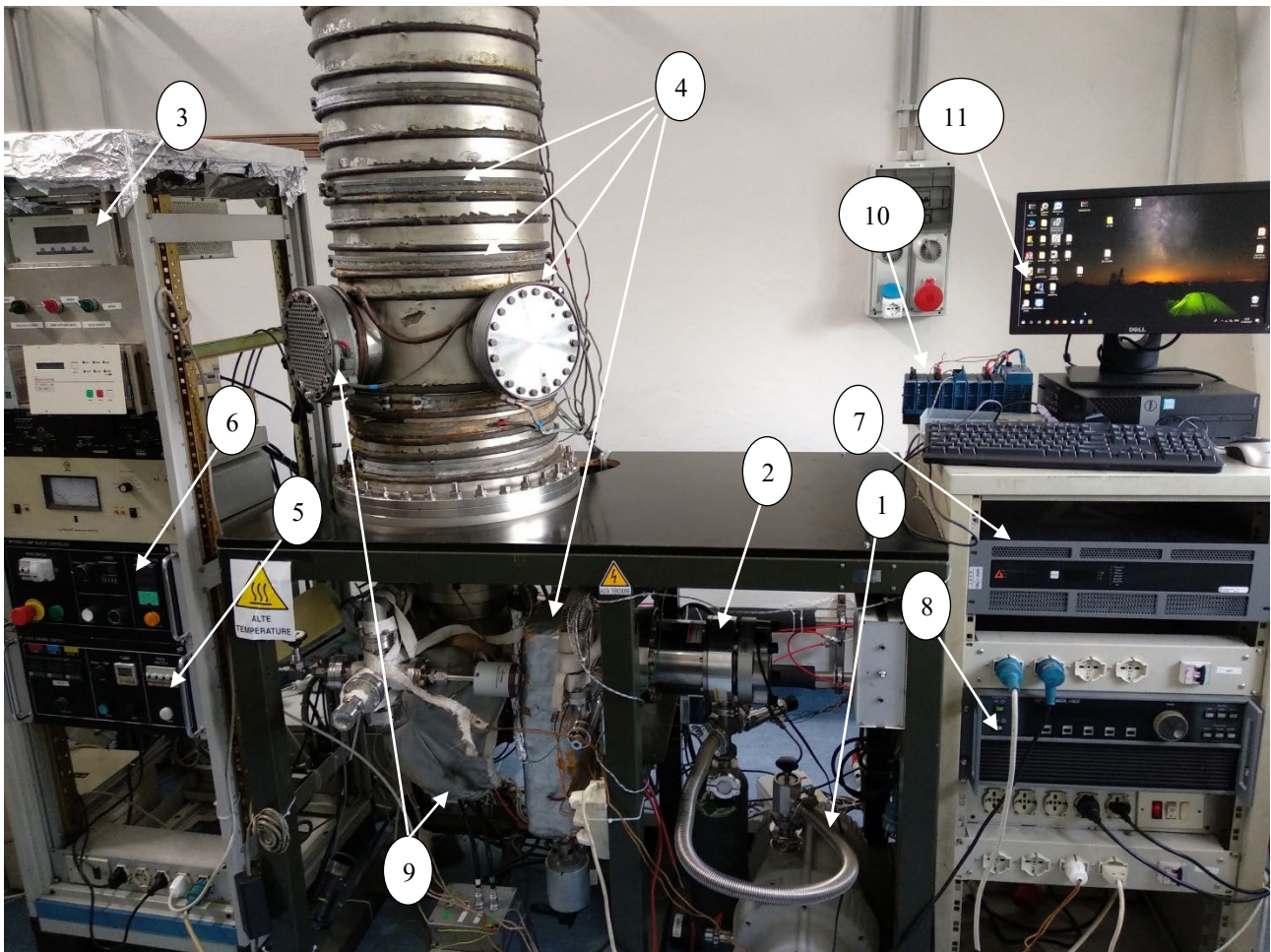


Figure 6.4 – View of the upgraded cavity sputtering system.

All the pumping systems were changed. It was decided to use oil-free scroll pump Edwards XDS 35i *(1)* with peak pumping speed 35 $m^3h^{-1}$, which reaches the maximum vacuum $1 \cdot 10^{-2}$ mbar. Using of the oil-free pump instead of the rotary pump is fundamental to avoid contamination of the vacuum system with oil due to the backstreaming effect.

Turbo molecular pump Edwards STP-451 *(2)* with rated speed 48000 rpm is used for reaching ultra-high vacuum. This pump is equipped with magnetic levitation bearing. All the contact between the rotor and the remainder of the pump is eliminated. Levitational turbo molecular pump is oil free, which is the main advantage of using this pump for avoiding vacuum system oil contamination.

Distance between internal parts of the vacuum chamber (QWR, niobium target, titanium nets) is small and external vibration of the system can cause shift of the assembled parts in respect to each other.

Three types of vacuum gauges were installed for control of the vacuum in the sputtering system at the different pressure regions: Pirani TPR 280 (measurement range: 1000 mbar - $5 \cdot 10^{-4}$ mbar), Pirani/Bayard-Alpert ion gauge PBR 260 (1000 mbar - $5 \cdot 10^{-10}$ mbar) and Cold Cathode gauge IKR 270 ($1 \cdot 10^{-2}$ mbar - $5 \cdot 10^{-11}$ mbar). All the vacuum gauges were connected to the Pfeiffer Maxigauge® TPG 366 *(3)*.

Baking process of the vacuum system is needed for removing the humidity and decreasing the amount of residual gasses in the system by heating. It is possible to reach lower pressure in the lower period of time with baking processing. Baking system is constructed of heating jackets *(4)*, divided into three independent zones, connected to the u.h.v. baking control unit *(5)*. These structures of the external baking system permit precise control of the baking and ability to heat different parts of the system at different temperatures.

Heating of the QWR cavity during the baking and sputtering processes is made by three internal infrared (IR) lamps with the power of 1000 W each, connected in parallel to the infrared lamp heater control unit *(6)*.

Two gas lines are connected to the sputtering system. Nitrogen is used for venting of the vacuum system and pure Argon gas N60 (99,9999 %) is used for the sputtering process. MKS flow meter with range 100 SCCM is assembled for better control of the argon inlet in the system and stable flux of the inert gas during the sputtering process.

Pinnacle® 12 kW *(7)* and Advanced energy MDX II 15 kW *(8)* power supplies are connected for application of the bias voltage to the substrate and current to the niobium cathode respectively during the sputtering process.

The system is also equipped with two quartz view ports CF 150 *(9)* from the side and from the bottom of the vacuum chamber for better monitoring of the deposition process.

All the electronic control units of the system were connected to the Compact FieldPoint National Instruments® cFP-2200 *(10)* for possibility of automatic control of the system via PC *(11)*.

QWR deposition is a long-term complicate process, which require constant control and data acquisition. Control program in LabVIEW® software was developed for simplification of the deposition processing.

## 6.2.4. Remote control software of the QWR sputtering system.

View of the control software of the sputtering process is shown on figure 6.5.
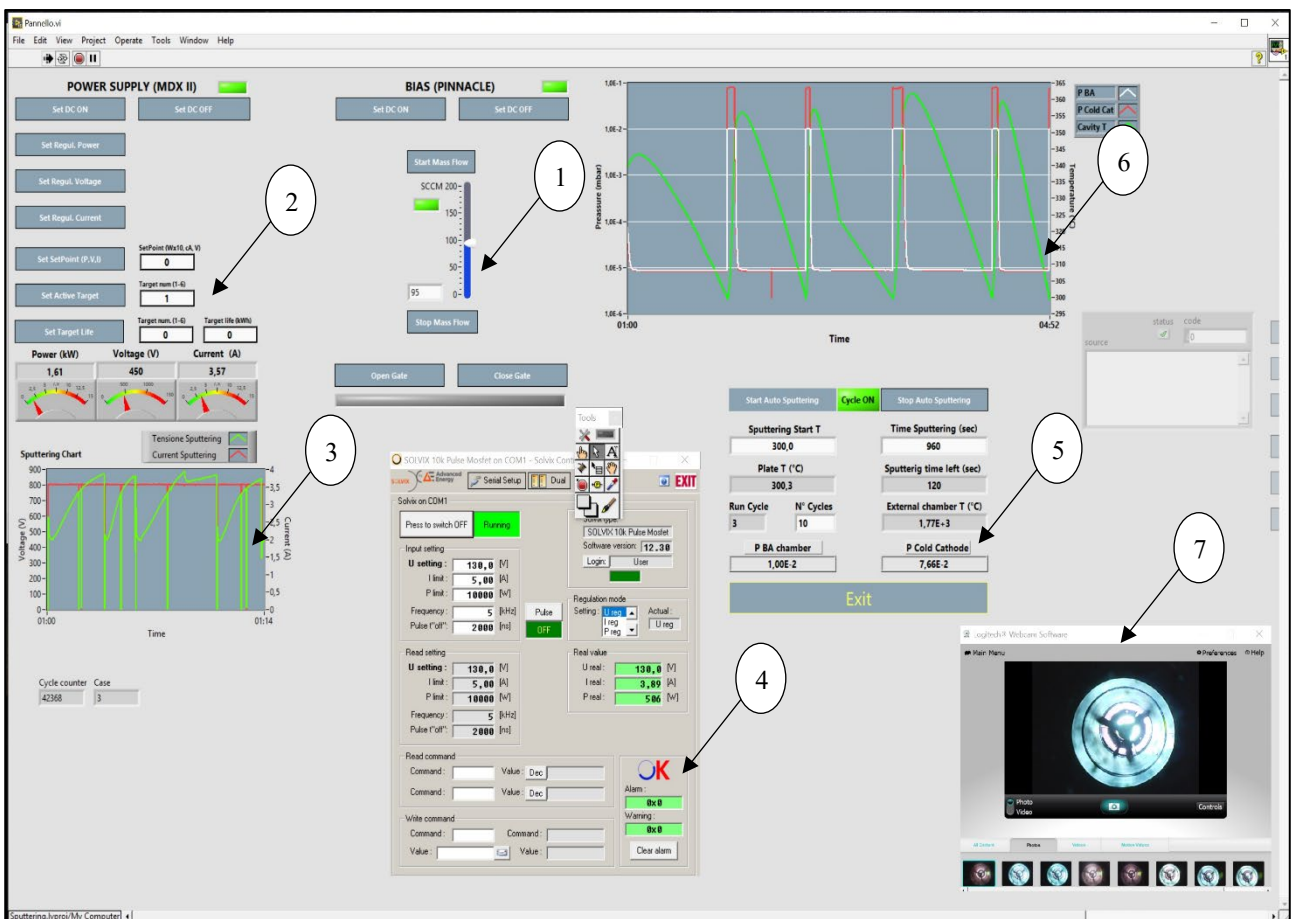


Figure 6.5 – Remote control software of the cavity sputtering system.

LabView program was designed to start the process in automatic mode.

Before the deposition process, all the sputtering parameters are set up in different parts of the software interface. Argon flux value *(1)* is defined to reach the sputtering pressure of the process. Niobium

deposition is performed with constant cathode current, which is set up in the cell *(2)*. Change of the cathode voltage and power can be observed from the graph *(3)*. Bias voltage is set up in the window *(4)*, where also is possible to control real values of bias current and power.

Number of sputtering cycles, QWR initial temperature and sputtering time is defined in the window *(5)*, where also possible to observe pressure of the vacuum system. QWR temperature change and pressure of the system is showed on the graph *(6)*. Overview of the sputtering activity inside the system can be done with the Logitech webcam *(7)*, assembled to the bottom view port of the system.

## 6.3. Plate sputtering system

### 6.3.1. Layout of the system

Bias diode sputtering process is decided to use for the production of the Nb/Cu plates for the ALPI QWR cavities. The layout of the plate sputtering vacuum system is shown on figure 6.6.
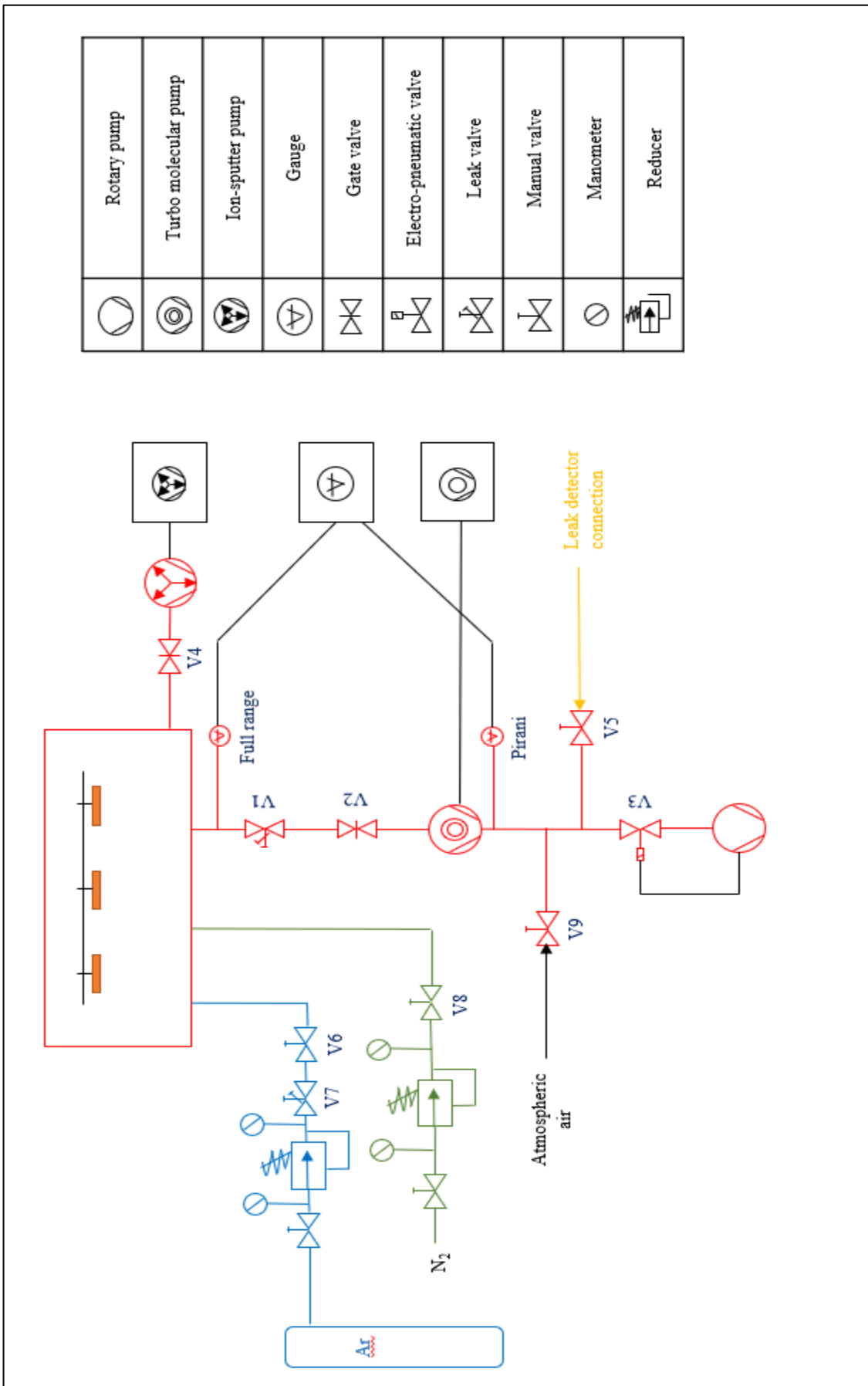
| | |
|---|---|
| Rotary pump | |
| Turbo molecular pump | |
| Ion-sputter pump | |
| Gauge | |
| Gate valve | |
| Electro-pneumatic valve | |
| Leak valve | |
| Manual valve | |
| Manometer | |
| Reducer | |

Figure 6.6 – Layout of the plate sputtering vacuum system.

As it is shown on figure 6.6, vacuum chamber is connected to two pumping lines. Main pumping line starts with the leak valve V1 and gate valve VAT V2. Leak valve V1 is used for regulation of the flux of argon gas, which is transported through the pumping line to the turbo molecular pump. Reduction of the gas flux prevents work of the turbo molecular pump at the high pressure during sputtering process. Rotary pump is connected to the electro pneumatic valve V3. Immediate closing of the valve V3 with stop of the rotary pump prevents backstreaming of the oil to the vacuum system.

An additional pumping line is used for reaching lower vacuum at ultra-high vacuum region, sufficient for the pure niobium deposit production. The additional pumping line is consisted of ion-gauge pump, connected through the VAT gate valve V4 to the vacuum chamber. The gate valve V4 is closed at the system pressure higher, than $10^{-5}$ mbar to prevent damaging of the ion-gauge pump at high pressure.

Pressure of the vacuum system is observed by the pressure sensors, which will be described in the next paragraph. Leak detection module is connected to the line between turbo molecular and rotary pumps through the leak valve V5.

Argon extra pure gas is used to perform the sputtering process. Argon gas line is connected to the vacuum chamber through shut off V6 and leak V7 valves.

After finish of the deposition process, vacuum system is vented by the nitrogen gas in the vacuum chamber region and by atmospheric air in the region of the main pumping line. Nitrogen cylinder is connected to the gas regulator and through the venting shut off valve V8 to the vacuum chamber. Venting of the pumping line by the atmospheric air is made through the leak valve V9.

Bias diode sputtering is complicate process, which requires application of different potentials to different parts of the vacuum system. Scheme of the electric connections for the plate sputtering system is shown on figure 6.7.
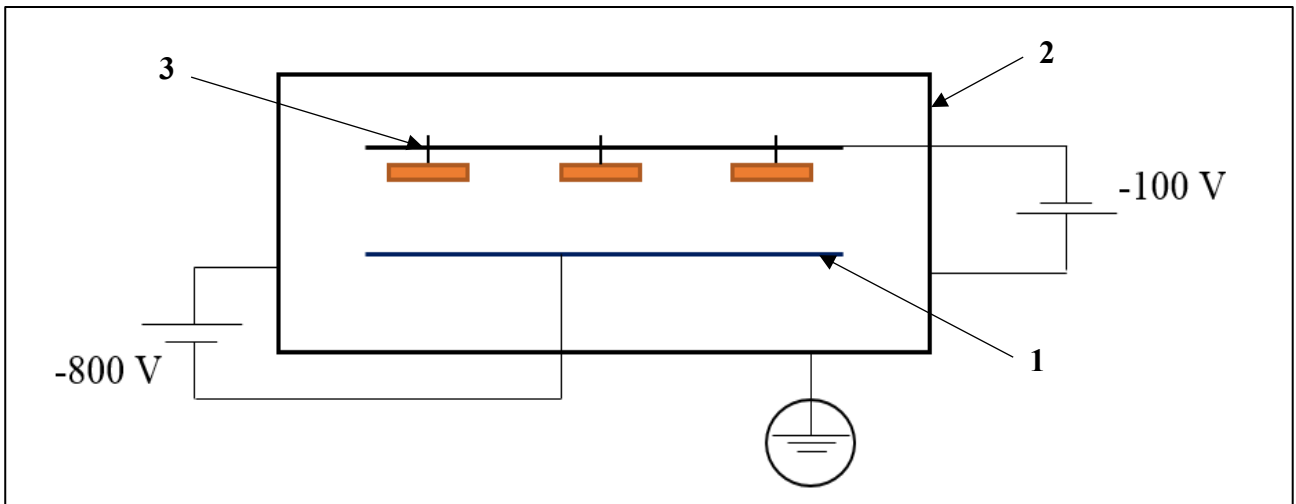
Figure 6.7 – Scheme of the plate sputtering system electric connection.

Sputtering process is performed at the constant cathode current. Voltage of -800 V is created between the niobium target *(1)* and the grounded chamber *(2)* to initialise the argon plasma ions bombardment of the niobium material and proceed niobium deposition.

Bias voltage of -100 V is created between QWR plates holding system *(3)* and vacuum chamber to process bias diode sputtering. Power supplies, described in paragraph 6.2.3 are used to apply negative potentials to the niobium target and copper plates substrate.

The assembly and upgrade of the plate sputtering system was made.

## 6.3.2. Refurbishing and upgrade of the system

Plate production requires simpler vacuum system construction in respect to the QWR sputtering due to planar geometry of the plates for the QWR cavities. It was decided to adapt vacuum system, which was used previously for ALPI RFQ production [66]. External view of the vacuum system for the plate sputtering process and internal view of the vacuum chamber are shown in figure 6.8.

|        |        |
| ------ | ------ |
| (a)    | (b)    |
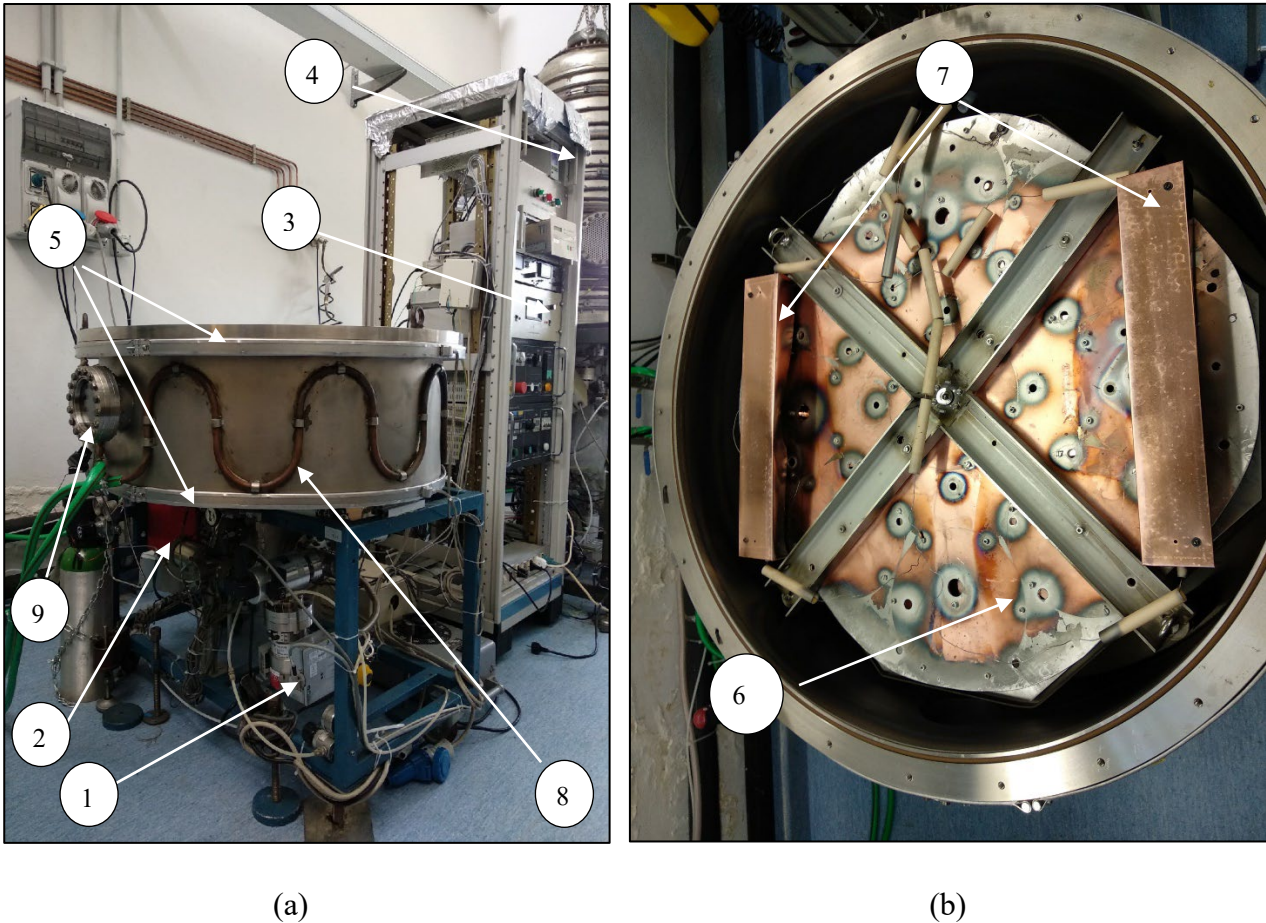
Figure 6.8 – External – (a) and internal – (b) view of the plate sputtering system.

Turbo molecular pump TMU 071 P *(1)* with rated speed 1500 Hz is connected to the control unit DCU 100. To the vacuum chamber is also assembled Varian StarCell® ion-gauge pump *(2),* which is connected to the StarCell® power unit 929-0172 *(3)*. Pumping of the vacuum chamber with turbo molecular and ion-gauge pumps simultaneously permits reaching lower vacuum, that is sufficient for the deposition of the high-quality superconductive niobium coatings.

Pfeiffer full range PKR 251 in the vacuum chamber and Pirani TPR 280 in the pump line after turbo molecular pump are used for the pressure measurements inside the plate sputtering systems. Both vacuum gauges are connected to the Pfeiffer DualGauge TPG 362 *(4)*.

Baking system of the plate sputtering system consists of the heater jackets *(5)*, divided onto 3 zones and connected to the baking control unit.

Plates are assembled to the plate holder *(6)*. Plate holder is mounted in the vacuum chamber in the way, that set-up distance between copper plates and niobium cathode of 20 – 40 mm. Heating of the

plates is processed by two infrared heating lamps *(7)* with power of 1000W, connected in parallel to the infrared lamp heater controller.

During the sputtering process vacuum chamber is cooled down with water circulation through the cooling line *(8)*. Quartz view port *(9)* was connected to the side of the chamber for possibility of constant observe of the sputtering process.

## 6.4. QWR test facility

## 6.4.1. Layout of the system

Cryostat system is used for characterisation of the superconductive performance of the coated QWR cavities. Schematic layout of the test cryostat is shown on figure 6.9.
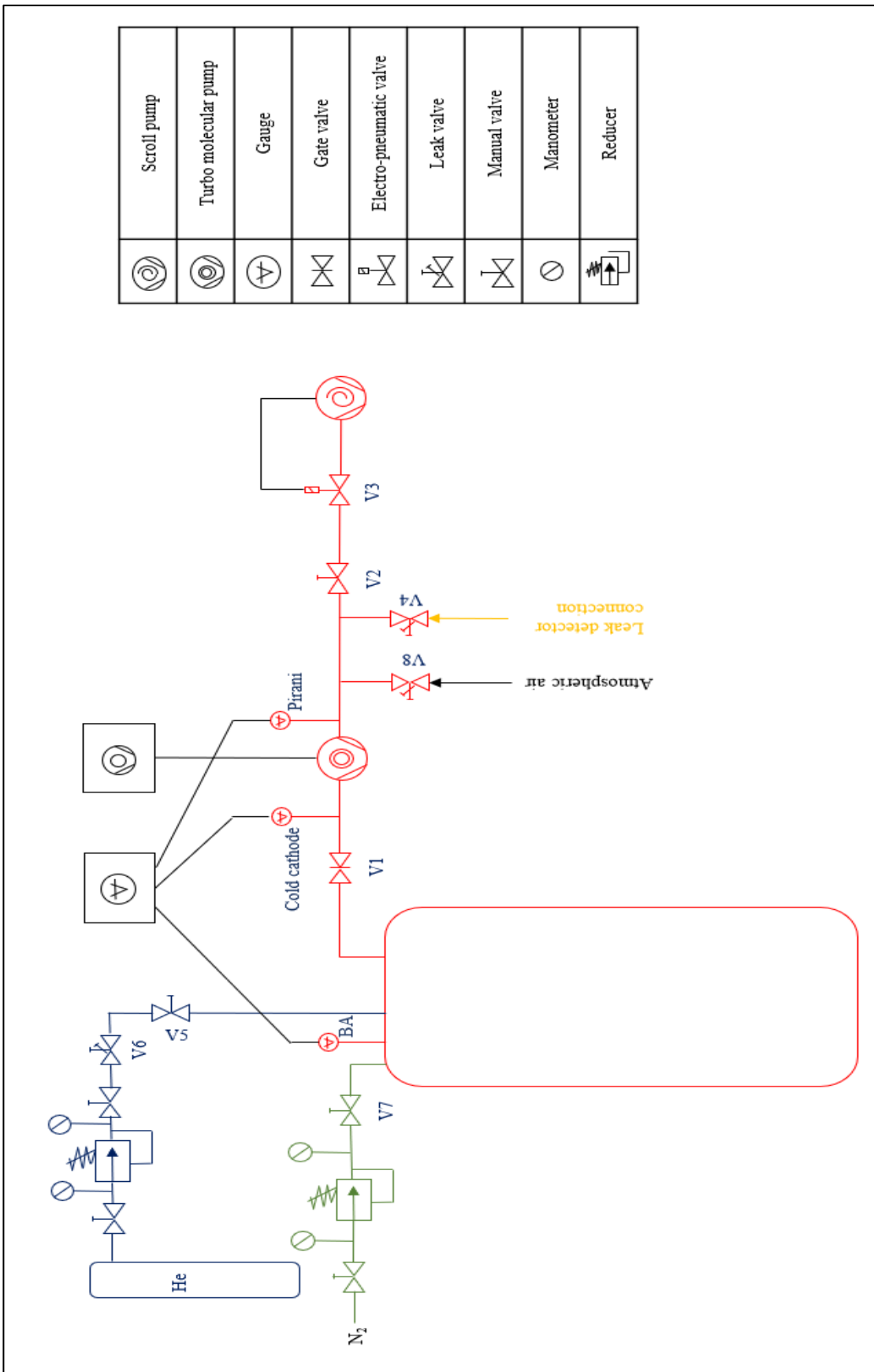
Figure 6.9 – Layout of the cryostat vacuum system.

Vacuum chamber of the cryostat is connected to the pumping line. Turbo molecular and scroll pumps are connected to the gate valve V1. Shut off V2 and pneumatic V3 valves are assembled between the turbo molecular pump and the scroll pump.

Pneumatic valve V3 is connected to the scroll pump, so, when the pump is switched off, V3 immediately close for preventing of the backstreaming of the air from the scroll pump, losing vacuum and damaging turbo molecular pump.

Leak detection unit is connected to the pumping line between turbo molecular and scroll pumps through the leak valve V4.

Two gas lines are connected to the vacuum line: high-pure helium and nitrogen gasses. High-pure helium gas is normally used for the low-temperature conditioning of the cavity (the process will be described in chapter 9). Helium gas line is connected to the cryostat chamber through the shut off V5 and leak V6 valves.

Venting of the vacuum chamber is made by the nitrogen gas, connected through the shut-off valve V7 to the system. Venting of the chamber beside the gate valve is made by atmospheric air, connected through the leak valve V8.

Test cryostat is a complicate system, which is constructed to perform RF measurements at low temperatures with usage of liquid helium and liquid nitrogen for cooling down of different system parts. Scheme of the cryostat vacuum chamber is shown on figure 6.9.
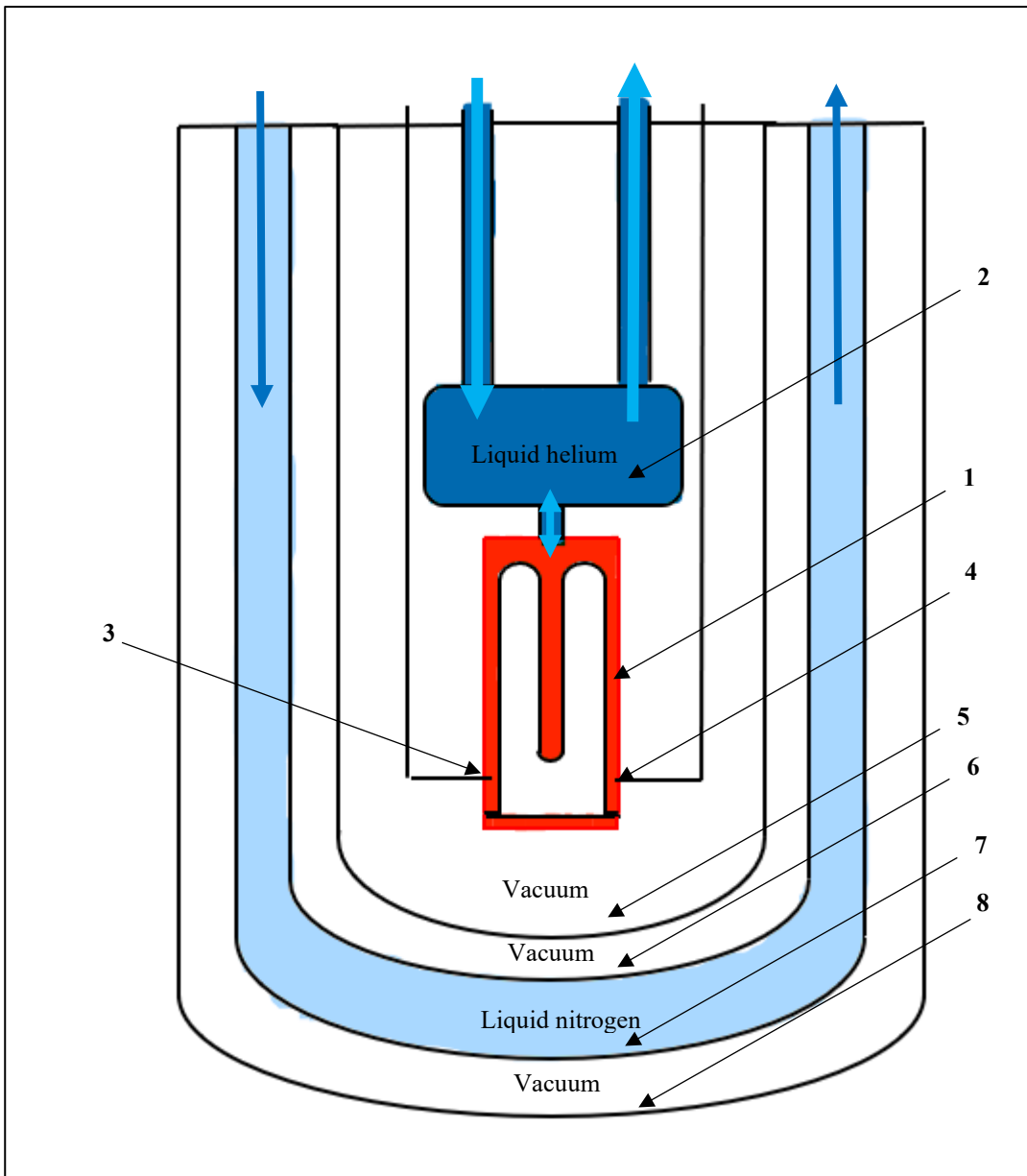
Figure 6.9 – Scheme of the cryostat vacuum system.

As shown on figure 6.9, Nb/Cu QWR cavity with plate *(1)* is connected to the liquid helium dewar *(2)* for cooling down of the cavity. Constant refill of the helium dewar with liquid helium is made during the RF measurement for maintaining the cavity temperature at 4,2 K. Coupler *(3)* and pick-up *(4)* antennas are connected to the cavity for transfer of the signal between the superconductive unit and the RF measurement system.

All the measured unit is placed in the vacuum chamber *(5)*. Three shields were constructed to the vacuum chamber walls to maintain the QWR temperature stable during the cryostat measurements and decrease liquid helium evaporation: internal vacuum shield *(6)*, liquid nitrogen shield *(7)*, external

vacuum shield *(8)*. Internal and external vacuum shields remain in static vacuum, meanwhile in the shield between them is transferred liquid nitrogen for cooling down of the chamber walls and stabilisation the vacuum chamber temperature. More detailed description of the preparation procedure for the RF measurements is written in chapter 9.

After schematic projection, refurbishing and upgrade of the cryostat was made.

## 6.4.2. Refurbishing of the cryostat

Cryostat system is used for the characterisation of the superconducting performance of the coated ALPI QWR cavities. There was a possibility to use the vacuum system, that was used for the RF measurements of the medium-β QWRs, sputtered 15 years before for the ALPI LINAC. The system for the QWRs testing needed modification and replacing of the old units onto the new ones after long term of inactivity [68]. View of the modificated cryostat system is shown on figure 6.10.
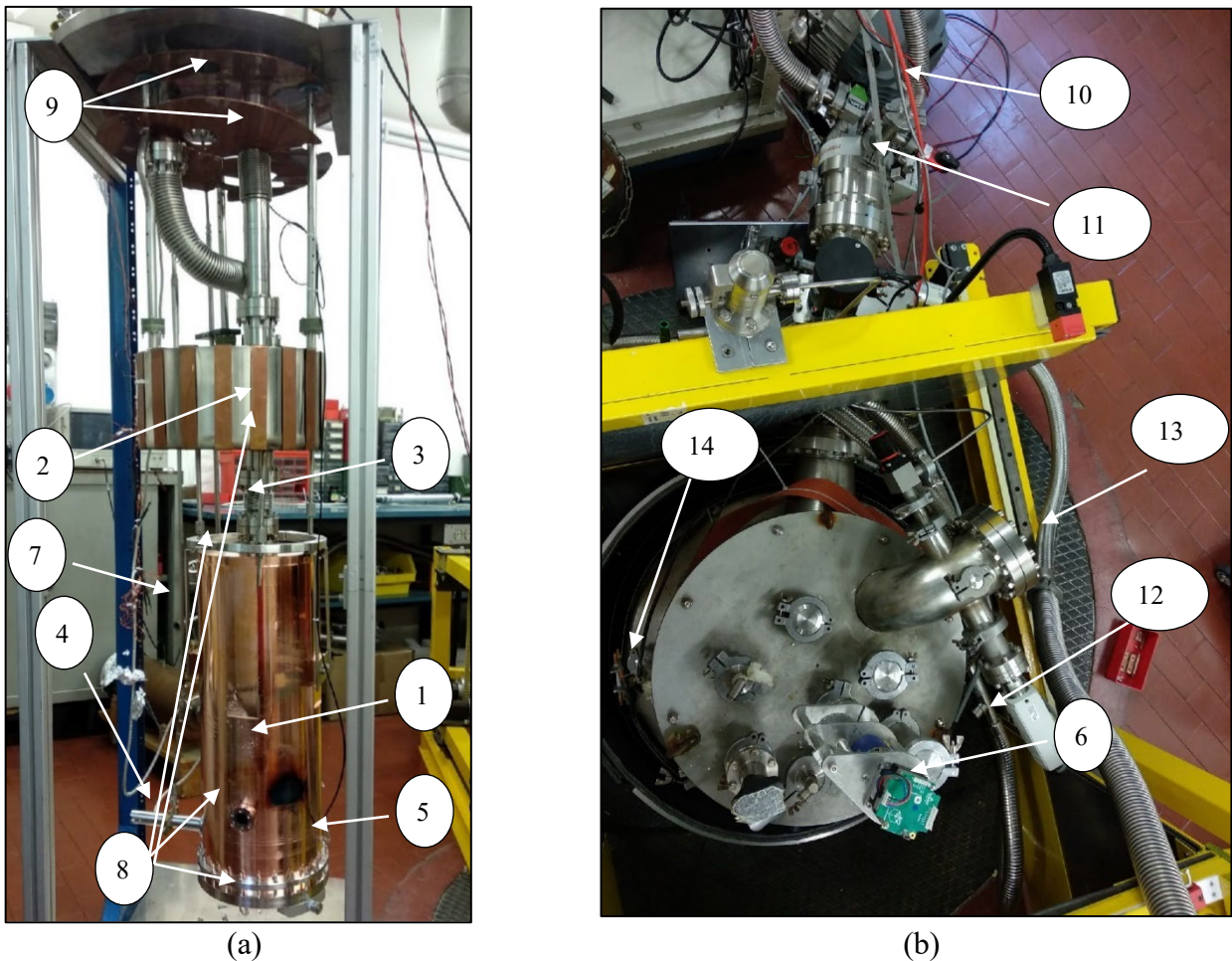


Figure 6.10 – Cavity stand – (a) and external view (b) of the ALPI QWR cryostat.

As shown on figure 6.10a, coated QWR cavity and plate *(1)* are connected to the helium dewar *(2)* through the liquid helium transfer line *(3)* for cooling down of the cavity during RF measurements.

Coaxial RF cables of the coupler *(4)* and pick-up *(5)* antennas were connected to the system for the RF signal transfer. Motor PD57-1-1161-TMCL *(6)* was connected to the coupler drive system *(7)* for the movement of the coupler antenna during the RF measurement.

Four Cernox-type thermometers *(8)* were assembled to the system for evaluation of the temperature within all the length of the cavity. All the thermometers of the system were connected to the temperature indicator SCI model 9300. Thermal copper shields *(9)* were placed on the top of the helium transfer line for reducing the heating effect of the top part of the stand onto the cavity.

Oil-free scroll pump nXDS 15i *(10)* and Pfeiffer turbo molecular pump TMU261P *(11)* were connected to the vacuum system for producing vacuum in the cryostat. Three vacuum sensors were connected to the cryostat: in the main chamber Pirani/Bayard-Alpert ion gauge PBR 260, in the chamber after turbo molecular pump Pfeiffer full range PKR 251 and between turbo molecular pump and scroll pump Pirani TPR 280. All the sensors were connected to the Pfeiffer Maxigauge® TPG 366 to observe the pressure at different regions.

Around the vacuum system there is cryostat shield, which is refilled with liquid nitrogen through the inlet *(12)* and outlet *(13)* for better cooling down of the system during the measurement. The level measurement of the liquid nitrogen *(14)* is connected to the liquid nitrogen level controller AMI 186.

# Chapter 7

# QWR SPUTTERING PARAMETERS

## 7.1. Introduction

Uniform coating has been demonstrated to enhance the performance of the accelerating cavities. To ensure niobium deposition along the entire QWR geometry, it is essential to study the process parameters. For this purpose, an analysis of the various sputtering parameters (current, bias, etc.) as well as the baking parameters, was carried out.

Niobium deposit should have good adhesion to the copper substrate with low internal tension for avoiding of cracks and delamination of the coating during accelerator operation of the superconductive structure. Chamber and substrate are prepared before the deposition process for decreasing the amount of impurities. High superconductive properties of the coating require as low as possible amount of contaminations in the coating.

## 7.2. QWR cavities deposition parameters

## 7.2.1. Methodology

The first aim of the project was the definition of the deposition parameters, at which the most possible uniform niobium coating along all the cavity surface substrate could be obtained.

Preparation of the copper substrate of the high–β ALPI QWR cavities is a structured process, which requires several days, starting from machining, tuning and chemical treatments (see chapter 8). Definition of the deposition parameters requires several sputtering tests. After deposition, characterisation of obtained niobium coating was made

It was decided to use test moke-up stainless steel cavity (Figure 7.1a) to simplify the process and decrease the cost of the sputtering procedure. The holes for the 9x9 mm quartz samples assemble are made along the external walls, inner conductor and top surface of the moke-up cavity (Figure 7.1b).

Quartz samples are used due to its low cost, good adhesion between niobium coating and quartz surface and flexibility to perform further analyses such as RRR, XRD, etc. The solution with moke-up cavity and quartz samples gave an opportunity to reduce R&D time. The usage of the copper QWR substrate needs long-term chemical surface preparation, complicate assembly on the sputtering system, deposition and eventually removal of the niobium deposit for further tests. The procedure of

the niobium deposition onto quartz samples requires only simplified chemical surface preparation and assemble of the quartz samples to the moke-up cavity.
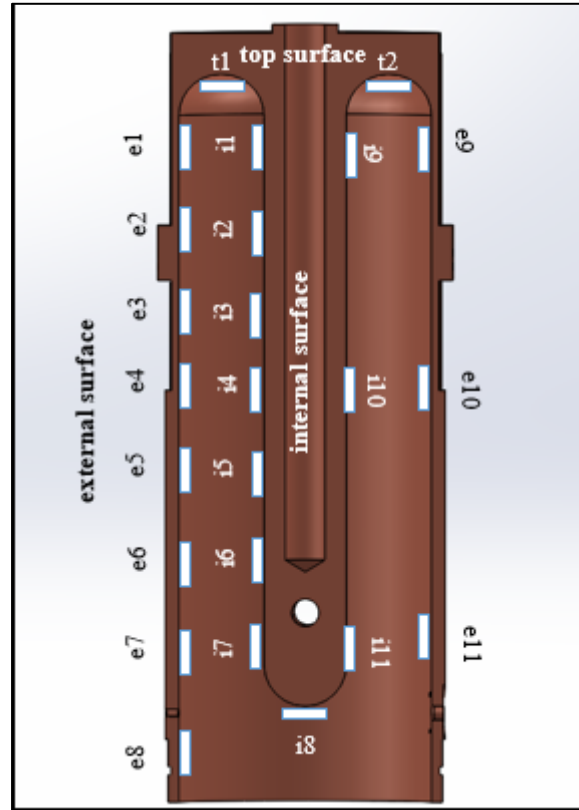


(a)                                                    (b)

Figure 7.1 – Scheme of the assembled mokeup cavity in the sputtering system (a) and quartz samples positioning (b).

Before the deposition process, quartz samples are initially cleaned in ultrasound bath in the solution of water and Rodacleen soap at the temperature 40 °C for 60 minutes. After cleaning, quartz samples were immersed in the ethanol and dried with compressed nitrogen gas. Next step is assembling of the dried quartz samples to the surface of the moke-up cavity. Quartz samples are fixed in different areas of the moke-up cavity to define niobium coating parameters within all the QWR internal surface.

After the assembling of the test cavity with quartz samples, the vacuum sputtering system is closed and pumped. Following step is baking and sputtering processes with specific parameters. After that the system is cooled down, vented and quartz samples are dismounted. The properties of the niobium coating on quartz samples are characterised and the parameters of the sputtering process are evaluated.

## 7.2.2. Baking parameters definition.

Before sputtering, baking process of the chamber and the substrate is applied for removing of the humidity and gasses, absorbed on the chamber and cavity walls. Temperature of the baking process, initial pressure and baking time are fundamental parameters for reaching low pressure and low contaminations of the vacuum system.

*Vacuum chamber temperature*

Assembled quartz view ports on the side and the bottom of the chamber are the main limitation of the system baking temperature. Overheating of the view port could cause damage of the quartz and leak in the system. For this reason, external baking system is divided onto the three zones. Zone with the view ports is heated at 120 °C (view port temperature according to the product specification should be in the range 20 – 200 ºC) and other part of the system is heated up to 200 °C. Further increase on the baking temperature in other regions of the system can cause temperature increase of the view ports.

*Initial pressure*

Heating up of the system at the pressure, higher then $10^{-3}$ mbar, causes oxidation of the walls of the system and possible contamination of the vacuum chamber. At the beginning of the baking, pressure increases on two - three orders of magnitude, which can be explained by desorption from the walls of humidity and residual gasses. For this reason, optimal initial pressure for starting the baking process is in the range of $10^{-5} – 10^{-6}$ mbar.

*Baking time*

Target pressure of the vacuum system after baking process is $10^{-8} – 10^{-9}$. This base vacuum is required for sputtering of the superconductive films with high superconductive characteristics. Experimentally was defined, that time, which is needed to reach optimal pressure is 72 – 96 hours.

*Substrate temperature*

The substrate temperature was defined to prevent annealing process of the copper material. Substrate temperature should not exceed 500 °C. Ideal temperature was defined in the range 400 – 500 °C. Results of the niobium deposition onto high – β QWR at the baking and sputtering temperatures, higher than the defined range, described in chapter 10.

### 7.2.3. Sputtering parameters definition

*Deposition thickness*

The ideal film thickness for the ALPI QWR cavities is 2-4 μm. This coating thickness is bigger, than the skin penetration depth but is not thick enough for pealing of the niobium deposit from the copper substrate due to different thermal contraction [69].

*Sputtering pressure*

The thickness uniformity is strongly dependent on the argon pressure at which discharge is driven. In the previous research of the ALPI QWR deposition [70] was defined, that the most uniform coating could be obtained at an argon pressure of $8 \cdot 10^{-2}$ mbar.

Due to the cathodic configuration of the sputtering system, deposition process of the ALPI QWR can be divided into three different regions, depending on the sputtering areas:

- the first region between the cathode and external cavity surface,
- the second region between the cathode and internal surface shaft,
- the third region between the top of the cathode and the top surface of the substrate.

Sputtering pressure is a crucial parameter, that could affect the internal stress (described in paragraph 5.5) and quality of the coatings.

With increasing of the pressure more than 0,2 mbar deposition rate of the internal part of the substrate increases in respect to external part of the cavity.

With lower pressure it is possible to obtain plasma holes and no niobium coating in some regions of the surfaces. The decrease in plasma density results in the creation of the plasma holes at low argon sputtering pressure. This can be explained using Paschen curve of the argon plasma discharge (Figure 7.2).
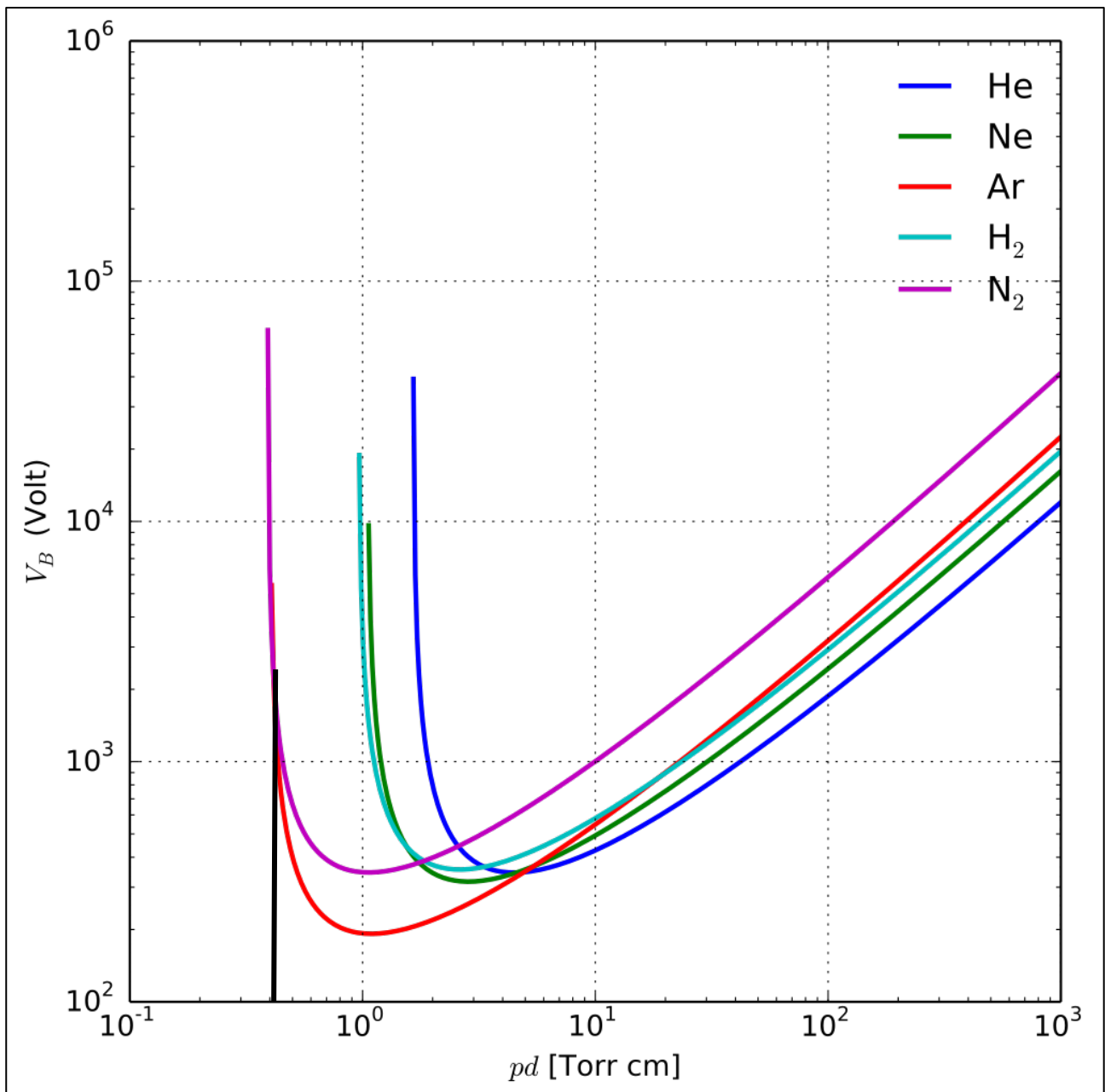
Figure 7.2 – Paschen curve of the voltage breakdown for helium, neon, argon, hydrogen, and nitrogen gasses [71].

As it is shown on figure 7.2, the breakdown voltage for the argon gas in the region before pd coefficient $4 \cdot 10^{-1}$ [Torr · cm] is very high. Initialisation of the voltage breakdown for the plasma production in this region is insufficient. Distance between QWR external shaft and niobium cathode cylinders in the constructed QWR sputtering system is 7 cm. In this case, the lowest pressure, needed for creation dense argon plasma without holes is 0,6 Torr ($8 \cdot 10^{-2}$ mbar).

Due to this research, it was decided to make the deposition process with the sputtering pressure in the range $8 \cdot 10^{-2} - 2 \cdot 10^{-1}$ mbar.

*Sputtering time*

During the sputtering process due to the bombardment of the ions, target and substrate surfaces are heated up because of the energy exchange. To avoid excessive heating of the copper substrate, the sputtering process is divided onto cycles of 15 minutes each. It was observed, that during 15 minutes of niobium deposition, QWR temperature increases of 60 – 70 ºC. After deposition, a pause of about 2 hours is carried out to allow the target to cool down and the QWR to recover to its initial temperature.

*Substrate temperature*

High substrate temperature is favorable for obtaining a clean film with a good superconductive structure and performance. The upper temperature limit is the cavity annealing temperature of 500ºC. It was therefore decided to start the sputtering process with the substrate at a temperature of 300°C in order to avoid reaching the annealing temperature during sputtering due to ion bombardment.

*Cathode parameters (current and tension)*

Niobium deposition process is made with stable cathode current and variable cathode voltage. Ideal cathode current is in the range 2 – 4 A due to the stability of the process.

Deposition of the niobium coating onto the ALPI QWR high-β cavity is a long-term process. Deposition rate of the bias diode sputtering process is relatively low. Taking in consideration all the deposition cycles and pauses for the system cooling down, total time for the sputtering process of 2 – 4 µm niobium deposit is in the range 36 – 60 hours depending on the cathode current. We observed that niobium deposition with cathode current lower than 2 A, was inefficient due to the increase of the sputtering time for deposition of the same niobium coating thickness.

On the other hand, we have observed that, at high sputtering current, deposition tension and temperature of the substrate increase too fast during the sputtering cycle. With the increase of the substrate temperature time of the pause between the deposition cycles is also increased. Due to these reasons, it was decided to perform niobium deposition at the cathode current, lower than 4 A.

Deposition of the quartz samples at 2; 3; 3,25; 3,5 and 4 A was made. The absolute cathode tension increase of 400 V was noticed during the sputtering cycle.

The superconducting properties of the obtained niobium films and performed measurements of the thickness of the coating obtained in the internal, external and top surface of the QWR, were characterized. Results of the film characterisation are described in the next paragraph.

*Bias voltage*

Initial cathode tension is an important characteristic for the sputtering process. As was noticed previously, during the sputtering cycle, absolute cathode voltage increases averagely on 400 V. Maintenance of the voltage in the range -400 – -900 V is important to prevent a fast increase of the substrate temperature. It was observed dependence between volt-ampere characteristic of the cathode and bias voltage of the substrate. So, initial cathode tension is one of the parameters, that were considered during bias voltage definition.

From the other side, bias voltage should not exceed -200 – -300 V for preventing a re-sputtering of the same deposited film. On figure 7.3 volt-ampere characteristic of the niobium cathode obtained at different biased voltages.
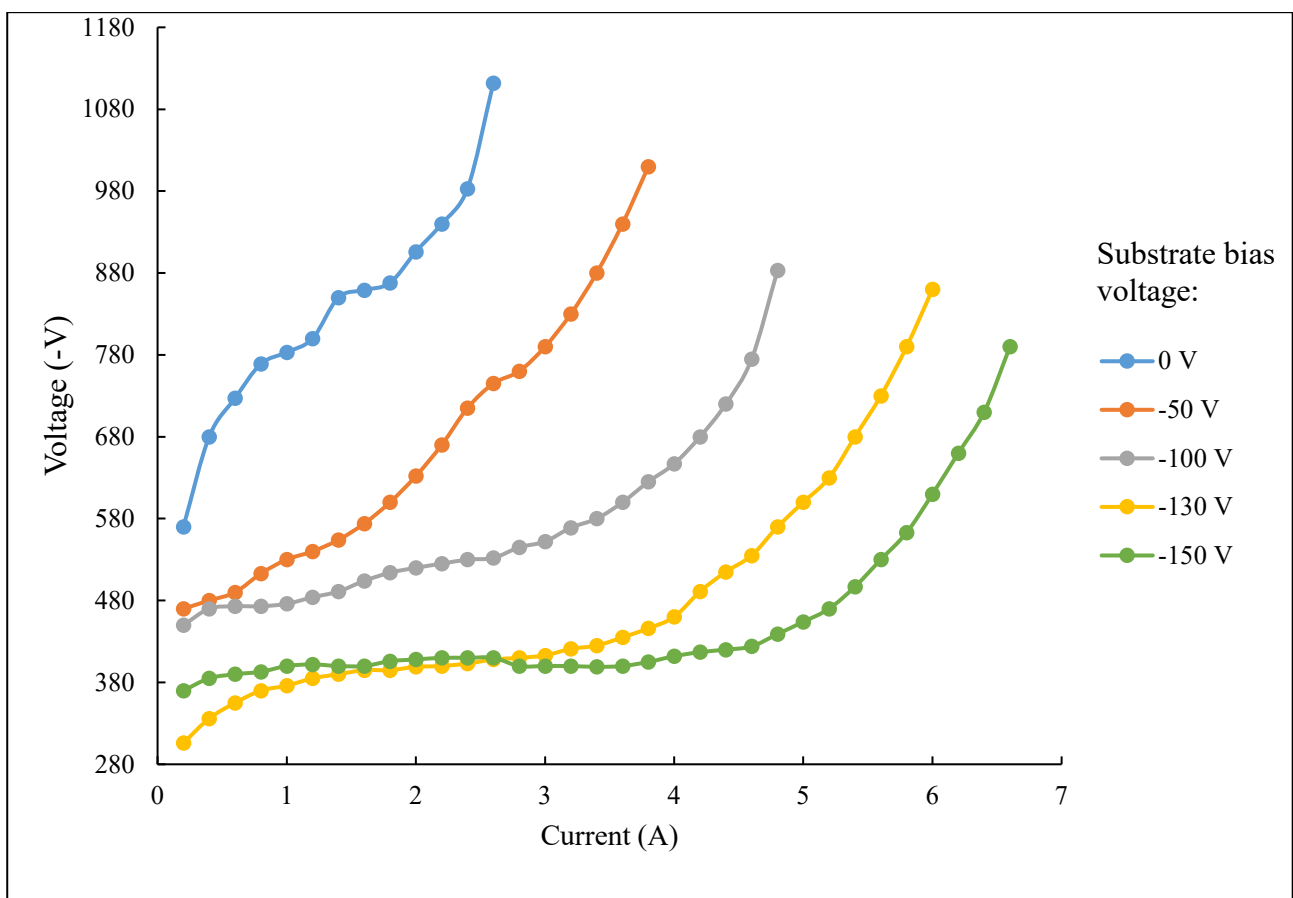


Figure 7.3 – Volt-ampere characteristic of the niobium cathode.

All the volt-ampere characteristics were measured with the constant argon pressure (0,1 mbar) and the same room temperature conditions (25°C of the niobium cathode). From figure 7.3 is seen strong dependence of the initial voltage of the cathode with the same current from the applied bias voltage. Without applying bias voltage, the maximum cathode current was 2,6 A. Applying a small bias voltage (-50 V; -100 V) is possible to reach higher cathode currents, but the initial cathode tension is too high in all the range of the cathode current.

Bias voltage of -130 V was chosen as optimal due to low initial cathode voltage at the 1 – 4 A and sufficiently lower value from the cathode tension (the lowest value is 306 V due to figure 7.3).

## 7.2.4. Niobium thin film characterisation.

Several niobium sputtering tests were carried out onto quartz samples to define the appropriate cathode current. Parameters of some experimental tests are summarised in table 7.1.

Table 7.1. Parameters of niobium sputtering tests.

| Parameters | Test 6 | Test 7 | Test 8 | Test 9 | Test 10 | Test 11 | Test 12 | Test 13 | Test 14 | Test 15 |
|---|---|---|---|---|---|---|---|---|---|---|
| Pre sputtering baking | | | | | | | | | | |
| Chamber temp., °C | - | 150 | 120 – 200 | | | | | | | |
| Lamps temp., °C | - | 400 | 350 | | | | | | | |
| Time, hours | - | 51 | 63 | 48 | 72 | 48 | 88 | 72 | 48 | 72 |
| Sputtering parameters | | | | | | | | | | |
| Full time, min | 60 | 165 | | | 150 | 160 | 165 | | 260 | 240 |
| Pressure, mbar | 0,08 - 0,2 | | | | | | | | | |
| Bias voltage, V | -130 | | | | | | | | | |
| Cavity temp., °C | 25 | 300 | | | | | | | | |
| Cathode current, A | 3 | 3 | 3 | 3,5 | 4 | 3,25 | 3,25 | 3,25 | 2 | 3,25 |

Main properties of the QWR Nb/Cu superconductive film, that characterise performance of the cavity at superconductive state, are uniformity and purity of the niobium deposit. Low relative thickness distribution within all the QWR surface is hardly reachable because of complicate substrate geometry. Deposition of the niobium occurs simultaneously in the internal, external, and top surface of the cavity due to the structure of the sputtering system. Ratio between surfaces of the external niobium cathode and external cavity walls is equal to 0,77. Meanwhile, ratio between the internal cathode surface and QWR inner conductor surface is 2,55. Calculations of these ratios are based on the high-β ALPI QWR cavity and niobium target of the QWR sputtering system working designs. High difference in ratios of the external and internal cavity surfaces and relative niobium target surface means high thickness

distribution within the QWR surface due to difference of the material amount, sputtered in different QWR regions.

During deposition on the quartz samples, the influence of the cathodic current on the coating thickness distribution was observed. Deposition tests were carried out with a sputtering current range of 2 – 4 A with a similar argon pressure, bias voltage, and initial substrate temperature. Cathode current was the only parameter changed. Thickness of the coating and deposition rate were measured for evaluation of the coating uniformity in the QWR, using a profilometer in different locations of the surface. Deposition rate of the different QWR areas at the different cathode currents is shown on figure 7.4.
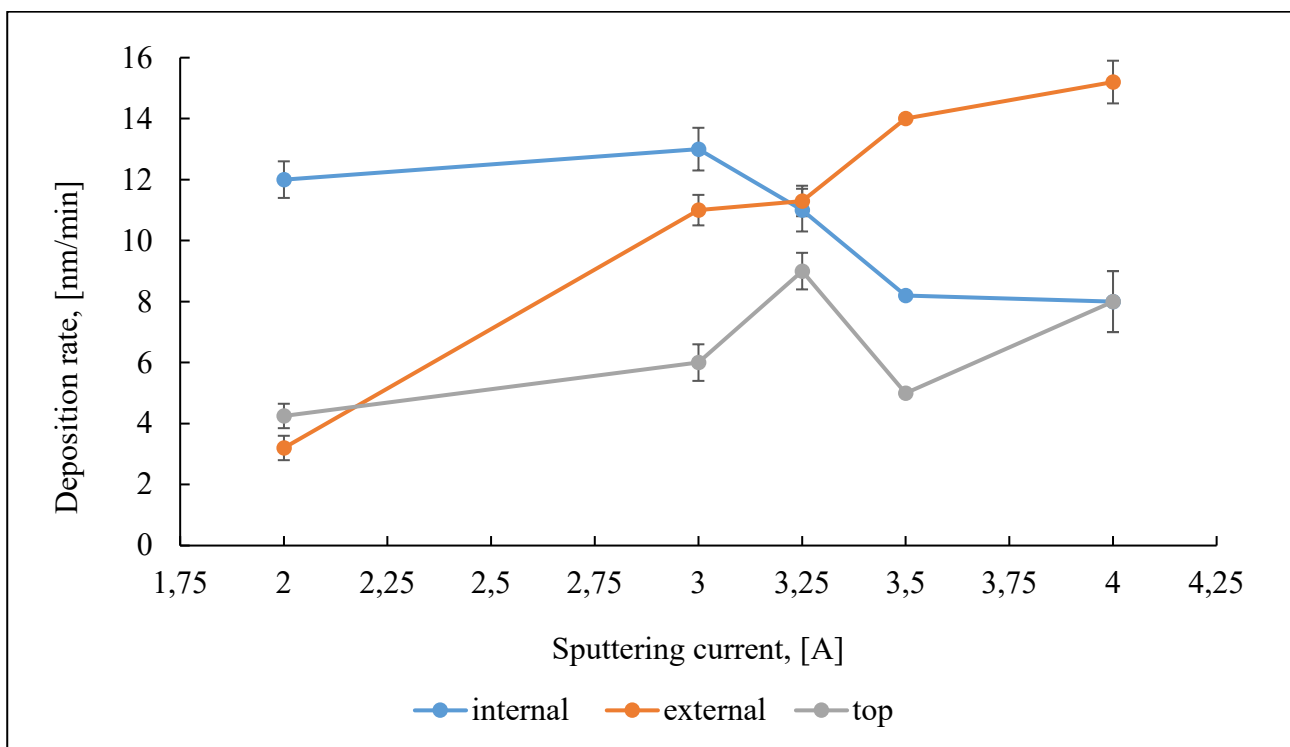
Figure 7.4 – Thin film deposition rate from the cathode current dependence.

The highest uniformity of the film thickness and deposition rate was achieved at the sputtering current of 3,25 A. At this parameters, average deposition rate of the external surface was 11,3 nm/min, internal – 11,0 nm/min and top surface – 9 nm/min.

The lowest uniformity was noticed at the sputtering current of 2 A. Sputtering process with cathode current of 2 A was made with longer period of deposition time (260 min.) in respect to the process with 3,25 A (165 min.). This data was used for the thickness distribution evaluation. Longer deposition time for the sputtering process at 2 A was performed to deposit enough amount of material,

which could be measured by the profilometer. Thickness distribution within the QWR surface at 3,25 A and at 2 A is shown on the figure 7.5.
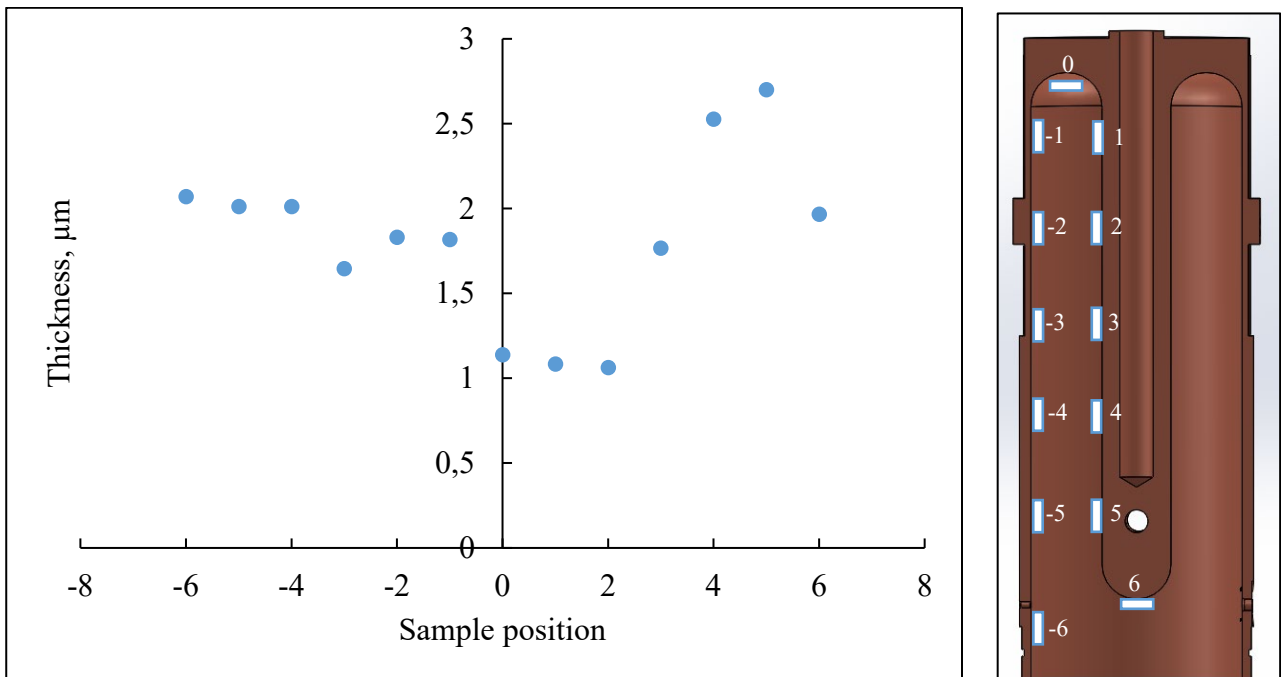


(a)
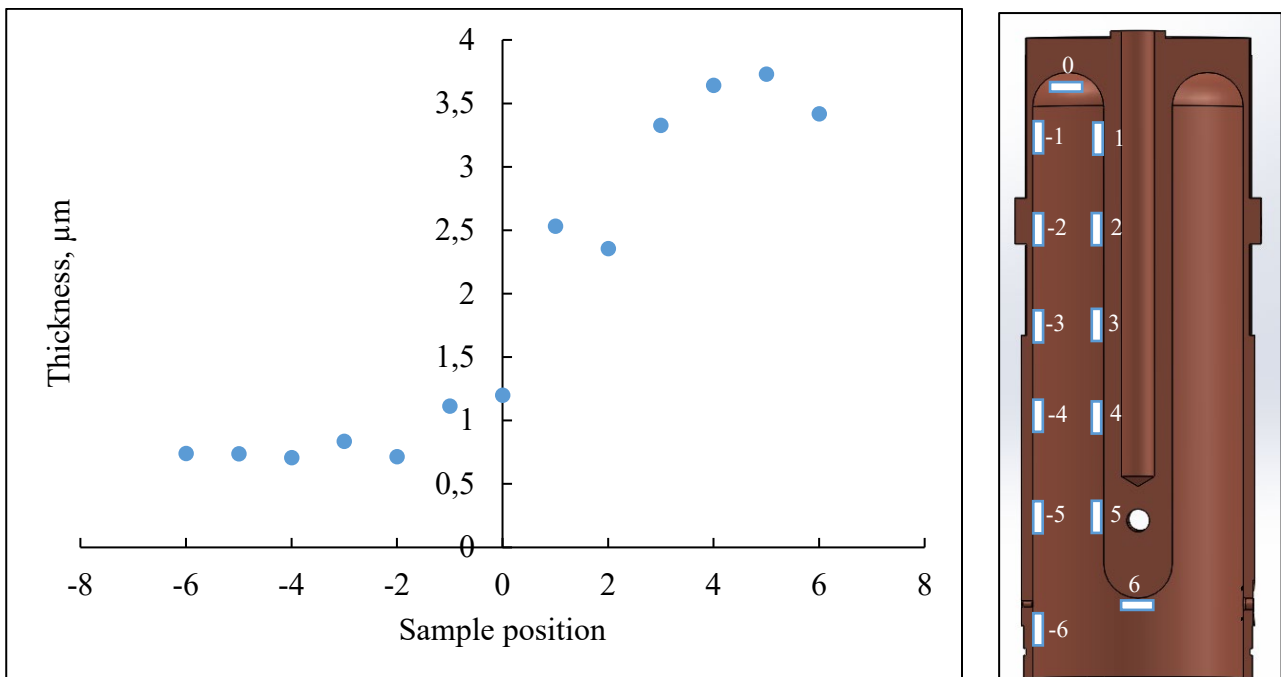


(b)

Figure 7.5 – Thickness distribution of the niobium film within QWR surface at the deposition process with the sputtering current: (a) – 3,25 A; (b) – 2 A.

As it is shown on the figure 7.5, thickness distribution of the niobium coating, obtained at the sputtering current 3,25 A is averagely similar at external and internal QWR surfaces with thickness minimum at the top surface. In case of niobium film, obtained at 2 A, thickness of the external niobium coatings approximately 4 times smaller, then on the QWR internal surface.

Obtaining a niobium film free of oxygen contamination is critical for achieving high QWR cavity performance. Main sources of the possible impurities in the coating are chamber residual gasses, leaks of the vacuum chamber and drawbacks during the cavity surface preparation. Main parameters, that characterise superconductive performance of the deposited niobium films are residual resistivity ratio and critical temperature. Measured RRR and $T_c$ of the deposits, obtained at different cathode currents are shown on figure 7.6.
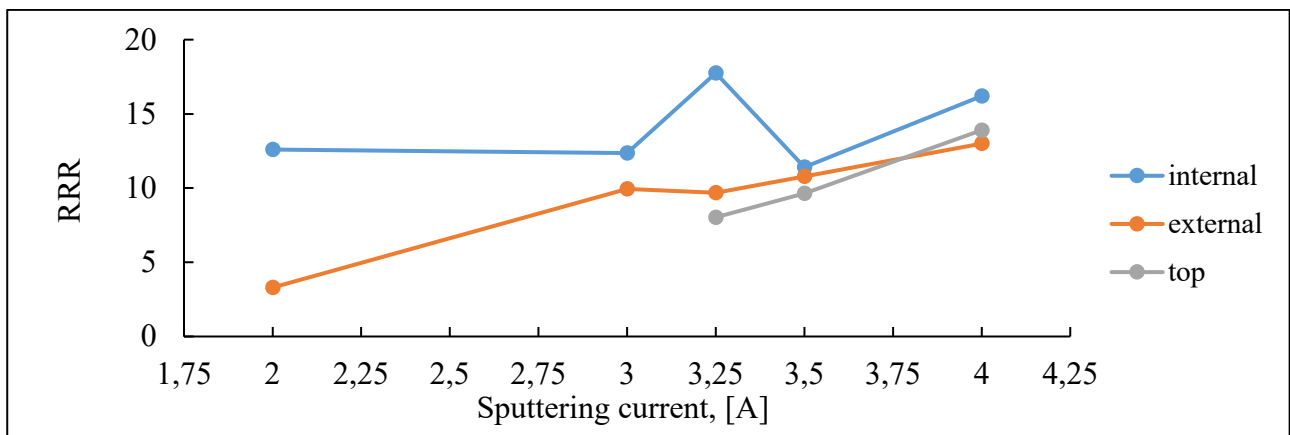


(a)
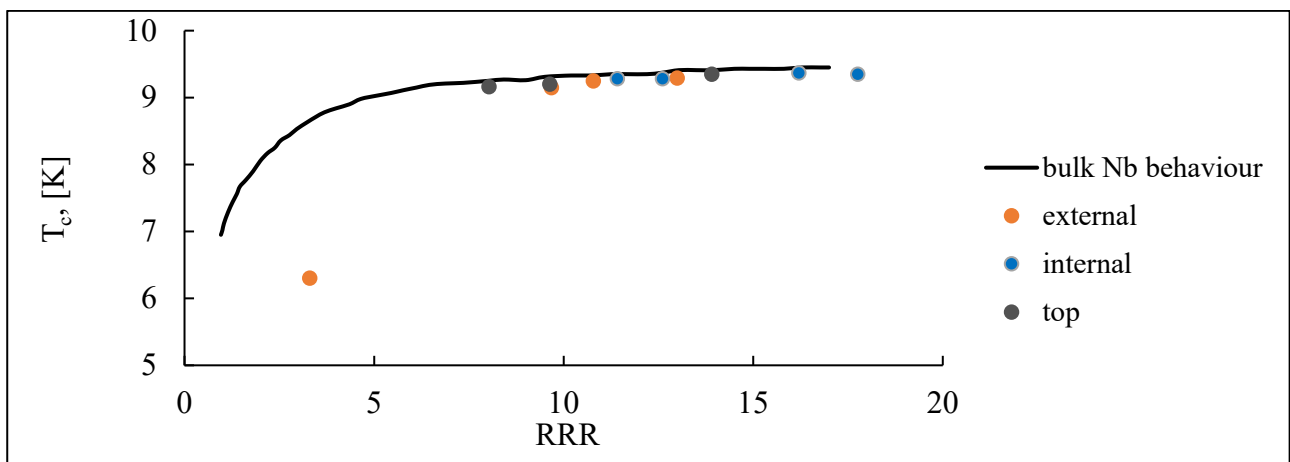


(b)

Figure 7.6 – Dependence of the triple R vs. the cathode current of the deposit – (a) and comparison of the obtained values of thin film critical temperature and RRR to the bulk niobium behaviour [72].

The RRR measurements showed, that niobium film, deposited at 3,25 A in the internal and external surfaces, has residual resistivity ratio, higher than 10 and in the top surface – slightly lower. At 3,5 A average RRR value within all the surface of the cavity is the most equivalent. Comparison of the critical temperature with RRR of thin film coatings to the bulk niobium behaviour showed similar results at the current range from 3 to 4 A which characterise high cleanliness of the niobium film, without oxygen interaction in the crystalline niobium structure [72].

It was noticed the lowest thickness distribution of the niobium deposit at 3,25 A of the cathode current (Figure 7.5a) and the lowest RRR distribution at the cathode current 3,5 A (Figure 7.6a). Ideal range of the cathode current due to uniformity and superconductive properties of the deposited niobium thin films is 3,25 – 3,5 A.

Scanning electron microscope analysis was made for evaluation of the niobium deposit growth. Niobium coating for the SEM analysis (Figure 7.7) was deposited at 3,5 A of the cathode current, 0,1 mbar and  -130 V of bias tension.
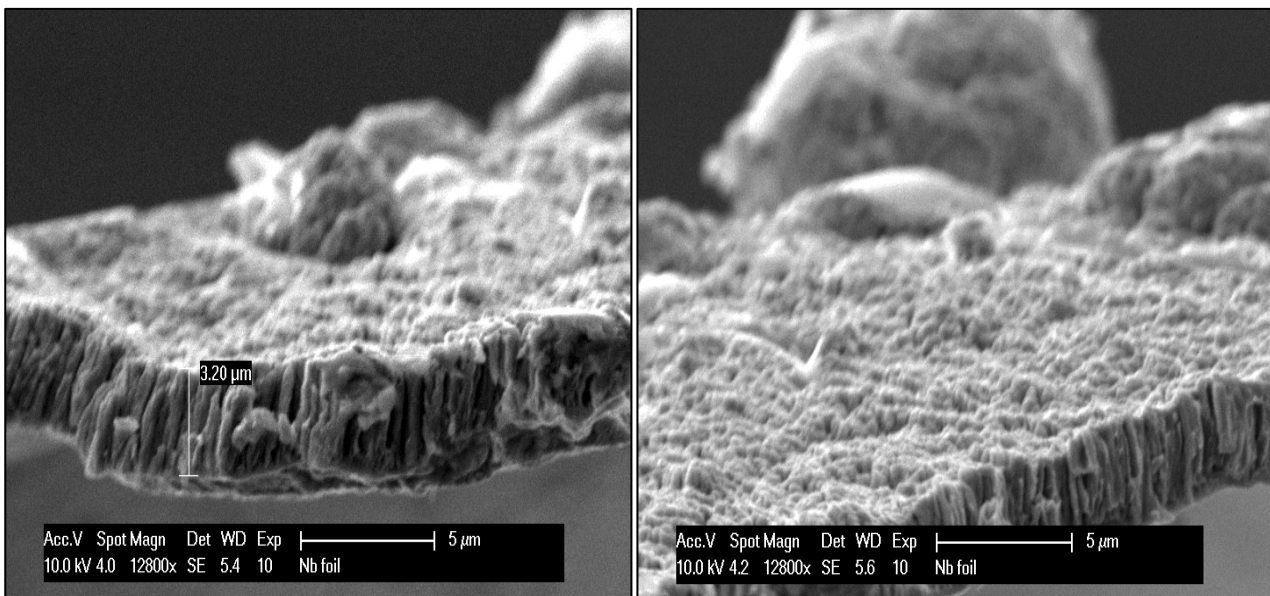


Figure 7.7 – Cross section of the deposited niobium film.

Due to the Thornton diagram (Figure 5.5), growth of the crystallite structure of the film, produced at defined previously parameters (T = 300°C; P = 0,1 mbar), is characterized by the transition zone. After the SEM analysis it was defined the dense columnar growth of the niobium deposit without intermediate pores which is critical important to the superconductive properties of the film. Dense film and low amount of the pores reduce amount of crystallite impurities, which produces normal

conductive islands in the superconductive state of the film and decreases quality of the superconductor in total.

## 7.2.5. Pulsed bias test.

The film microstructure is strongly dependent from the bias voltage [73]. Biasing of the substrate impacts on the orientation of the crystalline structure and increases superconductive properties of the niobium coatings.

Increasing of the niobium thin film superconductive properties could be done by implementation of the pulsed biasing of the substrate. It was decided to perform depositions of the niobium onto quartz samples with pulsed bias at 50, 100 and 150 kHz to define the influence of the bias tension onto superconductive properties and thickness distribution of the niobium coating. After the tests, deposition rate and superconductive properties of the obtained niobium films were evaluated. Results of the thin film analysis is shown on figure 7.8.
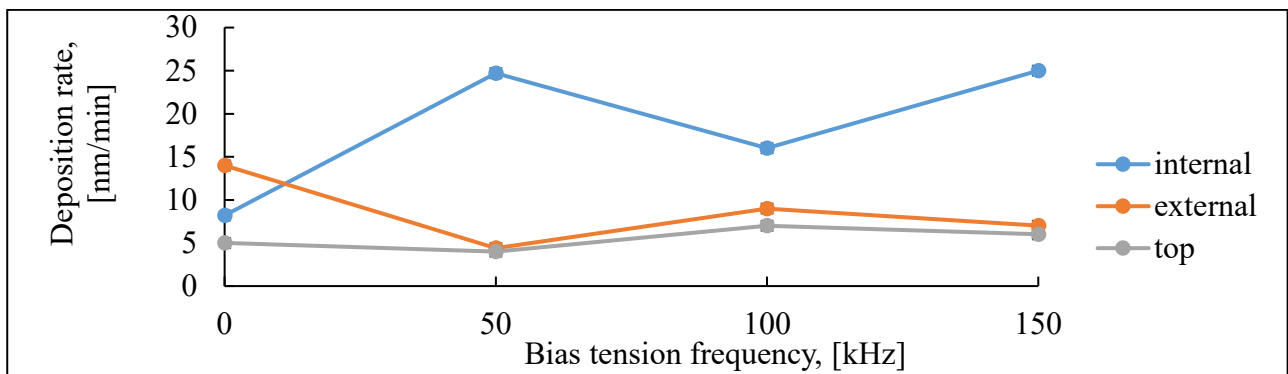


(a)



(b)
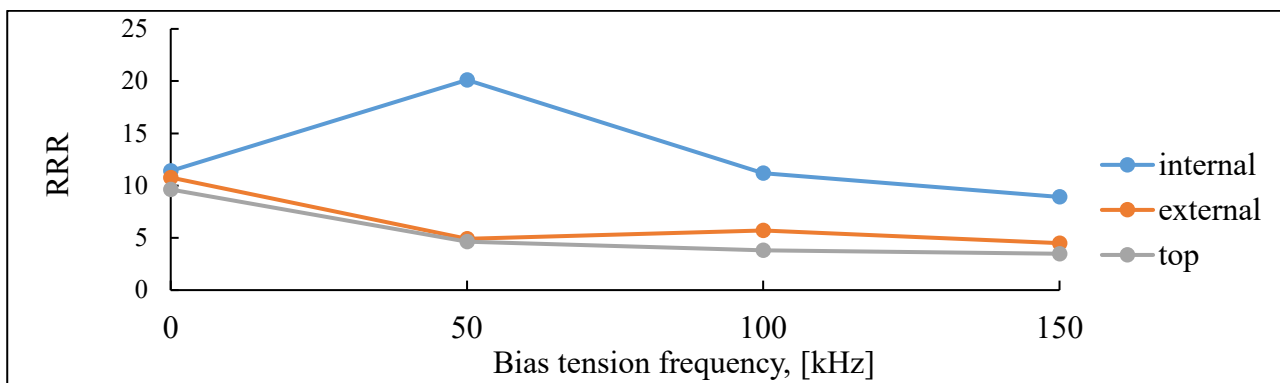
Figure 7.8 – Dependance of the deposition rate (a) and RRR (b) of the deposited thin films from the pulsed bias frequency.

Deposition tests were made at the cathode current 3,5 A with similar argon pressure (0,1 mbar) and bias voltage (-130 V). Frequency of the bias was the only modified parameter.

Profilometer and superconductive analysis of the coated films showed decreasing of the uniformity and superconductive properties of the film with increasing of the bias tension frequency. Thickness distribution of the coating was minimum at constant bias voltage and increased with further increase of the bias frequency (Figure 7.8a). From the graph on figure 7.8b is clearly seen constant decrease of the triple R of the coating with increase of the bias tension.

Evaluation of the niobium film properties showed degradation of the coating uniformity and RRR with implementation of the pulsed bias for the substrate. It was decided further usage of the DC bias during the ALPI QWR cavity production.

## 7.3. QWR plates parameters definition.

Thin niobium film was sputtered onto quartz samples for evaluation of the deposition rate, thickness, and superconductive properties of the deposited coating. For evaluation of the reproducibility of the process, several tests onto quarts samples were done.

Due to the planar geometry of the QWR plates and simple construction of the sputtering system (Figure 6.7), the only one variable parameter of the sputtering process was deposition time. All the other parameters, used for QWR plate deposition, were defined previously [66]. For all the deposition experiments same sputtering parameters were used: cathode current 12 A; bias voltage -100 V; sputtering pressure 0,2 mbar; initial substrate temperature 200 °C; total deposition time 60 min.

After deposition process, thickness, deposition rate, triple R and $T_c$ of the obtained niobium film were evaluated. Results of the thin film characterization are shown in table 7.2.

Table 7.2. Average results of the thin film characterization for proceeded experiments.

| Test #<br>Parameter | 1 | 2 | 3 |
|---|---|---|---|
| Thickness [μm] | 1,92 | 1,85 | 2,14 |
| Deposition rate [nm/min] | 32 | 31 | 36 |
| RRR | 16 | 18,7 | 15,9 |
| $T_c$, [K] | 9,36 | 9,32 | 9,36 |

Results of the thin film characterization show high reproducibility of the sputtering process with high superconductive properties of the deposited niobium coatings. Correspondence of the critical temperature to the residual resistivity ratio of thin films showed near values to the bulk niobium behavior, which characterizes high cleanliness and low impurity impact in the crystalline structure of the superconductive deposit.

Optimal sputtering parameters of the QWR plates were defined due to results of thin film characterization.

## 7.4. Conclusion

The best sputtering parameters for deposition of the Nb/Cu ALPI QWR cavities and plates were experimentally defined due to microstructural, superconductive and profilometer analysis of the coated niobium thin films onto quartz samples (Table 7.3).

Table 7.3. Optimal sputtering parameters for ALPI QWR cavities and plates production.

| Parameter | QWR cavity | QWR plate |
|---|---|---|
| **Baking process** | | |
| External chamber temperature, [°C] | 120 – 200 | 100 – 120 |
| Substrate temperature, [°C] | 450 | 350 |
| Baking time, [h] | 72 - 96 | |
| **Sputtering process** | | |
| Sputtering pressure, [mbar] | 0,08 – 0,2 | 0,2 |
| Cathode current. [A] | 3,25 – 3,5 | 12 |
| Bias voltage, [-V] | 130 | 100 |
| Total deposition time, [min] | 240 – 300 | 60 |
| Cycle time, [min] | 15 | 6 |
| Number of cycles | 16 - 20 | 10 |
| Initial substrate temperature, [°C] | 300 | 200 |

# Chapter 8

# METHODOLOGY OF QWR CAVITIES AND PLATES PRODUCTION

## 8.1. QWR cavities production

## 8.1.1. Introduction

The production of the ALPI QWR cavities consists of several steps, which are described in this chapter. A general scheme of the main steps of the ALPI QWR production procedure is shown on figure 8.1.
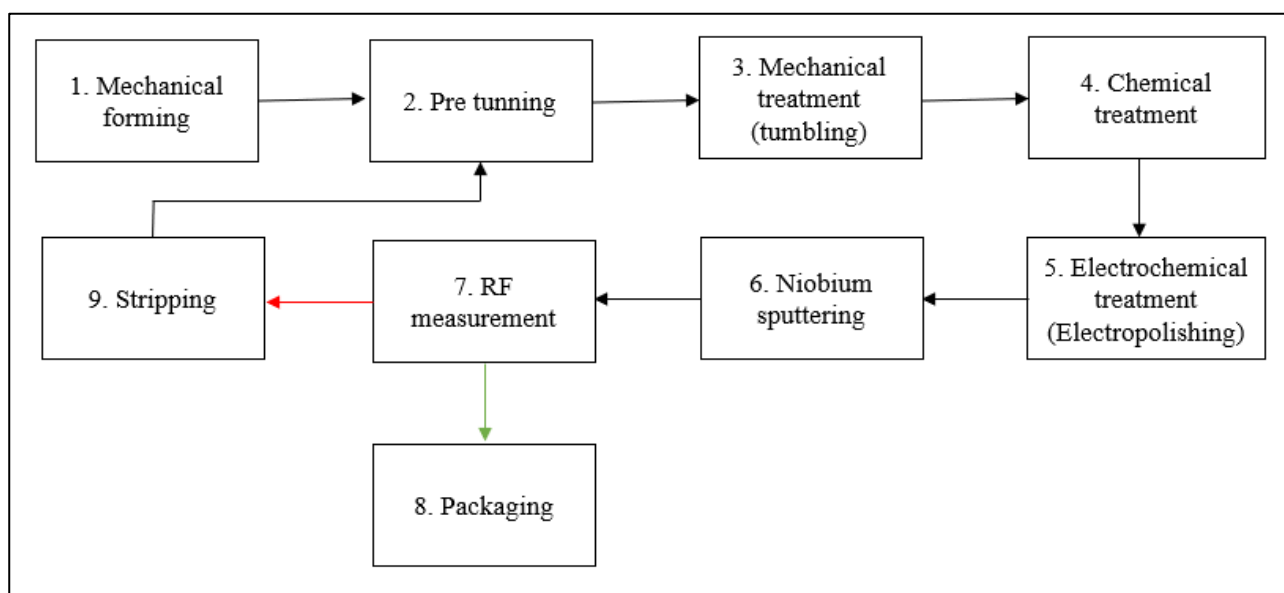


Figure 8.1 – Procedure of the ALPI QWR production.

The procedure in figure 8.1, which is used for production of the Nb/Cu high-β ALPI QWR cavities, can be detailed as follow:

    1. Mechanical forming.

The substrate of the QWR cavity is machined from the oxygen free copper using lathing technology from the bulk copper billet.

    2. Pre tuning.

The QWR cavities, assembled at the ALPI LINAC, work at frequency of 160 MHz and 4,2 K of temperature. Machining of the copper billet is needed for reaching the target frequency. Calculation of the frequency shift from the room temperature to the 4,2 K (paragraph 8.1.2) and methodology of the copper billet machining (paragraph 8.1.3) are described below.

3. Mechanical treatment

The surface of the copper billet after machining has high roughness. The deposited niobium thin film copies the morphology of the copper surface. High roughness of the niobium film increases field emission of the QWR during activity at low temperatures, which decreases superconductive performance of the cavity. One of the main goals of the copper substrate preparation before the sputtering process is to decrease roughness within all the copper cavity. Tumbling process is used to remove high peaks of the copper material. Methodology of the tumbling process is described in paragraph 8.1.4.

4. Chemical treatment.

After lathing, pre tuning and mechanical treatment of the copper QWR, residuals of organic, inorganic additives and machining oil remain over the copper surface. Main goal of the chemical treatment is to remove absorbed compounds from the copper surface in order to prevent pollution of the sputtering system and the consequent bad adhesion of the niobium coating to the substrate.

5. Electrochemical treatment.

Electrochemical treatment is used for further decrease of the copper surface roughness. Methodology of the chemical and electrochemical treatments are described in paragraph 8.1.5.

6. Niobium sputtering.

Deposition of the niobium film onto copper substrate is made after substrate surface preparation. Detailed niobium sputtering methodology is described in paragraph 8.1.6.

7. RF measurements.

Low temperature RF measurements allows to characterise the superconductive performance of the produced QWR cavities. Methodology of the RF measurements is described in chapter 9.

8. Packaging.

Cavity is packed and set for the assembling in the ALPI LINAC only when superconductive performance of the produced high-β QWRs is higher than the ALPI upgrade project target. Target superconductive performance and results of the RF measurements are described in chapter 10.

9. Stripping.

If superconductive performance of the produced high-β QWRs results lower than the ALPI upgrade project target, niobium coating is removed by the stripping process. After the stripping process, treatment, sputtering and RF measurement activity is repeated. Methodology of the stripping process is described in paragraph 8.1.7.

## 8.1.2. Frequency shift calculation.

The resonant frequency of the cavity $f$ is changed during cooling down process due to the QWR thermal expansion. Working frequency of the ALPI LINAC is 160 MHz at 4,2 K. For correct pre-tuning of the cavity, frequency variation due to the next parameters are evaluated [74]:

- thermal expansion, $\Delta f_{thermal}$;
- environment change, $\Delta f_{environment}$;
- surface impedance, $\Delta f_{impedance}$;
- mechanical treatment, $\Delta f_{treatment}$.

The resonance frequency change due to the thermal contraction is proportional to the linear dimension of the cavity by the equation:

$$f = C \cdot \frac{1}{L} \tag{8.1}$$

Where C is a constant. The frequency shift $\Delta f$ can be defined by the equation:

$$\frac{\Delta f}{f} = -\frac{\Delta L}{L} \tag{8.2}$$

For definition of the integrated dimension variation of copper, the function of thermal expansion of copper [75] was used.

$$\frac{\Delta L}{L} = \int_{4K}^{293K} \alpha\,(t)dt = 0,248\,\% \tag{8.3}$$

Frequency shift due to the copper thermal extraction is calculated as:

$$\Delta f_{thermal} = -0,248\% \cdot 160 \text{ MHz} = -396,8 \text{ kHz} \tag{8.4}$$

The change of the environment from vacuum to air also cause resonant frequency shift, which can be evaluated by the equation:

$$f_{air} = \frac{1}{\sqrt{\epsilon_0 \epsilon_r \mu_0} \lambda_{vac}} = \frac{f_{vac}}{\sqrt{\epsilon_r}} \tag{8.5}$$

Where $\lambda_{vac}$ is the wavelength in vacuum and $\epsilon_r$ is the relative electric permittivity, which can be calculated by the equation:

$$(\epsilon_r - 1) \cdot 10^6 = 210\frac{P_a}{T} + 180\left(1 + \frac{5580}{T}\right)\frac{P_w}{T} \qquad (8.6)$$

Where $T$ is the absolute temperature in K, $P_a$ and $P_w$ are vapour pressures of air and water in mm. Hg. The $\epsilon_r$ for air at 20°C and 50% of relative humidity is equal to 1,000647. The frequency shift due to the cavity transition from vacuum to atmosphere is equal to:

$$\Delta f_{environment} = f_{air} - f_{vacuum} = 160\ MHz \cdot \left(\frac{1}{\sqrt{\epsilon_r}} - 1\right) = -51,7\ kHz \qquad (8.7)$$

The surface impedance of copper at room temperature and niobium at 4,2 K is different and this can be another reason of frequency shift from the room temperature measurement to the superconductive state QWR measurement. Connection of the surface impedance and the cavity resonant frequency can be characterised by the formula:

$$\frac{1}{Q_0} - 2j\frac{\Delta\omega}{\omega_0} = \frac{R_s + jX_s}{G} \qquad (8.8)$$

Where $R_s$ and $X_s$ are surface resistance and surface reactance, $\omega_0$ is unperturbed frequency, which consider zero penetration depth and zero surface impedance, $\Delta\omega$ is frequency shift due to the finite surface reactance and $G$ is the cavity geometry factor. The connection of the surface reactance and frequency shift can be obtained by the transformation of formula (8.8) to:

$$X_s = -2G\frac{\Delta\omega}{\omega_0} \qquad (8.9)$$

The surface reactance for superconductors and normal conductors can be evaluated as:

$$X_s^{SC} = -2G\frac{\omega_{SC} - \omega_0}{\omega_0} = \omega_{SC}\mu_0\lambda \qquad (8.10)$$

$$X_s^{NC} = -2G\frac{\omega_{NC} - \omega_0}{\omega_0} = \omega_{NC}\mu_0\frac{\delta}{2} \qquad (8.11)$$

Where $\lambda$ is penetration depth (for niobium 32 nm), $\delta$ is the skin depth (average thickness of the ALPI QWR for niobium coating is 3 μm), geometry factor for the ALPI QWR is 29 (Figure 4.3b). The frequency shift can be obtained from the following equation:

$$\Delta f_{impedance} = \Delta\omega = \omega_{NC} - \omega_{SC} = \frac{\mu_0\omega_{SC}^2\left(\lambda-\frac{\delta}{2}\right)}{2G-\mu_0\omega_{SC}\left(\lambda-\frac{\delta}{2}\right)} \qquad (8.12)$$

The calculated frequency shift due to the substrate reactance variations is -19,7 kHz.
The total frequency shift due to the cooldown process can be calculated as:

$$\Delta f_{cooldown} = (-396,8\ kHz) + (-51,7\ kHz) + (-19,7\ kHz) = -468,2\ kHz \qquad (8.13)$$

The frequency shift is also connected with mechanical treatment of the QWR during pre-sputtering preparation procedure. This frequency shift can be estimated experimentally. By the measurement of the ALPI QWR resonance frequency before and after different preparation steps was defined frequency change of the cavity. Average shift after the tumbling process is -170 kHz, after chemical and electrochemical preparation is -20 kHz. Frequency shift due to mechanical treatment of the QWR can be calculated by the formula:

$$\Delta f_{treatment} = \Delta f_{tumbling} + \Delta f_{chemistry} = (-170\ kHz) + (-20\ kHz) = -190\ MHz \qquad (8.14)$$

Due to calculated and experimentally defined frequency shifts at different steps of the QWR production it is possible to define target resonance frequency for mechanical pre tuning process of the QWR copper billet:

$$f_{target} = f_{SC} + \Delta f_{cooldown} + \Delta f_{tretament} = 160,0 - 0,4682 - 0,190 = 159,3418\ MHz \qquad (8.15)$$

Target frequency of the copper QWR cavity at the room temperature is 159,3418 MHz.

## 8.1.3. Pre tuning process

Pre tuning process is made for adjusting the frequency of the QWR copper cavity to the target frequency. Frequency adjustment is done by removing copper material from defined region of the cavity, showed on figure 8.2.
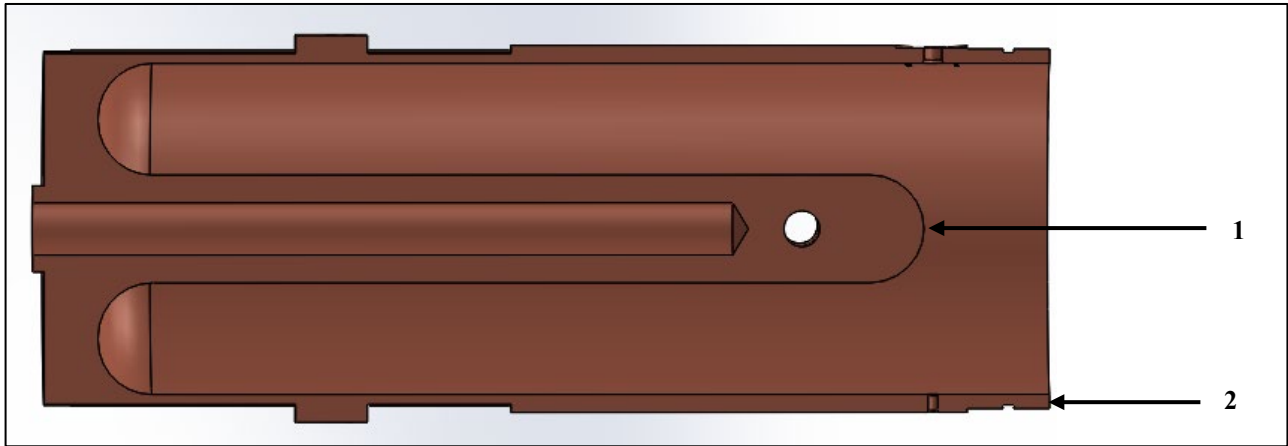


Figure 8.2 – Regions of the material removing from the cavity during QWR pre tuning process.

It was experimentally defined, that decreasing the length of the QWR inner conductor *(1)* on 1 mm increases QWR resonant frequency on 200 kHz. From the other side, removing 1 mm from the bottom external walls of the cavity *(2)* decreases resonant frequency on 10 kHz.

After forming of the cavity from the copper billet, it is transported for the frequency measurement. Resonant frequency of the cavity is measured with the network analyzer HP 8753E. Frequency measurement is made by S11 type when the signal is transferred to the cavity and after transferred back to the network analyzer through one antenna. Signal antenna is placed in the centre of the test plate, assembled to the cavity.

After definition of the QWR resonant frequency, difference between target and real frequencies ($\Delta f$) is calculated. According to the $\Delta f$, region and amount of the copper material removal is calculated. After calculations, QWR cavity is fixed to the lathe machine and copper material is removed from the defined cavity regions.

Process of the mechanical cavity pre tuning is shown on figure 8.3.
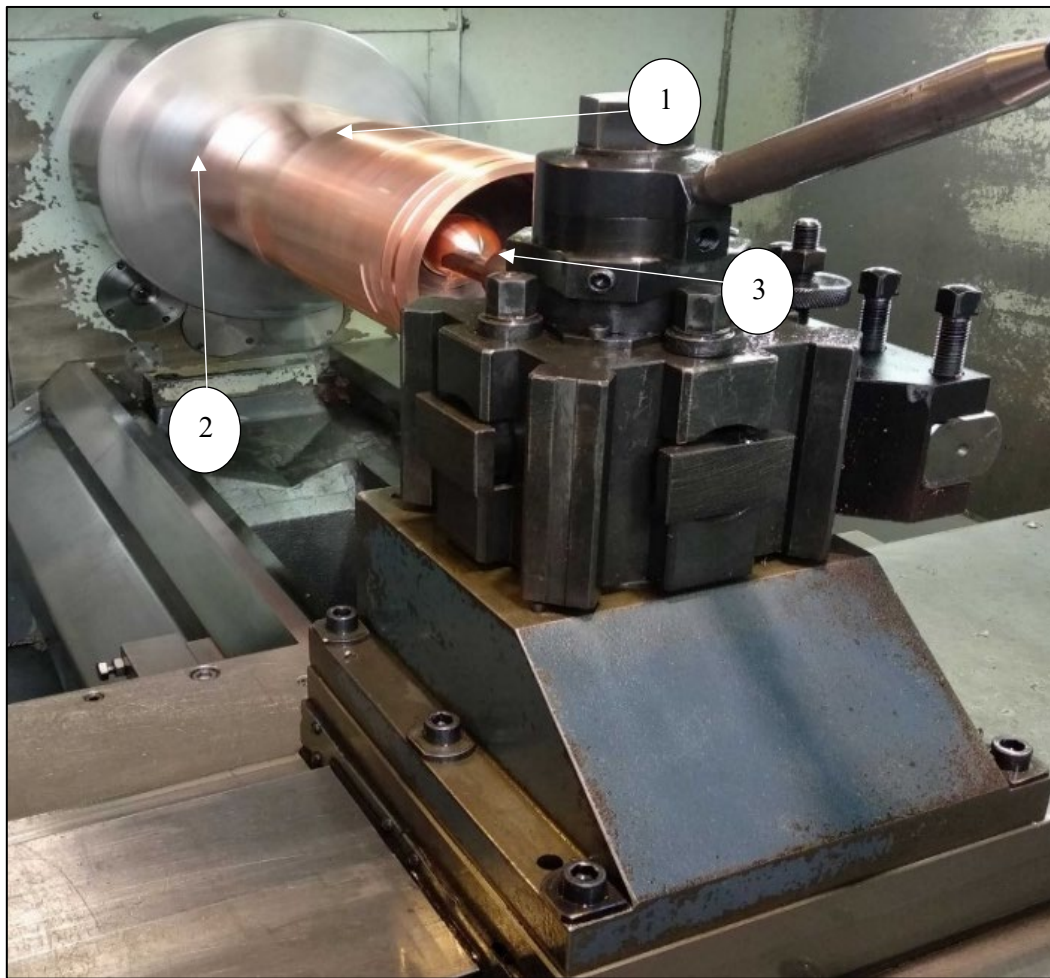


Figure 8.3 – Pre tuning process of the QWR cavity copper billet.

QWR copper billet *(1)* is fixed to the lathe *(2)* in the proper circular fixer. After fixing, rotation of the copper QWR starts and the copper material from specific part of the QWR is replaced with the corresponding tool *(3)*.

The procedure of the frequency measurement is repeated after the QWR lathe machining. In case of difference between real and target frequency, pre tuning process is repeated. If the QWR resonant frequency is similar to the target one, the cavity is transported to the surface preparation treatment.

## 8.1.4. Cavity mechanical treatment

Mechanical defects, cracks, oil and inorganic additives remains in the QWR cavity after forming and pre tuning of the copper billet. The copper surface has high roughness after the machining process. Mechanical surface treatment is needed for decreasing of the roughness and removing of the polluted layer of the copper material.

Research activity of the influence of the different surface treatments onto oxygen free copper planar surface roughness ($R_a$) was performed in INFN [76]. Atomic force microscopy (AFM) measurement of the surface roughness after the tumbling process showed $18{,}3 \pm 1{,}5$ nm of $R_a$. Surface roughness of the copper samples after electrochemical polishing (EP) was $11{,}5 \pm 0{,}7$ nm. Also, SEM microstructural analysis showed very smooth surface without pitting impact of the sample after EP. Electrochemical polishing is promising surface treatment methodology, but using of single EP process is insufficient, there is need of preliminary surface preparation. Tumbling effectively removes big surface defects, like scratches and cracks. Tumbling process as mechanical treatment is used for the QWR surface preparation.

QWR cavity, mounted to the tumbling system, is shown on figure 8.4.



(a)                                                    (b)
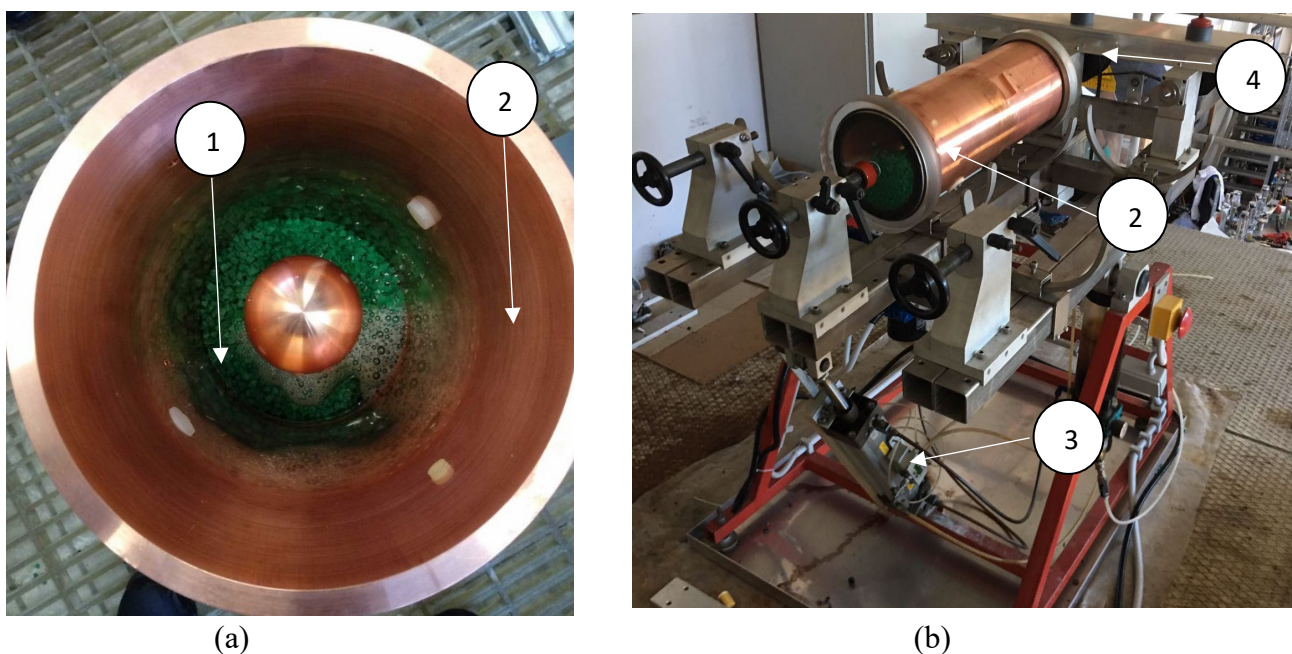
Figure 8.4 – Internal view of the QWR cavity during the tumbling process (a), mounted to the tumbling system (b).

Plastic abrasive compounds of the pyramid shape *(1)* are used for the tumbling process. Before the mechanical treatment, abrasive compounds with the tumbling solution (soap, citric acid, and water) are placed inside the QWR *(2),* and after cavity is mounted to the tumbling system.

Due to complex geometry, the cavity is placed under the angle to the ground obtaining more efficient removal of the material. Angle control of the QWR is regulated by the angle-regulation cylinder *(3)*. Rotation of the cavity with the motor system *(4)* is made for the uniform removal of the material within all the cavity surface.

## 8.1.5. Cavity chemical preparation

Chemical surface treatment is made after the tumbling process. Chemical treatment consists of several steps, which are: ultrasound cleaning, electrochemical polishing, chemical polishing, and passivation. Ultrasound cleaning of the QWR cavity is done for removing organic and inorganic impurities from the surface of the cavity, that may remain after the tumbling process. QWR copper cavity is immersed in the ultrasound bath with 5% NGL 17,40SUP (soap) solution. Ultrasound cleaning is performed at the temperature 60 ºC for 1 hour.

Afterwards the QWR cavity is moved to the EP bath. During electropolishing, cavity is connected to the power supply as an anode. Copper cylinder is used as a cathode for the QWR EP. Electrolytic solution for electropolishing consists of $H_3PO_4$ (85%)/ $C_4H_9OH$(99,5%) with a 3/2 volume rate. The process is performed for 210 min.

The next step is the chemical polishing that is made with the SUBU5 solution, which consists of 5 g/l $H_3NO_3S$, 1 g/l $C_6H_{11}NO_7$, 50 ml/l $C_4H_9OH$ and 50 ml/l $H_2O_2$. SUBU chemical treatment is used for chemical finishing of the cavity surface. The process is made at the temperature of 72 ºC for 3 – 5 min

Passivation process is made after chemical treatment for preventing the copper surface degradation. During passivation process on the copper surface forms protective oxide layer, which prevents further oxidation of the copper. Passivation process is made in 10g/l $H_3NO_3S$ solution for 4 - 5 min.

Water rinsing of the cavity is made during transport of the cavity from the SUBU to the passivation chemical bathes. Copper surface corrodes under influence of acid SUBU5 solution at hot temperature. The water rinsing process is critical, and it is performed to remove the SUBU5 solution from the inner surface of the cavity.

Ethanol rinsing of the cavity is made after passivation. Next step is drying of the cavity by the compressed nitrogen, packaging and QWR transportation to the sputtering laboratory.

Described tumbling and chemical preparation is a standard methodology, used for the copper surface preparation before the niobium deposition [77 – 80]. Parameters of the QWR surface preparation activity are mentioned in table 8.1.

## 8.1.6. Nb/Cu deposition process

QWR cavity is assembled to the sputtering system after chemical surface preparation. Three IR lamps are placed onto the resonator for heating the cavity during the baking and sputtering processes. Two thermocouples are fixed on the side and the top of the cavity to observe the QWR temperature during deposition. Next step is closing and pumping of the system.

Baking of the system and heating of the QWR is made at the parameters, described in table 7.3. After the baking process, vacuum chamber is cooled down with the water circulation in external chamber tubes. Cavity is cooled down from the baking temperature to the initial sputtering temperature, which remains during the chamber cooling down until the start of the niobium sputtering.

After vacuum chamber cooling down, sputtering process is started, using control software, described in paragraph 6.2.4.

Figure 8.5 shows modulation of the main sputtering parameters during two deposition cycles.
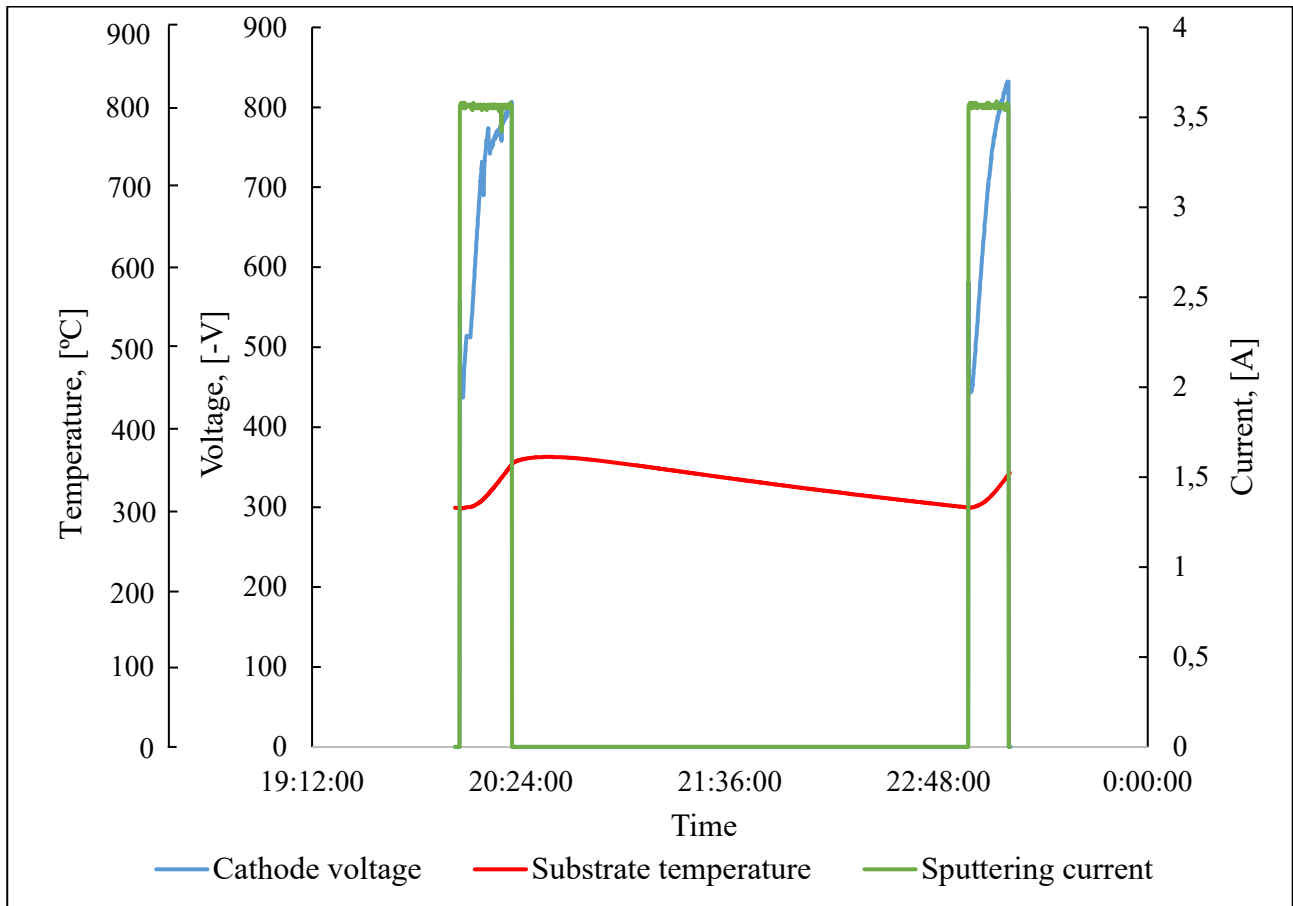


Figure 8.5 – Substrate temperature, cathode voltage and current change during two sputtering cycles.

During the sputtering cycle initial cathode voltage absolute value increases from 420 V to 800 V. The substrate temperature increases by 50 ºC and after the end of the run continues to rise by inertia for several minutes. After that substrate is cooled down to 300 ºC for the next cycle.

View of the internal surface of the QWR after each step of the production procedure is shown on figure 8.6.
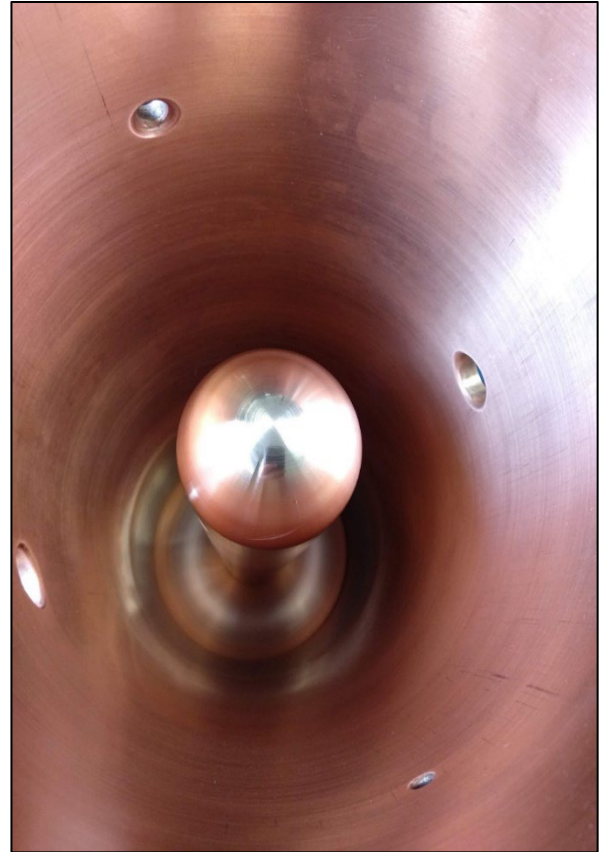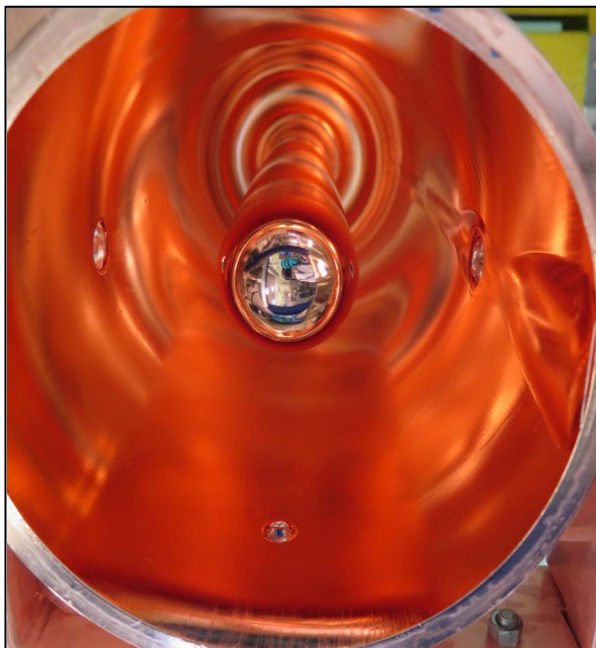
Figure 8.6 – View of the ALPI QWRs internal surface: (a) – after machining; (b) – after tumbling process; (c) – after chemical etching; (d) – after the sputtering process.

Produced Nb/Cu QWR cavity is disassembled from the vacuum system and moved to the chemical laboratory for dust-free water high pressure rinsing.

Production of one high-β Nb/Cu QWR is a long-term process. All the preparation steps from mechanical treatment to the assembling in the sputtering system is performed in 4 days. Baking, sputtering, and system cooling down process before venting takes another 10 days of activity. In total 2 weeks is needed for preparation and coating of 1 Nb/Cu high-β QWR cavity. 10 Nb/Cu high-β QWR cavities were coated with described methodology during research activity onto the ALPI upgrade of the SPES facility.

## 8.1.7. Stripping process

Methodology of the RF measurements is described in chapter 9. Niobium deposit is removed in case of visible defects, cracks, delamination of the niobium film from the substrate or low superconductive performance of the coated QWR cavity.

Water solution 48%HF, 50% HFB$_4$, and Stripaid with concentrations of 2,5%, 2,5%, and 100 g/l respectively is used for the stripping process. Niobium coating is oxidised with fluoboric acid (HFB$_4$) and after, created niobium oxide is dissolved by the hydrofluoric acid (HF). Cavity is placed vertically, and circulation of the stripping solution is made for 6 hours. After removal of the niobium coating, QWR chemical preparation methodology, described in paragraph 8.1.5 is repeated.

## 8.2. Plates production activity

Due to the planar substrate geometry, mechanical and electrochemical treatment for the QWR plates is unnecessary. Chemical treatment is used for the preparation of the copper plates to the sputtering process after mechanical forming. After cleaning, plates are assembled to the sputtering system. The deposition of the niobium onto copper substrate is made.

## 8.2.1. Chemical treatment of the QWR plates

First step of the plate chemical treatment is ultrasound cleaning. The same solution and parameters, as for QWR ultrasound cleaning, is used.

Ammonium persulfate treatment is made for removing part of the material and activation of the surface for polishing after ultrasound cleaning of the copper substrate. 20% (NH$_4$)$_2$S$_2$O$_8$ solution is used for the surface activation. Process is made at the temperature 20 ºC for 20 min.

Chemical polishing and passivation methodology of the plates treatment is similar to the QWR chemical polishing and passivation.

Before sputtering preparation steps of the QWR cavities and plates are described in table 8.1.

Table 8.1. Surface preparation treatments of the QWR cavities and plates.

| Preparation step | QWR cavities | QWR plates |
|---|---|---|
| Pre tuning | + | - |
| Mechanical tumbling | 48 – 72 hours | - |
| Chemical treatment | | |
| Ultrasound cleaning | 5% NGL 17,40Sub (soap) solution at 60 ºC for 1 hour | |
| Surface activation | - | 20% $(NH_4)_2S_2O_8$ at 20 ºC for 20 min. |
| Electropolishing | $H_3PO_4$ / $C_4H_9OH$ = 3/2 v.r.for 210 min. | - |
| SUBU | 5g/l $H_3NO_3S$; 1g/l $C_6H_{11}NO_7$; 50ml/l $C_4H_9OH$; 50 ml/l $H_2O_2$ at 72 ºC for 4 – 6 min. | |
| Passivation | 10 g/l $H_3NO_3S$ for 4 - 5 min. | |
| Rinsing | With water and ethanol. | |
| Drying | With compressed $N_2$. | |
| Packaging | + | |

## 8.2.2. Nb/Cu deposition

After substrate preparation, plates are assembled to the sputtering system. The pre-sputtering baking and sputtering processes with defined optimal parameters (Table 7.3) are made. View of the QWR plates surface before and after niobium deposition is shown on figure 8.7.



(a)                                                                              (b)

Figure 8.7 – View of the QWR ALPI plates before – (a) and after – (b) niobium deposition.

After deposition, the Nb/Cu QWR plates are transported to the chemical laboratory for the dust-free water high pressure rinsing.

9 copper plates were coated with described methodology during research activity onto the ALPI upgrade of the SPES facility.

## 8.3. Tuning system

Closed superconductive surface is necessary for the QWR activity in the superconductive state. RF measurements and LINAC activity is impossible for QWR cavities without assembled plates. In case of opened QWR usage, electric field, produced by the cavity, will be not concentrated on the QWR beam line and acceleration will be not performed.

Nb/Cu plates are used for the QWR cavities RF tests and LINAC activity. Plates should be assembled to the QWR cavities in the dust free environment to avoid contamination of the niobium surface. In INFN LNL plates are assembled to the QWRs in the clean room ISO 5 with the tuning system.

Another tuner function is adjustment of the operating frequency during QWR activity. The frequency change of the cavity at low temperatures can be caused by liquid helium fluctuations, QWR mechanical deformation and imperfections or vacuum instability due to the temperature change. Adjustment of the operation frequency is reached by mechanical movement of the plate and changing distance between the plate surface and the cavity inner conductor.

Tuner system view and design of the ALPI QWR are shown on figure 8.8.
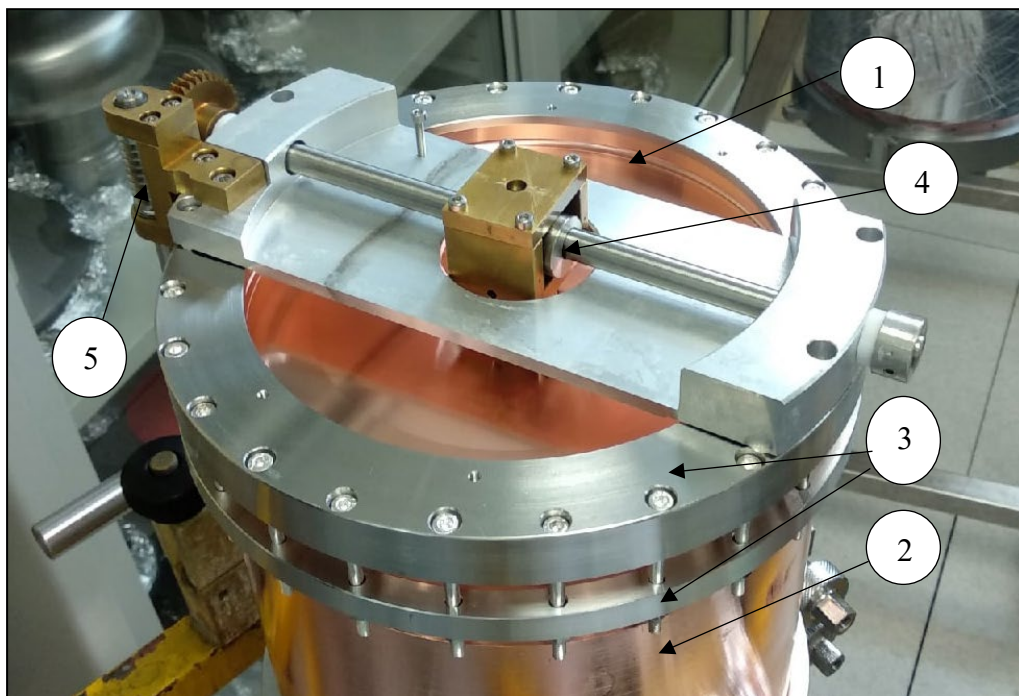


(a)
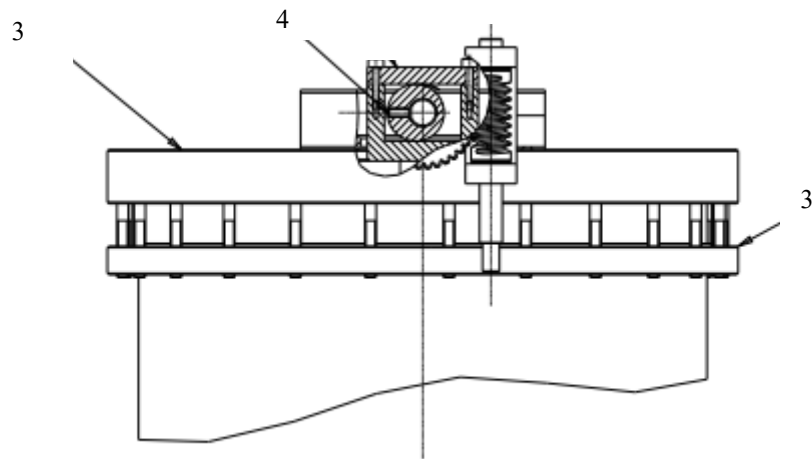
(b)

Figure 8.8 – ALPI QWR tuner (a) – view and (b) - design.

As shown on figure 8.8a, plate *(1)* is connected to the cavity *(2)* with the fixing flanges *(3)*. Strong electrical and thermal contact between cavity and plate surfaces is critical for the thermal stability of all the measured system.

Thermal distribution between QWR cavity and plate was noticed during the first RF measurements. Cooling down of the cavity is performed by immersing liquid helium inside the inner conductor (Figure 6.9). Plate cooling down occurs due to the thermal transfer between the cavity and plate. With bad attachment, temperature of the plate increases rapidly during the RF activity and passes the critical temperature, which causes transition to the normal conducting state of all the item.

It was decided to upgrade the tuner assembling methodology after facing this problem. The number of the fixing silvered screws M4 x 50 mm was doubled (from 12 to 24) for the cavity-plate assembling. It was decided also to close the screws with torque wrench with a similar force (3.2 N.m) to uniform the force along all the plate-QWR contact region.

Positioning of the plate is made by the concentric ring *(4)*, assembled from the top of the plate. Plate movement (Figure 8.8b) occurs in the range ±2.5 mm. in respect to the inner conductor, which gives frequency shift of the cavity of ± 15 kHz. Concentric ring is connected to the system of gearwheels *(5)*, which allows control of the plate position externally from the cryostat during RF measurements. The cavity is transported for the radiofrequency measurement in vacuum cryostat after tunning assembling.

# Chapter 9

# RF MEASUREMENTS

## 9.1. RF measurement system

The characterisation of the SRF cavities superconductive performance is made by providing low level RF signal into the cavity. Definition of the main QWR parameters is made by mathematical convert of the provided and received RF signal to the main cavity parameters.

Low temperature RF measurements define the main parameters of the QWR in superconductive state, such as the quality factor, accelerating voltage, acceleration field energy at certain power, stored energy, surface resistance and dissipated power. The main features of the QWR performance characterisation are quality factor ($Q_0$) and the dependence of the quality factor on the energy of acceleration field (Q – slope).

There are two ways to provide low level RF signal in the RF system: self-excited loop and generator driven signal. For the ALPI QWR cavity VCO-PLL (Voltage-Control Oscillator with Phase-Locked Loop) self-excited loop method with adjustment of the coupler position is used [47].

The apparatus for RF measurement, produced by S. Stark [81] take an advantage of the PC control (Figure 9.1). The system is connected to the signal generator, power meters, DC amplifier and frequency counter, which gives the possibility of the online control and half-automatic performance of the low temperature conditioning and RF measurement. RF signal is generated by the RF R&S SMN Generator. Signal is divided onto three loops, one of which is connected to the frequency counter Agilent 53131A through the attenuators. Second loop through I/Q modulator is transported to the input B of a phase detector. Third loop through the variable attenuator is transferred to a power amplifier. Power amplifier is used for adjusting the loop gain to avoid oscillations. After the RF signal passes through the Narda bidirectional coupler and arrives to the driven cavity coupler.

The pick-up signal from the cavity, through the variable gain amplifier, is transferred to the input A of the phase detector AD 8302. The phase error is produced by comparing the variable gain amplifier output signal with a frequency reference from the output of the phase shifter, which arrived there from the phase detector. The amplitude error is obtained by the comparison between the detected signal and a constant amplitude reference. Variable gain amplifier and phase detector correct the initial input signal and keep the difference of the phase at minimum. Adjusted signal goes after to the DC error amplifier, which then feeds the RF generator signal and closes the RF loop.
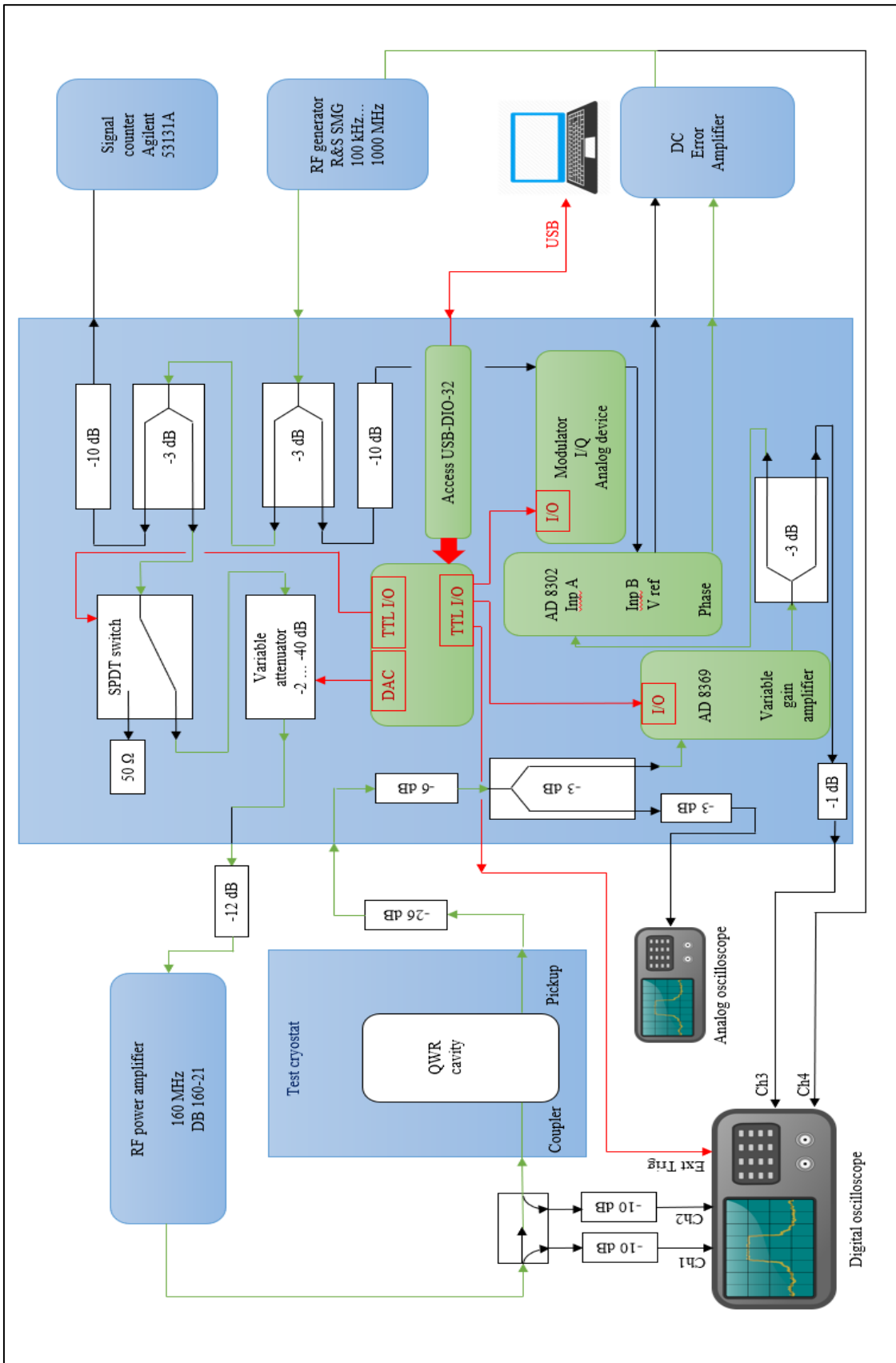
Figure 9.1 – The RF measurement system for ALPI QWR cavities.

## 9.2. Cryostat preparation for the RF measurements.

Test cryostat, described in chapter 6, is used for the RF measurements of the ALPI QWR cavities [82].

After assembling the QWR in the clean room, it is transported to the cryogenic laboratory and connected to the cryostat stand (Figure 9.2).
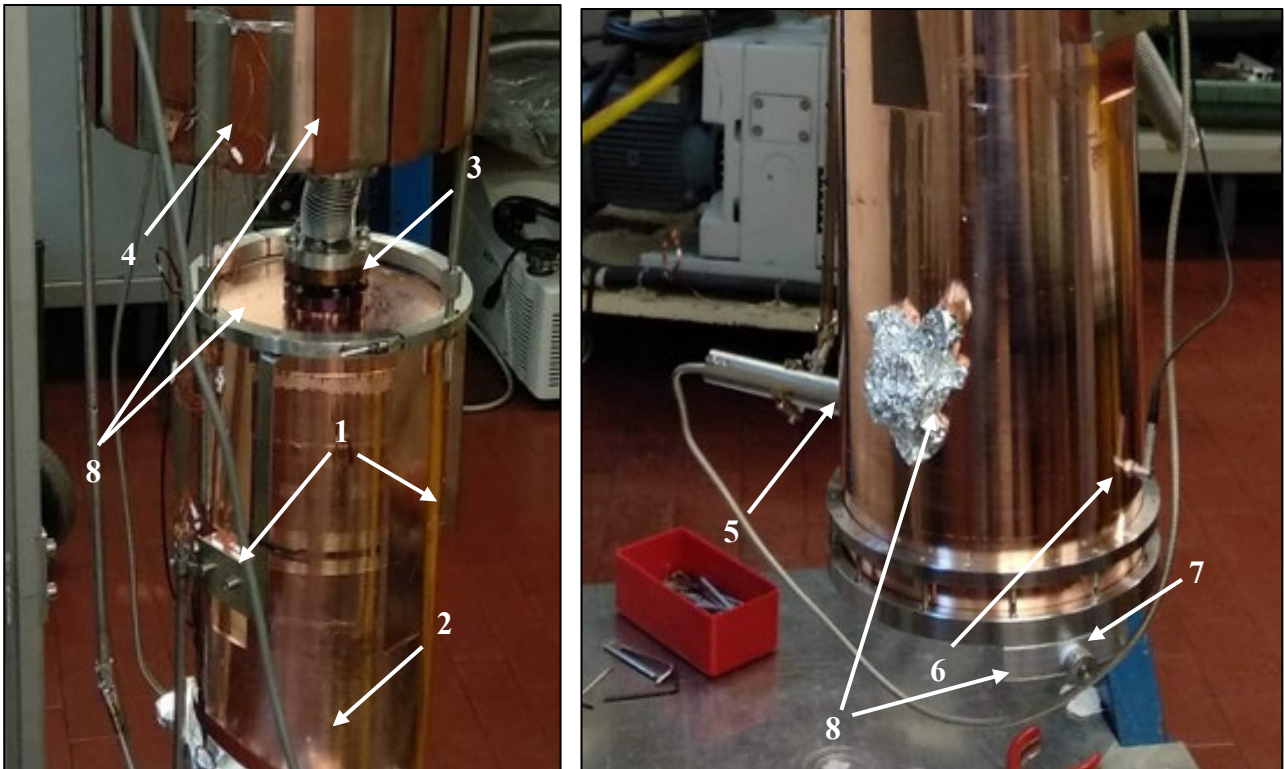


Figure 9.2 – QWR cavity, assembled to the cryostat stand.

The cavity is attached to the cryostat stand by connecting it to the holding jacket (1) with four M6 screws on the cavity sides (2). For cooling down of the cavity to the operating temperature (4,2 K) upper CF 35 flange *(3)* of the cavity is connected to the helium dewar *(4)*. Coupler *(5)* and pick-up *(6)* antennas are connected on the bottom sides of the cavity. Scheme of the cryostat is described in paragraph 6.4.1. Control system is connected to the tuner *(7)* for mechanical adjustment of the QWR frequency during the RF test. Four Cernox type diode thermometers *(8)* are connected along helium dewar and all the external cavity surface for online monitoring of the system temperature during the measurements.

After assembling, QWR frequency and RF signal of the antennas are checked.

Before performing the characterization of the resonator, it is essential to carry out a QWR baking in vacuum. This process is performed to clean the cavity walls from adsorbed humidity and residual gasses for reducing the multipacting effect. For the baking processing, infrared lamp is assembled in the helium line of the cavity. In parallel the external cryostat shield is refiled by liquid nitrogen for stabilization of the cavity temperature during RF operation and decreasing of the helium usage during the cavity cool down (Figure 6.9).

Multipacting occurs in the QWR cavities during initial RF signal transfer. Reasons and mechanisms of this effect are described in paragraph 4.8.2. Implementation of the low RF signals into the cavity at so-called multipacting regions is made for QWR multipacting level processing. This process is called conditioning (Figure 9.3). Conditioning of the cavity is made at normal conducting state ("high temperature" conditioning) for preliminary preparation of the superconductive coating and after cooling down of the resonator to superconductive state ("low temperature" conditioning) for final cleaning of the niobium deposit before the RF measurements.
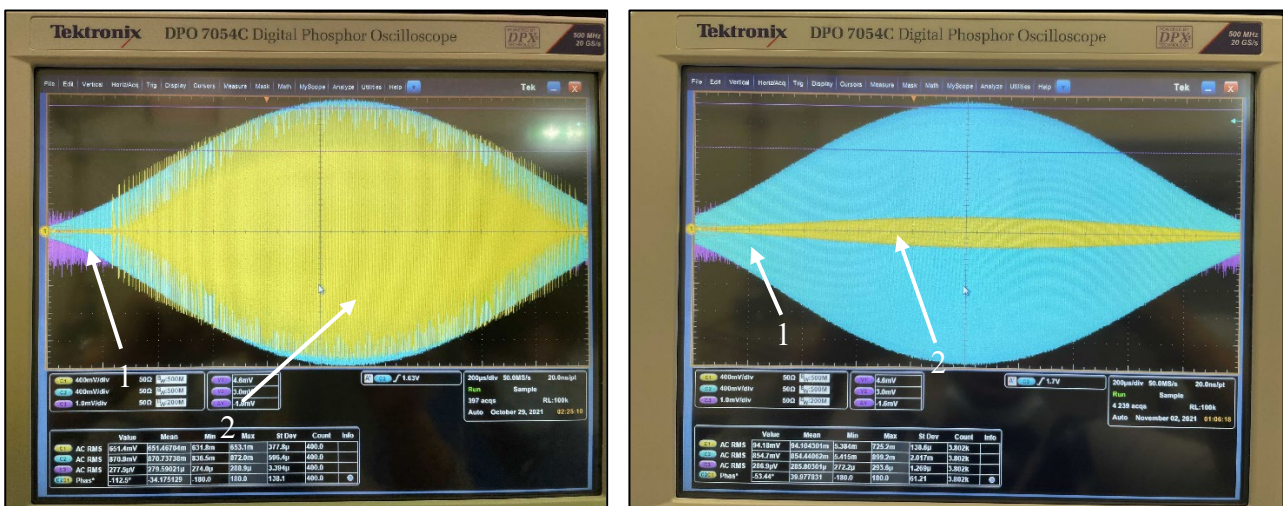


Figure 9.3 – RF signal (a) – before and (b) - after the "hot temperature" QWR conditioning.

At beginning of the "hot temperature" conditioning process, with stable implemented RF signal *(1)*, high reflected signal instabilities *(2)* are significant due to electron emittance from the surface structure. With constant impact of the RF signal onto superconducting coating, reflected power stabilize and multipacting effect vanishes. "Low temperature" conditioning is performed for increasing superconductive properties of the cavity by implementation of the RF signal to the cavity at superconducting state. Ultra-pure helium gas is used during the "low temperature" conditioning. Helium gas is fluxed into the vacuum chamber to reach system pressure of $10^{-7} – 10^{-5}$ mbar for the production of the helium plasma. Plasma ions bombard the niobium surface and clean the niobium

coating. The QWR conditioning at superconductive state is performed before and between different RF tests.

After baking and "hot temperature" conditioning of the QWR, the cryostat stand with the cavity are cooled down (Figure 9.4).
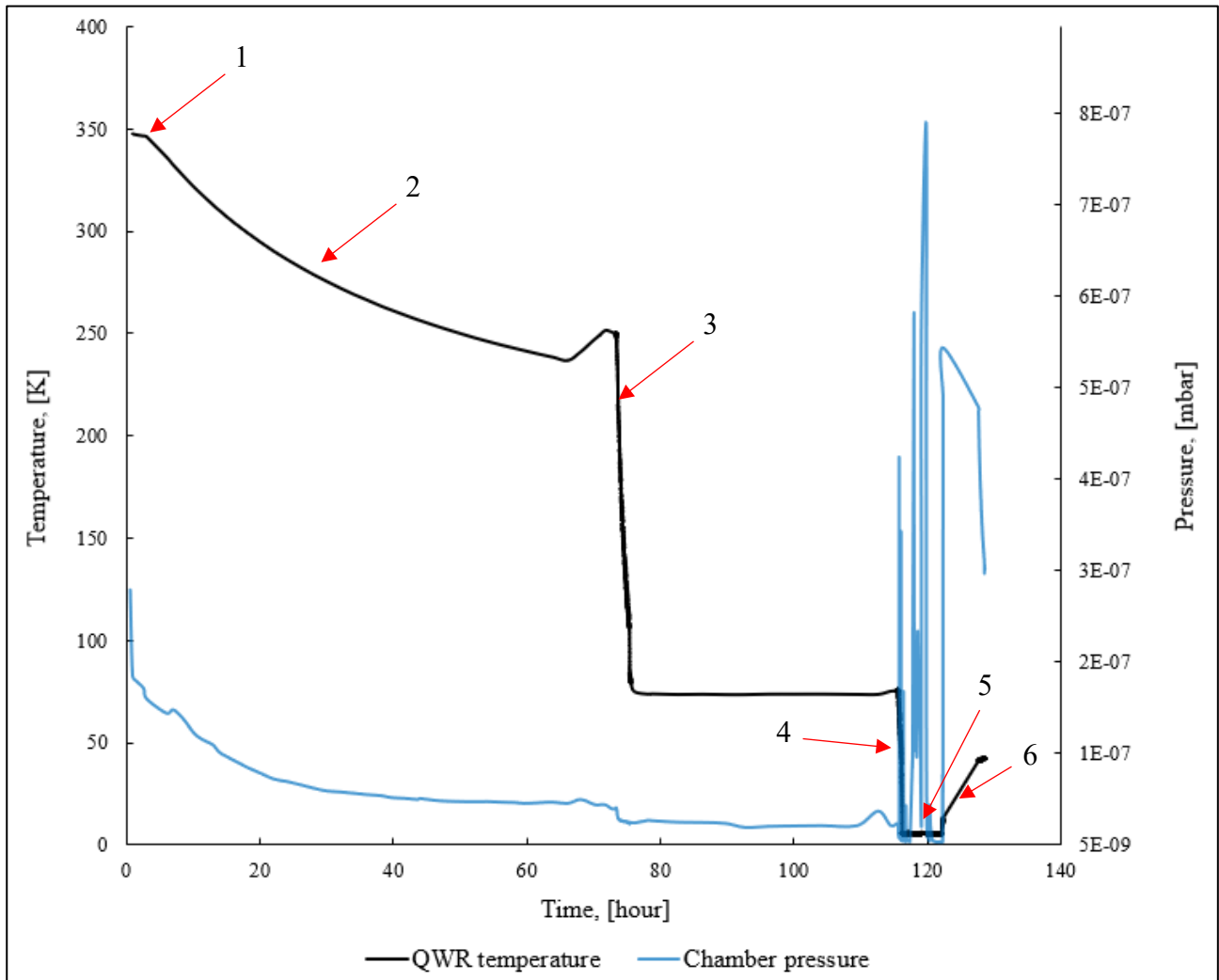


Figure 9.4 – Cavity temperature and chamber pressure change during system preparation and RF measurement procedure.

Cavity temperature behavior during vacuum cryostat activity can be divided on several significant regions, which corresponds to the specific process of the QWR treatment activity. Region *1* corresponds to the finish of the baking and "high temperature" QWR conditioning, after which cavity thermalizes in the vacuum system (region *2)*. Strong drop of the temperature from 270 K to 73 K (region *3)* occurs due to cooling down of the QWR by liquid nitrogen. Second strong temperature decrease (region *4)* corresponds to the QWR cooling down by liquid helium from 73 K to 4,2 K.

Following the transition of the QWR from normal to superconductive state, the RF measurement is performed (region *5*). Several picks of the chamber pressure during cryostat measurements can be explained by introduction of the extra pure helium gas in the chamber for the "low temperature" QWR conditioning. At the conclusion of the RF test, QWR temperature rises steadily to room temperature (region *6*).

The parameters of the preparation steps for ALPI QWR RF measurements are mentioned in table 9.1.

Table 9.1. RF test preparation treatment of the ALPI QWRs.

| Treatment | Parameters |
|---|---|
| Baking of the cavity | Temperature: 350 K; Time: 72 – 96 hours. |
| "Hot temperature" conditioning | Power: 1 – 72 W; Time: 72 – 96 hours. |
| QWR liquid nitrogen cooling down | From 270 K to 73 K. |
| QWR liquid helium cooling down | From 73 K to 4.2 K. |
| "Low temperature" conditioning | Helium pressure: 1E-07 – 1E-05 mbar; Power: 13 W. |

## 9.3. RF measurement methodology.

## 9.3.1. RF cables calibration.

Before carrying out the characterization of the resonator, it is essential to calibrate the cables, for correct reading and evaluation of the signal power, that is transferred through the coupler (forward line) and taken from the pick-up (reflected line) of the cavity.

In the first step, the forward line end is connected to a power meter for calibration of the line of the measurement system after the outlet of the bidirectional coupler. Real value of the signal can be seen in the forward outlet of the bidirectional coupler. The power meter measures the signal with error, which corresponds to the system cables attenuations. The difference between these two values is calculated in a correction coefficient, which should be input inside the measurement software.

Second step is calibration of the reflected line. Short circuit is placed in the end of the bidirectional coupler and signals, measured from the forward and reflected lines of the bidirectional coupler should be equal. In case of difference, correction coefficient should be placed in the measurement software.

The last apparatus of the RF system, that should be calibrated, is low level RF (LLRF) box. Calibration of the LLRF box starts from connecting coupler line to the pick-up line. After that, signal, that is seen on the channel 3 (Figure 9.3) of the digital oscilloscope should be the same as the signal that came out of the power amplifier. Corrected coefficient is put into the measurement software.

124

It is necessary to set the system frequency out of the QWR resonance frequency for calibration of the RF cables, that connects from the measurement system to the cavity. In this case input signal will be reflected from the cavity and will be high enough to perform the calibration. After setting up the frequency, bidirectional coupler output line should be connected to the pick-up cable of the QWR. The difference between forward and reflected signals of the bidirectional coupler will show the error, which should be considered due to the RF pick-up cable usage. After calibration of the pick-up cable, forward cable should be connected to the bidirectional coupler and the procedure repeats.

## 9.3.2. The decay measurement.

The decay measurement starts by pulsing the RF power on and off for determination if the cavity is over coupled ($\beta_{cpl} \gg 1$) or under coupled ($\beta_{cpl} \ll 1$). Stable gradient is calculated by the measured incident power $P_i$, reflected power $P_{ref}$, and peak-up power $P_{pk}$.

The cavity drive signal is turned off and the decay time constant $\tau_E$ is measured by the pulsed RF power meter. A view of the ALPI QWR decay measurement is shown on figure 9.5.
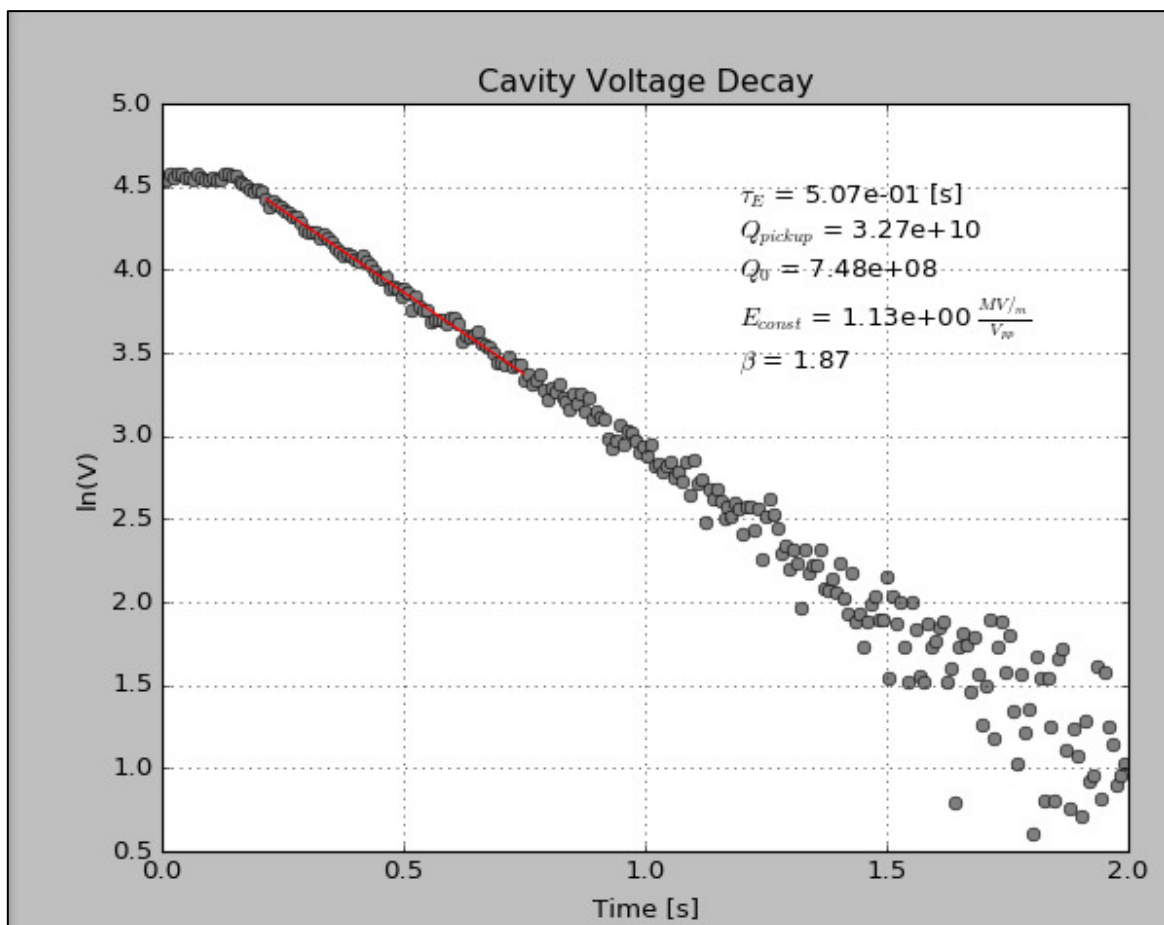


Figure 9.5 – The decay measurement curve of the HB 5 ALPI QWR cavity.

The $\tau_L$ is then used to calculate the $Q_L$ and, later, the quality factor of the cavity ($Q_0$). Theory of the QWR RF decay and Q-slope measurements is described in paragraph 4.9. The equations, used by the measurement software, are described below.

The loaded quality factor is characteristic of the QWR cavity including peak-up and coupler antenna, defined by the formula:

$$Q_L = \tau_L \omega \tag{9.1}$$

Where $\omega$ is the resonator frequency. The peak up quality factor is defined from the measured peak-up power:

$$Q_{pk} = \frac{\omega \cdot U}{P_{pk}} \tag{9.2}$$

The coupling factor is defined from the measured incident and reflected power by the formula:

$$\beta = \frac{1 + \sqrt{P_{ref}/P_i}}{1 - \sqrt{P_{ref}/P_i}} \tag{9.3}$$

After the coupling factor definition, correlated quality factor is defined by the formula:

$$\grave{Q_0} = Q_L \cdot (1 + \beta) \tag{9.4}$$

In the end, the QWR quality factor ($Q_0$) is defined with excluding of the coupling factor and peak-up quality factor:

$$Q_0 = \frac{\grave{Q_0} \cdot Q_{pk}}{Q_{pk} - \grave{Q_0}} \tag{9.5}$$

### 9.3.3. Quality factor in the function of the gradient measurement.

The measurement of the quality factor as function of the cavity accelerating field (so-called "Q-slope") is performed to evaluate the superconductive performance of the cavity.

Superconductive properties of the Nb/Cu QWR cavities are strongly dependent onto quality of the coating. As long as the power losses in the cavity walls are proportional to the stored energy, $Q_0$ should be constant with the gradient increase and $Q = f(E)$ should have linear behavior. This is typical for ohmic losses. In case of losses, such as field emission, quality factor will decrease nonlinear with

126

stored energy increasing, which will cause fast drop of the Q vs E function at a defined gradient. With increasing of the impurities number in the crystallite structure of the niobium coating, lattice defects and migration of the different gasses into the deposit Q-slope will be characterized by stronger dependance of the quality factor onto the energy of the acceleration field with the fast drop of Q at low gradient quantities.

The Q-slope measurement are made with increasing of the input power into the cavity and calculation of the quality factor by the formula:

$$Q = \frac{U \cdot \omega}{P_{Tran}} \tag{9.6}$$

Where $P_{Tran}$ is transmitted through the QWR power, and $U$ is stored energy, which is defined by the formula:

$$U = \frac{Q_{pk}P_{pk}}{\omega} \tag{9.7}$$

Decreasing of the reflected power and stabilization of the coupling parameters are made by mechanical movement of the coupler antenna in or out from the QWR cavity during the RF test. Example of the obtained Q-slope after ALPI QWR cavity RF measurement is shown on figure 9.6.
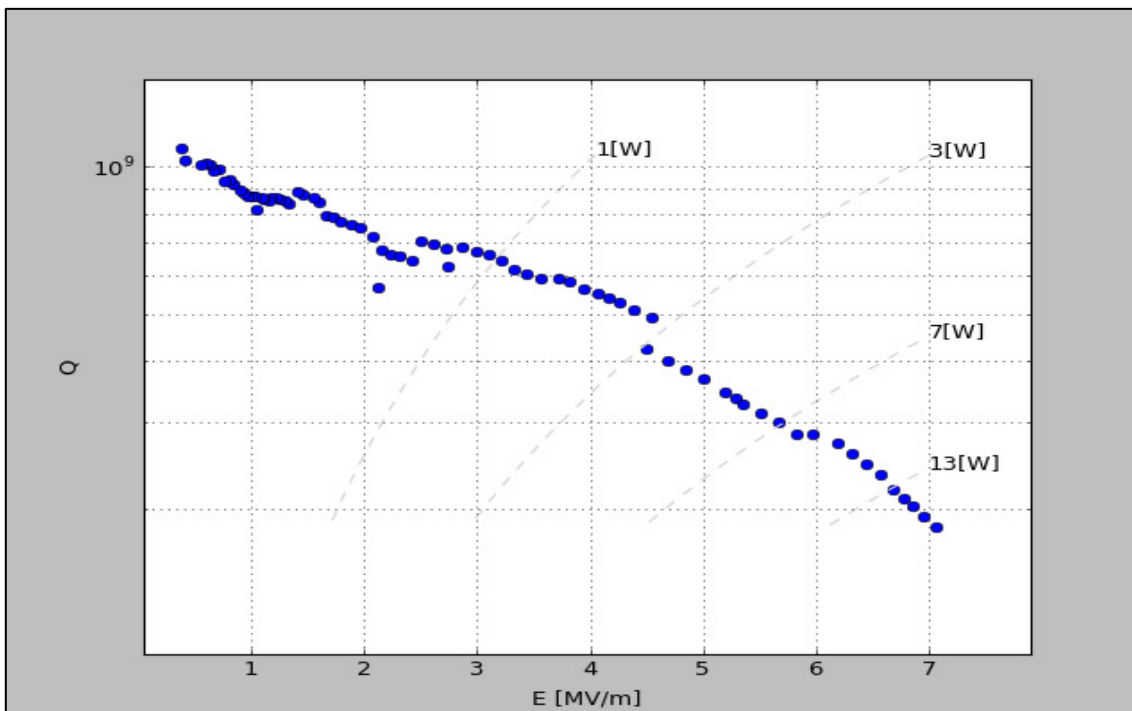


Figure 9.6 – The quality factor in function of the energy of acceleration field for HB 5 ALPI QWR cavity.

## 9.4. Results of the Nb/Cu QWR RF measurements.

RF testing is a complex and time-consuming process, taking 1 week to assemble and prepare the cryostat and a further week to cool the system and measure the resonator. One more week is required for the system heat up after the RF measurement. In total, it takes about 3 weeks to measure a cavity. 5 and 12 RF measurements of medium-$\beta$ and high-$\beta$ Nb/Cu QWR cavities respectively were done during the ALPI upgrade project activity.

Radiofrequency low temperature measurements, done in the framework of the ALPI upgrade project, can be divided onto two sections: Nb/Cu medium-$\beta$ QWR and Nb/Cu high-$\beta$ QWR tests.

The working power of the QWR cavities at the ALPI LINAC is 7 W. Target superconductive performance of the resonators, produced for the ALPI upgrade, is $Q \geq 10^8$; $E_{acc} \geq 4,5$ MV/m at 7 W. Produced Nb/Cu high-$\beta$ QWR cavities, which require appropriate superconductive performance, defined by the RF measurement, can be assembled to the ALPI LINAC. In case of insufficient superconductive characteristics, niobium coating from the QWR cavities is removed chemically by the stripping process, and the resonators are re-sputtered and remeasured.

## 9.4.1. Nb/Cu medium-$\beta$ QWR RF measurements.

Long term activity without any decrease in the superconductive performance of the QWR cavities is an important parameter, which characterise the reliability of the production technology. If the use of cavities in accelerators over a long period does not cause a degradation in produced QWR performance, the sputtering technology can be defined as optimal and can be used with the necessary modifications for the production of other types of resonators.

After long period of activity in the ALPI LINAC was decided to verify superconductive properties of the cavities, produced more than 15 years ago. Cryostat № 7 was disassembled from the LINAC. Last maintenance of this cryostat was done in 2007 and RF measurements of the cavities FC 40 and FC 44 was done for verification of the QWRs superconductive performance. View of the disassembled cryostat is shown on figure 9.7.

<table>
<tr><td>FC 40 (7-1)</td><td>FC 44 (7-4)</td></tr>
</table>
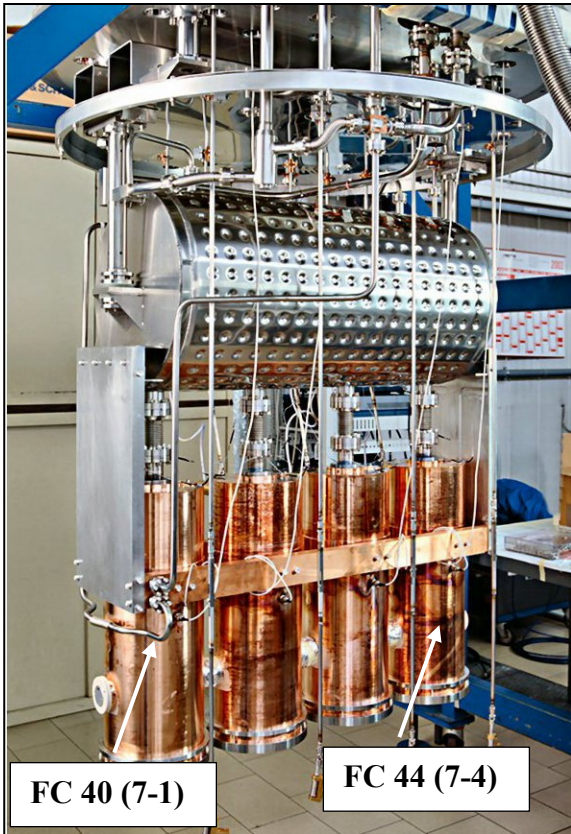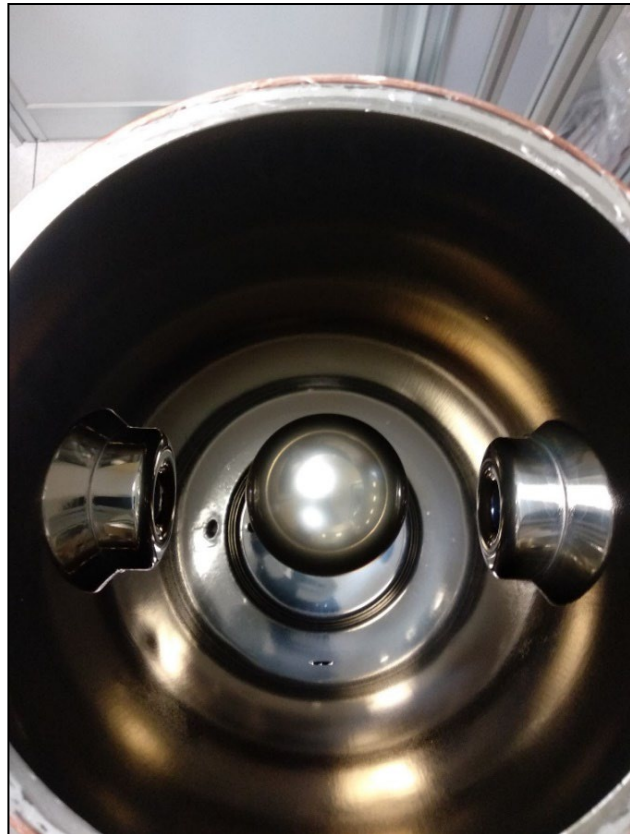
(a)                                                      (b)

Figure 9.7 – View of the disassembled cryostat № 7 – (a) and internal view of the QWR FC 44.

RF measurements of the medium-β cavities were made by the procedure, described in chapter 9. Results of the RF measurements (Table 9.2) and function of the quality factor to the gradient (Figure 9.8) are mentioned below.

Table 9.2. Results of the medium-β QWR cavities RF measurements.

| Cavity number | FC 40 (7-1) | | FC 44 (7-4) | |
|---|---|---|---|---|
| Date | 2007 | 2021 | 2007 | 2021 |
| $Q_0$ | | $2{,}78 \times 10^8$ | | $1{,}76 \times 10^8$ |
| Q [7W] | $1{,}4 \times 10^8$ | $1{,}31 \times 10^8$ | $1{,}34 \times 10^8$ | $8{,}69 \times 10^7$ |
| $E_{acc}$ [7W], MV/m | 3,8 | 3,63 | 3,79 | 3,15 |
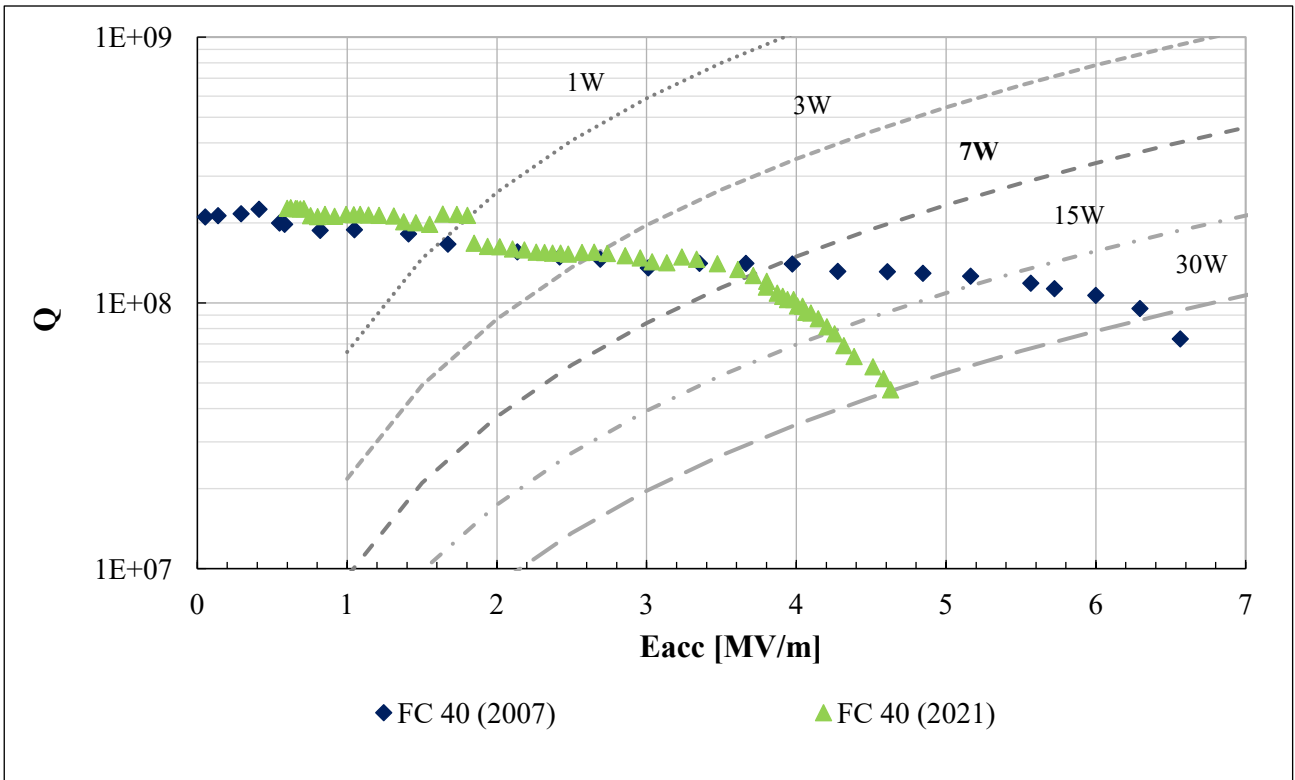
(a)
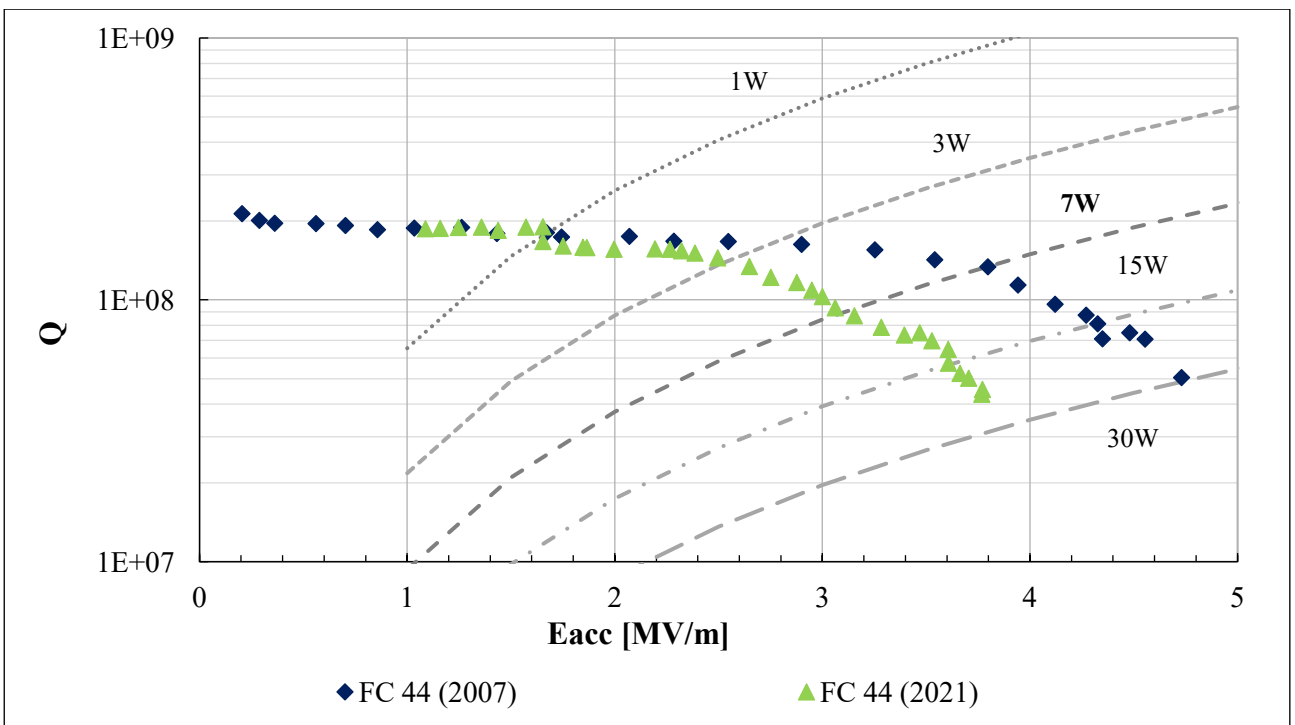


(b)

Figure 9.8 – RF measurement Q-slopes comparison of the 2007 and 2021 years of (a) FC-40 and (b) FC-44 QWRs.

As shown on figure 9.8a, quality factor dependance from the accelerating field is the same, as measured in 2007 until the input power 7 W. The Q-drop starts to be more significant with further gradient increase. This drawback can be removed by additional conditioning of the FC-40 cavity.

In case of FC-44 (figure 9.8b), the quality factor decrease is observed after 3 W of input power, but the Q-slope, measured in 2021 copies the form of the previous RF measurement, made in 2007. With the same low temperature conditioning, as in the case of FC-40 QWR, it is possible to increase the superconductive performance of the FC-44 cavity.

Difference between the superconductive performance at the ALPI LINAC operating power of the FC-40 and FC-44 cavities, measured in 2007 and 2021 years, is minimal. Quality factor curves of both cavities show similar behavior to ones, measured 14 years ago.

RF measurements of the Nb/Cu medium-β QWR cavities, produced more than 15 years ago and used in the ALPI linear accelerator for the long period, showed satisfactory results. The approach of the ALPI Nb/Cu medium-β QWR cavities production is reliable and can be used as basis for the development of Nb/Cu high-β QWR cavities production technology for the ALPI LINAC upgrade.

## 9.4.2. Nb/Cu high-β QWR RF measurement results.

After deposition, Nb/Cu high-β QWR cavities superconductive properties were evaluated by the methodology, described previously. Results of the RF measurements can be divided into two phases.

Cavities with superconducting properties appropriate to the ALPI upgrade project were packaged for the ALPI LINAC assembly. Nb/Cu high-β QWRs with delaminated niobium coating and low superconductive performance are delivered again to the chemical laboratory. Niobium coating from these cavities is removed chemically by stripping process. The copper substrate is subsequently prepared according to the procedure described in chapter 8. Then sputtering is carried out again, followed by RF tests.

Table 9.3 summarizes the results of the first RF measurement cycle of the Nb/Cu high-β QWRs, Figure 9.9 highlights the dependence of the quality factor on the energy of the acceleration field.

Table 9.3. RF measurement results of the first produced Nb/Cu high-β QWR cavities.

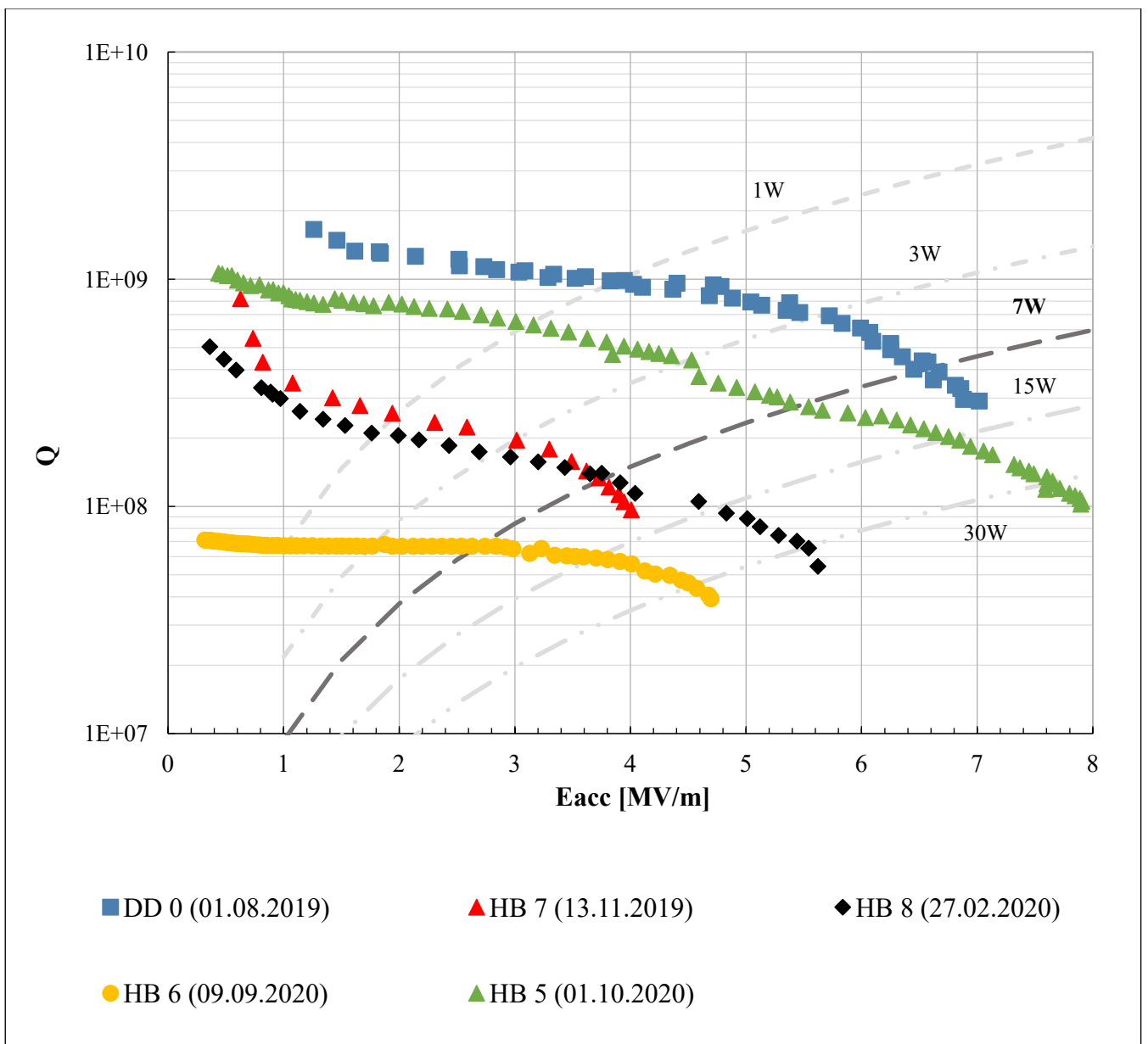| Cavity № | Date | $Q_0$ | Q [7W] | $E_{acc}$ [7W], MV/m | $R_s$, [nΩ] |
|---|---|---|---|---|---|
| **The project target** | | | $\geq 1 \cdot 10^8$ | $\geq 4,5$ | |
| **DD 0** | 01.08.2019 | $2,1 \cdot 10^9$ | $4,3 \cdot 10^8$ | 6,5 | 14 |
| **HB 7** | 13.11.2019 | $4,5 \cdot 10^8$ | $1,4 \cdot 10^8$ | 3,7 | 90 |
| **HB 8** | 27.02.2020 | $1,5 \cdot 10^8$ | $1,4 \cdot 10^8$ | 3,8 | 195 |
| **HB 6** | 09.09.2020 | $7,6 \cdot 10^7$ | $6,7 \cdot 10^7$ | 2,6 | 383 |
| **HB 5** | 01.10.2020 | $7,6 \cdot 10^8$ | $1,8 \cdot 10^8$ | 5,5 | 38 |



Figure 9.9 – Q-slopes of the first produced Nb/Cu high-β QWR cavities.

At the end of the first cycle of RF measurements, we observed that the superconducting properties of several produced resonators achieved the required performance. The superconducting performance of the DD 0 cavity was the highest. However, following cryogenic testing of this cavity, delamination of the niobium coating from the top surface of the inner conductor occurred.

Due to the delamination, this cavity could not be assembled in the accelerator and the coating was removed.

Niobium coating of the HB 5 and HB 8 cavities after deposition had mirror-like view without delamination from the copper substrate within all the QWR inner surface. During RF measurements of the HB 5 cavity was defined superconductive QWR performance, that reached the project target. Due to successful RF measurements and high quality of the niobium coating, HB 5 cavity was packed for the ALPI assembling. RF measurements of HB 8 cavity showed medium superconductive performance with quality factor and energy of acceleration field, slightly lower from the accelerator target.

The measurement of HB 8 cavity was done with the plate, sputtered before. At that point, plate deposition system upgrade was in process and new plates were not produced. The low-quality plate niobium coating could decrease the superconductive performance of the HB 8 cavity. We decided to repeat RF measurements of this cavity increasing "low temperature" conditioning and replacing the old plate onto the new one.

Delamination of the niobium coating in the inner conductor and beam ports surface was observed in the QWRs HB 7 and HB 6. Low superconductive properties and bad adhesion of the coating can be explained by the internal stress of the niobium deposit and wrong distance of the counter electrode in respect to the QWR inner conductor. During the first and second sputtering cycles different sputtering pressures and counter electrode – QWR distance were tested. The influence of these parameters onto superconductive performance of the QWR cavities will be described in chapter 10.

Following stripping, the cavities DD 0, HB 6 and HB 7 were treated again by classical chemical processes (EP, chemical etching, and passivation). In a second step, these cavities were re-coated, and a second cycle of RF measurements was performed. Cavity HB 8 was also re-measured with the modified tuner system, new produced plates, and a further conditioning process.

Results of the second RF measurement cycle (Table 9.4) and quality factor dependence from the acceleration field (Figure 9.10) are mentioned below.

Table 9.4. RF measurement results of the second cycle of the Nb/Cu high-β QWR cavities.

| Cavity № | Date | $Q_0$ | Q [7W] | $E_{acc}$ [7W], MV/m | $R_s$, [nΩ] |
|---|---|---|---|---|---|
| **The project target** | | | $\geq 1 \cdot 10^8$ | $\geq 4,5$ | |
| **DD 0** | 23.07.2020 | $1,0 \cdot 10^9$ | $1,8 \cdot 10^8$ | 4,5 | 28 |
| **HB 7** | 03.12.2020 | $1,4 \cdot 10^8$ | $8,7 \cdot 10^7$ | 3,1 | 207 |
| **HB 8** | 23.06.2021 | $3,0 \cdot 10^8$ | $1,7 \cdot 10^8$ | 4,2 | 96 |
| **HB 6** | 10.09.2021 | $9,2 \cdot 10^7$ | $4,6 \cdot 10^7$ | 2,2 | 315 |
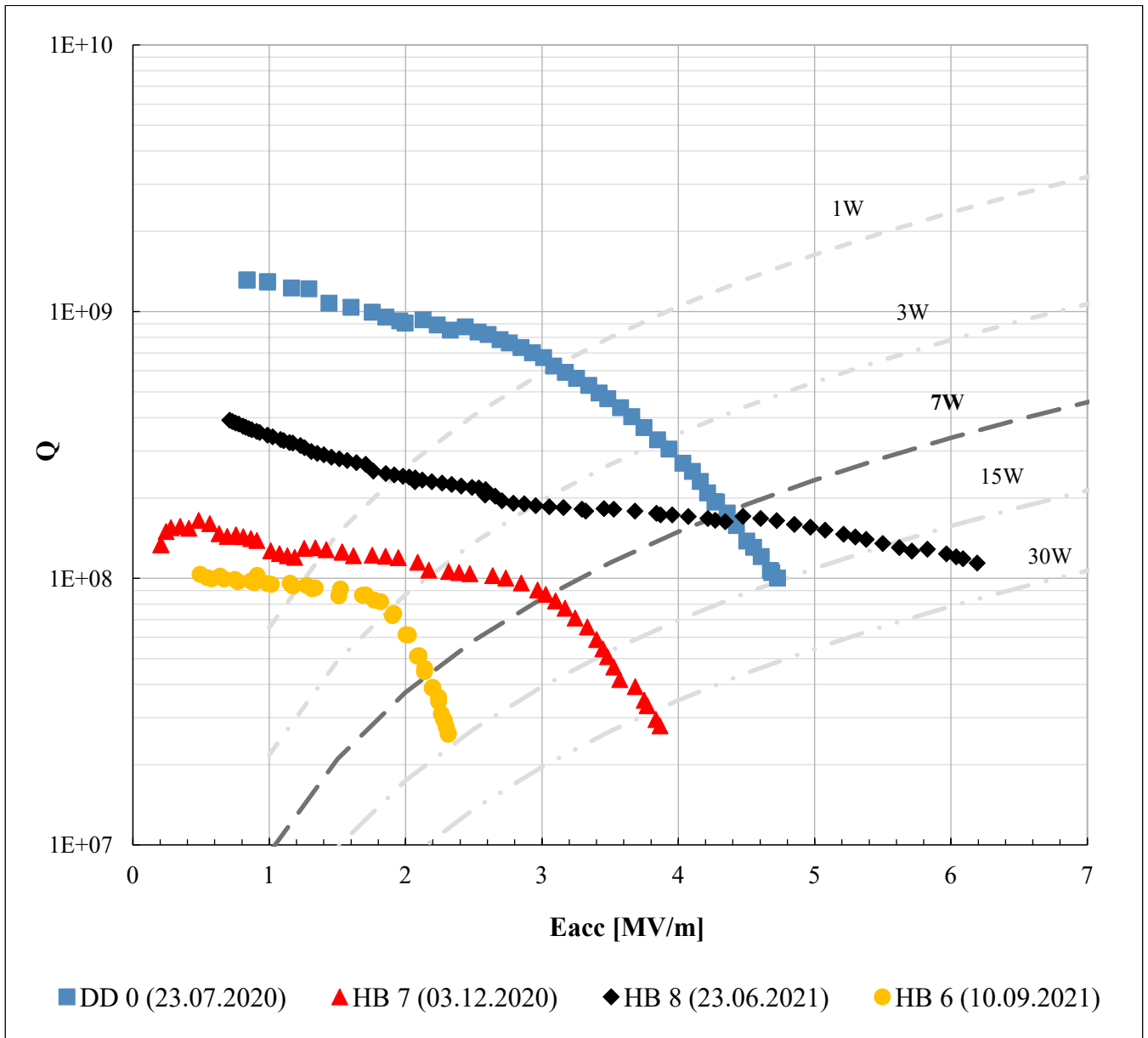


Figure 9.10 – Q-slopes from the second cycle rf measurement of the Nb/Cu high-β QWR cavities.

From the second cycle of the RF measurements results is confirmed that cavities DD 0 and HB 8 showed superconductive performance similar to the ALPI target. With additional low temperature conditioning it is possible to increase the quality factor and the gradient at 7 W of HB 8 cavity. Due to this, the last resonator is ready for assembly in the accelerator. DD 0 cavity will be sent for further RF tests.

The cavities HB 6 and HB 7 showed similar superconductive performance. With the increase of the input power, the quality factor of both cavities is stable at first and after sudden Q-drop appeared (for HB 6 cavity – at 3 W and for HB 7 – at 7 W of the input power). This Q-slope behavior and low $Q_0$ values can be caused by a coating with numerous trapped impurities. Increasing input power impurities starts to overheat and exceed the critical temperature, creating islands of normal conductivity state and increasing of the power dissipation in the cavity walls. This Q-drop dependence is typical of low-quality superconducting films, which consequently must be removed as described above, with chemical techniques in order to re-deposit the resonators.

# Chapter 10

# RESULTS AND DISCUSSION

## 10.1. Analysis of Nb/Cu high-β QWR deposition results.

### 10.1.1. Introduction

After defining the sputtering parameters (chapter 7) and methodology for production of the copper high-β Nb/Cu QWR (chapter 8), the deposition of niobium coatings onto copper QWR substrates was carried out. Compared to the planar surface of the quartz samples, copper QWR substrate has a complicated circular geometry with several critical positions with rounded areas such as the top surface and the terminating part of the inner conductor. The main goal of the niobium deposition onto copper QWRs is to sputter high quality niobium coating without delamination from any part of the cavity surface.

High stress inside of the coating can cause cracks of the niobium deposits and delamination from the copper surface. Bad adhesion of the niobium to copper surface decreases superconductive performance of the produced cavity. On the delaminated region during transition of the cavity in superconductive state occurs so-called "normal conductive islands", which decrease the quality factor of the cavity. During acceleration activity, due to normal conductance and high resistance of the copper spots, normal conductive islands are heated up and the temperature of the nearby niobium coating increases. The non-superconductive surface area in the cavity increases, which further decreases the superconductive performance of the cavity and creates a cascade effect.

Delamination of the deposited layer at some points on the cavity surface may cause further delamination of the coating during long-term operation. For this reason, the use of the delaminated cavity in the accelerator is not permitted. The problems encountered during the deposition of Nb/Cu high-β QWR and the proposed solutions will be described in this chapter.

### 10.1.2. High temperature Nb/Cu high-β QWR deposition.

With increasing of the baking temperature of the system it is possible to perform desorption of the residual gasses from the sputtering system walls and cavity surface more efficient. After high temperature baking a lower base pressure can be achieved, which will decrease the amount of impurities in the niobium coating and increase superconductive properties.

In addition, the decrease in internal stress of the thin film is possible with the increase in sputtering temperature (paragraph 4.9). High internal stress causes defects in the crystal structure and a decrease of the superconductive performance of the niobium film.

It was decided to make one resonator deposition at the high baking temperature, around 550 ºC and consequently a sputtering with the resonator at a temperature of 450 ºC. All the other sputtering parameters remained constant. View of the deposited niobium coating is shown on figure 10.1.



(a)                                                         (b)
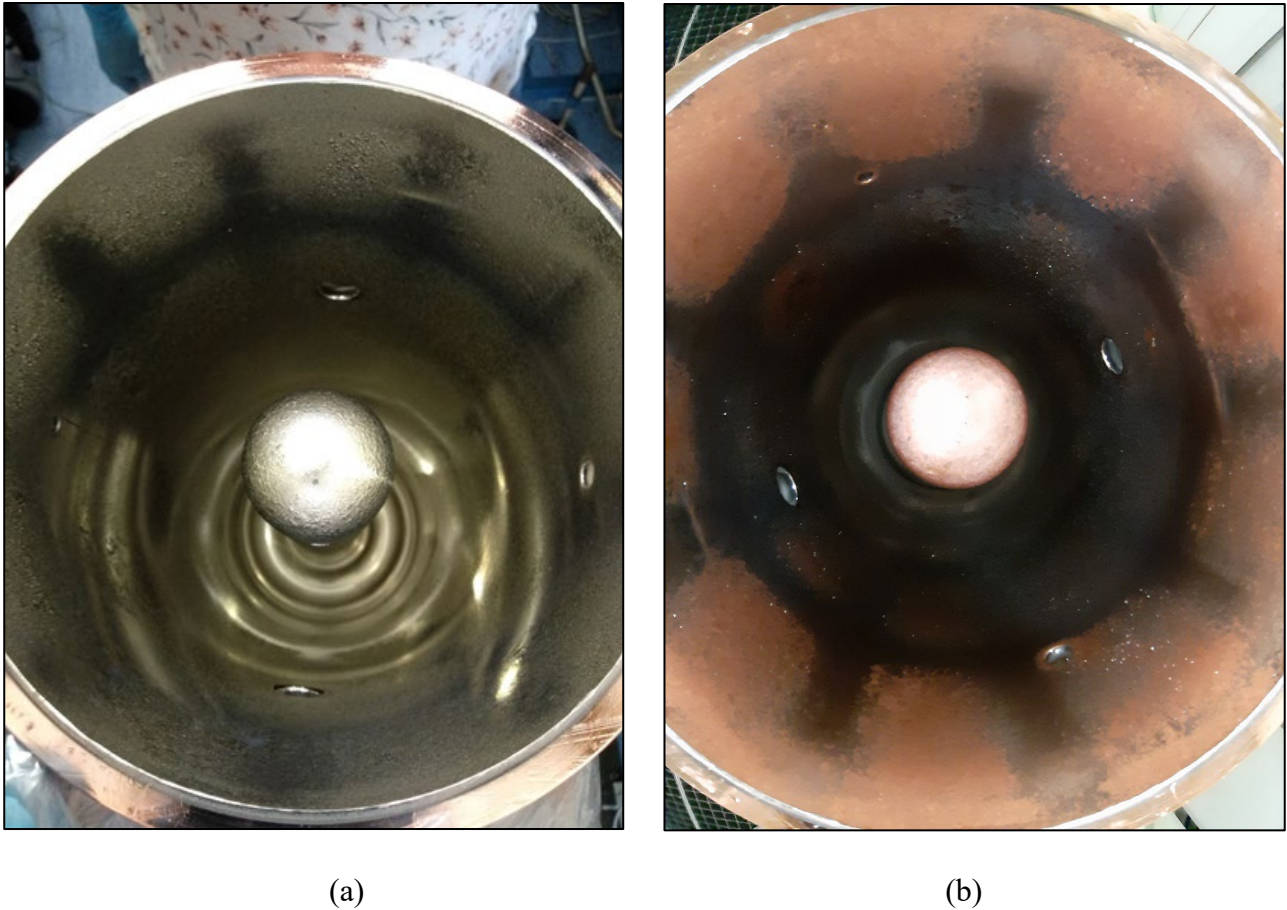
Figure 10.1 – View of the sputtered niobium coating at high temperature (a) – before and (b) – after high pressure rinsing.

As shown on figure 10.1a, a low quality deposit with high surface delamination was obtained during high temperature sputtering. High internal stress of the coated niobium caused delamination from the big internal surface area of the substrate just after high pressure rinsing (Figure 10.1b). This effect can be caused by annealing process of the copper material at high temperatures (Figure 10.2).
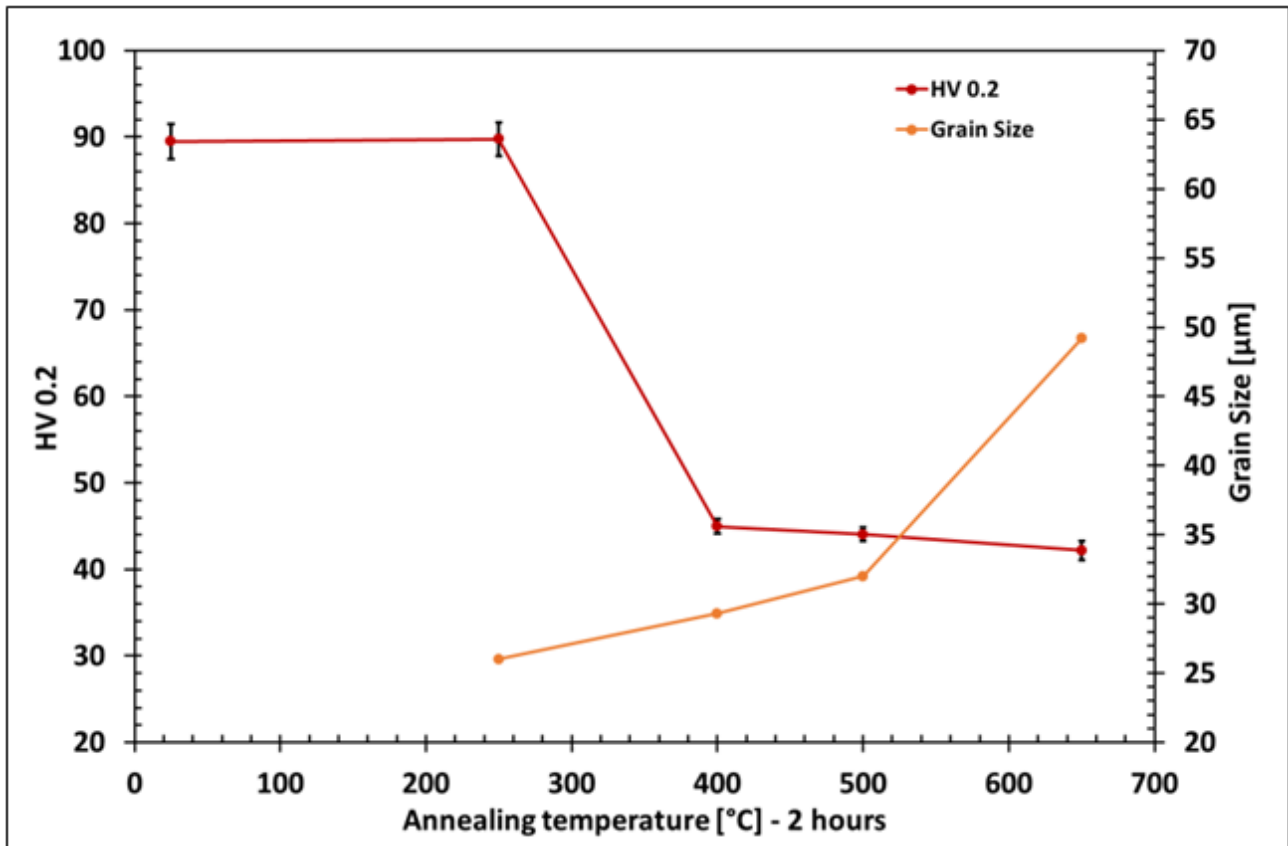
Figure 10.2 – Hardness and grain size change of the copper with the temperature increase [83].

As shown on figure 10.2, at high temperature, hardness of the copper material decreases until 400 ºC and at 500 ºC grain size starts to increase, which corresponds to the annealing of the copper material. The annealing process of the substrate during deposition could cause desorption of the niobium coating. Due to that, temperature of the substrate during baking and sputtering process should not overcome 500 ºC.

## 10.1.3. Delamination of the niobium coating.

Following unsuccessful high temperature deposition, it was decided to lower the temperature to the standard parameters. After the deposition of several high-β QWR cavities a systematic drawback was noticed, shown on figure 10.3.
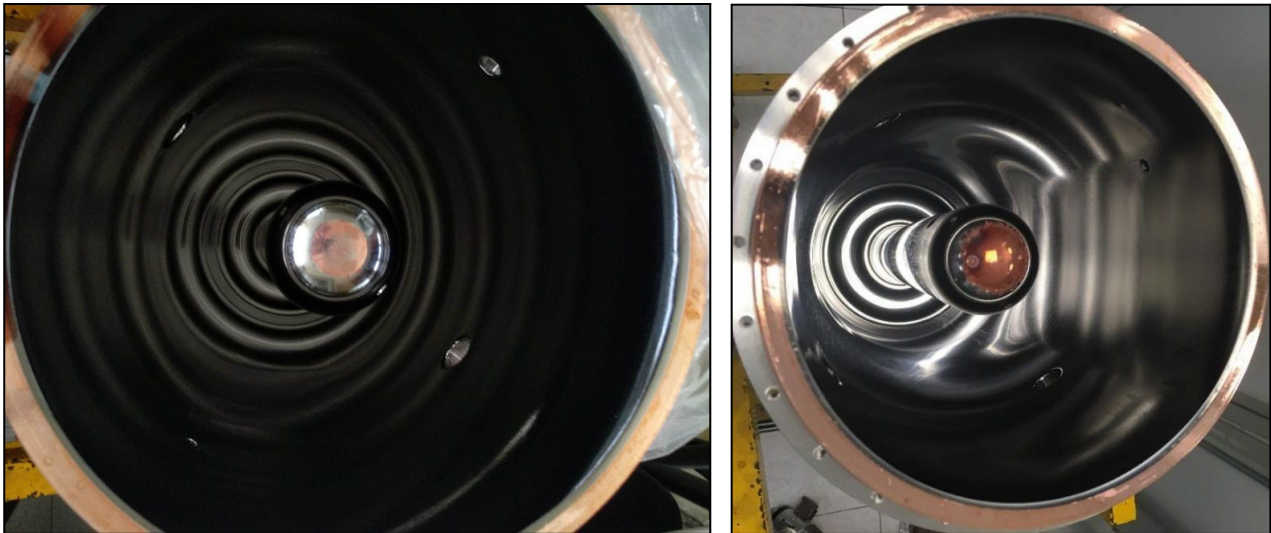
<center>(a)                                           (b)</center>

Figure 10.3 - View of the sputtered (a) – HB 6 and (b) – DD 0 cavities.

In some cases (HB 6, HB 7) delamination of the coating at the bottom of the inner conductor was observed at the time of water pressure rinsing after disassembling of the cavity from the sputtering system. In another case (DD 0) desorption occurred at the same place after two weeks of maintenance in the ISO5 cleanroom.

Possible reason of coating delamination in these specific spots can be high internal tension of the niobium deposit. Due to small radius and the highest electric field density nearby the bottom part of the inner conductor, deposition rate in this specific place is the highest within all the surface of the cavity.

The desorption problem was only observed at the bottom of the inner conductor. The niobium coating "copied" the surface of the substrate without visible defects or delamination, producing a mirror-like film on all other cavity surfaces.

Higher thickness of the niobium coating in some specific area of the QWR cavity can be explained by higher amount of the high energy incident ions in the nearby area. Sputtering yield change with incident ion energy. Sputtering yield and thickness of the deposit increases with increasing of the $Ar^+$ ion energy [49].

The balance of the plasma ions amount is possible due to electric field equilibrium. To reduce electric field density at the bottom cavity surface and consequently the thickness of the inner conductor coating, it was decided to modify the position of the counter electrode with respect to the bottom of

the cavity. Finite element method (FEM) analysis was used for simulation of the counter electrode-cavity distance influence onto the density of the electric field (Figure 10.4).



(a)            (b)            (c)

(d)      (e)      (f)
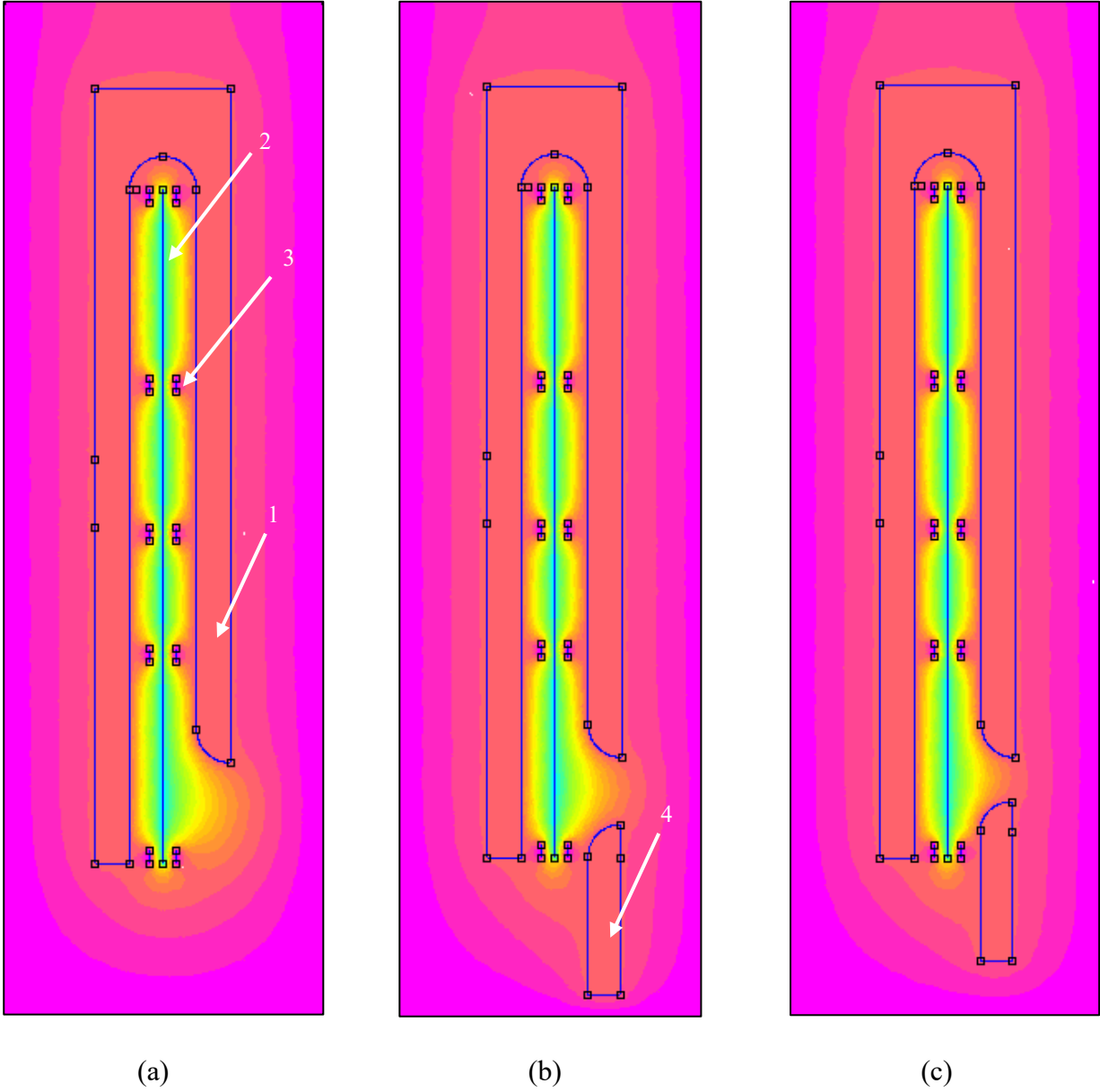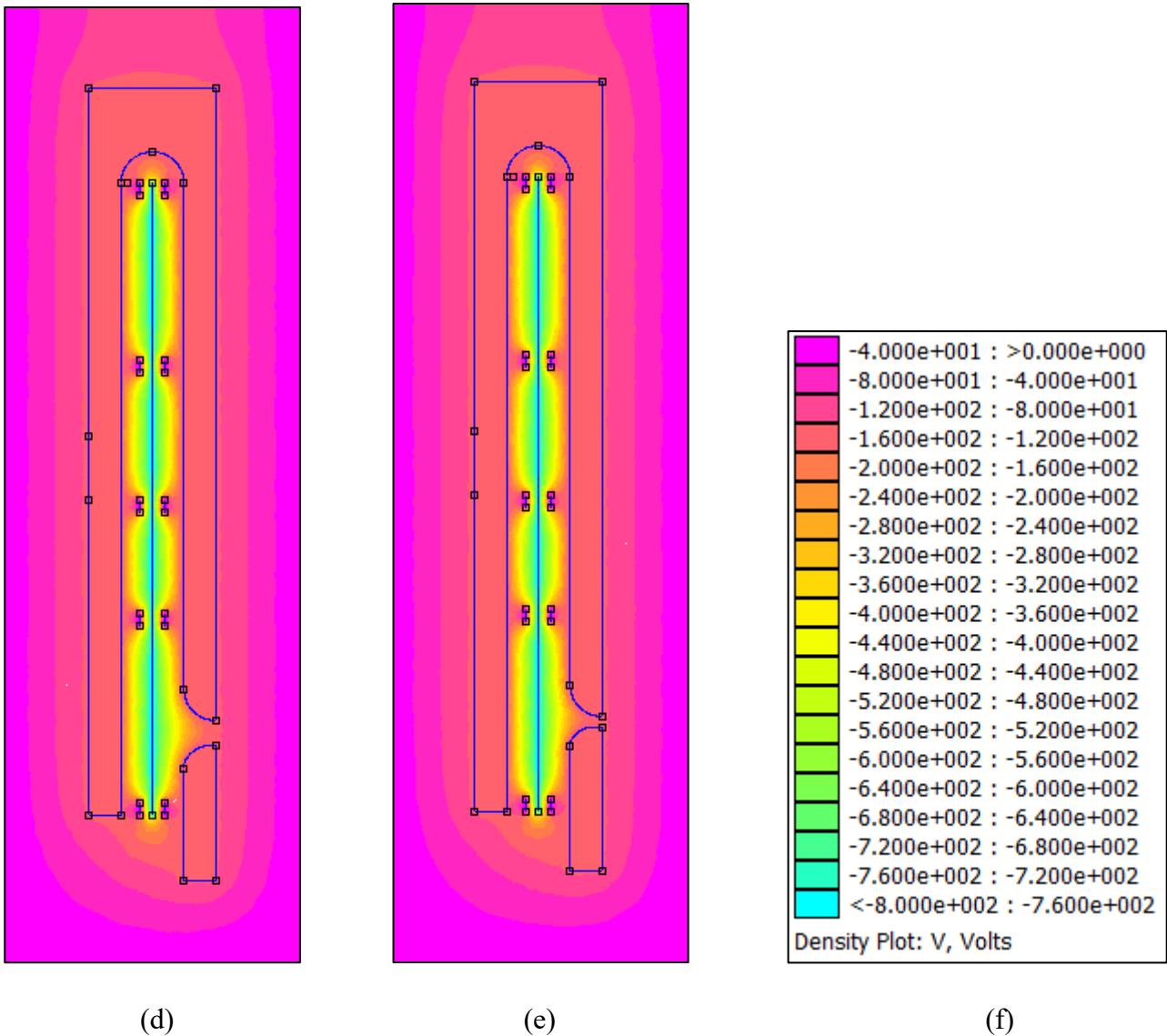
Figure 10.4 – Electric field simulation using software FEM 4.2. with different distance of the counter electrode from the inner conductor at (a) – without counter electrode; (b) – 50 mm; (c) – 40 mm; (d) – 30 mm; (e) – 20 mm. with the voltage distribution – (f).

To perform these simulations, the voltage applied to the electrodes during the sputtering process was used. For the QWR cavity (1) and the counter electrode (4) the same voltage of -130 V was applied, for the niobium target (2) -800 V and for the ground net (3) 0 V.

As shown on the figure 10.4a, counter electrode usage is essential to obtain a similar distribution of voltage and electric field. High plasma density in the area near the inner conductor without counter electrode causes high deposition rate of niobium atoms, which produces internal tension of the niobium coating with further delamination. Same situation is observed at too high distance between QWR inner conductor and counter electrode (Figure 10.4b).

142

Too small distance between counter electrode and QWR cavity will cause shielding of the cavity by counter electrode and low thickness of the niobium deposit (Figure 10.4e).

FEM simulations have made possible the definition of the optimum distance between the counter electrode and the cavity, which is 40 - 30 mm. At this distance electric field density is similar within all the cavity surface, which gives the possibility to overcome shielding effect and increase mean free path of the niobium atoms due to lower plasma-injected atoms interaction.

Sputtering pressure is another deposition parameter, which influences onto internal tension of the niobium film. The increase of the sputtering pressure decreases internal stress of the niobium film (paragraph 5.5). Due to this reason, it was decided to increase the sputtering pressure from $8 \cdot 10^{-2}$ mbar to 0,1 mbar for decreasing the total stress of the deposited films.

The resonators visible in figure 10.5 was obtained by increasing the sputtering pressure and assembling the counter electrode at the previously defined distance.
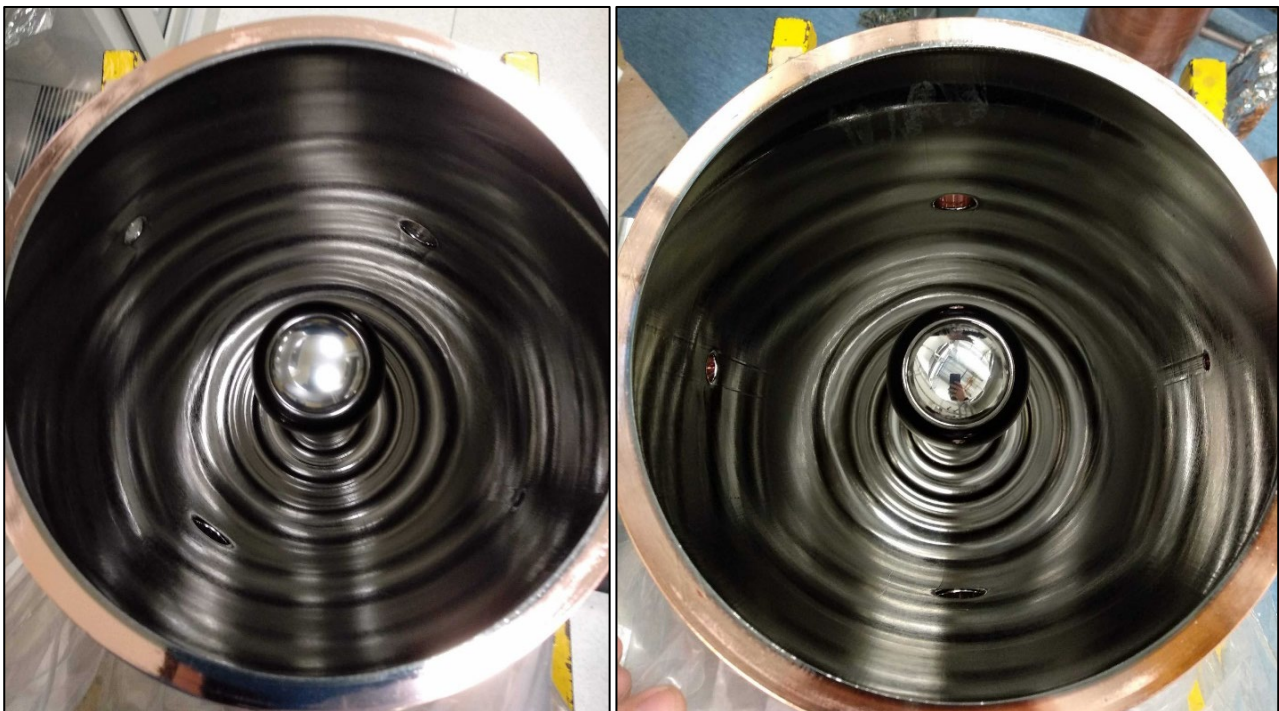


(a)                                                        (b)

Figure 10.5 – View of the sputtered (a) – HB 5 and (b) – HB 8 cavities.

By using an adapted sputtering pressure and a suitable distance between the inner conductor and the counter electrode, a resonator with an excellent coating with a mirror-like surface was obtained within

the entire QWR surface, without any delamination. An evaluation of the quality of the niobium coating is carried out by means of RF tests.

## 10.2. Analysis of the Nb/Cu high-β QWR low temperature measurement.

During low-temperature cavity measurements, a correlation between QWR superconducting performance and the specific parameters of the sputtering processes was observed. In this chapter will be described influence of different parameters variation onto superconductive performance of the produced QWR cavities.

*Sputtering process parameters*

A dependence between quality factor and superconducting performance was observed for some sputtering parameters, such as sputtering pressure and counter electrode – QWR distance. Quality factor in function of the sputtering parameters is shown on figure 10.6. In the figure are presented quality factor QWR values, obtained during: [1] – first RF measurements cycle; [2] – second RF measurements cycle.



(a)
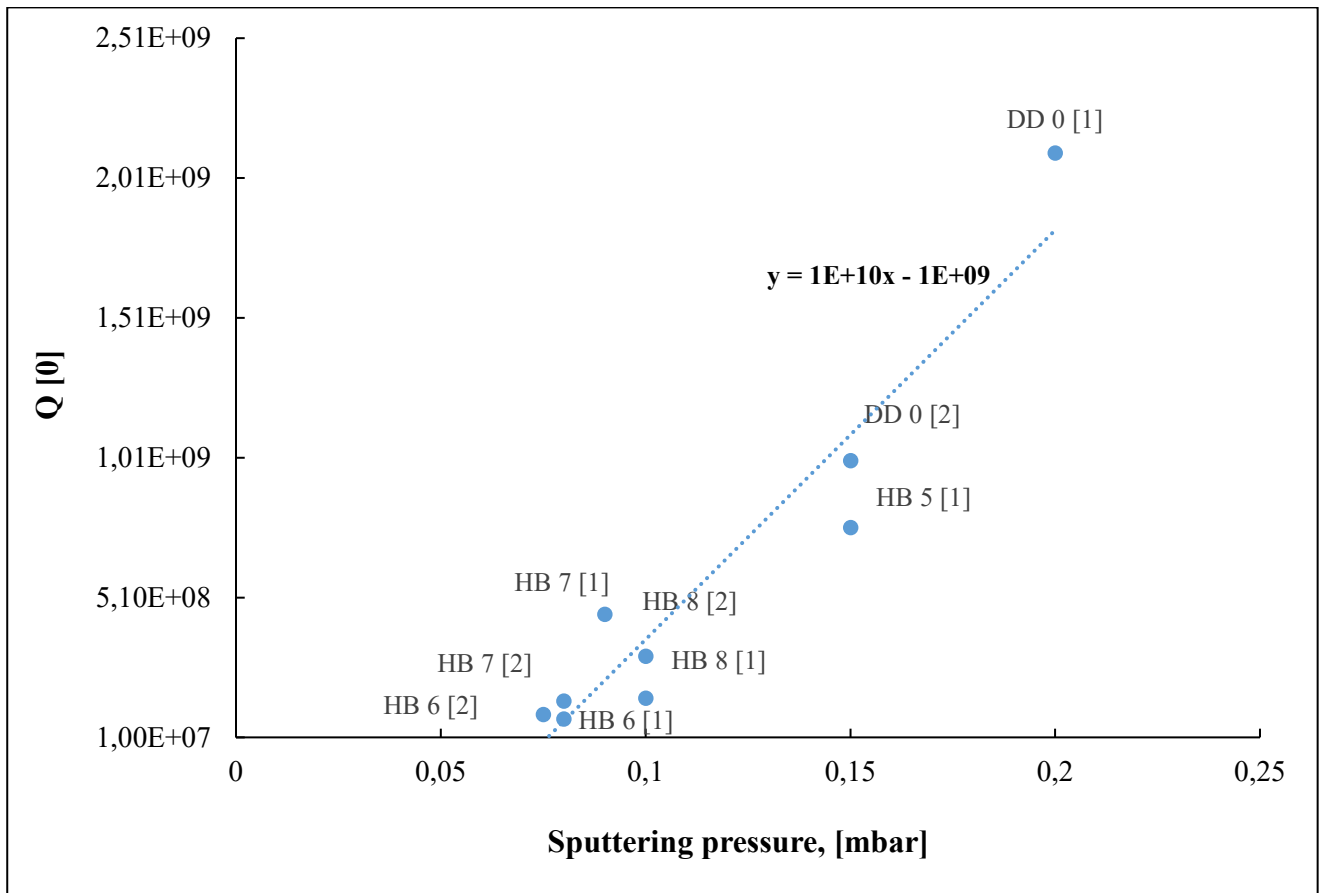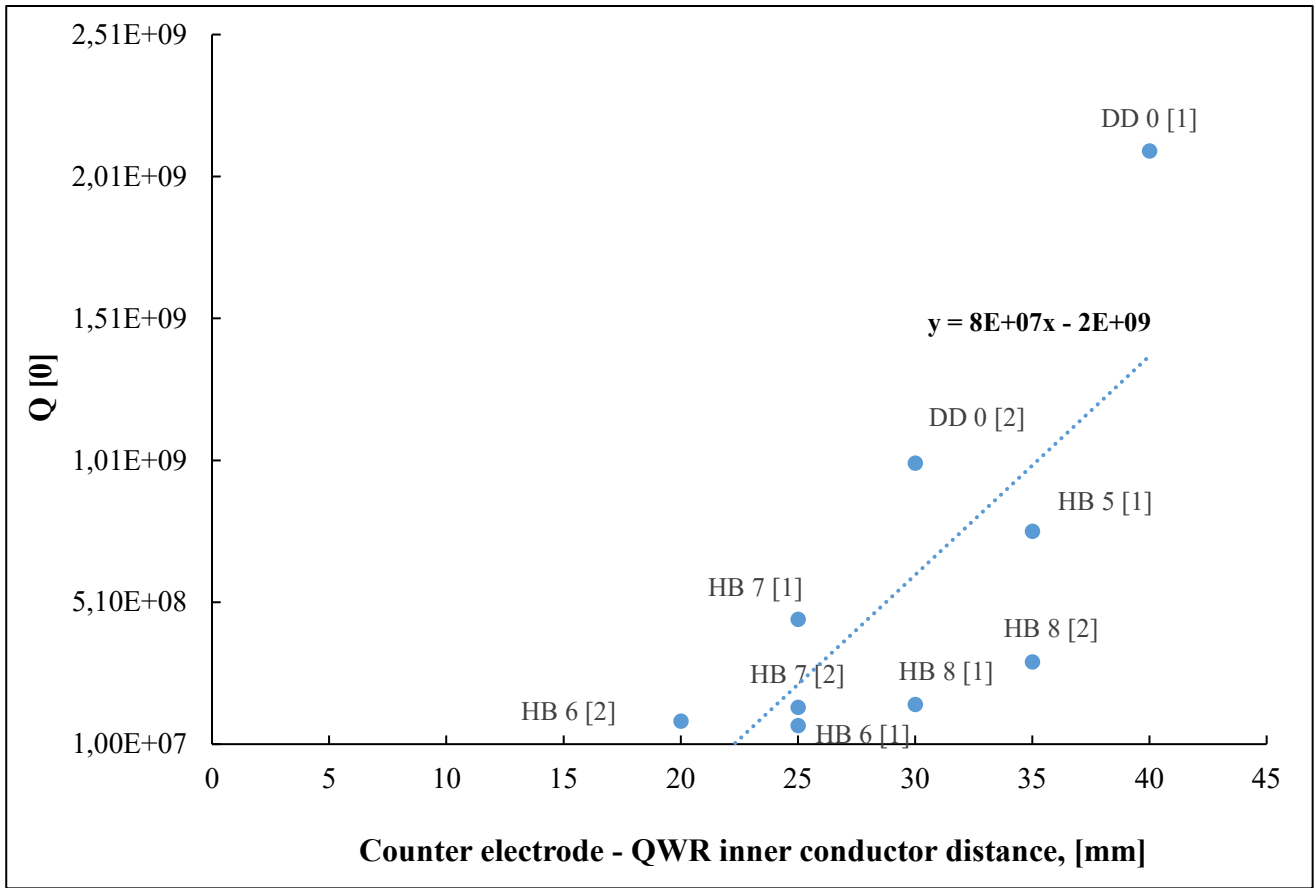
Figure 10.6 – Quality factor dependance from the sputtering parameters: (a) – argon deposition pressure; (b) – counter electrode-QWR inner conductor distance.

As was explained in paragraph 10.1.2., variation of the counter electrode-QWR distance and the sputtering pressure it is possible to change internal stress of the niobium coating. With high internal coating stress there is higher probability of crystallite defects production during stress release. Crystalline defects and impurities increase surface resistance of the film in superconductive state, which decreases, consequently, QWR superconductive performance.

Figure 10.6a shows that increasing the sputtering pressure from 0.07 to 0.2 mbar and the distance between the electrode and the QWR from 20 to 40 mm will significantly increase the quality factor of the resonator. That's parameters change corresponds to the R&D described in paragraph 10.1. A considerable improvement in the quality of the deposited film is obtained by increasing the pressure and distance. Thin film was mirror-like, without delamination.

Due to the influence of the sputtering parameters onto film morphology and QWR superconductive performance it is recommended to use sputtering pressure 0,2 mbar and distance between counter electrode and QWR inner conductor of 40 mm.

*Low temperature conditioning*

It is possible to decrease the number of emitted electrons from the resonator by the input of the stable power in the superconductive QWR. This effect will lead to decrease the power, dissipated in the cavity walls, and increase of the cavity quality factor. Conditioning process in superconductive state is normally used for overpassing the Q-quench, which can appear in all the range of the applied gradient and is caused by imperfection of the niobium coating.

Normally, 13 W of transmitted power was used during the conditioning process. During this process temperature of the cavity increases, which causes increasing of the liquid helium evaporation, used for the QWR cooling. Time of the conditioning treatment is limited by the amount of liquid helium, which is used to keep the QWR cavity with the tuner in the superconductive state.

Table 10.1 and Figure 10.7 show the effect of the conditioning process on the quality performance of the resonator. The data shows the example of the cavities with the best (DD 0) and worst (HB 6) superconducting performance of the first measurement cycle.

Table 10.1. RF measurement results before and after conditioning treatment.

| Cavity № | DD 0 [1] | | HB 6 [1] | |
|---|---|---|---|---|
| Parameters | Before | After | Before | After |
| $Q_0$ | $1{,}75 \cdot 10^8$ | $2{,}1 \cdot 10^9$ | | $7{,}6 \cdot 10^7$ |
| Q [7W] | $2{,}15 \cdot 10^8$ | $4{,}3 \cdot 10^8$ | - | $6{,}7 \cdot 10^7$ |
| $E_{acc}$ [7W], MV/m | 4,9 | 6,5 | - | 2,6 |
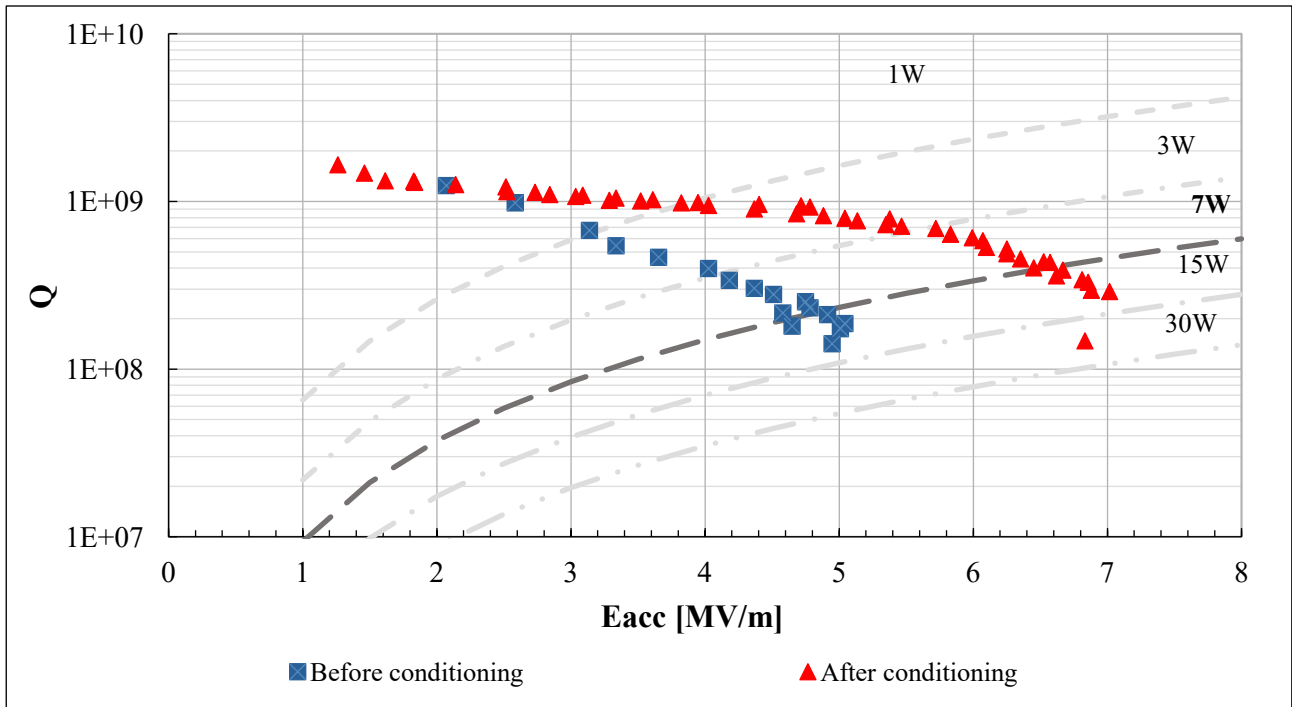
(a)
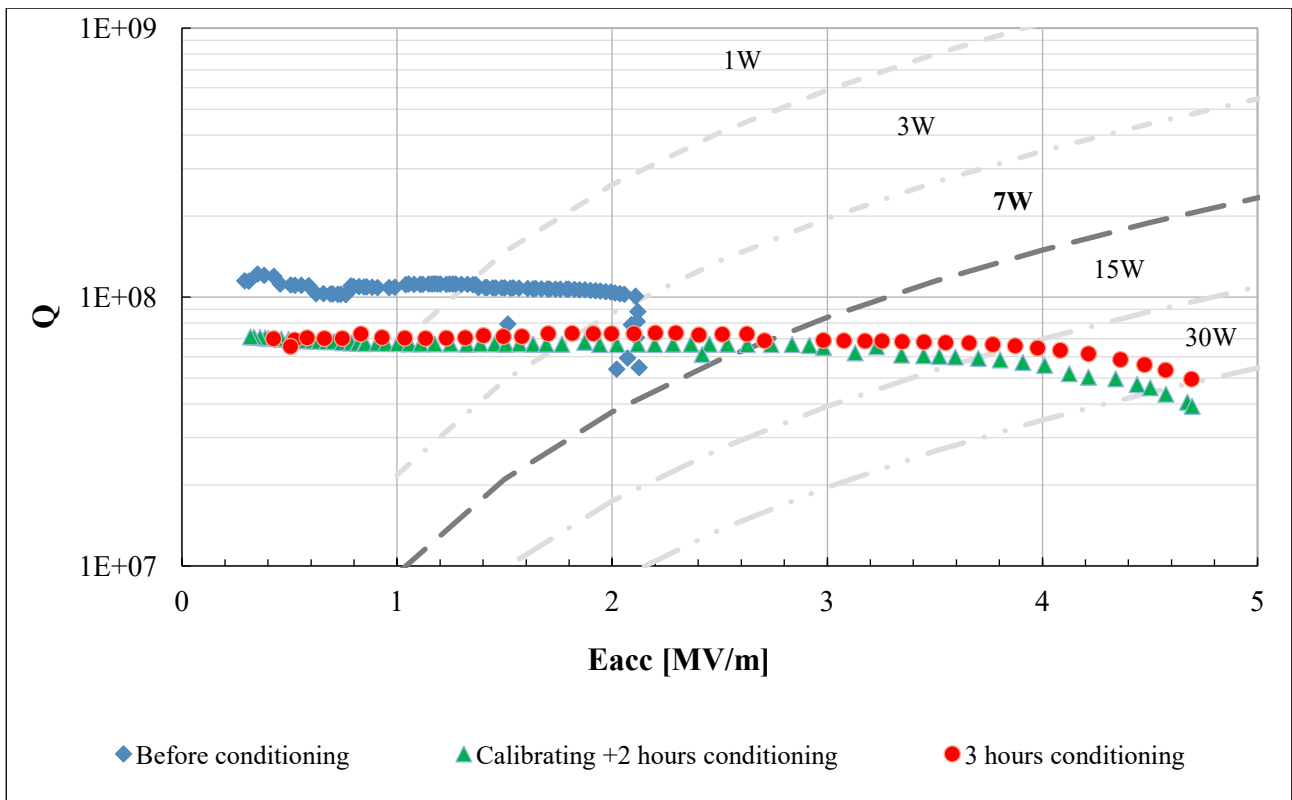


(b)

Figure 10.7 – Q-slopes of the (a) – DD 0[1] and (b) – HB 6 [1] cavities before and after low temperature conditioning.

Conditioning treatment effect was noticeable within all the RF measurements.

In case of DD 0 [1] RF measurement (Figure 10.7a) shows strong Q-drop from the low electromagnetic fields before the conditioning treatment. The Q-factor showed a strong dependence on the gradient, and we could achieve a maximum field of 5 MV/m. This Q-drop value could not be exceeded even by increasing the power transmitted in the cavity. After conditioning process which lasted 3 hours, significant change of the DD 0 performance was observed. Q-slope, starting from the smallest gradient number up to 6 MV/m, showed linear behavior with further gradient increase up to 7 MV/m, which is rather promising result for the QWR cavities.

Same influence of the conditioning treatment onto HB 6 superconductive performance was noticed. First run of the RF measurements of the cavity was blocked at the energy of acceleration field of 2 MV/m. After recalibration of the system and conditioning in superconductive state, Q-drop effect vanished, and Q-slope of the HB 6 cavity showed linear dependence with the gradient increase up to 4 MV/m with final reached gradient 4,7 MV/m.

Low temperature conditioning is necessary procedure for the QWR RF measurements, which increases the superconductive performance of the resonator.

The limiting factors of the conditioning process in the Legnaro National Laboratory are the maximum energy of the acceleration field, which is limited to 15 MV/m (due to radioprotection rules), and the time we can keep the cavity in a superconductive state depending on the availability of liquid helium, which generally is limited to 550 liters per test.

## 10.3. Comparison of the achieved results with current ongoing projects.

For the evaluation of the produced high-β QWR superconductive performance it is useful to compare measured superconductive characteristics with QWR cavities, used in the linear accelerators. RF measurements data of the cavities, confirmed for the accelerator assemblance (HB 5; HB 8) and two DD cavity measurements were used for the comparison of the superconductive performance.

The most evident comparison, that can give an idea of the achieved results, is superconductive performance of the high-β Nb/Cu QWR cavities, installed and operated in the ALPI LINAC high-β section. Cryostat # 19, produced and assembled in 2001, composed by 4 high-β QWR cavities, has been in constant use in recent decades. The Q-slopes of the cavities from the cryostat # 19 and resonators, produced within the ALPI upgrade project are showed in figure 10.8.
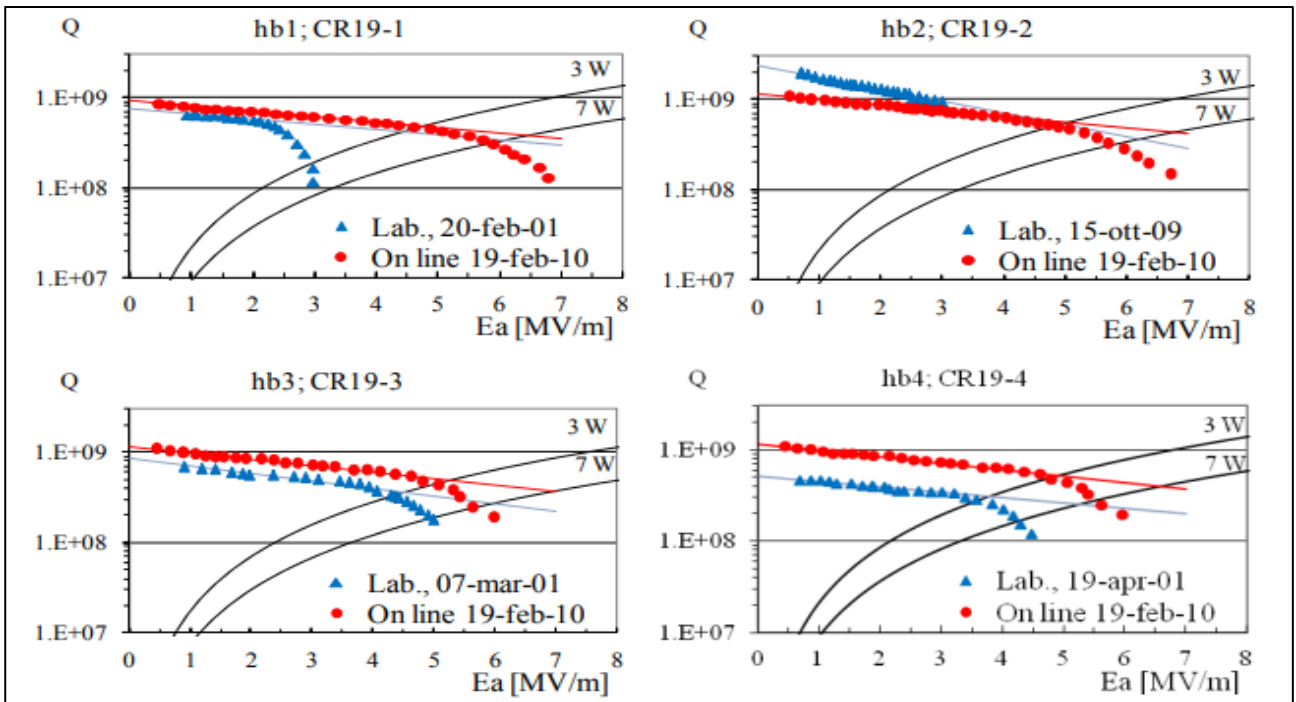
(a)
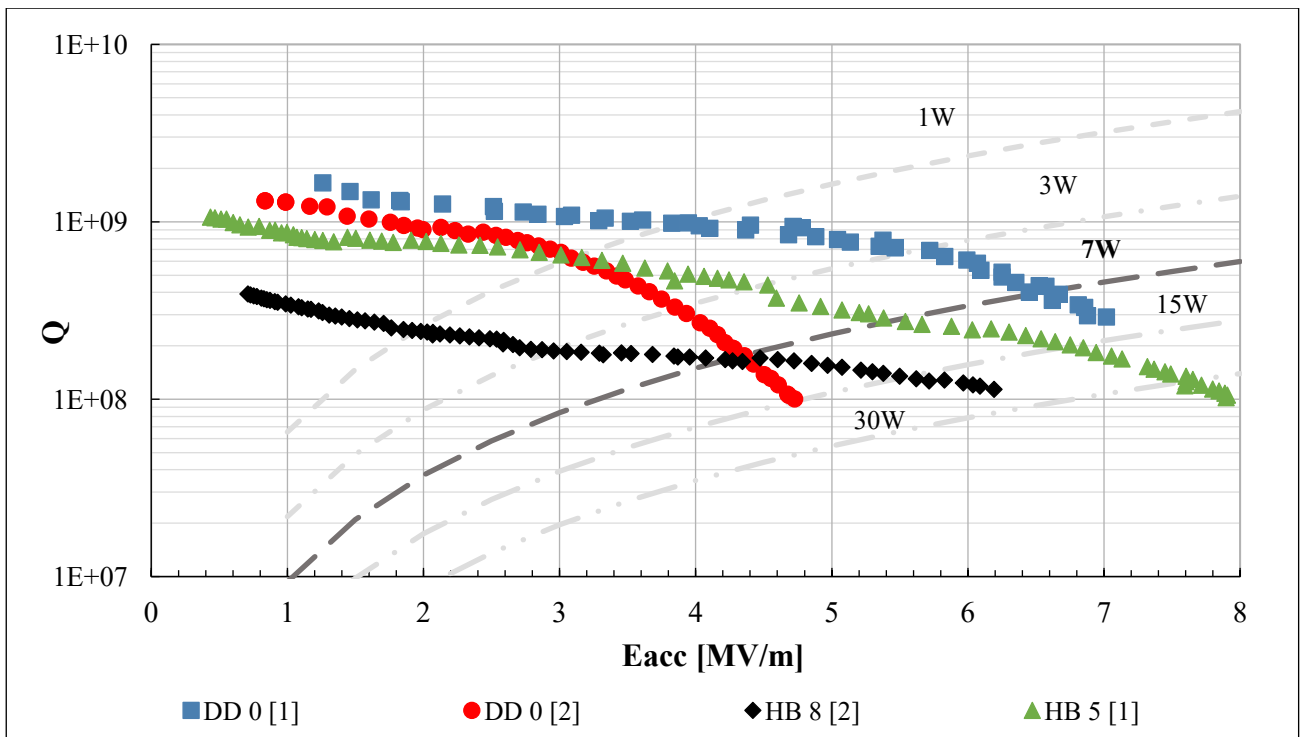


(b)

Figure 10.8 – Comparison between (a) – laboratory (blue) and on-line (red) Q-curves of the high-β resonators installed in ALPI cryostat CR19 [18] and (b) – laboratory measured Q-curves, produced in the framework of the ALPI upgrade project.

After the last maintenance in 2009, cavities of the 19th cryostat were assembled to the LINAC line and helium conditioning at 100 W for several hours was made. The Q-slope shift from laboratory to online measurement, which can be noticed in the figure 10.15a can be explained by high power treatment of the QWRs, which cannot be done in research laboratory environment.

Average value of the 19th cryostat high-β cavities gradient at the ALPI working power due to the laboratory measurements is in the range of 4 – 5 MV/m with the quality factor in the order of magnitude $10^8$. Superconductive properties of the produced high-β Nb/Cu QWR cavities for the ALPI upgrade are 4,5 – 5,5 MV/m with Q in the same order of magnitude.

Produced superconductive cavities showed promising results of the RF measurements. Further treatment of these cavities after assembling into LINAC by high power helium conditioning can significantly increase cavities superconducting performance.

Another project currently in operation, consisting of sputtered niobium quarter-wave resonators, is HIE-ISOLDE, described in chapter 2. Since the working power and QWR geometry of the cavities, used in the ALPI and HIE-ISOLDE projects is different, it is incorrect to compare Q-slopes and quality factors of both QWRs.

Surface resistance is basic parameter, that characterize superconductive performance of the QWR thin film, considering cavity construction (geometry factor). Reported surface resistance of the HIE-ISOLDE QWR cavities, measured at 4,2 K is in the range 20 – 80 nΩ with average value of 65 nΩ [84, 85]. Surface resistance of the QWRs, produced within the ALPI upgrade project is in the range 14 – 96 nΩ with average of 44 nΩ at the same temperature.

The surface resistance of the QWRs, produced for the HIE ISOLDE and ALPI upgrade projects, are similar. These results suggest that the proposed Nb/Cu QWR production technology is a technology that provides resonators with excellent performance and is also reliable over the time (paragraph 9.4.1).

# Chapter 11

# CONCLUSIONS

The main goal of this work has been the development of the high-β Nb/Cu superconductive QWR cavities production technology for the ALPI LINAC upgrade in the framework of the SPES project.

The research activity during this project can be divided into several stages. The first stage has dealt with the refurbishing of the vacuum systems, used for production and characterisation of the superconductive ALPI QWR cavities and plates. Vacuum systems for QWR sputtering and test cryostat were cleaned, refurbished and upgraded. The main upgrade has concerned on the electronic control systems, vacuum gauges, pumps, baking jackets and lamps. Power supplies of the sputtering systems were renewed. After reassembling, plasma cleaning of the sputtering systems niobium targets was done. The main upgrade of the vacuum cryostat has concerned the renewal of the temperature measurement system, tuner fixer and movement of the coupler antenna.

The next step was testing the sputtering systems for the definition of the deposition parameters and verification of the sputtering reliability. More than 20 deposition tests onto quartz samples were done in order to define the baking and sputtering temperature, deposition current, argon pressure and bias voltage for the QWR sputtering process. The possibility of the pulsed bias voltage application to the substrate was tested. Several sputtering tests onto quartz and copper substrate were done to verify the deposition parameters and quality of the produced coating of the plates.

After the definition of the sputtering parameters, the high-β QWR copper cavity deposition was performed. A high temperature niobium deposition was done. Several drawbacks during the Nb/Cu QWR deposition were faced (delamination of the niobium coating from different regions of the copper substrate) and solved by variation of the certain sputtering parameters. The methodology for the substrate preparation, baking, and sputtering processes of the Nb/Cu high-β QWR cavities was defined.

RF measurements in the refurbished test cryostat were done for the evaluation of the superconductive performance of the produced QWR cavities. The methodology for the tuner assembling was modified. RF measurements of the Nb/Cu high-β QWR cavities were defined.

In conclusion, 10 high-β Nb/Cu ALPI QWR cavities and 9 plates were produced during the final stage of this research activity. More than 15 low temperature measurements at 4,2 K of the produced high-β and tested medium-β Nb/Cu ALPI QWR cavities were done.

A correlation between QWR superconductive performance and sputtering process parameters was defined, after data analysis of the cavities RF measurements. With a variation of the argon gas sputtering pressure and distance between counter electrode and QWR inner conductor, it is possible to obtain niobium deposit without delamination from the copper QWR substrate and with high superconductive cavity performance.

RF measurements of the cavities, produced by the developed methodology showed promising results in comparison to the superconductive characteristics of the cavities, implemented in the current ongoing projects.

Superconductive characteristics of three produced QWR cavities overpassed the target performance, needed for the assembling in the ALPI LINAC.

Developed methodology of the Nb/Cu high-$\beta$ superconductive QWR cavities production is reliable, due to measured results and can be used for the high-$\beta$ QWRs production for the further upgrade of the ALPI linear accelerator.

# REFERENCES

[1] V. Palmieri et al., "Niobium sputter-coated copper quarter wave resonators", ICEC 15 Proceeding, Vol.34, pp.773 – 776, 1994;

[2] D. Franco, "An innovative cylindrical magnetron sputtering source for the deposition of HIE-ISOLDE superconducting Nb/Cu QWRs", Ferrara: PHD Thesis, University of Ferrara, 2015;

[3] V. Palmieri et al., "Niobium sputtered quarter wave resonators", Nuclear Instruments and Methods in Physics Research A328, pp.280 – 284, 1993;

[4] INFN, "ALPI" [Online]. Available: https://www.lnl.infn.it/alpi/;

[5] INFN, "SPES" [Online]. Available: https://web.infn.it/spes/;

[6] G. Bisoffi et al., "ALPI Setup as the SPES Accelerator of Exotic Beans", INPC 2013, pp.1 – 4, 2014; Available: http://www.epj-conferences.org;

[7] P.A. Posocco et al., "The ALPI Super-conducting accelerator upgrade for the SPES Project", Proceeding of LINAC08, pp.109 – 111;

[8] F.T. Cole et al., "Accelerator Physics and Engineering", Encyclopedia of Physical Science and Technology, Cornell University, USA, 2003, pp. 27 – 53;

[9] C.S. Hopper et al., "Superconducting spoke cavities for high-velocity applications", Physical review special topics – accelerators and beams, 16, 2013;

[10] H. Podlech, "Superconducting versus normal conducting cavities", CERN Yellow Report CERN-2013-001, pp. 151 – 170;

[11] S. De Silva, "Superconducting Cavities of Interesting Shapes (Non-Elliptical Cavities)", Talk of the SRF 2019 tutorial session, Dresden, Germany, 2019;

[12] Y. Kadi et al., "HIE-ISOLDE. Technical Design Report of the Energy Upgrade", CERN Yellow Reports: Monographs, Volume 1, 2018;

[13] G. Fortuna et al., "THE ALPI PROJECT AT LEGNARO NATIONAL LABORATORY", Proceedings of The Third Workshop on RF Superconductivity, Argonne National Laboratory, Illinois, USA, pp. 399-404;

[14] . G. Fortuna et al., "Status of ALPI and Related Developments of Superconducting Structures", LINAC 96, pp. 905-909;

[15] A.M Porcellato et al., "ON LINE PERFORMANCE AND UPGRADING OF ALPI RESONATORS", Proceedings of the 1999 Workshop on RF Superconductivity, La Fonda Hotel, Santa Fe, New Mexico, USA, pp. 174-178;

[16] A.M. Porcellato et al., "NIOBIUM SPUTTERED QWRS", Proceeding of the 12th International Workshop on RF Superconductivity, Cornell University, New York, USA, pp. 118 – 122, 2005;

[17] A.M. Porcellato et al., "NB SPUTTERED CU QWR: A 20 YEARS EXPERIENCE FROM AN IDEA TO THE ROUTINE BEAM ACCELERATION", 2007;

[18] A.M. Porcellato et al., "PERFORMANCE OF ALPI NEW MEDIUM BETA RESONATORS", Proceeding of HIAT 2012, Chicago, USA, pp. 73 – 79, 2012;

[19] G. Prete et al., "The SPES Project at the INFN-Laboratori Nazionali di Legnaro", INPC 2013, 2014; Available: http://dx.doi.org/10.1051/epjconf/20146611030;

[20] R.G. Sharma, "Superconductivity: Basics and Applications to magnets", Volume 214, 2015;

[21] V. Shmidt, "Introduction into superconductive physics", vol. 2, pp 5 -10, 2000;

[22] H. Ibach, H. Lűth, "Solid-state physics", Fourth edition, Springer, p.295, 2003;

[23] N.W. Ashcroft, I. Mermin, "Solid state physics", Cornell University, pp.726 – 728, 1976;

[24] J. Bardeen et al, "Theory of superconductivity," Physical review, vol. 108, p. 1175, 1957;

[25] A. Pippard, "Superconductivity" Proc.Roy sos, vol. A, n. 203, p. 98, London 1950;

[26] J. Waldram, "Surface Impedance of Superconductors", Adv. Physics, vol. 1, p. 13, 1964;

[27] H. Padamsee et al., "RF Superconductivity for Accelerators", New York: John Wiley & Sons, 1998;

[28] G. Ciovati, "AC/RF Superconductivity", Virginia, USA, 2015;

[29] V. Palmieri, "Superconducting resonant cavities", LNL-INFN (REP), Naples, Italy, 1991;

[30] H. Padamsee, "RF superconductivity science, technology and applications", NY. USA: WilleyVCH, 2008;

[31] I. Ben-Zvi, "Quarter Wave Resonators for Beta~1 Accelerators", Proceeding of SRF 2011, Chicago, USA, 2011, pp. 637 – 645;

[32] INFN, "The ALPI accelerator" [Online].

Available: https://www.lnl.infn.it/index.php/en/accelerators-3/alpi;

[33] G. Barbato, "Electrodeposition of tantalum and niobium using ionic liquid," University of Toronto, Toronto, 2009;

[34] W. Singer, "RRR-Measurement Techniques on High Purity Niobium"/W. Singer, A. Ermakov, X. Singer/ TTC-Report, 2010;

[35] H. Padamsee, "The science and technology of superconducting cavities for accelerators", Supercond. Sci. Technol., 14, 2001, R28 – R51;

[36] P. Bayer et al., "A Collection of Selected High Field Q-Slope Studies, Models and Comments", Review of Q-drop in SRF cavities, 2006, pp. 4-6, TD-05-56;

[37] B. Visentin, "Improvements of Superconducting Cavity Performance at High Accelerating Gradients", EPAC 1998, Stockholm, Vol. III, p. 1885, TUP07B;

[38] B. Visentin, "High Field Q-Slope and Oxygen Diffusion", presentation at the 2005 workshop on RF superconductivity, July 2005, Ithaca, USA;

[39] J. Halbritter, "Material Science of Nb RF Accelerator Cavities: where do we stand 2001", 10th Workshop on RF Superconductivity, Tsukuba - JAPAN (2001) - MA006;

[40] V. Palmieri, " The Problem of Q-Drop in Superconducting Resonators Revised by the Analysis of Fundamental Concepts from RF-Superconductivity Theory", Proceedings of 12th Workshop on RF Superconductivity, Ithaca (2005), p. 162;

[41] V. Palmieri and R. Vaglio, "Thermal contact resistance at the Nb/Cu interface as a limiting factor for sputtered thin film RF superconducting cavities," Supercond. Sci. Technol., vol. 29, no. 015004, 2016;

[42] C. Benvenuti et al., "Study of the surface resistance of superconducting niobium films at 1.5 GHz", Physica, Genova, Switzerland, 1999;

[43] C. Benvenuti et al., "CERN studies on niobium coated 1.5 Ghz copper cavities", Proc. 10th Workshop on RF Superconductivity, Tsukuba, Japan, 2001;

[44] H. Padamsee, "SRF Accelerators Flourish In a Golden Age," presented at the 6th International Particle Accelerator Conference, Richmond, VA, USA, 2015;

[45]  B. Bonin, R.W. Röth "Q degradation of niobium cavities due to hydrogen contamination", Particle Accelerators, Vol. 40 , 1992, pp. 59 – 83;

[46] P. Kneisel, B. Lewis and L. Turlington, "Experience with High Pressure Ultrapure Water Rinsing of Niobium Cavities", Proceedings of the 6th Workshop on RF Superconductivity, 1993;

[47] T. Powers, "Theory and practice of cavity RF test systems," presented at the Proceedings of 12th In. Workshop on RF Superconductivity (SRF2005), Cornell University, Ithaca, New York, USA, 2005;

[48] C. Pira, "Nb thick films in 6 GHz superconducting resonant cavities", Padua, PhD Thesis, University of Padova, 2019;

[49] J. Vossen, "Thin Film Processes"/ J. Vossen, W. Kern/USA, 1991;

[50] A. Rockett, Lecture notes; "Sputter deposition of thin films", University of Illinois, U.S.A., 1998;

[51] D.M. Mattox, "Handbook of Physical Vapour Deposition (PVD) Processing"/ Mattox D.M./ USA, 2010;

[52] W. Kiyotaka, "Handbook of Sputter Deposition Technology" /W. Kiyotaka, H. Shigeru/ New Jersey, USA, 1992;

[53] M. Ohring, "Material Science of Thin Films", Academic press, 2002, pp. 145 – 202;

[54] D.M. Hoffman, "Handbook of vacuum science and technology" / D.M. Hoffman, B. Singh, J.H. Thomas/ USA, 1997;

[55] R. Frerichs, "Superconductive Films made by Protective Sputtering of Tantalum or Niobium", Journal of Applied Physics, 33 (5), May 1962, pp. 1898 – 1899;

[56] J.M. Seeman, "Bias sputtering: its techniques and applications", Vacuum, Vol. 17 (3), March 1967, pp. 129 – 177;

[57] R. Vratny, D.J. Harrington, "Tantalum Films Deposited by Asymmetric AC Sputtering", Journal of the Electrochemical Society, May 1965, pp. 484 – 489;

[58] W.A. Grant, G. Carter, "Ion Trapping and Gas Release Phenomena", Vacuum, 15 (10), Oct. 1965, pp. 477 – 490;

[59] B. A. Movchan, A. V. Demchishin, "Structure and Properties of Thick Condensates of Nickel, Titanium, Tungsten, Aluminum Oxides, And Zirconium Dioxide in Vacuum", Fiz. Metal. Metalloved., vol. 28, p. 653, 1969;

[60] J.A. Thornton, "Influence of Apparatus Geometry and Deposition Conditions on the Structure and Topography of Thick Sputtered Coatings", Journal of Vacuum Science Technology, Vol. 11 (4), Jan 1974, pp. 666 – 670;

[61] A.L. Kameneva "Models of Structural Zones for Sputtered and Evaporated Thin Films", Research Journal of Pharmaceutical, Biological and Chemical Sciences, 6 (5), Sept 2015, pp. 464 – 474;

[62] J.A. Thornton, D.W. Hoffman, "Stress-related effects in thin films", Thin Solid Films, 171 (1), 1989, pp. 5 – 31;

[63] H. Windischmann, "Intrinsic stress in sputter-deposited thin films", Critical Reviews in Solid State and Materials Sciences, 1992, pp. 547-596;

[64] C. T. Wu, "Intrinsic stress of magnetron-sputtered niobium films", Thin Solid Films, 64 (1), 1979, pp. 103 – 110;

[65] "DEKTAK 8 advanced development user manual", Veeco Instruments Inc., USA, 2004;

[66] D. Franco Lespinasse et al., "Niobium Coating of Copper RFQs Plates by Biased Diode Sputtering", LNL-INFN (REP), V.242, Legnaro, Italy, 2016;

[67] A. Tsymbaliuk et al., "Refurbishing of the System for Niobium Sputtering of the High-β Superconducting QWR Cavities for ALPI Upgrade for the SPES Project", LNL-INFN (REP), V.258, Legnaro, Italy, 2019;

[68] S. Palazzese et al., "Refurbishing, assembling and preliminary test of the cryostat for QWR cavities.", LNL-INFN (REP), V.258, Legnaro, Italy, 2019;

[69] A.M. Porcellato et al., "Production, installation and test of Nb-sputtered QWRs for ALPI", Pramana – journal of physics, vol.59, N.5, 2002, pp. 871 – 880;

[70] V. Palmieri et al., "Niobium sputtered quarter wave resonators", Nuclear Instruments and Methods in Physics Research, 1993, pp.280 – 284;

[71] F. Ghaleb, H. Loukil, A. Belasri, "Breakdown Voltage in Electrical Discharge for Gases", in Proc. HTTPP, June 2014;

[72] J.R. Rairden, C.A. Neugebauer, "Critical temperature of niobium and tantalum films", Proceedings of the IEEE, 52(10), 1964, 1234–1238;

[73] V. Palmieri et al., "Sputtering of niobium thin films onto copper quarter wave resonators", Proceeding of the Fifth Workshop on RF Superconductivity, Hamburg, Germany, 1991, pp. 473 – 486;

[74] P. Zhang et. al., "Frequency pre-tuning of the niobium-sputtered quarter-wave resonator for HIE-ISOLDE project at CERN", Nuclear Instruments and Methods in Physics Research A, 797, 2015, pp. 101 – 109;

[75] N.J. Simon et al., "Properties of Copper and Copper Alloys at Cryogenic Temperature", NIST Monograph 177, New York, USA, 1992;

[76] C. Pira et al., "IMPACT OF THE Cu SUBSTRATE SURFACE PREPARATION ON THE MORPHOLOGICAL, SUPERCONDUCTIVE AND RF PROPERTIES OF THE Nb SUPERCONDUCTIVE COATINGS", in Proc. SRF 2019, Dresden, Germany, 2019, pp. 935 – 939;

[77] S. Stark et al., "Niobium Sputter-Coated QWRs", in Proc. SRF`97, Padova, Italy, Oct.1997, pp. 1156 – 1163;

[78] W. Venturini Delsolaro et al., "Nb Sputtered Quarter Wave Resonators for the HIE-ISOLDE", in Proc. SRF`13, Paris, France, Sep.2013, pp. 767 – 772;

[79] H. Vogel et al., "Production of Nb/Cu Sputtered Superconducting Cavities for LHC", in Proc. SRF`99, Santa Fe, NM, USA, Nov. 1999, pp. 437 – 439;

[80] C. Benvenuti et al., "Superconducting Cavities Produced by Magnetron Sputtering", in Proc. SRF`87, Lemont, IL, USA, Sep.1987, pp. 445 – 468;

[81] S. Stark et al., "Recent Upgrade of Ultra-Broadband RF System for Cavity Characterization," in Proceedings of 16th International Conference on RF Superconductivity (SRF2013), Paris, France, 2013;

[82] V. Palmieri et al., "Installation in the LNL ALPI linac of the first cryostat with four niobium quarter wave resonators", Nuclear Instruments and methods in physics research, Vol. 382 (A), 1996, pp. 112 – 117;

[83] E. Cantergiani, "Characterisation of OFE copper", CERN Internal Report;

[84] W. Venturini Delsolato et al. "Lessons learned from the HIE-ISOLDE cavity production and cryomodule commissioning", SRF2017, TUXAA02, Lanzhou, China;

[85] N. Jecklin et al. "Niobium coating for the HIE-ISOLDE QWR Superconducting accelerating cavities", Proceeding of SRF2013,TUP073, Paris, France.